The Dissertation Committee for Paul Michael Alvey II Certifies that this is the approved version of the following dissertation:

Self-Assembly of Electron-Rich and Electron-Poor Naphthalene Rings

Committee:

Brent L. Iverson, Supervisor

C. Grant Willson

Christopher W. Bielawski

Bradley J. Holliday

C. Buddie Mullins

Self-Assembly of Electron-Rich and Electron-Poor Naphthalene Rings

by

Paul Michael Alvey II, B.S.

Dissertation

Presented to the Faculty of the Graduate School of

The University of Texas at Austin

in Partial Fulfillment

of the Requirements

for the Degree of

Doctor of Philosophy

The University of Texas at Austin

May 2013

Dedication

To my parents

Acknowledgements

I want to first thank Professor Brent Iverson for his support and guidance. I am forever grateful for the research opportunity and the lessons he bestowed unto me. I thank my fellow group members for their support, feedback and friendship. My conversations with Joe Reczek and Valerie Bradford were truly influential. A special thanks to friends and former coworkers Garen Holman, Chelsea Martinez, Michael Elmuccio and Stevan Samuel for making my experience an enjoyable one. Thank you to Cameron Peebles for his friendship and company in lab which got me through the last two years. As Sean Connery said, "you're the *dog** now, *man**!" Thank you to Mark and Kelly Pogson for the countless meals, bone-breaking ninja techniques (sorry Stevan), holiday gatherings, and many other memorable experiences. Again, thank you to the entire group and I wish you all success in your future endeavors.

I must thank the Willson, Bielawski, Anslyn and Sessler groups for sharing their equipment and knowledge. In particular, many thanks to Rob Ono and Hao Tang. I also cannot forget Michael Jacobsson, Adriel Salazar, Leo Joyce, Jason Zbieg, and Pedro Metola who provided much needed distractions (and help) throughout the years. I appreciate the friendship and help from all those I was unable to list here as well!

I only made it this far because of the motivation and support from my parents and sister. I cannot thank them enough for their frequent phone calls and trips to Austin which meant more to me than they know. And finally, I want to thank Allie and the whole Leander family for their care and support.

Self-Assembly of Electron-Rich and Electron-Poor Naphthalene Rings

Paul Michael Alvey II, Ph.D.

The University of Texas at Austin, 2013

Supervisor: Brent L. Iverson

Molecular self-assembly through non-covalent interactions is an integral part of countless natural and synthetic materials. The Iverson group specifically focuses on aromatic donor–acceptor interactions and the subsequent self-assembly of molecules containing these functionalities. The work has predominately utilized association between the electron-rich 1,5-dialkoxynaphthalene (DAN) and the electron-deficient 1,4,5,8-naphthalenetetracarboxylic diimide (NDI) to create numerous self-assembled structures through intramolecular or intermolecular aromatic donor–acceptor interactions. The self-assembly and inherent electronic properties of aromatic units have made them attractive candidates for nature-inspired molecules, molecular machines and organic electronic materials.

The focus of these D–A interactions now shifts from an aqueous environment as solid state aromatic D–A interactions are promising modes of driven self-assembly for molecular architectures geared towards material applications. Aromatic units have long been applied in areas such as organic electronic materials due to their inherent charge transport properties. NDI has become a molecule of considerable interest among the organic electronics community due its electron transporting properties and ability to self-assemble. Therefore a thorough understanding of NDI and DAN–NDI self-assembly in the solid state should be of importance for the improvement and development of

molecular architectures for organic electronic devices. The following dissertation chapters focus on NDI or its aromatic D–A complex with DAN.

Chapter 2 investigates an unusual thermochromic behavior that occurred in our previous study when several solid state DAN:NDI mixtures lost their characteristic red color while crystallizing from the mesophase. Chapter 3 describes the synthetic progress towards a rigid, non-conjugated DAN–NDI molecule that retains electrostatic complementarity and ultimately led us to explore solid state non-covalent interactions of conjugated aromatic NDI–donor polymers. Chapter 5 describes an approach to synthesize conjugated NDI polymers and a diyne NDI to serve as an important synthetic intermediate. The work in chapter 6 tests the solid state association between neutral aromatic donor and acceptor polymer strands.

The work enhances the present understanding of these D–A interactions in different phases. The results also support recent discussions about aromatic stacking dominated by interactions between highly polarized groups on the periphery of aromatic units rather than overall polarization of the aromatic ring itself (*i.e.* D–A interactions).

Table of Contents

List of Tables

List of Figures

List of Schemes

Chapter 1

Aromatic Donor–Acceptor Interactions: Macroscopic Organization

1.1 MOLECULAR SELF-ASSEMBLY

Molecular self-assembly through non-covalent interactions is an integral part of countless natural and synthetic materials. Nature has long provided the gold standard for self-assembly through non-covalent interactions. While large covalent networks comprise protein and deoxyribonucleic acid (DNA) macromolecules, a delicate system of non-covalent hydrogen bonding, van der waals, metal coordination, and desolvation interactions dictate the actual molecular folding and assembly. It is this folding and assembly that controls the function of proteins and DNA, emphasizing the importance of these non-covalent interactions.

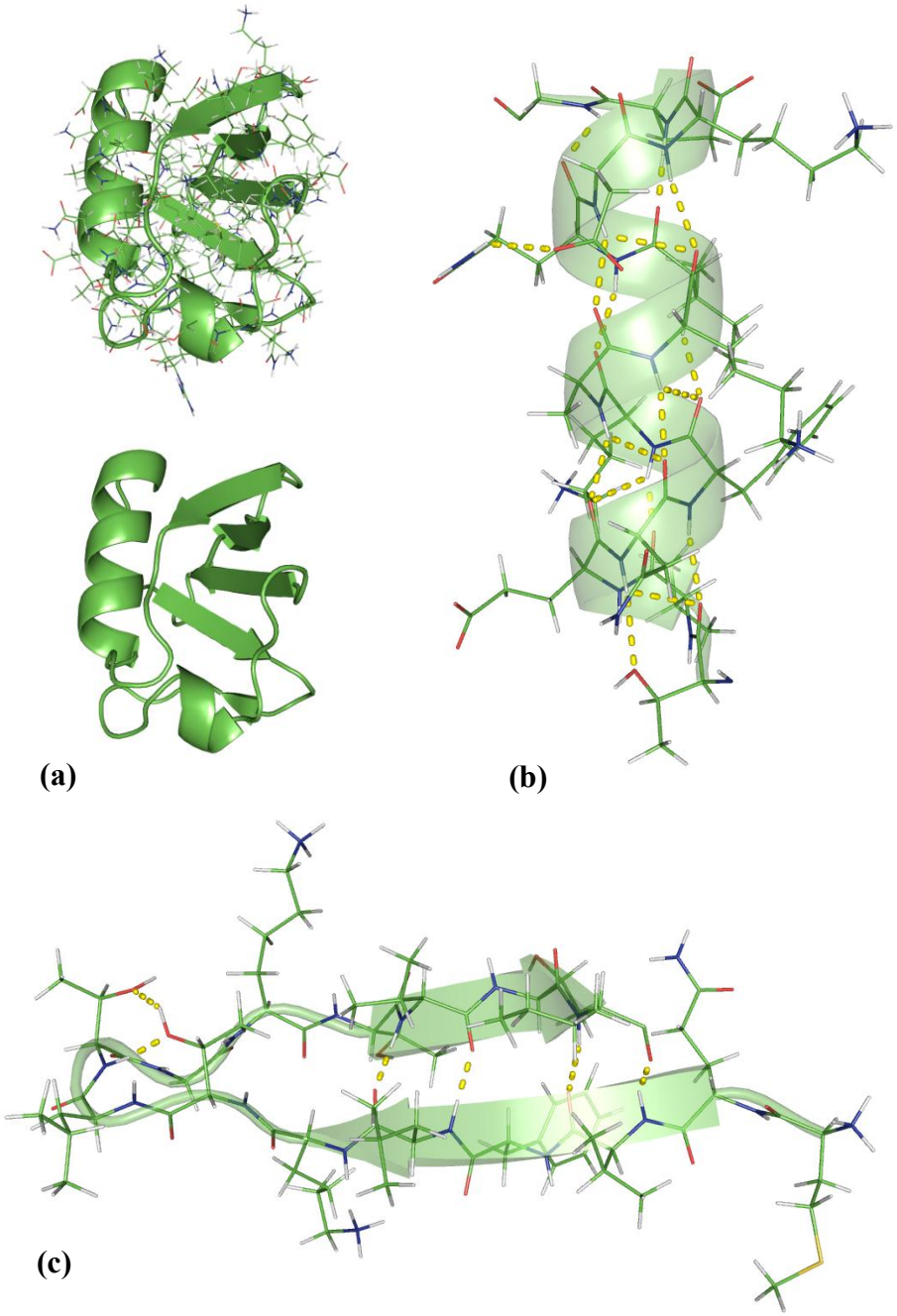

Figure 1.1 (a) Tertiary structure and cartoon representation of Ubiquitin (1). (b) Close up view of the alpha helix in Ubiquitin (hydrogen bond = dashed yellow line). (c) Close up view of a beta sheet in Ubiquitin (hydrogen bond = dashed yellow line).

Proteins are involved in nearly all biological functions on the cellular level. They can offer structural support, defend against foreign invaders, and carry out catalytic reactions. Proteins are most often assembled from only twenty distinct amino acids connected by amide bonds. In conjunction with the side chains of the amino acid residues, the backbone amide functionalities participate in hydrogen bonding patterns and serve to stabilize the three-dimensional structure of fully folded proteins (Figure 1.1a). Protein tertiary structure is built from secondary structural units such as alpha helixes (Figure 1.1b) and beta sheets (Figure 1.1c).

The tertiary and or quaternary structure controls its biological function. For example, enzymes adopt a precise three-dimensional shape, enabling the binding of a particular substrate within the active site. Once the enzyme binds its specific substrate, it can carry out its catalytic functions. The catalytic activity of proteins is therefore contingent on precise molecular folding and associated non-covalent interactions.

Many proteins also bind metal ions (metalloproteins) to perform specific functions or to drive self-assembly. Metals predominately coordinate to nitrogen, oxygen and sulfur atoms of amino acid residues within the protein. A transcription factor protein, for instance, binds specific DNA sequences to promote or block the transfer of genetic information during transcription. Many transcription factors require zinc for folding, typically through interactions with cysteine or histidine amino acid residues.

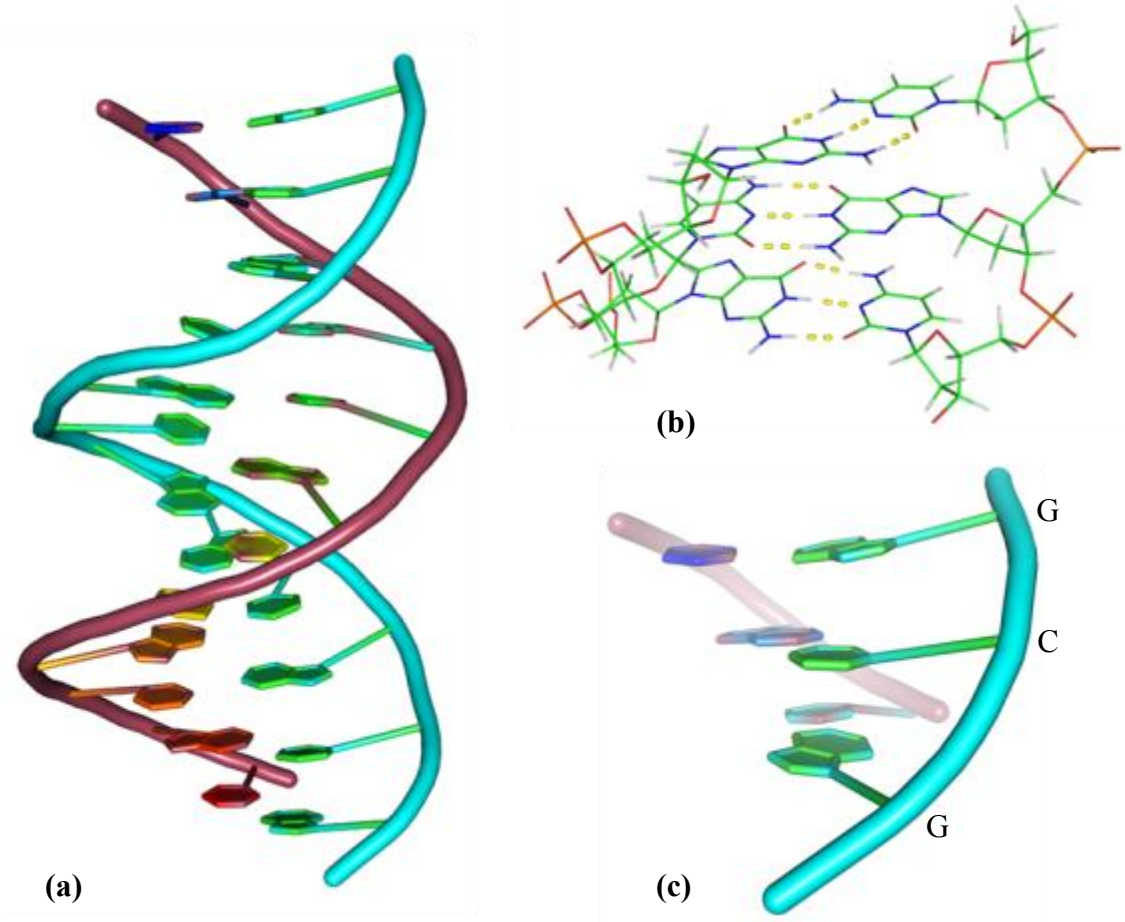

Figure 1.2 (a) The Cidofovir DNA duplex which shows the characteristic double-helix (2). (b) Complementary pairing of GCG and CGC bases (hydrogen bond = yellow dashed line). (c) Base stacking of GCG bases (labeled along the backbone) in a single strand of DNA.

DNA also relies on a complex system of non-covalent interactions to maintain its folded shape. A strand of DNA consists of a sequence of nucleotide bases (Guanine = G, Cytosine = C, Adenine = A, and Thymine = T). These nucleotides are attached to sugar residues and the sugar residues are connected through phosphodiester linkages to form a single strand of DNA. Two complementary strands join together to form the intertwined structure characteristic of DNA, the double-helix (Figure 1.2a).

Intermolecular hydrogen bonds between complementary nucleotide residues align and bind two individual DNA strands together (Figure 1.2b). Because hydrogen bonds are relatively weak interactions heat or mechanical force can pull apart these complementary strands. The ability to easily separate DNA strands facilitates the replication of DNA. Interactions between the stacked nucleotide bases (base stacking) within the individual strands add to the overall stability of the DNA double-helix (Figure 1.2c), while desolvation of the aromatic faces of the bases upon stacking is thought to provide a significant driving force for the formation of the double-helix structure.

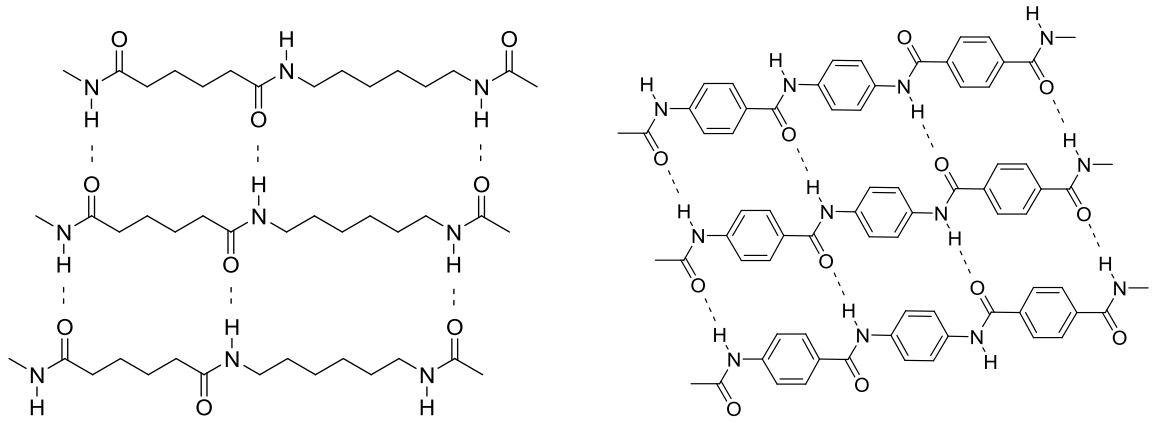

Nylon **Kevlar**

Figure 1.3 Hydrogen bonds present in Nylon and Kevlar.

The physical and electronic properties of many materials are dependent on the overall macromolecular structure. Studying macromolecular structure is a high priority in the field of supramolecular chemistry, where much research focuses on the predictable structural control of synthetic materials. Scientists now borrow organizational motifs from nature and employ non-covalent interactions for the development and application of truly novel synthetic materials (3; 4). Hydrogen bonding is perhaps the most common non-covalent interaction used to achieve higher order structures in synthetic applications. Materials like nylon and Kevlar greatly rely on hydrogen bonds to achieve their characteristic strength (Figure 1.3) and exemplify the collective strength that is possible when these relatively weak intermolecular interactions reinforce each other during macromolecular assembly.

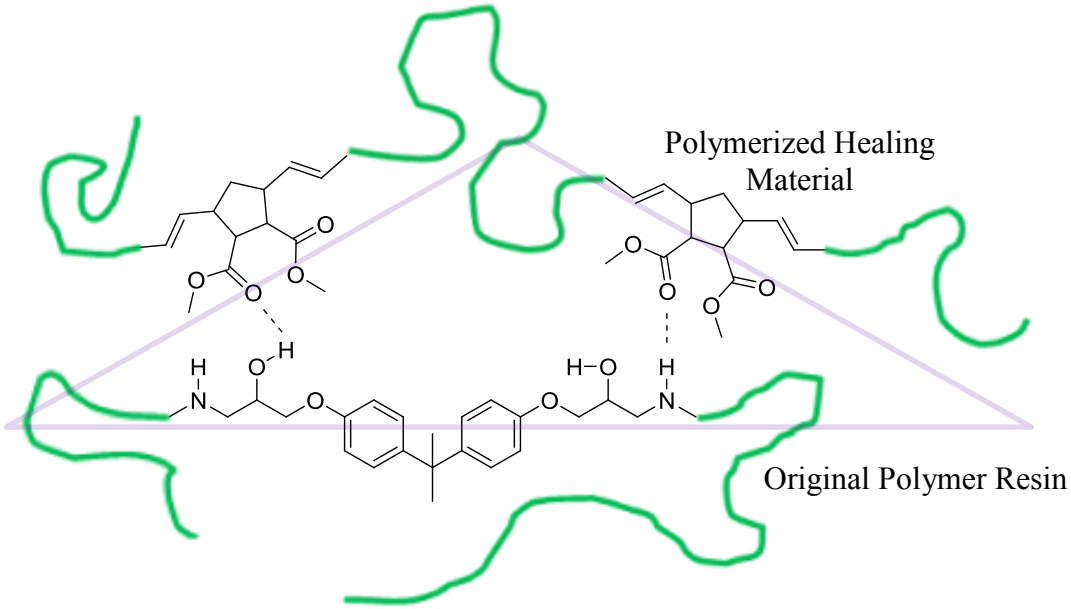

Figure 1.4 Schematic representation of a polymerized healing agent adhering through hydrogen bonds to a polymer resin that has sustained a crack (purple triangle) through hydrogen bonds.

A recent example by Moore *et al*. incorporates hydrogen bonding interactions as an adhesion promoter in a poly-dicyclopentadiene (poly-DCPD) self-healing material (5). Grubbs' catalyst and microcapsules containing DCPD monomers are embedded within the poly-DCPD material. When a crack develops within the polymer, microcapsules will break and release monomer into the crack. The newly free DCPD monomers then undergo polymerization with the Grubbs' catalyst embedded in polymer to repair the crack and complete the polymer healing process. To improve the healing properties of poly-DCPD, Moore incorporated hydrogen bonding donor and acceptor sites on the poly-DCPD and encapsulated healing monomer (Figure 1.4). The hydrogen bonds allow the healing material to better adhere to the original polymer and form a more entangled network along the fracture site.

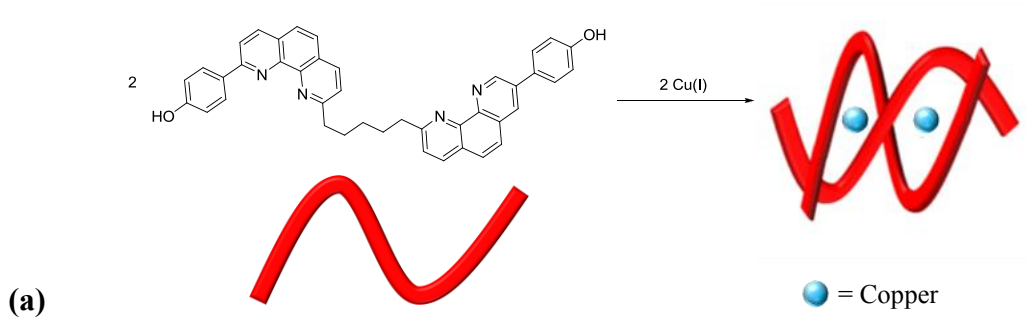

(a)

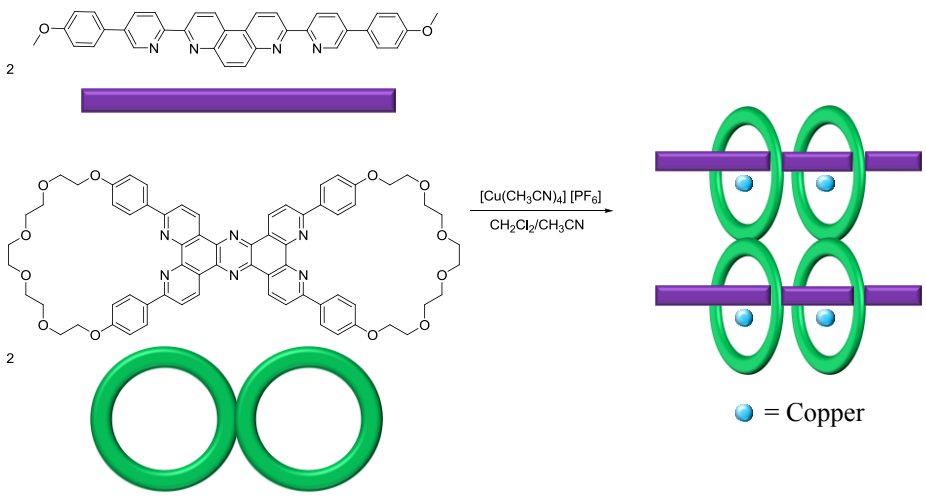

(b)

Figure 1.5 Examples of small molecule organization through copper templates.

Metal coordination has been applied to numerous monomeric and polymeric systems to achieve complex structural motifs. Metals can template two (Figure 1.5a) (6) or more (Figure 1.5b) (7) small molecules to form twisted and interlocked organizational motifs. Weder *et al*. reported low mass, rubbery polymers that assemble through zinc-binding interactions with nitrogen (Figure 1.6) (8). Metal-binding monomers can assemble in the presence of zinc to form polymer networks that can undergo a reversible assembly with UV light. The zinc–polymer structure is electronically excited with UV light and releases heat that temporarily disengages its zinc–polymer bonds. The polymer relaxes after irradiation and reassembles its zinc–polymer bonds. The polymer is a promising material for a new class of self-healing materials that can regenerate under local doses of UV light.

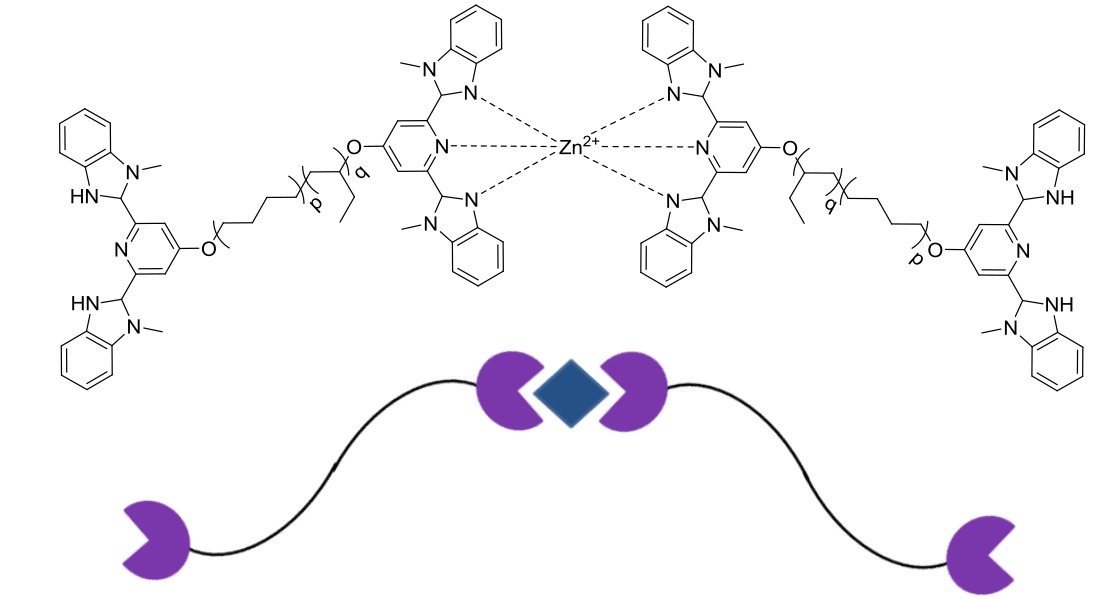

(a)

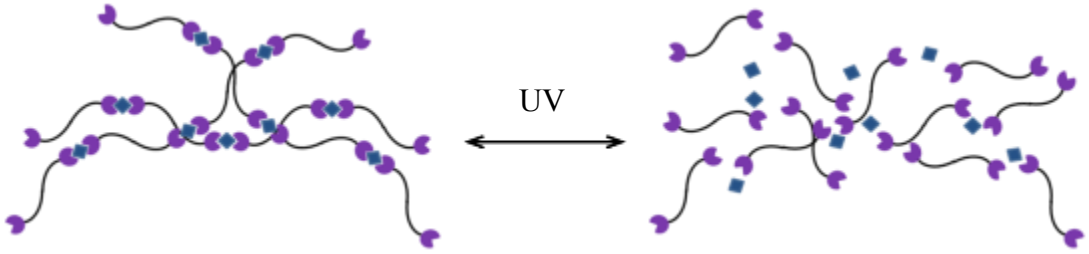

(b)

Figure 1.6 (a) Polymer that forms through metal-binding monomers (purple-black strands) and zinc (blue diamond) and (b) its reversible assembly under UV light.

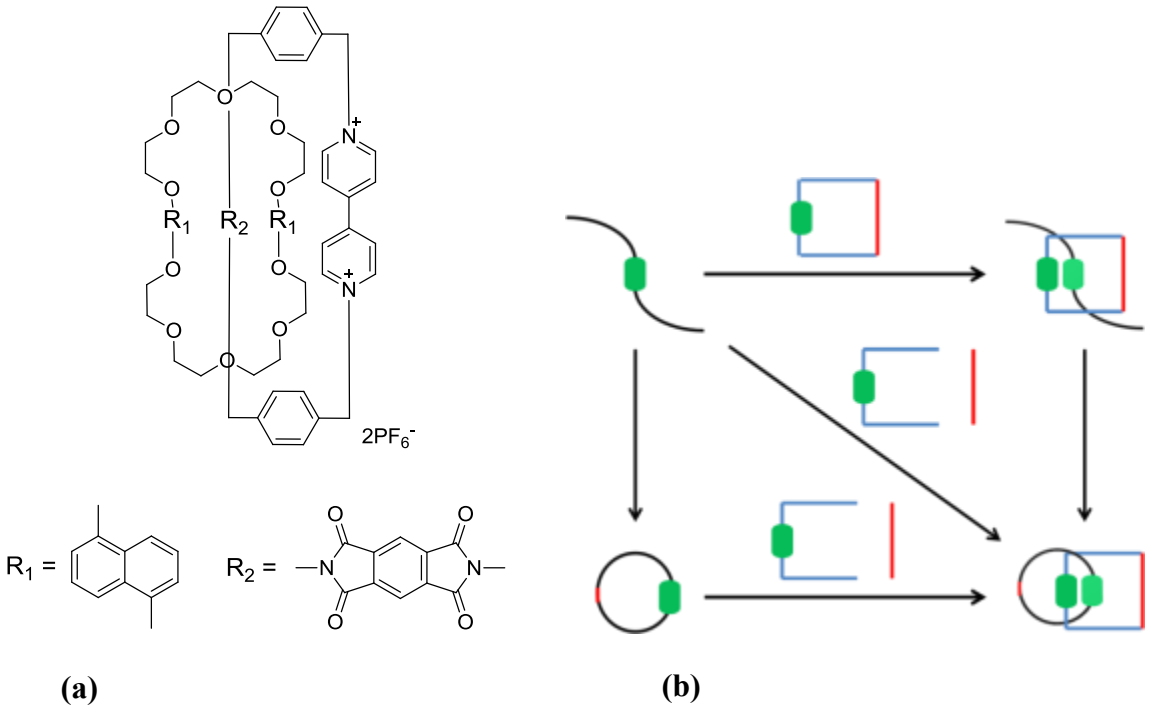

Figure 1.7 (a) Methods to template catenane structures through interactions between aromatic units. Green cylinders represent aromatic units. (b) A catenane structure synthesized by an aromatic–aromatic template.

Although interactions between aromatic units have historically received less attention than hydrogen bonding or metal coordination, they have been used in a variety of folding and self-assembling systems. Like metal coordination, interactions between aromatic units have been used to template catenane structures (Figure 1.7a). Separate strands that contain an aromatic unit can interact to form a threaded structure and cyclized with a ring closure reaction (Figure 1.7b). The intermolecular interaction between the aromatic units facilitates both the threading of two independent strands and the correct orientation for ring closure (9). Stoddart *et al*. employed these aromatic–aromatic template principles for a series of novel rotaxane systems. The rotaxane in Figure 1.8 displayed reversible intermolecular interactions between aromatic units that can be attenuated under different redox conditions (10).

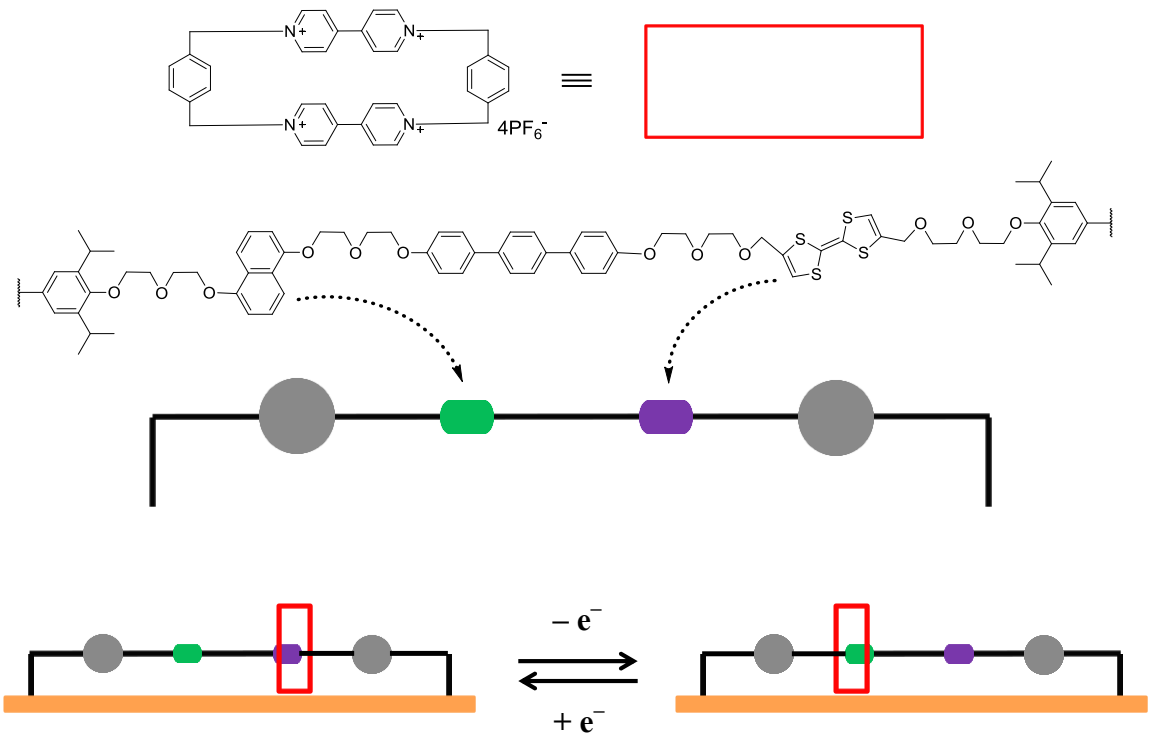

Figure 1.8 The aromatic containing ring of this rotaxane switches between aromatic substituents (green and purple) under different redox conditions.

The following dissertation describes the design, synthesis, and application of materials that incorporate non-covalent interactions between aromatic groups. The self-assembly and inherent electronic properties of aromatic units have made them attractive candidates for nature-inspired molecules, molecular machines and organic electronic materials. The growing interest in these non-covalent interactions highlights the importance of uncovering the subtle details that control self-assembly induced by aromatic–aromatic interactions. The next generation of these aromatic systems has the potential to create truly unique supramolecular architectures with desirable behavior and electronic properties.

1.2 INTERACTION BETWEEN AROMATIC UNITS: A STACKING MODEL

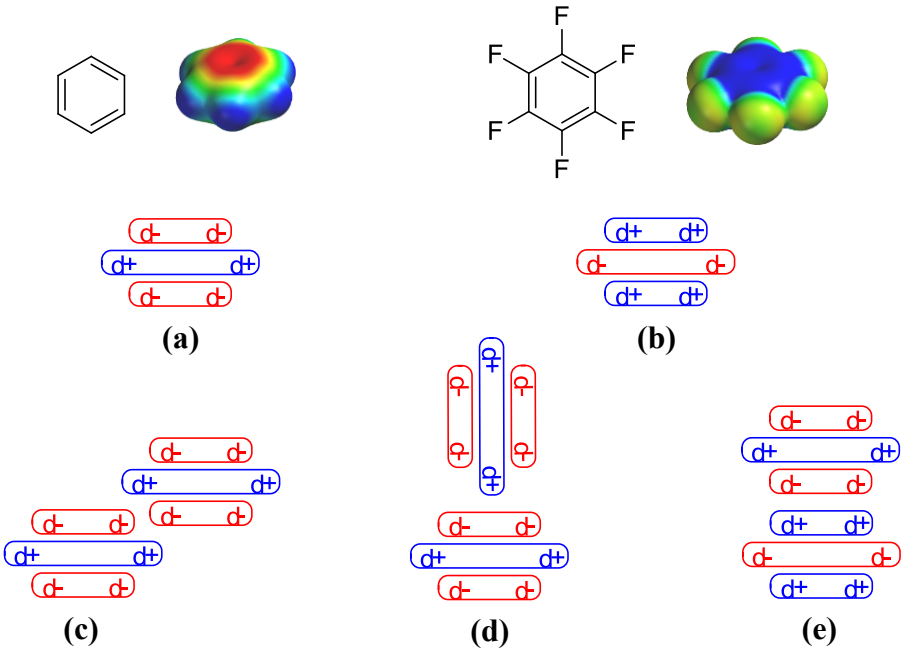

Figure 1.9 The polar/pi model of aromatic stacking with the (a) electron-rich benzene and the (b) electron-deficient hexafluorobenzene. Typical stacking modes are (c) offset face-to-face, (d) edge-to-face, and (e) face-centered stacking. Models were generated with the same electrostatic potential color scale in Spartan using the DFT B3LYP G-31* method.

The traditional model for interactions between aromatic units was established by Hunter and Sanders in 1990 (11). Known as the polar/pi model, it predicts aromatic stacking geometry using the quadrupole moment that arises from pi electron density on polarized aromatic rings. Aromatic rings like benzene are electron-rich (partial negative charge) on its top and bottom faces and electron-deficient (partial positive charge) along its periphery (Figure 1.9a). The Hunter and Sanders model proposes that two benzene molecules will interact or stack in such a way as to maximize complementary electrostatics. Since a face-centered interaction will result in electrostatic repulsion, the

model predicts that two benzene molecules will interact in an offset face-to-face (Figure 1.9c) or an edge-to-face (Figure 1.9d) fashion. Experimental as well as theoretical investigations have verified that benzene molecules prefer an edge-to-face or perpendicular arrangement in solution, as a liquid, and in the solid state (12; 13; 14; 15).

The benzene example illustrates the interaction between two electron-rich aromatic molecules. Yet substitution on the aromatic ring can enhance, alter, or completely reverse the overall quadrupole moment and greatly impact the type of interaction between two aromatic molecules. The fluorine atoms on hexafluorobenzene can completely reverse the quadrupole moment such that the aromatic core is electron-deficient and its periphery is electron-rich (Figure 1.9b). Although a face-centered interaction is unfavorable between two molecules of hexafluorobenzene due to the same reasons given for benzene, a face-centered interaction is favorable between molecules of hexafluorobenzene and benzene. The face-centered interaction between benzene and hexafluorobenzene is known as an *aromatic donor–acceptor interaction* (Figure 1.9e) where benzene is the donor (electron-rich) and hexafluorobenzene is the acceptor (electron-deficient). Experimental evidence for this complex was first reported in 1960 (16). The terminology is broadly applied to face-centered stacking between aromatic molecules with different but complementary polarization.

More recent models for aromatic−aromatic interactions by Waters (17), Houk and Wheeler (18), and later by Wheeler (19) emphasize the importance of substituents. This model of local electrostatics asserts that through-space interactions between polarized atoms on substituents along the aromatic periphery control the interaction between stacked aromatic units ("local electrostatics" model). The through-space interactions of local electrostatic interactions even clarifies some observed aromatic stacking behavior that opposes polar/pi predications. For the most part though, geometry predictions made

by both Wheeler and Hunter−Sanders models for stacked aromatic molecules are in agreement with each other. In actuality, a combination of both models may best describe the mechanisms behind aromatic−aromatic interactions and one should consider both models while predicting or assessing stacked aromatic molecules.

1.3 INTERACTION BETWEEN AROMATIC UNITS: DAN AND NDI

The Iverson group focuses on electron-rich 1,5-dialkoxynaphthalene (DAN) (Figure 1.10a), electron-deficient 1,4,5,8-naphthalenetetracarboxylic diimide (NDI) (Figure 1.10b), and their aromatic donor−acceptor (D−A) complex (Figure 1.10d, e). Crystal structures (Chapter 2) show that DAN and NDI as individual components usually adopt either an edge-to-face or an offset face-to-face (parallel displaced) stacking mode to best alleviate repulsive forces. When mixed, DAN and NDI stack in an alternating, face-centered fashion to maximize complementary electrostatic interactions (Figure 1.10c). The electrostatic potential map of DAN and NDI (Figure 1.10a, b) shows that they possess complementary quadrupole moments, which favors D–A stacking as predicted by Hunter and Sanders. Local electrostatic interactions between the oxygen atoms of DAN and the polarized carbonyl groups of NDI may also drive D–A association as described by Houk and Wheeler. In addition, these local electrostatic interactions appear to dominate the self-association of NDI units and result in an offset face-to-face stacking mode (Chapter 2, 4).

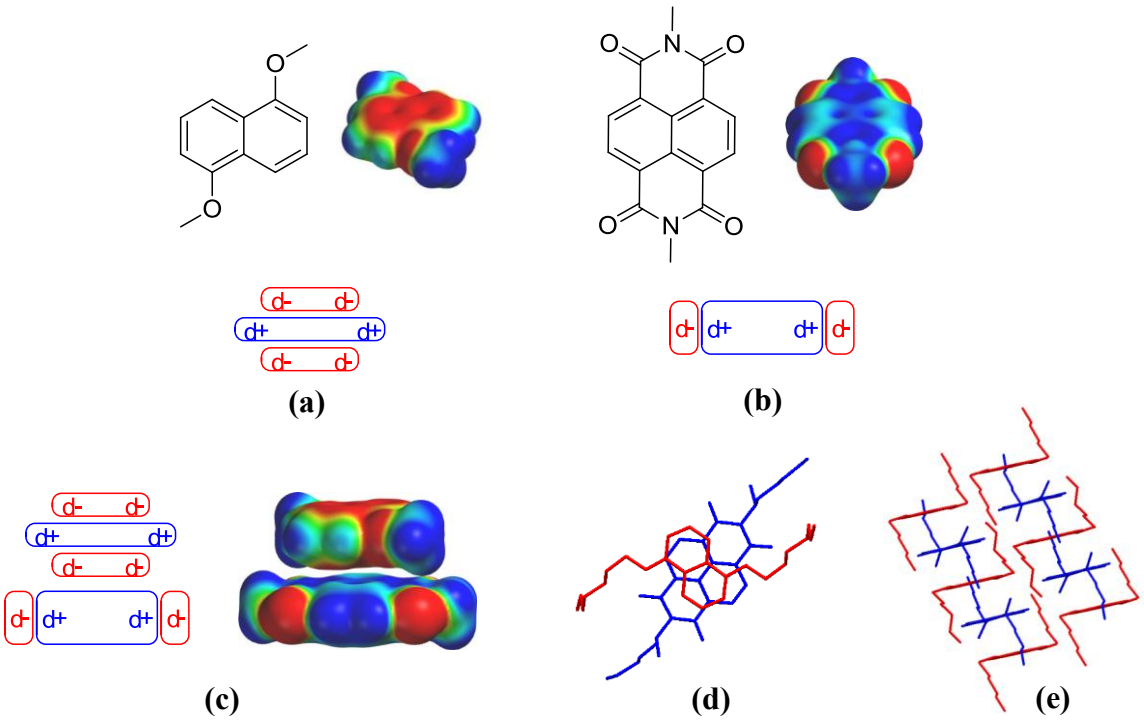

Figure 1.10 The D–A complex (c) that arises between (a) electron-rich DAN and (b) electron-deficient NDI along with (d, e) crystal structures of the D–A complex. Models were generated with the same electrostatic potential color scale in Spartan using the DFT B3LYP G-31* method.

Thus far, only electrostatic factors have been described as a driving force for aromatic–aromatic association. In water, though, solvophobic (hydrophobic) effects play a substantial role in DAN–NDI interactions. The electrostatic and hydrophobic contribution towards solution self-assembly was explored by Mark Cubberly who used ^{1}H NMR to tabulate the association constants of DAN–NDI monomers (20). Monomers with tetraethylene glycol side-chains (Figure 1.11) were synthesized to provide sufficient solubility in a variety of solvents. Association constants were recorded in deuterated solvent of different polarity for DAN–DAN, NDI–NDI, and 1:1 DAN–NDI.

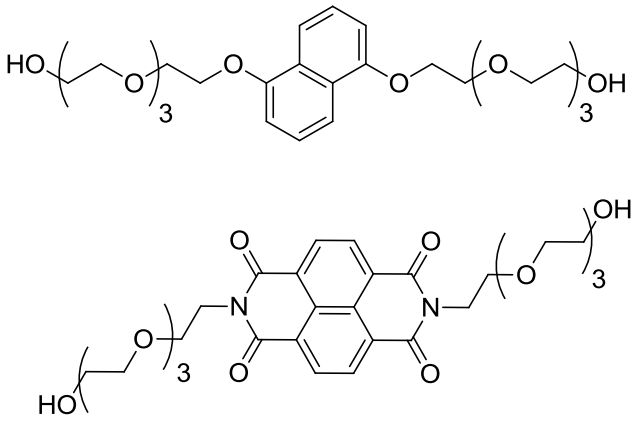

Solvent	DAN–DAN	NDI–NDI	DAN–NDI
$CDCl_3$	-	-	2
DMSO-d_6	1	2	3
CD_3CN	1	3	11
CD_3OD	1	8	30
D_2O	20	245	2045

Figure 1.11 Association constants of DAN, NDI, and 1:1 DAN–NDI for the derivatives shown above in a variety of deuterated solvents of different polarity.

The association constants of DAN–DAN, NDI–NDI, and DAN–NDI all increased with increasing levels of solvent polarity (top to bottom of table, Figure 1.11). DAN–NDI showed the most dramatic increase which suggested that complementary electrostatics is important for association. The association constant dramatically increased for DAN–DAN, NDI–NDI, and DAN–NDI upon switching from methanol to water (Figure 1.11). This substantial increase was indicative of strong solvophobic effects.

An explanation for the differences among the association constant values was rationalized using crystal structures. It was found that the association constant trends

obtained in this study correlate well with the amount of aromatic surface that each type of packing mode (offset face-to-face for NDI, edge-to-face for DAN, face-centered for DAN–NDI) exposes to the solvent. Specifically, DAN–DAN association had the lowest constant because its edge-to-face stacking mode exposes the most surface area of the three modes to the solvent. In contrast, DAN–NDI association had the highest constant because the face-centered stacking exposes the least surface area to the solvent. NDI–NDI association had an intermediate constant because the offset face-to-face stacking mode exposes an amount of aromatic surface area to the solvent that is between the edge-to-face and face-centered stacking modes. The study revealed that electrostatic contributions certainly impact the aromatic D–A association, but these results also indicated that solvophobic factors are a primary driving force for DAN–NDI association in water.

1.3.1 Intramolecular DAN−NDI Interactions

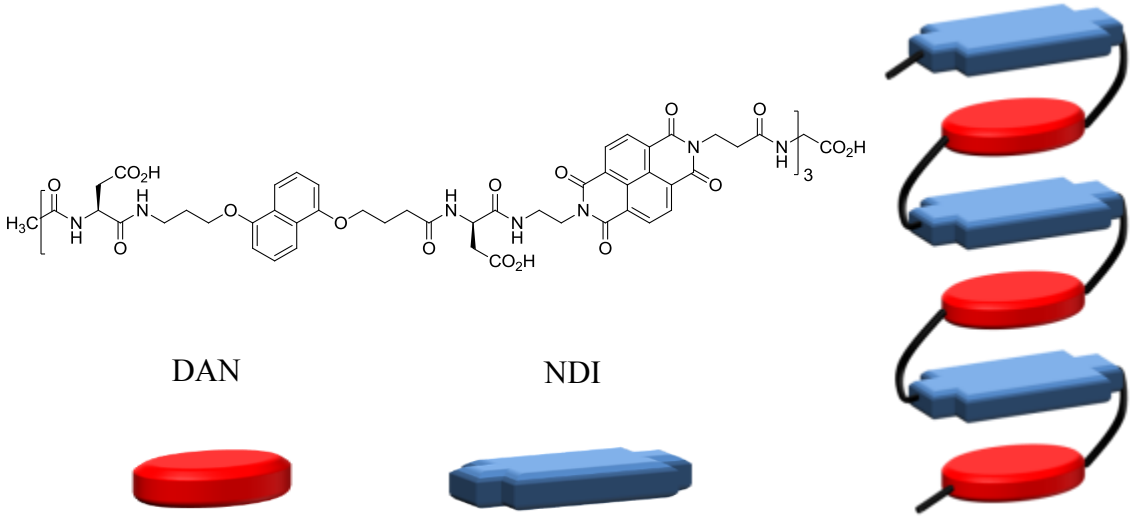

Figure 1.12 The structure of the first aromatic electron D–A oligomer (left) and its representative pleated stacking mode (right).

Scott Lokey was responsible for the first synthetic molecule designed to self-assemble into a secondary structure in water through aromatic D–A interactions (21). This type of molecule is known as an *aedamer* (*a*romatic *e*lectron *d*onor–*a*cceptor olig*omer*). The first aedamer was an aspartic acid linked molecule composed of alternating DAN and NDI units (Figure 1.12). The aedamer formed a pleated structure in water so that the DAN and NDI units were aligned in a face-centered manner to minimize the exposed aromatic surface area and to maximize face-to-face electrostatics. The alternating pleated structure was corroborated by UV-vis spectroscopy and ^{1}H NMR. The self-assembly resulted in strong hypochromism compared to the individual monomers (similar to DNA). The close proximity and face-centered geometry of DAN and NDI within the aedamer structure also yielded orbital mixing and a charge transfer (CT) complex that gave a characteristic red color in solution. ^{1}H NMR further showed an

upfield shift of the aromatic protons due to ring current effects from DAN and NDI units in close proximity to each other.

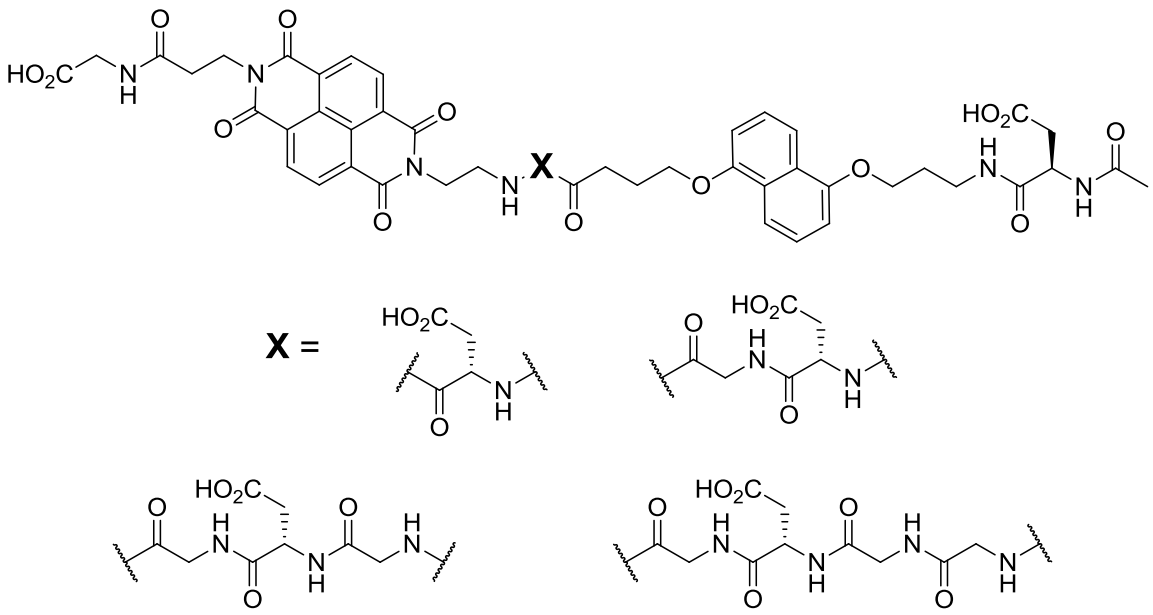

Figure 1.13 A DAN–NDI dimer that incorporated different amino acid linker units. Several of the investigated linkers are shown above.

Spurred by the results of Lokey's aedamer, the Iverson group embarked on numerous studies to further refine the stacking mechanisms behind the pleated aedamer structure. Andrew Zych synthesized a series of ten dimers comprised of DAN and NDI units tethered together by different amino acid linker residues (Figure 1.13) (22). The amino acid linkers imparted different lengths and degrees of rigidity to the aedamer structure. UV-vis and NMR spectroscopy was consistent with folded structures for all ten dimers. Only the exact orientation of DAN and NDI with respect to each other was linker dependent. Molecular modeling suggested a dynamic interaction between DAN and NDI with different possible conformations that all have a face-centered geometry.

	Designation	λ_{CT} (nm)	ε_{CT} ($M^{-1}\cdot cm^{-1}$)	% Hypochromism
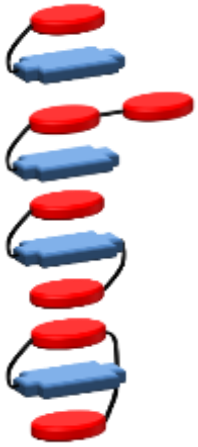	Dimer	526	380	45
	Control Trimer	510	490	48
	Linear Trimer	532	700	57
	Non-linear Trimer	532	670	60

Figure 1.14 The CT absorbance (λ_{CT}), molar absorptivity (ε_{CT}), and percent hypochromism (at 382 nm) of four derivatives used to study connectivity effects. Percent hypochromism = 100 × [1 – (absorbance at 382 nm without CTAB / with excess CTAB)].

Greg Gabriel tethered together DAN and NDI with aspartic acid residues to form a dimer and three trimer molecules to study the effect of aromatic D–A connectivity (Figure 1.14) (23). It was possible to switch between a pleated and a hairpin structure by simply changing the order of DAN and NDI within the trimer scaffold. Hypochromism represents a UV-vis absorption decrease due to stacked aromatic units (21). The spectroscopic characteristics of stacked DAN–NDI can be altered using the cationic detergent, cetyltrimethyl ammonium bromide (CTAB). The result is unstacked DAN–NDI and these spectroscopic characteristics resemble the combination of those obtained with isolated DAN and NDI monomers. The percent hypochromism in this study was determined for each derivative (Figure 1.14) using the naphthalene absorption difference at 382 nm between stacked and unstacked (with excess CTAB) molecules.

The second DAN unit of the control trimer was connected by a rigid linker to prohibit it from adopting the pleated structure. 2D ^{1}H NMR also indicated that the second DAN unit of the control trimer was not in contact with the NDI unit. Since the

outside DAN unit was unable to participate in the aromatic D–A stacking (Figure 1.14), the absorbance characteristics and percent hypochromism of the control trimer were similar to those of the dimer.

The CT absorption, molar absorptivity, and percent hypochromism for the linear and non-linear trimers agreed with previously reported values of stacked DAN–NDI–DAN (21). The linear trimer formed the expected pleated structure while the non-linear trimer adopted a hairpin arrangement such that the NDI on the end inserted itself between the two DAN units (Figure 1.14). 2D ^{1}H NMR supported a non-linear trimer structure in which the NDI was placed between the two DAN units.

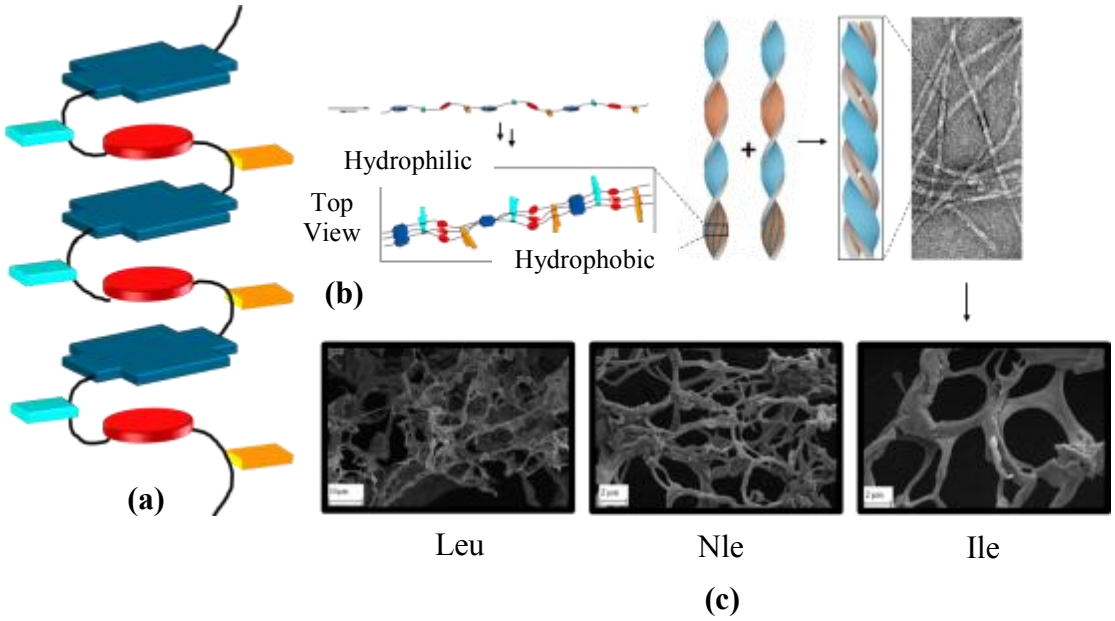

Figure 1.15 (a) Amphiphilic aedamer (teal squares = hydrophilic residues, gold squares = hydrophobic residues). (b) Proposed aedamer conformation change upon heating and a top view of associated linear aedamer strands. The strands associate into a twisted helix with hydrophilic (light blue) and hydrophobic (light orange) faces that can further associate into fibers. (c) SEM images of hydrogel networks that result from fiber assembly. The hydrophobic residue is listed below each image. Reprinted (adapted) with permission from (24). Copyright (2008) American Chemical Society.

The former studies showed that DAN–NDI association is extremely tolerant of both the type of linker and the order of the DAN and NDI units along the molecule. In other words, DAN and NDI will associate into their pleated D–A complex in water if the linker yields enough flexibility to do so. Up to this point, only hydrophilic amino acids like aspartic acid of the original aedamer were used to tether together the aromatic components. Although aspartic acid aided in solubilizing the aedamer and its shorter derivatives, the Iverson group discovered that incorporating hydrophobic residues into the aedamer resulted in hydrogel formation at elevated temperatures (25). Valerie Bradford synthesized several of these amphiphilic aedamers with aspartic acid and several different hydrophobic residues like leucine, norleucine, and isoleucine (24). The

DAN and NDI are tethered together such that the one side of the pleated aedamer structure has hydrophilic amino acid residues and the other side has hydrophobic amino acid residues (Figure 1.15a). The amphiphilic aedamers showed the characteristic red color from face-centered D–A association in water but irreversibly lost the red color around 80 °C. Not only did the solution lose its characteristic CT, the solution turned into a viscous hydrogel.

Scanning electron microscopy (SEM) showed that the hydrogel contained large molecular networks (Figure 1.15b). The different hydrophobic residues had little effect on the hydrogel transition temperature but SEM micrographs showed that different hydrophobic residue resulted in unique and characteristic hydrogel morphology. Cameron Peebles conducted a structural analysis on aedamer fibrils that were isolated from dilute hydrogel solutions. Experimental evidence from the fibril study supported the proposal that the aedamers reorganize during the thermal transition from a pleated, face-centered D–A structure into an offset, helically stacked NDI–NDI structure (Figure 1.15c). Atomic force microscopy and molecular modeling further suggest that these individual fibrils associate through hydrophobic and hydrophilic interactions into the large hydrogel networks observed by SEM.

The unique aspect of the amphiphilic aedamer is that it can irreversibly transition between two secondary structures using aromatic–aromatic interactions. The amphiphilic aedamer can also undergo its irreversible transition when seeded with pre-formed hydrogel material, similar to amyloid formation which occurs from misfolded proteins (26). The aedamer work demonstrates that intramolecular D–A interactions are a powerful tool for self-assembly and have the potential to template novel secondary structures with interesting properties such as irreversible conformational switching.

1.3.2 Intermolecular DAN−NDI Interactions

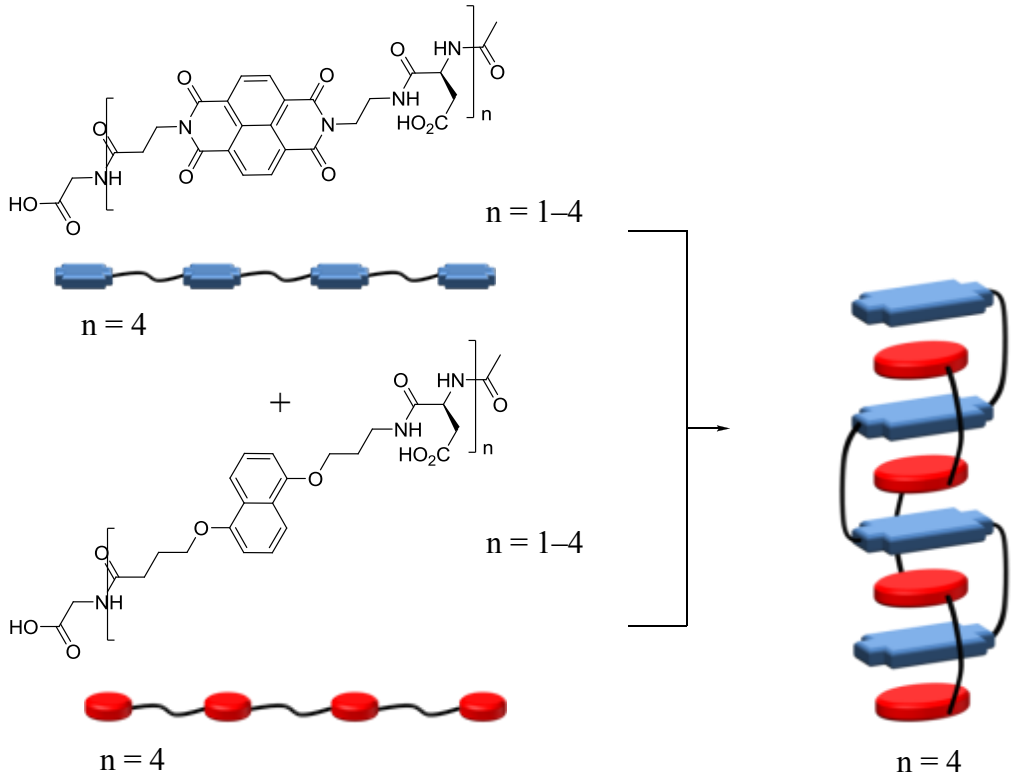

(a) **(b)**

Duplex	K_a (M^{-1})	ΔG° (kcal·mol^{-1})	ΔH° (kcal·mol^{-1})	ΔS° (cal·mol^{-1}·K^{-1})
n = 2	2.7 x 10^3	–5.0	–12.3	–23.0
n = 3	4.5 x 10^4	–6.8	–17.7	–34.2
n = 4	3.5 x 10^5	–8.1	–19.3	–35.3

(c)

Figure 1.16 (a) Structures of DAN and NDI oligomers and (b) the 1:1 DAN–NDI heteroduplex for oligomers n = 4 (right). (c) ITC energy parameters at 318 K for 1:1 oligomer mixtures (n = 1–4).

The association of separate DAN and NDI oligomers in water was demonstrated by Greg Gabriel and their energy parameters were determined with isothermal titration calorimetry (ITC) (27). DAN and NDI oligomers of up to four units in length (Figure 1.16a) engaged in heteroduplex formation through intermolecular D–A interactions (Figure 1.16b). The ITC data best fit a 1:1 model of DAN–NDI association, results that were corroborated with an NMR Job plot. Interestingly, the heteroduplex binding affinity (K_a) increased with each additional aromatic unit in the DAN and NDI oligomer (Figure 1.16c). Conclusive evidence for 1:1 DAN–NDI binding was acquired using polyacrylamide gel (PAGE) titration experiments. PAGE gels use charge density to discriminate and separate different materials. A PAGE gel titration showed that a 1:1 DAN–NDI oligomer ratio traveled farther than either the individual DAN or NDI oligomer. Furthermore, any excess oligomer at ratios other than 1:1 traveled less than the 1:1 complex.

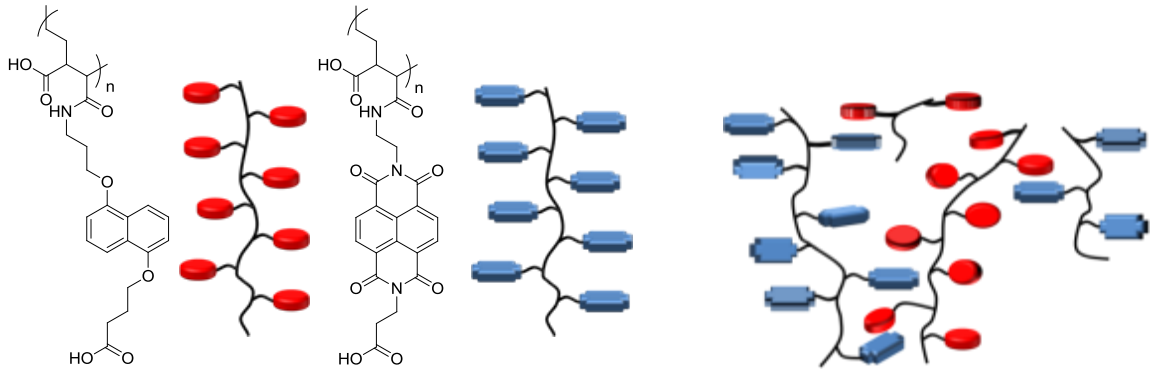

(a) **(b)**

Figure 1.17 (a) Structures of DAN and NDI polymers. (b) The proposed stacking of DAN and NDI polymers.

The proportional increase in binding affinity between DAN and NDI oligomers inspired the investigation of DAN and NDI polymer association. The premise was that water soluble polymers that contain many DAN or NDI units would yield excellent intermolecular association. Joe Reczek synthesized slightly water soluble (under basic conditions) DAN and NDI polymers by functionalizing poly(ethylene-*alt*-maleic anhydride) (Figure 1.17a) (28). A CT band was present in mixtures of DAN and NDI polymer mixtures indicating D–A association. Thin polymer films were analyzed by AFM and SEM. Surface features were as follows: the NDI polymer showed a smooth surface, the DAN polymer showed small miscelle-like objects, and the combination of DAN and NDI polymers showed large macrostructures which was indicative of an interconnected polymer network.

The mixture of DAN and NDI polymers was also precipitated in an acidic solution through a small needle to form delicate fibers. The delicate nature of the fibers was attributed to an overall small percentage of DAN–NDI interactions within the polymer network as shown in Figure 1.17b. Independent DAN or NDI polymers did not form fibers on precipitation in an acidic solution. The DAN–NDI fiber is a fine example

of a molecular assembly driven by intermolecular interactions. It may also serve as an initial step towards the realization of separate macromolecules that can recognize and assemble with each other through aromatic D–A interactions in a manner previously accomplished only by non-covalent interactions such as hydrogen bonding.

1.3.3 Solid Phase DAN−NDI Interactions

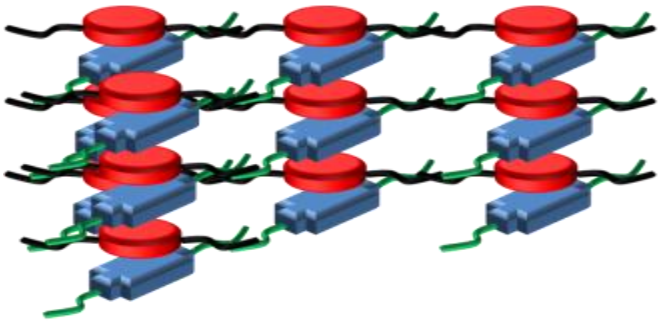

Figure 1.18 The assembly of DAN and NDI monomers in the liquid crystalline state.

Joe Reczek discovered that 1:1 mixtures of DAN and NDI monomers can form liquid crystals (29). DAN and NDI monomers were synthesized using a series of different alkyl groups. The 1:1 mixtures of these monomers displayed liquid crystalline properties with phase transition temperatures that correlated in a relative way to the melting points of the individual monomers. The liquid crystalline state of these mixtures exhibited a strong CT band and characteristic red color of DAN–NDI association. Interestingly, some mixtures lost their red color upon crystallization and experimental evidence suggested that these mixtures separated into discrete DAN and NDI domains. The DAN and NDI monomers stacked in columns composed of alternating D–A units (Figure 1.18), a model corroborated by UV-vis spectroscopy as well as single-crystal and

variable temperature powder X-ray diffraction studies. The DAN–NDI system not only offered a high level of phase tunability, it demonstrated face-centered DAN–NDI association in the absence of solvophobic effects. Furthermore, ordered assemblies driven together in the absence of solvent are of interest for solid and thin film material applications.

1.3.4 Additional Literature DAN−NDI Examples

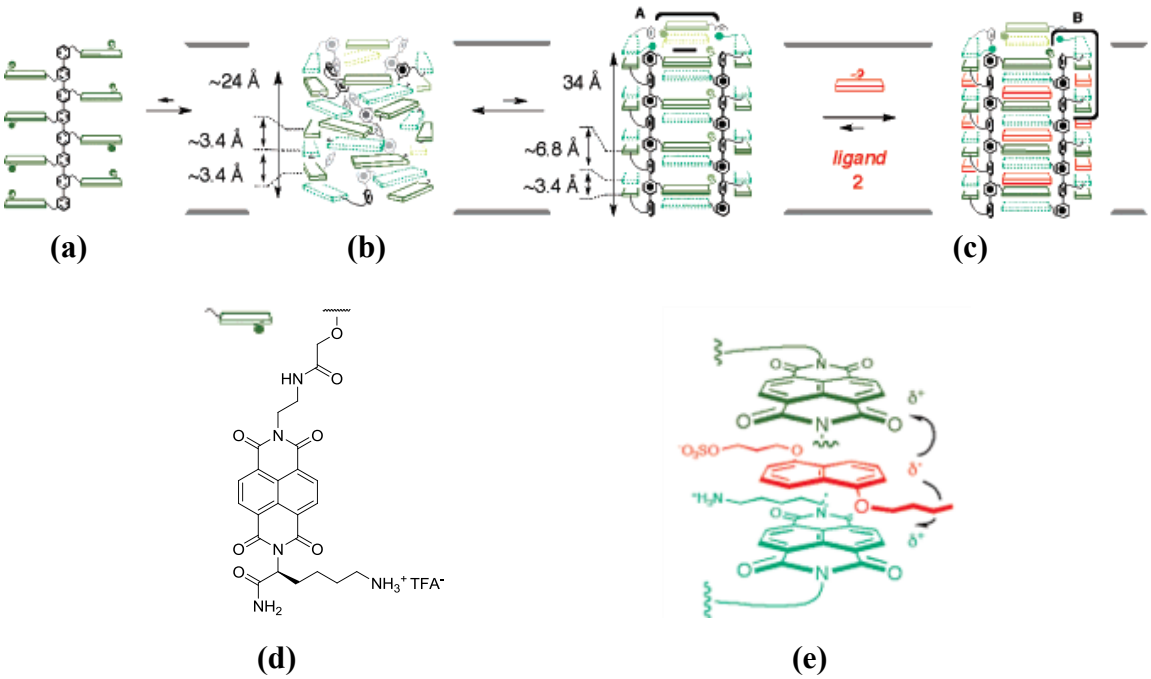

Figure 1.19 (a) Rigid-rod scaffold with eight NDI units (light green squares). (b) Twisted helix with closed channel. (c) Intercalation of DAN units (red squares) and reorganization into barrel structure with open channel. (d) Structure of NDI unit. (e) Molecular model of DAN–NDI stacking within barrel structure. Reprinted (adapted) with permission from (30). Copyright (2005) American Chemical Society.

Other groups have employed DAN–NDI interaction to drive the self-assembly of some truly novel supramolecular systems. Matile *et al*. used DAN–NDI association to template a synthetic ion channel (30). A rigid-rod scaffold was synthesized with a *p*-octiphenyl backbone and eight NDI units (Figure 1.19a, d). This scaffold adopted a twisted helix structure which lacked space for ions to pass through its internal cavity (Figure 1.19b). The addition of DAN monomers facilitated a conformational change into an open barrel structure that allowed the passage of ions (Figure 1.19c). A red solution was observed due to face-centered DAN–NDI association (Figure 1.19e). Experimental evidence and modeling supported that DAN–NDI interaction forced the rigid-rod scaffold to untwist into the barrel structure. The barrel structure provided enough space within its internal cavity to transport ions with some selectivity.

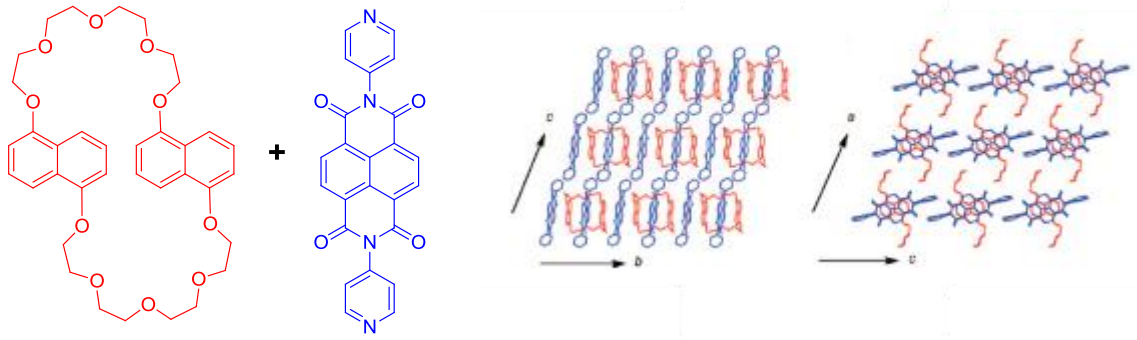

(a) **(b)**

Figure 1.20 (a) DAN and NDI components from the mechanical grinding investigation and (b) the X-ray crystal structure that shows a 2:1 complex. Reprinted (adapted) with permission from (31). Copyright (2009) American Chemical Society.

Liu *et al*. demonstrated that DAN–NDI association can be induced by solid state grinding (31). Solid DAN crown ethers and NDI derivatives were mechanically ground

together to selectively form a red solid composed of alternating D–A units (Figure 1.20a). The binary mixtures formed 1:2 complexes where one NDI unit threaded the DAN crown ether and another NDI unit associated alongside one of the DAN units in the crown ether (Figure 1.20b). All of the aromatic units were aligned in a face-centered fashion. Mechanical grinding yielded yet another way to induce DAN–NDI association and provided a fine example of host–guest chemistry in the solid state.

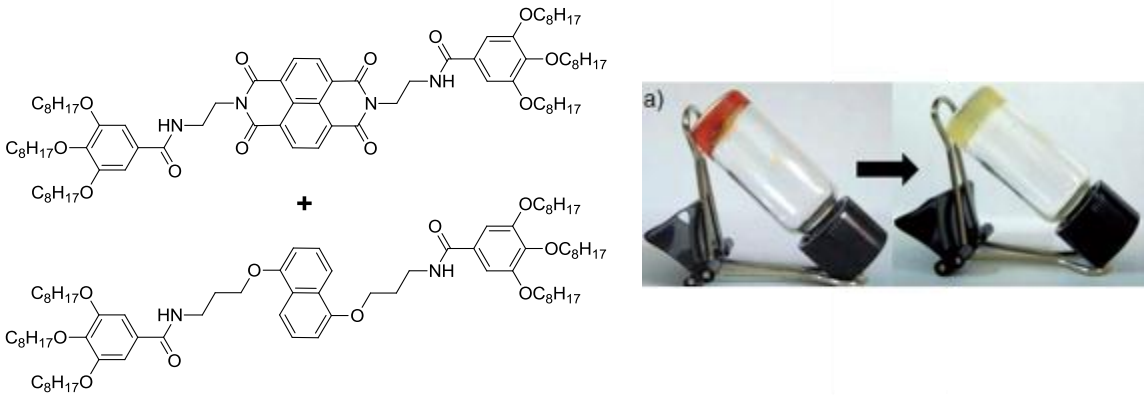

(a) **(b)**

Figure 1.21 (a) DAN and NDI monomers that form a gel through DAN–NDI association and (b) the gel transition upon standing at room temperature from a system of alternating DAN–NDI monomers (red color) to separate DAN and NDI components (loss of red color). Reprinted (adapted) with permission from (32). Copyright (2012) John Wiley and Sons.

Ghosh *et al*. investigated a series of *bis*-amide functionalized DAN and NDI monomers (32). These materials formed gels in non-polar solvents through hydrogen bonds and/or aromatic D–A interactions (Figure 1.21a). Gels composed of individual monomers were colorless while some gels composed of DAN–NDI monomer mixtures produced a red gel and CT complex (Figure 1.21b). The DAN–NDI assembly was strongly influenced by solvent polarity as well as the distance between the aromatic core and the amide functionality along the side chain (*i.e.* spacer length). DAN and NDI

monomers with different spacer lengths produced a gel composed of segregated DAN and NDI assemblies. The DAN–NDI mixtures only assembled into an alternating D–A arrangement when the spacer length was approximately equal on both monomers. Interestingly, these DAN and NDI monomers still segregated into discrete DAN and NDI assemblies upon standing in highly non-polar solvents (*e.g.* methylcyclohexane) (Figure 1.21b). This mode of aromatic chromophore self-sorting is relevant to many organic electronic applications.

1.4 CHEMISTRY AND SCOPE OF NDI

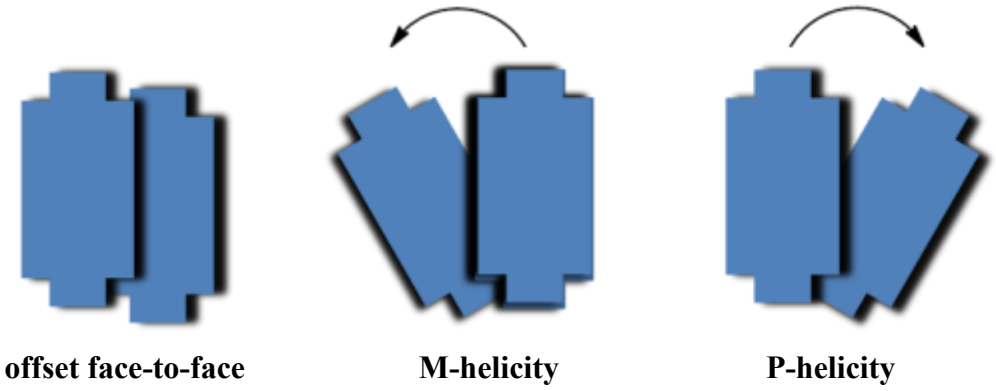

Figure 1.22 Observed modes of NDI–NDI association.

NDI is the focus of many applications in the areas of supramolecular and materials chemistry. The neutral and planar properties of NDI enable them to drive the self-assembly of numerous molecular systems. NDI units adopt an offset face-to-face or sometimes a helically stacked arrangement (Figure 1.22). NDI–NDI association most likely results from complementary local electrostatics between carbon and oxygen atoms on the imide functionalities of adjacent NDI molecules, as described by Houk and

Wheeler. NDI–NDI association is responsible for the self-assembly of numerous nanostructures that include nanotubes, helical nonofibers, twisted nanoribbons, and stacked nanosheets (Figure 1.23).

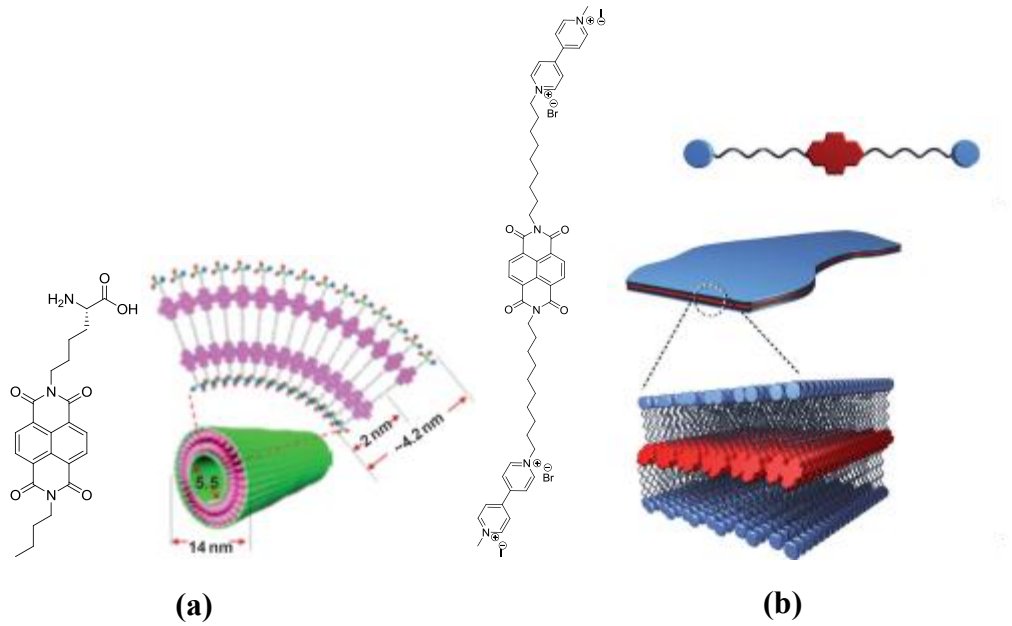

Figure 1.23 Two examples of self-assembled nanostructures driven by NDI–NDI association where NDI is represented by (a) light purple and (b) red. Figures (a) and (b) reprinted (adapted) with permission from (33) and (34). Copyright (2012) John Wiley and Sons.

The importance of NDI self-assembly is exemplified by the physical properties of NDI. Aromatic molecules with well-defined redox and spectroscopic properties are popular candidates for organic electronic applications. NDI possesses respectable electron mobility and can form stable radical anions. NDI generally exhibits a strong absorption (below 400 nm) and a weak emission (7 nm stokes shift). Along with their ability to self-assemble, the electronic properties of NDI have made them suitable components for photoinduced electron transfer and n-type semiconductor studies (35).

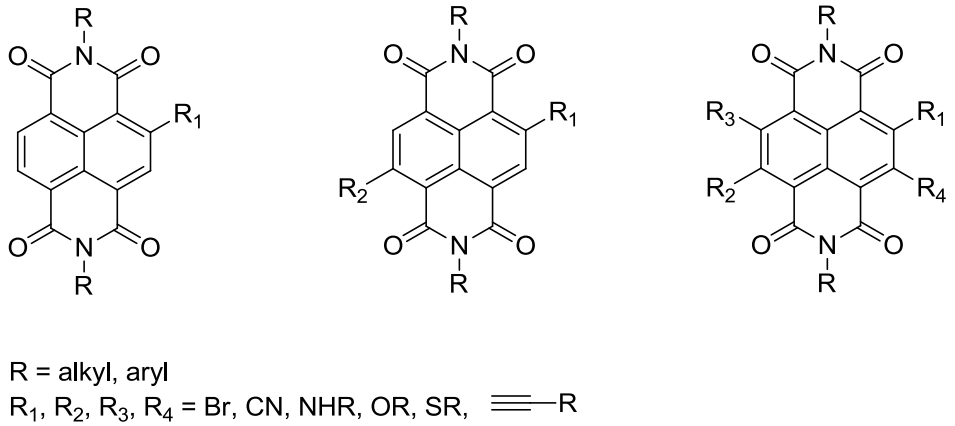

Figure 1.24 Common core functionalized NDI derivatives.

The most significant advancement of NDI chemistry has been the selective bromination of its aromatic core (36) and subsequent functionalization (Figure 1.24). The ability to fine-tune and obtain desired optical properties (*e.g.* absorbance, emission) by appending functional groups directly onto the NDI aromatic core has extended the reach of NDI chemistry into the area of organic solar cells (Chapter 4). Core functionalized NDI units also exhibit improved n-type character with enhanced electron mobility and spin coating properties which benefit organic thin film transistors. Several of these NDI molecules are shown in Figure 1.25. Continued fundamental and application-based research focuses on next generation materials that exploit these organizational, physical, and electronic properties of NDI (37).

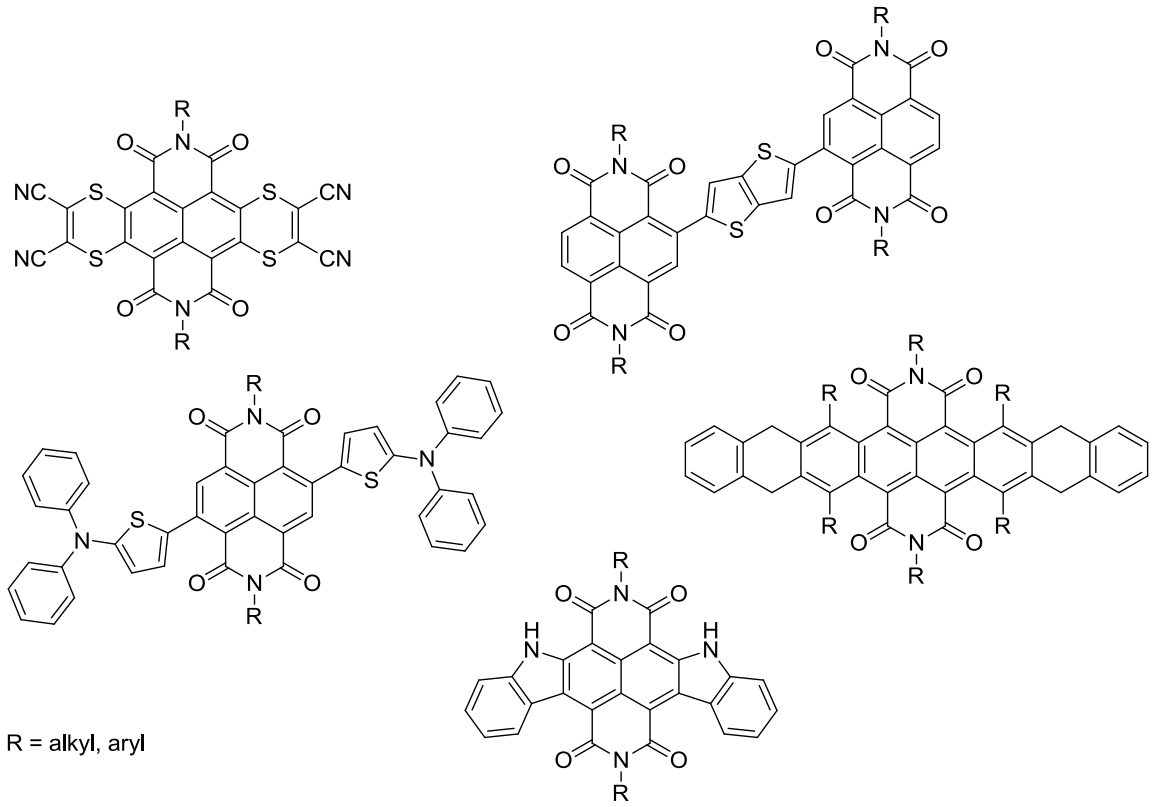

Figure 1.25 A few core functionalized NDI derivatives investigated for organic electronic device applications.

1.5 OVERVIEW OF AROMATIC DONOR AND ACCEPTOR PROJECTS

The Iverson group has predominately explored DAN–NDI and their aromatic D–A interactions in water. The focus of these D–A interactions did not shift from an aqueous environment until the discovery of DAN–NDI liquid crystalline phases. These solid-phase aromatic D–A interactions are promising modes of driven self-assembly for molecular architectures. Aromatic units have long been applied in areas such as organic electronic materials due to their inherent charge transport properties. NDI, though, has become a molecule of interest among the organic electronics community due its electron transporting properties and ability to self-assemble. Therefore a thorough understanding of NDI and DAN–NDI self-assembly should be of importance for the improvement and development of molecular architectures for organic electronic devices. The following dissertation chapters focus on NDI or its aromatic D–A complex with DAN.

Chapter 2

Thermochromic Aromatic Donor-Acceptor Materials

2.1 CHAPTER SUMMARY

2.1.1 Introduction

Chapter 1 describes general aromatic D–A interactions and how they can serve as a versatile tool for affecting 2D and 3D molecular architectures. Our group has employed the electrostatic complementarity of DAN and NDI to control molecular assembly in water and in the absence of solvent. Chapter 2 extends our DAN–NDI work in the absence of solvent. This chapter describes our investigation of the unusual thermochromic behavior that occurred in our previous study when several of the DAN:NDI mixtures lost their characteristic red color while crystallizing from the mesophase.

2.1.2 Goals

The goal of this chapter is to answer the question: *Are there structural features associated with certain DAN and NDI derivatives that account for the thermochromic behavior of their corresponding mixtures?* Knowledge of such parameters would not only allow us to predictably control mesophase transition temperatures of these systems, it would also allow us to control thermochromic behavior through careful component selection.

2.1.3 Approach

In order to investigate the origins of the thermochromic behavior, DAN and NDI side chains were systematically altered and their 1:1 mixtures studied. Ten different

DAN derivatives and five different NDI derivatives were prepared and all fifty of their possible 1:1 mixtures were examined. The individual derivatives and mixtures were analyzed by differential scanning calorimetry (DSC), UV-vis spectroscopy, polarized optical microscopy (POM), and X-ray crystallography to establish correlations between the thermochromic behavior of the mixtures and the structural properties of the DAN and NDI components.

2.1.4 Results

1:1 molar mixtures of DAN and NDI derivatives form highly tunable, columnar mesophases with a dark red color due to a charge transfer absorbance derived from alternating face-centered stacking. Most DAN:NDI mixtures undergo a dramatic color change from dark red to an almost colorless material upon crystallizing from the mesophase. Macroscopic morphology of the solid does not change during this process.

We previously speculated that the presence or absence of steric interactions due to side chain branching on the aromatic units controlled the level of color change associated with crystallization. Results from the present study further refine this conclusion including a key crystal structure that provides a structural rationale for the observed results (38).

2.2 BACKGROUND

The assembly of molecules in *solution* via stacking of electron-deficient (acceptor) and electron-rich (donor) aromatic units has proven to be a versatile tool for affecting 2D and 3D molecular architectures (20; 39; 40; 41; 42; 43; 24; 27; 23; 21; 44; 45; 46; 47; 48; 49; 11). The *solid-state* assembly of D–A complexes has also been

achieved through co-crystallization, grinding, and spin-coating techniques (50; 51; 52; 53; 16; 29). In addition, well-defined macromolecular assemblies have been constructed using either bulk blends of individual or covalently linked liquid crystalline donor-acceptor components (54; 55; 56; 57; 58; 59; 60; 61; 62; 63; 64). Liquid crystalline mixtures of donor-acceptor molecules offer a high degree of phase tunability relative to single component systems (56; 29; 65) and may possess enhanced and interesting opto-electronic properties (66; 67; 68; 69; 70; 71; 72; 73). A prominent example using aromatic donor and acceptor liquid crystals involves the assembly of linear charge-transfer (CT) channels (74; 75) while mesophase columns of segregated donor and acceptor molecules have been proposed as promising structures for organic photovoltaic applications (76; 77).

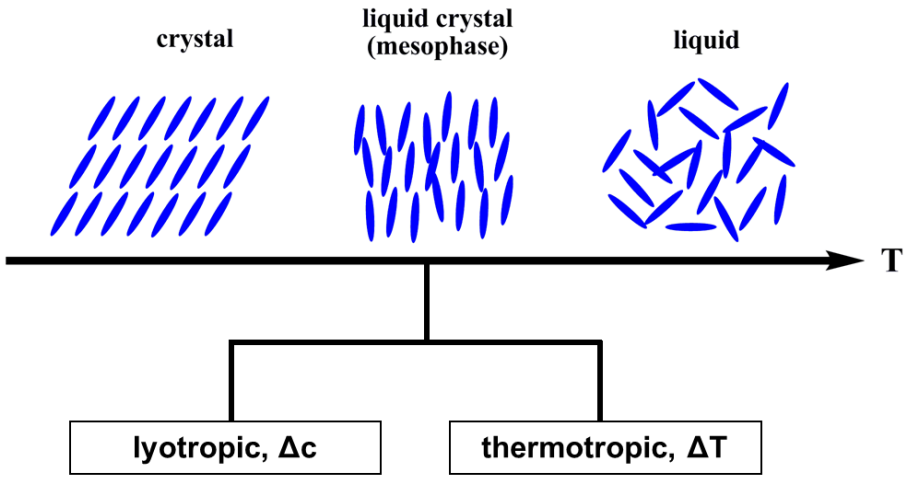

Figure 2.1 States of matter as temperature (T) increases.

The mesophase or liquid crystalline phase is the state of matter that lies between a crystalline solid and a liquid (Figure 2.1). The mesophase has both the order of a

crystalline solid and the disorder of an isotropic liquid. In fact, there are many types of mesophase such as nematic, smectic, and other soft crystalline states that describe a wide range of molecule alignment and bulk order. A mesophase is often induced by concentration effect (lyotropic) or by heat (thermotropic). The systems described in our studies are thermotropic liquid crystals. These materials undergo a phase transition upon heating that transforms them from a crystalline solid into a liquid crystalline state. Further heating results in another transition(s) that either transforms them into additional liquid crystalline phases or into the isotropic liquid state (78).

We have previously reported that 1:1 molar mixtures of appropriately derivatized electron-rich 1,5-dialkoxynapthalene (DAN) and electron-deficient 1,4,5,8-naphthalenetetracarboxylic diimide (NDI) units form mesophases over moderate temperature ranges (29). These mixtures exhibited dark red isotropic and mesomorphic phases, and often dark red crystalline phases as well. The dark red color was attributed to a DAN–NDI charge transfer absorbance due to the columnar face-centered stacks of alternating DAN and NDI units. The presence of alternating DAN–NDI stacks was further supported by polarized optical microscopy, UV-vis spectroscopy, and X-ray powder diffraction studies.

An interesting feature of the D–A stacks of DAN and NDI units is that attached side chains orient in orthogonal directions. Possibly for this reason, it proved possible to predict and thus fine-tune mesophase transition temperatures through side chain manipulation (29). In particular, the isotropic-mesophase transition correlated well with the NDI side chain identity, while the mesophase-crystalline phase transition temperature correlated well with the DAN side chain identity. One series of mixtures underwent an instantaneous and dramatic color change from dark red to an almost colorless off-white upon crystallization suggesting a loss of face-centered DAN–NDI stacking. X-ray

powder diffraction studies indicated that the DAN and NDI components in this series separated into individual microdomains during the crystallization process. Herein is reported a series of systematic studies that further explore this interesting thermochromic behavior of DAN–NDI materials.

2.3 RESULTS

2.3.1 Component Synthesis and Design

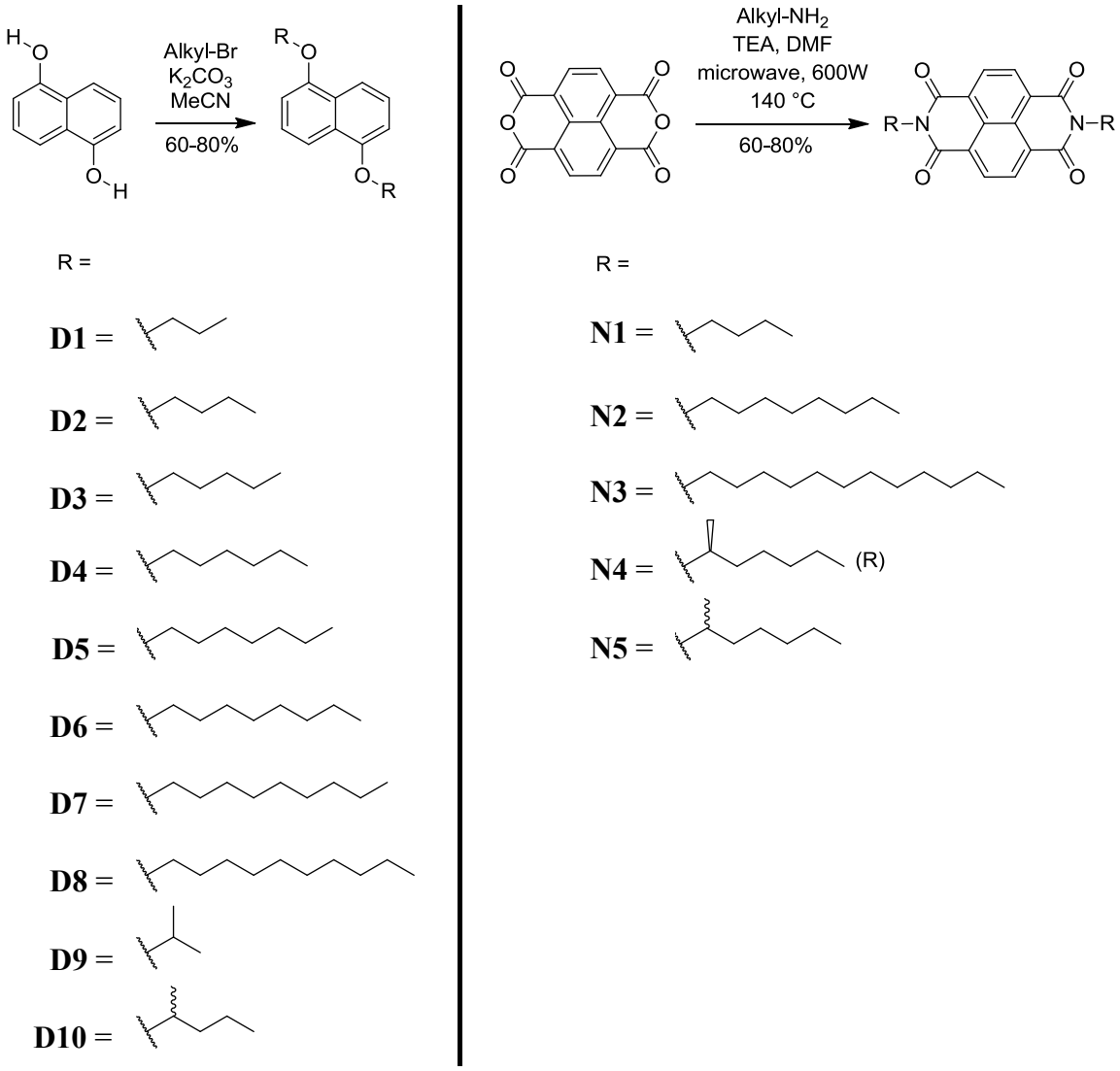

Scheme 2.1 DAN and NDI derivatives used in this study.

DAN and NDI derivatives were synthesized as described previously (29) with slight modification (79) (Scheme 2.1). Because our previous study revealed that the mesophase–crystallization phase transition temperature correlated with the DAN side

chain identity, a series of DAN units with increasing alkyl chain lengths (**D1**–**D8**) were created to investigate systematically the effects of side chain length on the mesophase–crystalline phase transition behavior of the DAN:NDI mixtures. DAN components with alkyl chains of one or two carbons evaporated readily during these experiments. Noting that the instantaneous color changes seemed characteristic of mixtures containing the diisopropyl DAN derivative in our previous study, branched alkyl chains were included (**D9**, **D10**) to study possible steric interactions. NDI derivatives **N1**–**N5** were selected as representative NDI units possessing three different alkyl chain lengths as well as branching.

2.3.2 Component Characterization

derivative	T_c °C (ΔH KJ mol^{-1})		
D1	97 (–20)		
D2	95 (–25)	⟶	78 (–24)
D3	70 (–44)		
D4	81 (–61)		
D5	64 (–47)		
D6	76 (–71)		
D7	59 (–39)		
D8	81 (–87)		
D9	98 (–36)		
D10	24 (–22)		
N1	226 (–23)	⟶	160 (–3)
N2	181 (–32)		
N3	160 (–27)	⟶	145 (–8)
N4	156 (–23)		
N5	117 (–24)		

Table 2.1 Temperatures (T_c) and associated enthalpies of crystallization (ΔH) obtained by DSC upon cooling at 5 °C/min.

The individual components were analyzed by differential scanning calorimetry (DSC) to quantify transition temperatures as well as crystallization characteristics. DSC data for the components was collected on cooling after the second heating cycle at a rate of 5 °C/min. Component phase transition temperatures and associated enthalpies of crystallization are listed in Table 1.1. The crystallization temperatures of the linear components generally decreased in an odd-even fashion (**D1**>**D3**>**D5**>**D7** and **D2**>**D4**, **D8**>**D6**) and higher magnitude transition enthalpies were usually observed with the longer alkyl chain derivatives.

The data in Figure 2.2a–c reveal that DAN units with alkyl substituents containing 4 or fewer carbons (**D1**, **D2** and **D9**) resulted in crystallization heat flows (peak intensities) that were 2-3 times larger than the other DAN derivatives that had more broad exotherms. **N1** and **N2** also produced narrow, intense exotherms compared to the other NDI components (Figure 2.2d). Branched or racemic alkyl chains resulted in lower crystallization points and broader transitions. The broad crystallization peaks of **D10** and **N5**, Figure 2.2c–d, occurred at the lowest temperatures and were among the least energetic (in terms of ΔH) derivatives of this investigation. **D2**, **N1** and **N3** underwent two transitions, the origin of which is unclear at this time but this behavior has previously been observed with long chain NDI derivatives (29). Significant supercooling effects were observed for those derivatives with intense crystallization exotherms, particularly **D1**, **D2**, and **D9** (Figure 2.2e).

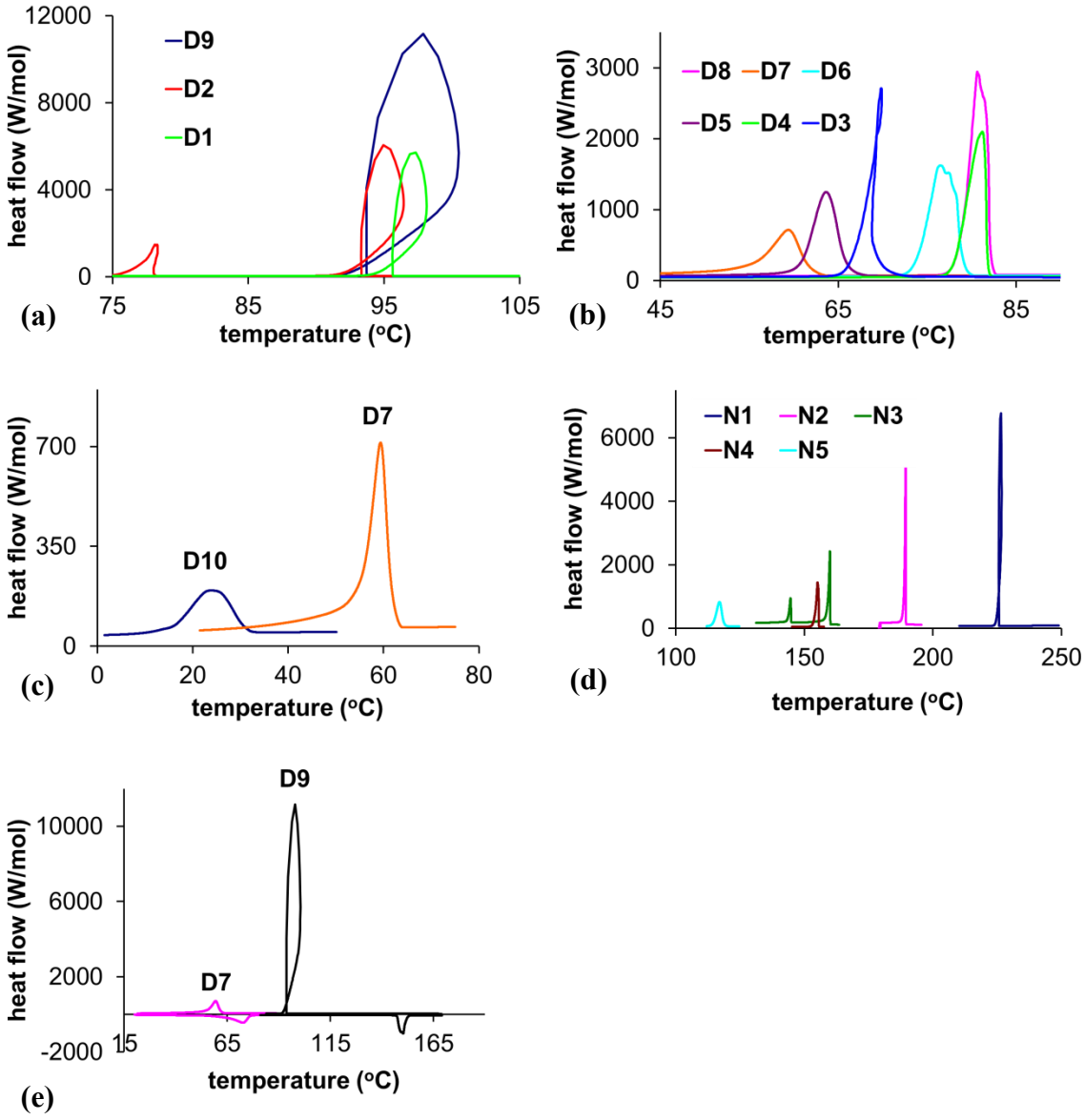

Figure 2.2 DSC traces upon cooling at 5 °C/min for all DAN and NDI derivatives. (a) **D1**, **D2**, and **D9** traces. (b) **D3**–**D8** traces. (c) **D10** with the **D7** trace for comparison. (d) NDI traces (**N1**'s additional crystalline phase modification was omitted for clarity). (e) **D9** heating and cooling cycles at 5 °C/min exhibited a significant supercooling effect, whereas **D7** showed little supercooling.

2.3.3 X-ray Crystallography

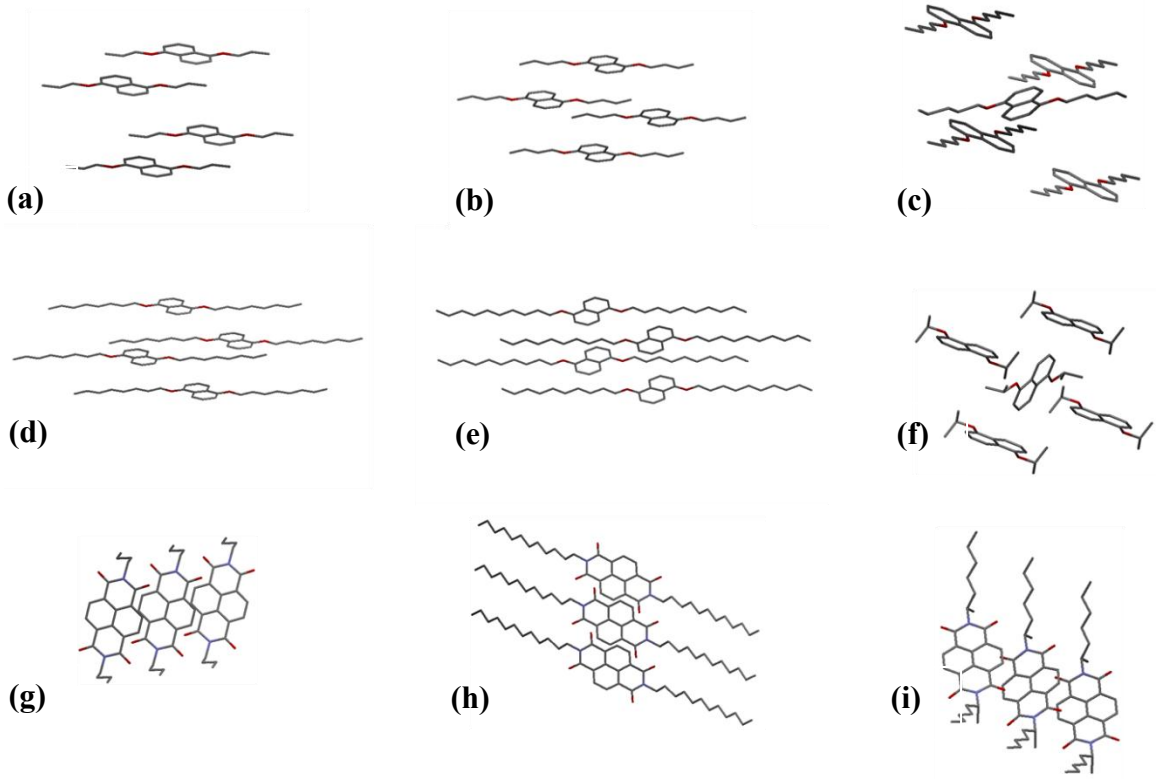

Figure 2.3 X-ray single-crystal structure of (a) **D1**, (b) **D2**, (c) **D3**, (d) **D6**, (e) **D8**, (f) **D9**, (g) **N1**, (h) **N3**, and (i) **N4**.

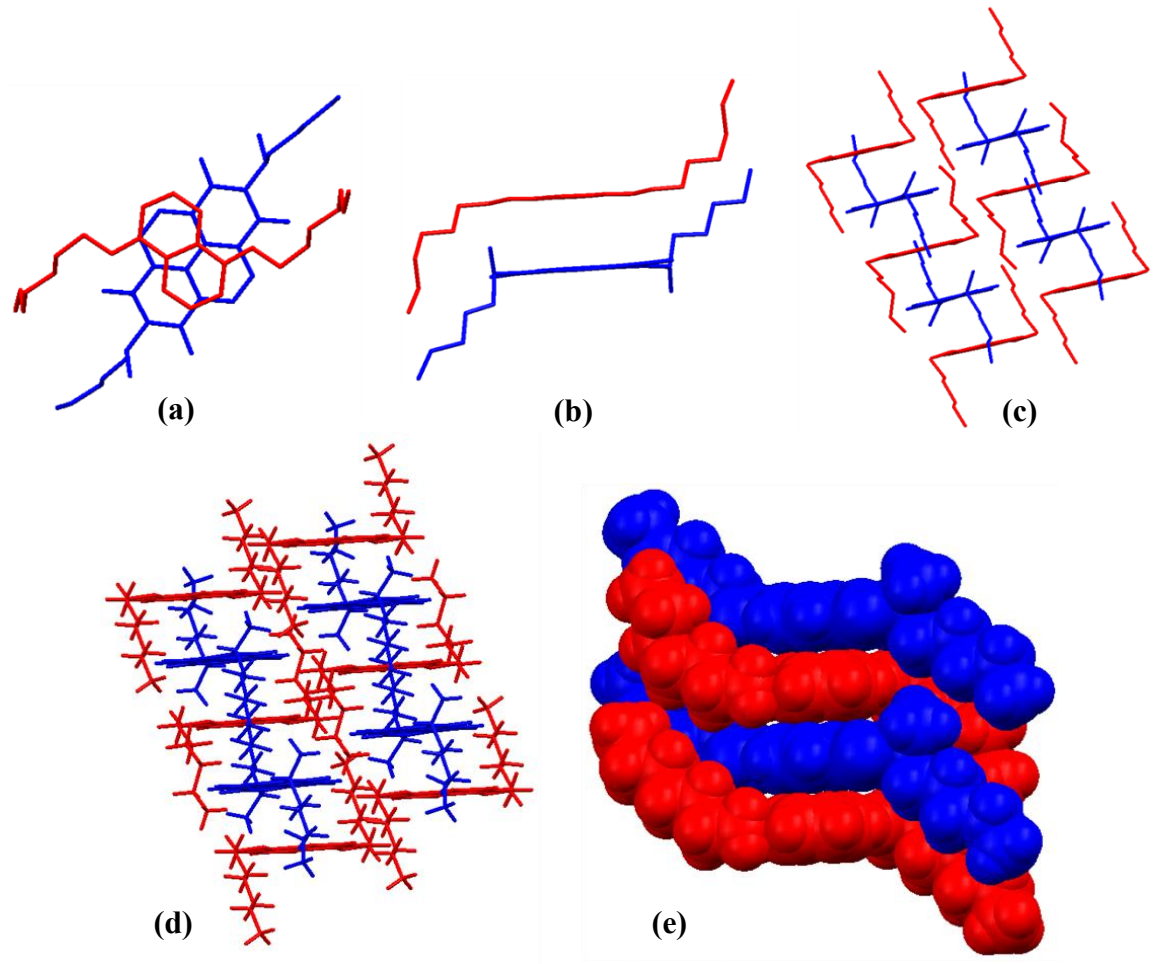

Figure 2.4 X-ray single-crystal structure of cocrystal **D5**:**N4**. Structures (a–c) are presented without hydrogen atoms for clarity. (d) Packing with the hydrogen atoms. (e) Space-filled structures with hydrogen atoms.

Single crystal data were obtained for homo-crystals of several DAN units to look for a correlation between crystal structure and the other properties examined in this study. In all cases, the DAN units packed in a herringbone (Figure 2.3c or 2.3f) or a completely offset planar fashion (Figure 2.3a–b and d–e). Structures of several NDI derivatives were also determined and were found to stack in an offset face-to-face fashion as shown in Figure 2.2g–i. A cocrystal of **D5**:**N4** (Figure 2.4) shows the aromatic donor-acceptor stacking mode that leads to the characteristic dark red color of these crystalline materials.

2.3.4 Mixtures

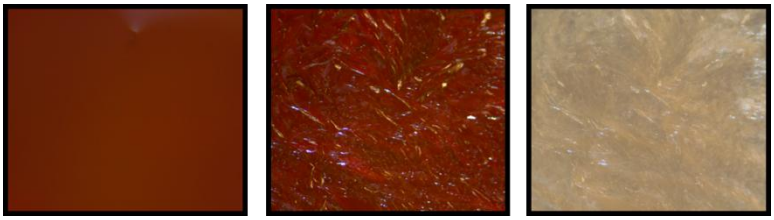

(a) **(b)** **(c)**

Figure 2.5 Thermochromic behavior taken under 5X magnification for **D8**:**N3** on cooling: (a) 145, (b) 110, and (c) 60 °C.

Mesophases were prepared by melting together 1:1 molar mixtures of solid DAN and NDI derivatives in the absence of solvent. All 50 combinations of **D1**–**D10** and **N1**–**5** were investigated. The lower melting point component (generally the DAN residue) melted first, thereby dissolving the higher melting point component. A liquid crystalline phase persisted until a completely isotropic mixture formed. As expected based on our previous results (29), the mixture clearing temperature corresponded reasonably well with the crystallization temperature of the NDI derivative and the mixture crystallization temperature corresponded reasonably well with the crystallization temperature of the DAN component upon cooling. In all cases, the liquid crystalline and isotropic phases exhibited a deep red color that is characteristic of the DAN–NDI charge transfer (CT) band, indicating face-centered stacks with alternating DAN–NDI units. Upon crystallization, the mixtures either remained dark red or lost their dark red color, indicating the preservation or loss of alternating DAN–NDI stacks (Figure 2.5). Mixtures containing N5 did not appear to produce a liquid crystalline phase.

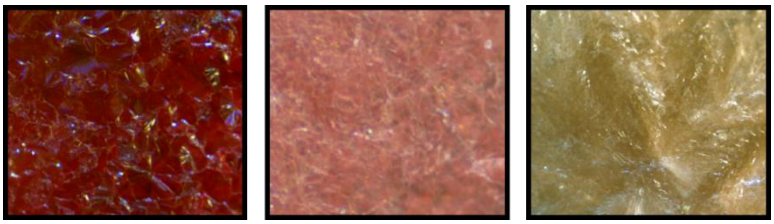

(a) **(b)** **(c)**

Figure 2.6 Representative colors for bulk crystalline phases taken under 5X magnification: (a) **D9**:**N5**, (b) **D4**:**N2**, and (c) **D7**:**N3**.

Representative examples of crystalline colors are shown in Figure 2.6. **D1**–**D8**:**N4** and **D1**–**D9**:**N5** retained a dark red (Figure 2.6a) color upon crystallization. Some mixtures such as **D4**–**8**:**N2** appeared to exhibit a light pink crystalline color (Figure 2.6b) while all other mixtures completely lost their red intensity (Figure 2.6c) within a few minutes of cooling to the crystallization temperature.

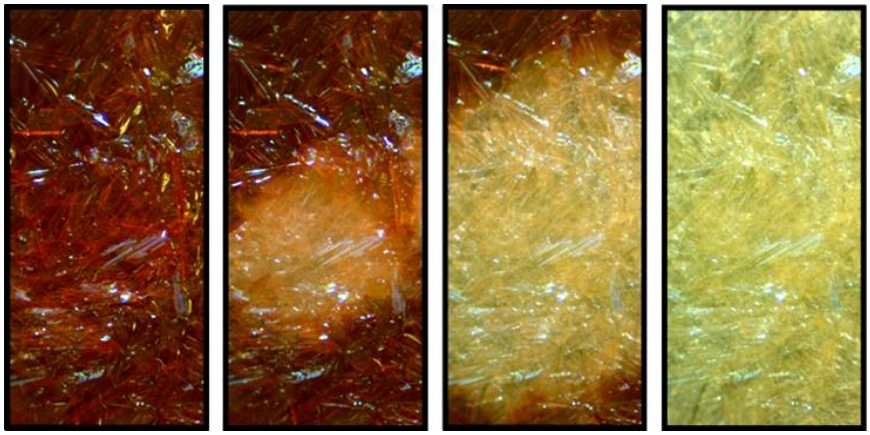

Figure 2.7 Deep red mesophase to off-white crystalline phase color change (5X magnification) that occurred over approximately 20 s of cooling for the **D8**:**N1** mixture.

A representative color change process is depicted in Figure 2.7 with a sample of **D8**:**N1**. The color change began in the center of the sample as it was located over the

center of the heating stage (an area that cools first), then radiated outward with time until the entire sample was no longer red. This transition took about twenty seconds to complete. Importantly, the *macroscopic morphology, i.e. surface features, of the solid did not change during this process*, indicating reorganization at the microdomain level consistent with our previous observations (29).

2.3.5 UV-vis Spectroscopy

Thin crystalline films were examined using UV-vis spectroscopy to monitor the presence of the CT band by melting equimolar DAN:NDI mixtures between two glass slides. Interestingly, placing the mixtures between the glass slides slowed the rate of color change upon crystallization compared to samples without a top cover. Therefore, in order to insure completion of the phase transition, UV-vis spectra were collected after the mixtures cooled for at least 5 minutes following attainment of the crystallization temperature (29). Mixtures containing **D10** had to be placed at 20 °C for ten minutes to ensure complete crystallization. Representative UV-vis spectra are shown in Figure 2.8. A UV-vis spectrum for each crystalline DAN:NDI mixture is located in Figure 2.15. The thermochromic behavior was recorded as the retention or loss of the CT absorbance (Table 2.2). Those mixtures that maintained a deep red color upon crystallization (most mixtures with **N4** and **N5**) exhibited the expected strong CT absorbance in their crystalline state (Figure 2.8a). Mixtures that changed color from deep red to pink (**D4**–**D8**:**N2**) displayed a CT absorbance dramatically reduced in intensity and red shifted (Figure 2.9). The CT absorbance of the pink samples can be better visualized upon subtraction of the **D9**:**N2** spectrum, which cancels some of the background scattering (Figure 2.10). The extremely small, red shifted absorption profile is consistent with a

crystalline state in which an incomplete separation of the alternating D–A molecules has taken place, leading to the faint pink color.

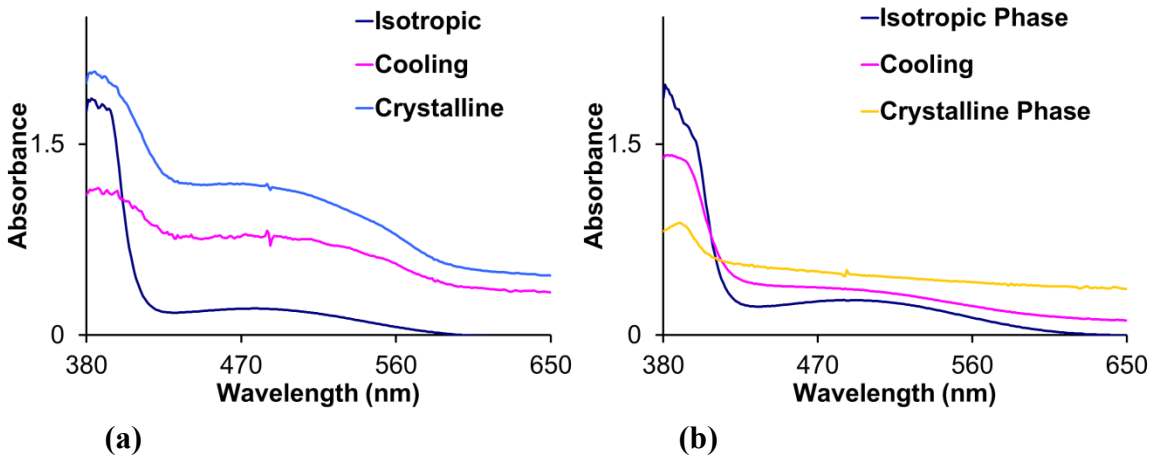

Figure 2.8 Representative UV-vis spectra on cooling for (a) **D7**:**N4** (retention of CT) and (b) **D7**:**N3** (loss of CT).

	N1	**N2**	**N3**	**N4**	**N5**
D1	–	L	L	R	R
D2	–	L	L	R	R
D3	–	L	L	R	R
D4	–	P	L	R	R
D5	L	P	L	R	R
D6	L	P	L	R	R
D7	L	P	L	R	R
D8	L	P	L	R	R
D9	–	–	L	L	R
D10	–	–	L	L	L

Table 2.2 The thermochromic behavior is reported as the retention (R), change to pink (P), or loss (L) with respect to the observed deep red color of the mesophase upon crystallization. Dashes indicate component evaporation.

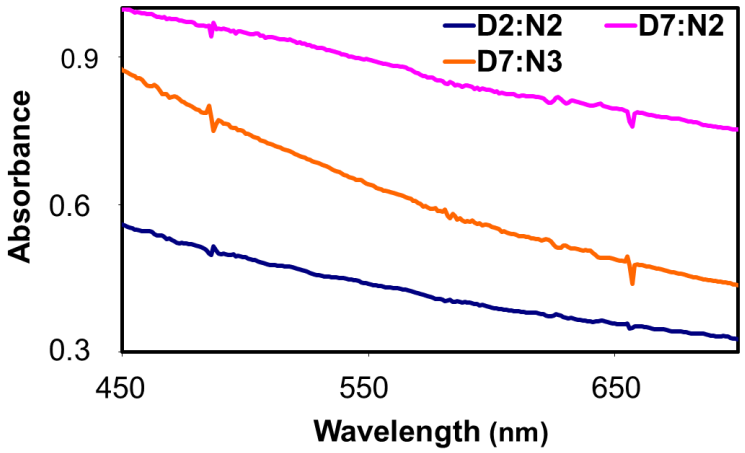

Figure 2.9 Expanded CT region and slight absorption for crystalline **D7**:**N2** (pink). **D2**:**N2** (loss of red color) and **D7**:**N3** (loss of red color) are shown for comparison.

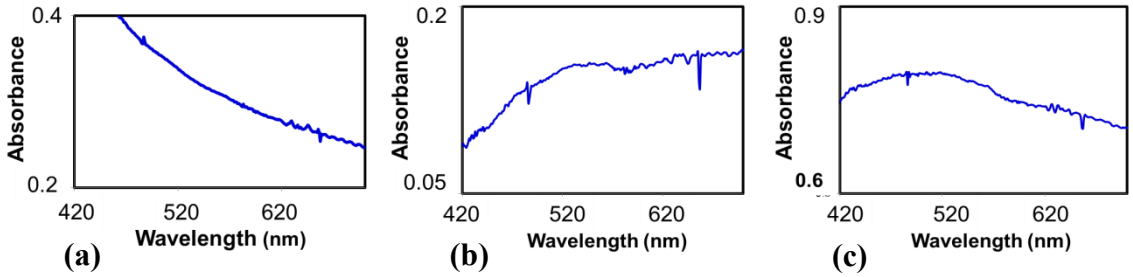

Figure 2.10 UV–vis spectra of the CT region for representative mixtures in the **N2** series with **D9**:**N2** subtraction correction: (a) **D9**:**N2**, no CT band; (b) **D8**:**N2**, slight CT absorption; (c) **D7**:**N2**, slight CT absorption.

2.3.6 Differential Scanning Calorimetry

The phase transitions of the mixtures were characterized using DSC. Phase transition temperatures and energies measured at a cooling rate of 2 °C/min for the mixtures of **D1**–**10** with **N1**–**N5** are given in Tables 2.3–7. All mixtures measured, except those that contained **N5**, produced at least two transition temperatures that indicated mesophase formation. **D10**:**N5** was extremely slow to crystallize and transition temperatures were not obtained for this mixture by DSC.

derivative		T_{c1}	→	T_{c2}	→	T_{c3}	
D1:**N1**				**D1** evaporated			
D2:**N1**				**D2** evaporated			
D3:**N1**				**D3** evaporated			
D4:**N1**				**D4** evaporated			
D5:**N1**	iso	188 [–13]	→	72 [–31]	→	55 [–87]	cr
D6:**N1**	iso	182 [–4]		71[a] [–82]			cr
D7:**N1**	iso	176 [–13]	→	71 [–19]	→	53 [–43]	cr
D8:**N1**	iso	182 [–8]		74[a] [–93]			cr
D9:**N1**				**D9** evaporated			
D10:**N1**				**D10** evaporated			

Table 2.3 Temperatures (°C) and enthalpies (KJ/mol) in brackets for phase transitions determined by DSC upon cooling 2 °C/min. T_c is a transition upon cooling; iso = isotropic and cr = final crystalline state. [a]Transition is composed of multiple peaks.

derivative		T_{c1}	→	T_{c2}	→	T_{c3}	
D1:**N2**				**D1** evaporated			
D2:**N2**	iso	137 [–10]	→	86 [–28]	→	81[a] [–22]	cr
D3:**N2**	iso	139 [–8]	→	64 [–47]			cr
D4:**N2**	iso	148 [–7]	→	78 [–63]			cr
D5:**N2**	iso	138 [–9]	→	60 [–55]			cr
D6:**N2**	iso	140 [–8]	→	76 [–74]			cr
D7:**N2**	iso	146 [–7]	→	68 [–68]			cr
D8:**N2**	iso	141 [–86]	→	78 [–92]			cr
D9:**N2**				**D9** evaporated			
D10:**N2**	iso	144 [–10]	→	41 [–0.6]			cr

Table 2.4 Temperatures (°C) and enthalpies (KJ/mol) in brackets for phase transitions determined by DSC upon cooling 2 °C/min. T_c is a transition upon cooling; iso = isotropic and cr = final crystalline state. (a) Transition is composed of multiple peaks.

derivative		T_{c1}		T_{c2}		T_{c3}	
D1:**N3**	iso	132 [–7]	→	86 [–22]			cr
D2:**N3**	iso	134 [–7]	→	85 [–25]	→	73 [–15]	cr
D3:**N3**	iso	129 [–11]	→	66 [–46]			cr
D4:**N3**	iso	131 [–10]	→	77 [–67]			cr
D5:**N3**	iso	123 [–21]	→	60 [–49]			cr
D6:**N3**	iso	123 [–21]	→	75 [–72]			cr
D7:**N3**	iso	129 [–14]	→	66 [–71]			cr
D8:**N3**	iso	133 [–17]	→	78 [–85]			cr
D9:**N3**	iso	125 [–7][a]	→	132[a] [–38]			cr
D10:**N3**	iso	131 [–17]	→	120 [–0.4]			cr

Table 2.5 Temperatures (°C) and enthalpies (KJ/mol) in brackets for phase transitions determined by DSC upon cooling 2 °C/min. T_c is a transition upon cooling; iso = isotropic and cr = final crystalline state. (a) Transition is composed of multiple peaks.

derivative		T_{c1}		T_{c2}		T_{c3}	
D1:**N4**				**D1** evaporated			
D2:**N4**	iso	116 [–4]	→	103 [–17]	→	83 [–9]	cr
D3:**N4**	iso	121 [–7]	→	99 [–18]	→	65 [–22]	cr
D4:**N4**	iso	129 [–5]	→	122 [–41]	→	72 [–5]	cr
D5:**N4**	iso	133 [–11]	→	124 [–35]			cr
D6:**N4**	iso	123[a] [–5]	→	121[a] [–40]			cr
D7:**N4**	iso	124 [–7]	→	112 [–35]			cr
D8:**N4**	iso	115 [–7]	→	99 [–20]	→	61 [–18]	cr
D9:**N4**	iso	115 [–10]	→	80 [–42]	→	76 [–49]	cr
D10:**N4**	iso	122 [–11]	→	20 [–15]			cr

Table 2.6 Temperatures (°C) and enthalpies (KJ/mol) in brackets for phase transitions determined by DSC upon cooling 2 °C/min. T_c is a transition upon cooling; iso = isotropic and cr = final crystalline state. (a) Transition is composed of multiple peaks.

derivative		T_{c1}	→	T_{c2}	→	T_{c3}	
D1:**N5**	iso	95 [–0.7]	→	84 [–5]			cr
D2:**N5**	iso	98 [–42]	→	89 [–3]	→	63 [–1]	cr
D3:**N5**	iso	95 [–37]	→	61 [–10]			cr
D4:**N5**	iso	111 [–52]	→	77 [–3]			cr
D5:**N5**	iso	110 [–54]	→	50 [–11]			cr
D6:**N5**	iso	110 [–59]	→	73 [–3]			cr
D7:**N5**	iso	106 [–58]	→	55 [–3]			cr
D8:**N5**	iso	94 [–55]	→	74 [–16]			cr
D9:**N5**	iso	106 [–50]	→	81 [–3]			cr
D10:**N5**	iso	–	→	–			cr

Table 2.7 Temperatures (°C) and enthalpies (KJ/mol) in brackets for phase transitions determined by DSC upon cooling 2 °C/min. T_c is a transition upon cooling; iso = isotropic and cr = final crystalline state. Dashes indicate no observed exothermic transitions.

2.3.7 Polarized Optical Microscopy

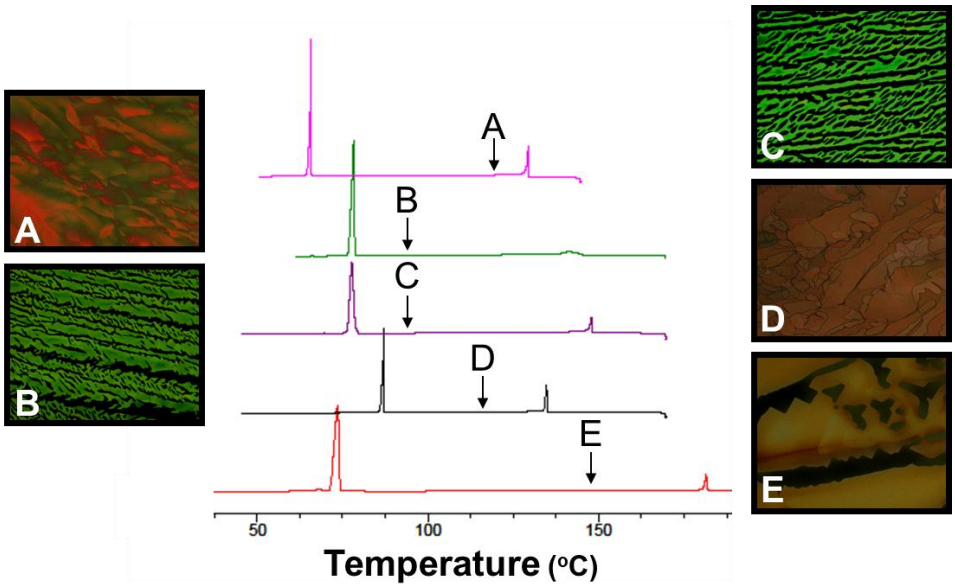

Figure 2.11 Optical textures and associated DSC traces for representative 1:1 mixtures at 10X magnification. Arrows indicate optical texture temperatures: (a) **D3**:**N3**, 118 °C; (b) **D8**:**N2**, 92 °C; (c) **D4**:**N2**, 90 °C; (d) **D1**:**N2**, 117 °C; (e) **D8**:**N1**, 147 °C.

Mesophase texture visualization and transition temperature confirmation were performed using polarized optical microscopy (POM). Samples were placed between glass cover slips and analyzed upon cooling from the isotropic phase at a rate of 5 °C/min. Textures (Figure 2.11) were consistent with those previously reported for DAN:NDI mixtures (29). The long sheet-like dendritic or mosaic patterns are characteristic of columnar mesophases (78).

2.3.8 Field-Effect Transistors

The charge transport properties of select DAN:NDI mixtures that either exhibited a color change upon crystallization (**D9**:**N4**) or remained red upon crystallization (**D7**:**N4**) were investigated by incorporating them as the active layer in an organic field-effect transistor (OFET). A general schematic of the bottom-contact OFET used in this study is illustrated in Figure 2.12. A two weight percent toluene solution of **D9**:**N4** or **D7**:**N4** was drop-casted onto the wafer and allowed to evaporate slowly until a film effectively covered the channel region between source/drain electrodes (Figure 2.13a and 2.13c). The wafer was then heated at 90 °C to remove residual solvent.

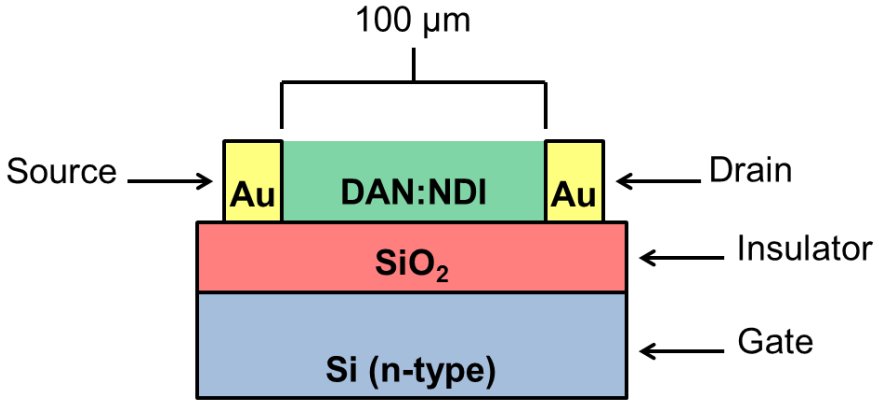

Figure 2.12 General schematic of the bottom-contact OFET device.

Measurements were taken at room temperature and at an elevated temperature within the liquid crystalline temperature range for each mixture. Device images show a macroscopic change to a more fluid mesophase at elevated temperatures (Figure 2.13b and 2.13d). Output and transfer characteristics for **D9:N4** and **D7:N4** in the mesophase and crystalline phase are shown in Figure 2.14.

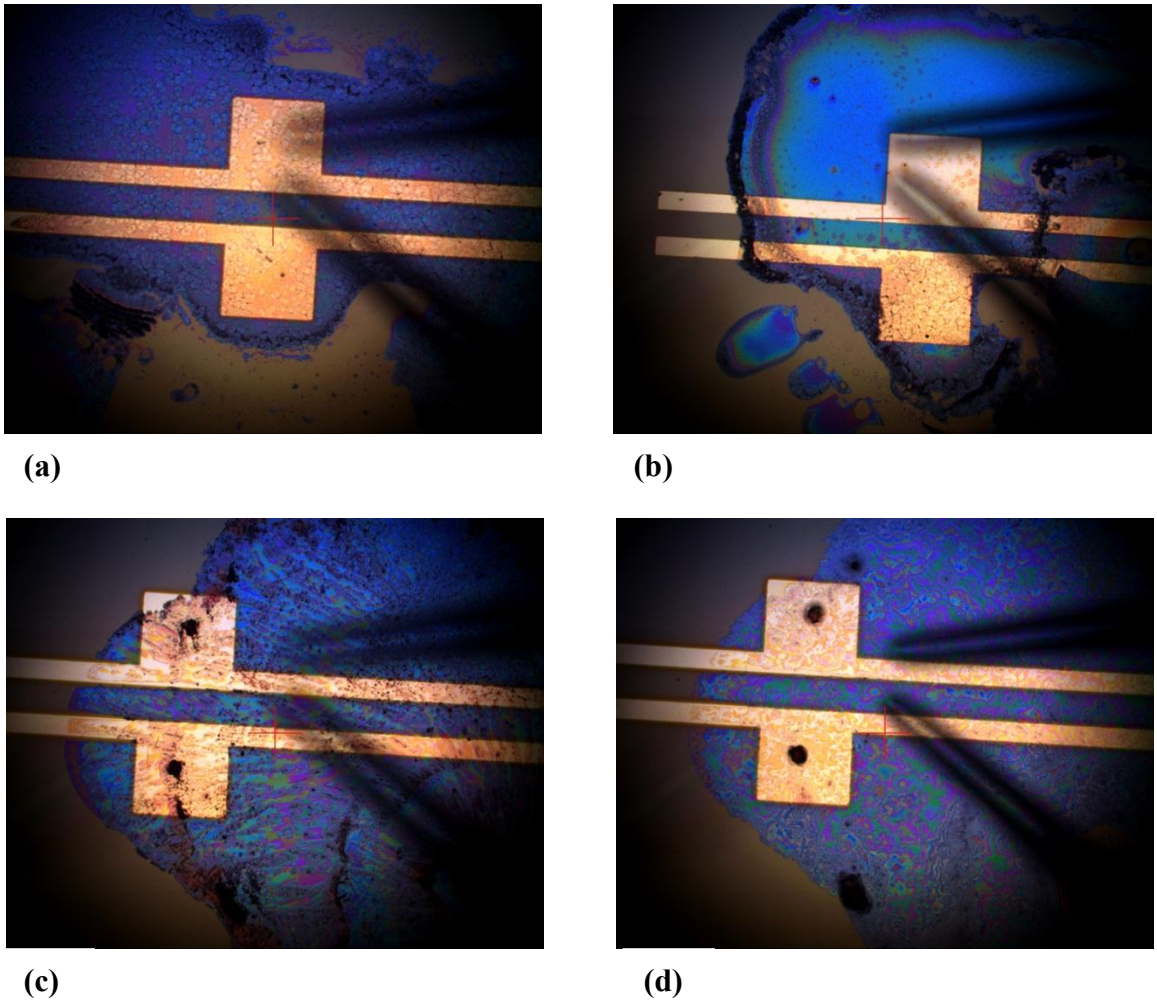

Figure 2.13 OFET devices images for (a) **D9**:**N4** at 25 °C; (b) **D9**:**N4** at 100 °C; (c) **D7**:**N4** at 25 °C; (d) **D7**:**N4** at 115 °C.

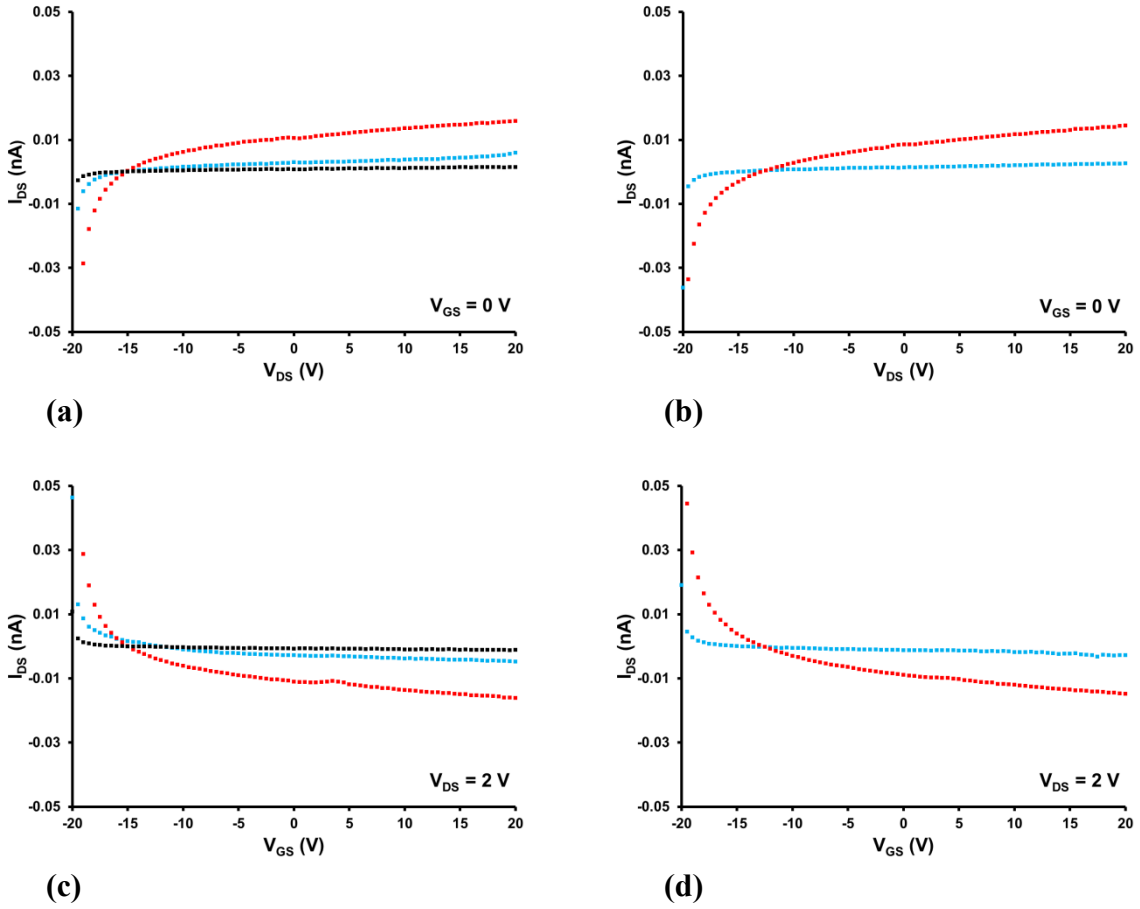

Figure 2.14 Output (a–b) and transfer (c–d) characteristics of OFET devices for (a) **D9**:**N4** at 25 °C (blue), **D7:N4** at 25 °C (red), blank electrode at 25 °C (black), (b) **D9**:**N4** at 100 °C (blue), **D7:N4** at 115 °C (red), (c) **D9**:**N4** at 25 °C (blue), **D7:N4** at 25 °C (red), blank electrode at 25 °C (black), (d) **D9**:**N4** at 100 °C (blue), **D7:N4** at 115 °C (red).

2.4 DISCUSSION

2.4.1 Individual Component Crystallization Behavior

The DSC traces of **D1**–**D10** (Table 2.1 and Figure 2.2) revealed that several DAN derivatives (**D1**, **D2** and **D9**) exhibited looping patterns upon crystallization. The peak intensities for these derivatives were among the largest seen in this study and their observed crystallization temperatures were several degrees lower than their melting temperatures. In other words, these samples behaved as supercooled liquids during the cooling cycle. Once nucleation occurred, crystals grew rapidly, leading to self-heating that was manifest in the observed looping traces (80; 81). Taken together, the relatively large heat flows and higher crystallization temperatures indicated that **D1**, **D2** and **D9** produced a highly crystalline material with a rapid growth process once nucleation had begun. Of the NDI derivatives examined, **N1** and **N2** had relatively large heat flows and showed some self-heating behavior, indicating that these also formed highly crystalline materials upon nucleation.

Those components with longer side-chains such as **D3**–**D8** and **N3** resulted in more gradual exotherms at lower temperatures that were less intense and exhibited negligible supercooling behavior. Presumably, the longer side-chains slowed down the organization process during crystallization. With the exception of the short-chain **D9** derivative, branching (**D10**, **N4**–**5**) lowered the exotherm intensity and crystallization temperature significantly. The racemic nature of the **D10** and **N5** (as compared to enantiomerically pure **N4**) analogues also complicated the crystallization process as they had the lowest crystallization temperatures and the least intense exotherms of any derivatives examined.

We initially sought to determine if there was a correlation between an individual component's crystallization behavior and the presence or absence of significant color

change of the 1:1 mixtures made from it. Overall, derivatives with relatively intense exothermic transitions like **D1**–**D3** and **N3** also exhibited the highest melting temperatures, an indication that these derivatives make particularly stable homo-crystals. Such stability would provide a possible thermodynamic driving force for phase separation during the mesophase to crystal transition of mixtures. However, high melting temperature is not the only important parameter for unstacking during mixture crystallization as all derivatives with linear side chains produced mixtures that unstacked, regardless of the individual component crystallization properties.

2.4.2 Individual Component Structure

Structures of several representative DAN and NDI units were obtained to compare crystalline structures to measured properties such as the DSC traces. In all of the DAN X-ray structures, the aromatic core units stacked in a planar offset or herringbone manner, never in an arrangement involving any parallel aromatic stacking. On the other hand, all NDI structures obtained in this study contained an offset face-to-face aromatic stacking mode. For the DAN component structures obtained, no obvious correlation between the modes of aromatic stacking, *i.e.* herringbone vs. planar offset, and the DSC traces of the DAN components was seen. For example, **D1** and **D3** exhibited very similar DSC traces with moderate heat flow and some looping behavior, but **D1** crystallized in a planar offset mode, while **D3** crystallized in a herringbone arrangement (Figure 2.3). Similarly, although individual NDI derivatives exhibited different DSC traces, all of their crystals showed similar packing. To a first approximation, then, it appears appropriate to attribute the DSC behavior to side-chain

packing interactions rather than the aromatic stacking mode of the DAN or NDI derivatives.

2.4.3 Mesophase Behavior of Mixtures

DSC studies of most mixtures exhibited at least two transitions, consistent with mesophase formation (Tables 2.3–7). Optical textures obtained through POM supported the formation of columnar mesophases (Figure 2.12). The only mixtures that did not appear to form a true mesophase were those with **N5**, possibly a manifestation of its racemic nature. The DSC data for the various mixtures was consistent with the previously reported trend that major transition temperatures correlated in a *relative way* to the transition temperatures of the components. For example, **D4**:**N2** crystallized at 78 ºC (**D4** = 81 °C) and **D6**:**N2** crystallized at 76 ºC (**D6** = 76 °C). Clearing point temperatures occurred around 180 ºC with **N1** (**N1** = 226 °C), 140 °C with **N2** (**N2** = 181 °C) and 130 °C with **N3** (**N3** = 160 °C). A likely explanation for these correlations is that the DAN and NDI side chains are positioned orthogonal to each other in the face-centered DAN–NDI stack, so they behave independently of each other, consistent with their behavior in pure form. This observation is consistent with our previous report (29) as well as the X-ray crystallography results reported here, and supports the hypothesis that side-chain interactions dominate phase transition behavior.

2.4.4 Thermochromic Behavior of Mixtures

The present study was intended to investigate the thermochromic behavior of DAN:NDI mixtures in a systematic fashion. Here, only **D1**–**8**:**N4** and **D1**–**9**:**N5** remained dark red upon crystallization, while all other mixtures examined lost their red mesophase

color. There are at least two explanations for the observed thermochromic behavior. In one scenario, separation into DAN and NDI microdomains occurs during the crystallization process (29). Alternatively, the aromatic units could rearrange to give an overall altered but homogeneous packing in which the alternating aromatic stacking is diminished, such as in a herringbone arrangement or some other offset packing. Our previous results using X-ray powder diffraction studies verified that in the case of **D9**:**N4** the observed thermochromicism was the result of separation into DAN and NDI microdomins upon crystallization (29). Unexpectedly, several crystalline mixtures, especially those involving **N2**, exhibited a light pink color (Figure 2.6 and Table 2.2). The light pink color of these mixtures (for example **D7**:**N2**) could result from incomplete separation into microdomains or, in the second scenario, a novel packing mode with a modified or diminished CT absorbance (Figure 2.9 and Figure 2.10).

It is worth noting that the color change associated with mixtures containing **D9** occurred more rapidly that with the other DAN derivatives with linear side chains, happening almost instantaneously versus a few seconds for the straight-chain derivatives. The rapid color change associated with **D9** in this study is consistent with our previous observations (29). A reasonable explanation for this behavior is that the steric strain resulting from the isopropyl side chain of **D9** in close proximity to the NDI aromatic core increases the rate of component separation during crystallization.

2.4.5 Cocrystal Structure

The crystallographic structure obtained for the deep red **D5**:**N4** mixture showed face-centered stacks of alternating DAN:NDI units (Figure 2.4a–e). The component side chains are positioned in an orthogonal fashion as expected (29). The branched NDI side

chains are oriented above and below the NDI plane and, importantly, appear to surround the DAN units while in the alternating stacks (Figure 2.4d–e). Close inspection reveals that indeed the **N4** branch methyl group is likely to serve as a steric barrier to unstacking, perhaps "locking in" the alternating aromatic stack enough for it to persist in the crystalline state.

2.4.6 Charge Transport Properties

Samples of **D9:N4** and **D7:N4** both lacked the typical characteristics of a semiconductor. I_{DS}–V_{DS} (Figure 2.14a–b) and I_{DS}–V_{GS} (Figure 2.14c–d) were relatively linear throughout the sweep widths. A scan of a blank electrode was included with those of the crystalline mixtures at room temperature and there was little difference between them (Figure 2.14a and 2.14c). In addition, there was little change in terms of charge transport properties when the crystalline mixtures were heated into the mesophase (Figure 2.14b and 2.14d).

Charge transport properties are often dependent on molecular orientation. Future studies should consider functionalizing the SiO_2 surface with various alkyl-silanes to aid/alter molecular orientation along the SiO_2–semiconductor interface. The current study was also conducted in air which is generally suitable for p-type organic semiconductors. But n-type organic semiconductors often require an inert atmosphere as anion charge carriers are vulnerable to moisture and oxygen. Therefore, if possible, these samples should be analyzed with a semiconductor characterization instrument that operates under an inert atmosphere with variable temperature control.

2.5 CONCLUSION

A more complete understanding of intermolecular DAN–NDI interactions in different phases has emerged from the present work. In particular, complementary electrostatic interactions between the aromatic cores apparently dominate the DAN–NDI packing arrangement when some or all of the side chains are mobile, verified by the characteristic red color due to alternating face-to-face stacking in the isotropic and mesophases with all mixtures. During crystallization, however, the interactions of the side chains appear to become dominant, often leading to dramatic thermochromism as unstacking of the aromatic cores leads to loss of the CT absorption and corresponding red color.

A lack of thermochromic behavior during the mesophase to crystalline phase transition was seen with mixtures containing **N4** and **N5**. The **D5**:**N4** cocrystal (Figure 2.4) revealed that the methyl group of the branched side chain on **N4** virtually encloses **D5** within the stack, apparently preventing unstacking during crystallization. Interestingly, the **D9**–**10**:**N4** mixtures did undergo a color change, indicating that DAN side chain branching can serve as a stacking deterrent even in the presence of such a presumed NDI rearrangement barrier.

The present study has shown that careful selection of DAN and NDI components not only permits a high degree of mesophase tunability but also *controllable thermochromism*. For example, the change from a deep red mesophase to a deep red or an off-white solid could be adjusted by changing branching on the NDI side chain while maintaining the same DAN component. Future work will aim to refine these relationships; in particular the stereochemical effects of the components as well as develop DAN and NDI mixtures exhibiting robust mesophase behavior at or around room temperature.

2.6 EXPERIMENTAL

2.6.1 General Methods

All starting materials and solvents were commercially available and used without further purification. NMR spectra were taken on a 400 MHz spectrometer in $CDCl_3$. TLC was performed on silica gel plates and column chromatography was carried out using silica gel. Optical microscopy was carried out using standard glass microscope cover slips on a microscope equipped with a hot stage and digital camera. Polarized optical microscopy was carried out using an Olympus BX60 microscope equipped with a Mettler FP82HT hot stage and digital camera. Experimental melting points of the individual components were obtained using DSC and recorded as a temperature range on the second heating cycle at 5 ºC/min. UV-vis spectra were taken of equimolar DAN:NDI mixtures using glass microscope slides. I-V characteristics were measured using an Agilent 4155C precision semiconductor parameter analyzer. OFET fabrication: the gate electrode was an n-type silicon wafer (resistivity 1–10 Ω•cm), the gate dielectric was an SiO_2 layer thermally grown at 1000 °C for 10 h (thickness of 230 nm, capacitance of 18.4 nF/cm^2), and the gold source/drain electrodes (thickness of 50 nm) were thermally evaporated through a shadow mask with W/L = 20. All compounds were synthesized in a 60–80% yield using modifications of previously reported methods (79; 29). A CEM Microwave Accelerated Reaction System (model MARS®) was used to synthesize the NDI derivatives.

2.6.2 Generic DAN Preparation

To a solution of 1,5-dihydroxynaphthalene (1 eq) and K_2CO_3 (5 eq) in CH_3CN (0.1 M) was added 1-bromo-alkane (2.4 eq). The solution was heated to reflux and

allowed to stir for 24 h. The solution was filtered while hot and concentrated under reduced pressure. The crude product was purified twice by column chromatography (20% CH_2Cl_2/ 80% Hexanes) to afford the symmetrical DAN derivative. Suitable crystals for X-ray crystallographic analysis were obtained through slow evaporation from CH_2Cl_2.

2.6.3 Generic NDI Preparation

A DMF (0.1 M) solution consisting of 1,4,5,8-naphthalenetetracarboxylic dianhydride (1 eq), TEA (2.4 eq), and 1-amino-alkane (2.4 eq) was placed in a microwave reactor at 600W. The temperature ramped for 2 min until it reached 140^{o}C and was held at that temperature for 12 min. Once cooled, the solution was placed in a refrigerator for several hours. The precipitated product was removed by vacuum filtration. The crude product was purified by column chromatography (70% CH_2Cl_2/ 30% Hexanes) to afford the symmetrical NDI derivative. Suitable crystals for X-ray crystallographic analysis were obtained through slow evaporation from CH_2Cl_2.

2.6.4 Cocrystal Structure

Suitable crystals for X-ray crystallographic analysis of **D5**:**N4** were obtained by slow evaporation of a 1:1 molar mixture of **D5** and **N4** from toluene.

2.6.5 Component Characterization

1,5-*Bis*(propyloxy)naphthalene (D1). Mp 113-117°C; ^{13}C NMR (400 MHz, $CDCl_3$) δ 154.3, 126.5, 124.7, 113.7, 105.0, 69.3, 22.4, 10.5 ppm; ^{1}H NMR (400 MHz, $CDCl_3$) δ 7.86 (d, J = 8.4 Hz, 2H), 7.35 (t, J = 7.6 Hz, 2H), 6.84 (d, J = 7.6, 2H), 4.09 (t, J = 6.4

Hz, 4H), 1.94 (m, 4H) 1.13 (t, J = 7.6 Hz, 6H) ppm; CI-HRMS (positive ion) calculated for $C_{16}H_{20}O_2$, 244.1463; found 244.1462.

1,5-*Bis*(butyloxy)naphthalene (D2). Mp 110-112°C; ^{13}C NMR (400 MHz, $CDCl_3$) δ 154.7, 126.8, 125.0, 114.0, 105.2, 67.8, 31.4, 19.5, 14.0 ppm; ^{1}H NMR (400 MHz, $CDCl_3$) δ 7.86 (d, J = 8.8 Hz, 2H), 7.36 (t, J = 7.6 Hz, 2H), 6.83 (d, J = 7.6, 2H), 4.14 (t, J = 6.4 Hz, 4H), 1.91 (m, 4H), 1.61 (m, 4H), 1.03 (t, J = 7.2 Hz, 6H) ppm; CI-HRMS (positive ion) calculated for $C_{18}H_{24}O_2$, 272.1776; found 272.1773.

1,5-*Bis*(pentyloxy)naphthalene (D3). Mp 82-87°C; ^{13}C NMR (400 MHz, $CDCl_3$) δ 154.56, 126.7, 124.9, 113.9, 105.1, 68.0, 28.9, 28.3, 22.4, 14.0 ppm; ^{1}H NMR (400 MHz, $CDCl_3$) δ 7.87 (d, J = 8.4 Hz, 2H), 7.36 (t, J = 7.6 Hz, 2H), 6.84 (d, J = 7.6 Hz, 2H), 4.13 (t, J = 6.4 Hz, 4H), 1.94 (m, 4H), 1.56 (m, 4H), 1.46 (m, 4H), 0.98 (t, J = 7.2 Hz, 6H) ppm; CI-HRMS (positive ion) calculated for $C_{20}H_{28}O_2$, 300.2089; found 300.2090.

1,5-Bis(hexyloxy)naphthalene (D4). Mp 90-93°C; ^{13}C NMR (400 MHz, $CDCl_3$) δ 154.9, 126.8, 125.0, 114.0, 105.2, 68.2, 31.9, 29.33, 26.29, 22.7, 14.1 ppm; ^{1}H NMR (400 MHz, $CDCl_3$) δ 7.85 (d, J = 8.4 Hz, 2H), 7.35 (t, J = 7.6 Hz, 2H), 6.83 (d, J = 7.6 Hz, 2H), 4.12 (t, J = 6.4 Hz, 4H), 1.92 (m, 4H), 1.57 (m, 4H), 1.39 (m, 8H), 0.93 (t, J = 6.4 Hz, 6H) ppm; CI-HRMS (positive ion) calculated for $C_{22}H_{32}O_2$, 328.2402; found 328.2405.

1,5-*Bis*(heptyloxy)naphthalene (D5). Mp 72-82°C; ^{13}C NMR (400 MHz, $CDCl_3$) δ 154.8, 126.8, 125.0, 114.0, 105.2, 68.2, 31.8, 29.3, 29.1, 26.3, 22.6, 14.1 ppm; ^{1}H NMR (400 MHz, $CDCl_3$) δ 7.85 (d, J = 8.4 Hz, 2H), 7.35 (t, J = 7.6 Hz, 2H), 6.82 (d, J = 7.6

Hz, 2H), 4.11 (t, *J* = 6.8 Hz, 4H), 1.92 (m, 4H), 1.56 (m, 4H), 1.34 (m, 12H), 0.91 (t, *J* = 6.8 Hz, 6H) ppm; CI-HRMS (positive ion) calculated for $C_{24}H_{36}O_2$, 356.2715; found 356.2715.

1,5-*Bis*(octyloxy)naphthalene (D6). Mp 86-94°C; ^{13}C NMR (400 MHz, $CDCl_3$) δ 154.5, 126.6, 124.8, 113.9, 105.1, 68.0, 31.7, 29.25, 29.17, 29.12, 26.1, 22.5, 14.0 ppm; ^{1}H NMR (400 MHz, $CDCl_3$) δ 7.86 (d, *J* = 8.8 Hz, 2H), 7.35 (t, *J* = 7.6 Hz, 2H), 6.83 (d, *J* = 7.6 Hz, 2H), 4.12 (t, *J* = 6.4 Hz, 4H), 1.92 (m, 4H), 1.57 (m, 4H), 1.32 (m, 16H), 0.91 (t, *J* = 6.8 Hz, 6H) ppm; CI-HRMS (positive ion) calculated for $C_{26}H_{40}O_2$, 384.3028; found 384.3030.

1,5-*Bis*(nonyloxy)naphthalene (D7). Mp 75-84°C; ^{13}C NMR (400 MHz, $CDCl_3$) δ 154.7, 126.8, 125.0, 114.0, 105.2, 68.2, 31.9, 29.57, 29.45, 29.33, 29.29, 26.3, 22.7, 14.1 ppm; ^{1}H NMR (400 MHz, $CDCl_3$) δ 7.85 (d, *J* = 8.4 Hz, 2H), 7.36 (t, *J* = 8.0 Hz, 2H), 6.83 (d, *J* = 7.6 Hz, 2H), 4.12 (t, *J* = 6.8 Hz, 4H), 1.92 (m, 4H), 1.57 (m, 4H), 1.30 (m, 20H), 0.90 (t, *J* = 6.8 Hz, 6H) ppm; CI-HRMS (positive ion) calculated for $C_{28}H_{44}O_2$, 412.3341; found 412.3341.

1,5-*Bis*(decyloxy)naphthalene (D8). Mp 94-97°C; ^{13}C NMR (400 MHz, $CDCl_3$) δ 154.7, 126.8, 125.0, 114.0, 105.2, 68.2, 31.9, 29.6, 29.6, 29.4, 29.3, 26.3, 22.7, 14.1 ppm; ^{1}H NMR (400 MHz, $CDCl_3$) δ 7.84 (d, *J* = 8.4 Hz, 2H), 7.34 (t, *J* = 8.0 Hz, 2H), 6.82 (d, *J* = 7.6 Hz, 2H), 4.12 (t, *J* = 6.4 Hz, 4H), 1.92 (m, 4H), 1.54 (m, 4H), 1.28 (m, 24H), 0.89 (t, *J* = 7.2 Hz, 6H) ppm; CI-HRMS (positive ion) calculated for $C_{30}H_{48}O_2$, 440.3654; found 440.3655.

1,5-*Bis*(isopropoxy)naphthalene (D9). Mp 147-153°C; ^{13}C NMR (400 MHz, $CDCl_3$) δ 153.7, 128.2, 125.2, 114.7, 107.4, 70.6, 22.4 ppm; ^{1}H NMR (400 MHz, $CDCl_3$) δ 7.89 (d, *J* = 8.1 Hz, 2H), 7.40 (t, *J* = 7.5 Hz, 2H), 6.90 (d, *J* = 7.5 Hz, 2H), 4.76 (m, 2H), 1.49 (d, *J* = 6 Hz, 12H) ppm; ESI-MS (positive ion, M + H^+) calculated for $C_{16}H_{20}O_2$+ H, 245; found 245 (29).

1,5-*Bis*(pentan-2-yloxy)naphthalene (D10). Mp 47-70°C; ^{13}C NMR (400 MHz, $CDCl_3$) δ 153.7, 127.8, 124.9, 114.1, 106.6, 73.8, 38.8, 19.7, 18.8, 14.1 ppm; ^{1}H NMR (400 MHz, $CDCl_3$) δ 7.84 (d, *J* = 8.8 Hz, 2H), 7.34 (t, *J* = 8.0 Hz, 2H), 6.85 (d, *J* = 7.2 Hz, 2H), 4.58 (m, 2H), 1.88 (m, 2H), 1.68 (m, 2H), 1.55 (m, 4H), 1.40 (d, *J* = 6.0 Hz, 6H) 0.97 (t, *J* = 7.6 Hz, 6H) ppm; CI-HRMS (positive ion) calculated for $C_{20}H_{28}O_2$, 300.2089; found 300.2086.

2,7-Dibutyl-benzo[*lmn*][3,8]phenanthroline-1,3,6,8-tetraone (N1). Mp 232-239°C; ^{13}C NMR (400 MHz, $CDCl_3$) δ 162.7, 130.8, 126.6, 126.5, 40.7, 30.1, 20.9, 13.8 ppm; ^{1}H NMR (400 MHz, $CDCl_3$) δ 8.71 (s, 4H), 4.17 (t, *J* = 7.6 Hz, 4H), 1.71 (m, 4H), 1.44 (m, 4H), 0.97 (t, *J* = 7.2 Hz, 6H) ppm; CI-HRMS (positive ion, M + H^+) calculated for $C_{22}H_{22}N_2O_4$+ H, 379.1613; found 379.1660.

2,7-Dioctyl-benzo[*lmn*][3,8]phenanthroline-1,3,6,8-tetraone (N2). Mp 184-187°C; ^{13}C NMR (400 MHz, $CDCl_3$) δ 162.8, 130.9, 126.6, 126.6, 41.0, 31.8, 29.27, 29.17, 28.0, 27.1, 22.6, 14.1 ppm; ^{1}H NMR (400 MHz, $CDCl_3$) δ 8.74 (s, 4H), 4.18 (t, *J* = 8.0 Hz, 4H), 1.73 (m, 4H), 1.36 (m, 20H), 0.87 (t, *J* = 6.4 Hz, 6H) ppm; CI-HRMS (positive ion, M + H^+) calculated for $C_{30}H_{38}N_2O_4$+ H, 491.2910; found 491.2906.

2,7-Didodecyl-benzo[*lmn*][3,8]phenanthroline-1,3,6,8-tetraone (N3). Mp 161-163°C; ^{13}C NMR (400 MHz, $CDCl_3$) δ 162.8, 130.9, 126.6, 126.6, 41.0, 31.9, 29.61, 29.58, 29.51, 29.40, 29.33 (one overlapping peak), 28.1, 27.1, 22.7, 14.1 ppm; ^{1}H NMR (400 MHz, $CDCl_3$) δ 8.74 (s, 4H), 4.18 (t, J = 7.6 Hz, 4H), 1.73 (m, 4H), 1.24 (m, 36H), 0.87 (t, J = 6.8 Hz, 6H) ppm; CI-HRMS (positive ion, M + H^+) calculated for $C_{38}H_{54}N_2O_4$+ H, 603.4162; found 603.4158.

2,7-Di(R-heptan-2-yl)benzo[*lmn*][3,8]phenanthroline-1,3,6,8-tetraone (N4). Mp 166-177°C; $[\alpha]^{24}$ D+82.2 (*c* 0.6 CH_2Cl_2); ^{13}C NMR (400 MHz, $CDCl_3$) δ 163.6, 141.1, 131.1, 127.0, 50.7, 33.6, 31.8, 26.9, 22.8, 18.5, 14.2 ppm; ^{1}H NMR (400 MHz, $CDCl_3$) δ 8.74 (s, 4H), 5.28 (m, 2H), 2.19 (m, 2H), 1.91 (m, 2H), 1.61 (d, J = 7.2 Hz, 6H), 1.30 (m, 12H), 0.85 (t, J = 7.5 Hz, 6H) ppm; ESI-MS (positive ion, M + H^+) calculated for $C_{28}H_{34}N_2O_4$+ H, 463; found 463[1].

2,7-Diheptan-2-yl-benzo[*lmn*][3,8]phenanthroline-1,3,6,8-tetraone (N5). Mp 145-150°C; ^{13}C NMR (400 MHz, $CDCl_3$) δ 162.8, 130.4, 126.3, 126.2, 50.0, 32.9, 31.1, 26.2, 22.0, 17.8, 13.5 ppm; ^{1}H NMR (400 MHz, $CDCl_3$) δ 8.71 (s, 4H), 5.26 (m, 2H), 2.18 (m, 2H), 1.92 (m, 2H), 1.58 (d, J = 7.2 Hz, 6H), 1.26 (m, 12H), 0.82 (t, J = 7.5 Hz, 6H) ppm; CI-HRMS (positive ion, M + H^+) calculated for $C_{28}H_{34}N_2O_4$+ H, 463.2597; found 463.2593.

2.6.6 Retention or Loss of CT Absorbance upon Crystallization

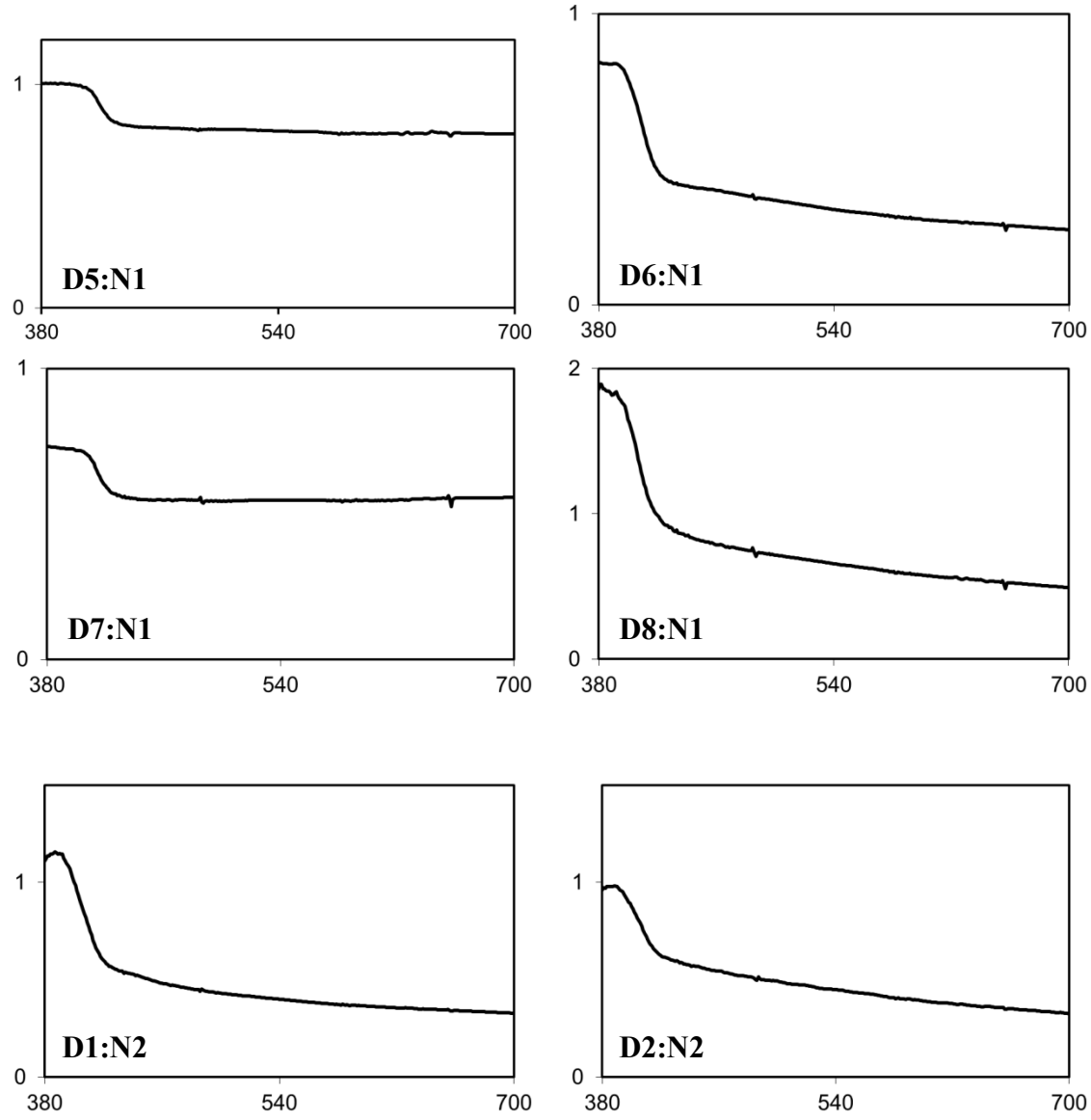

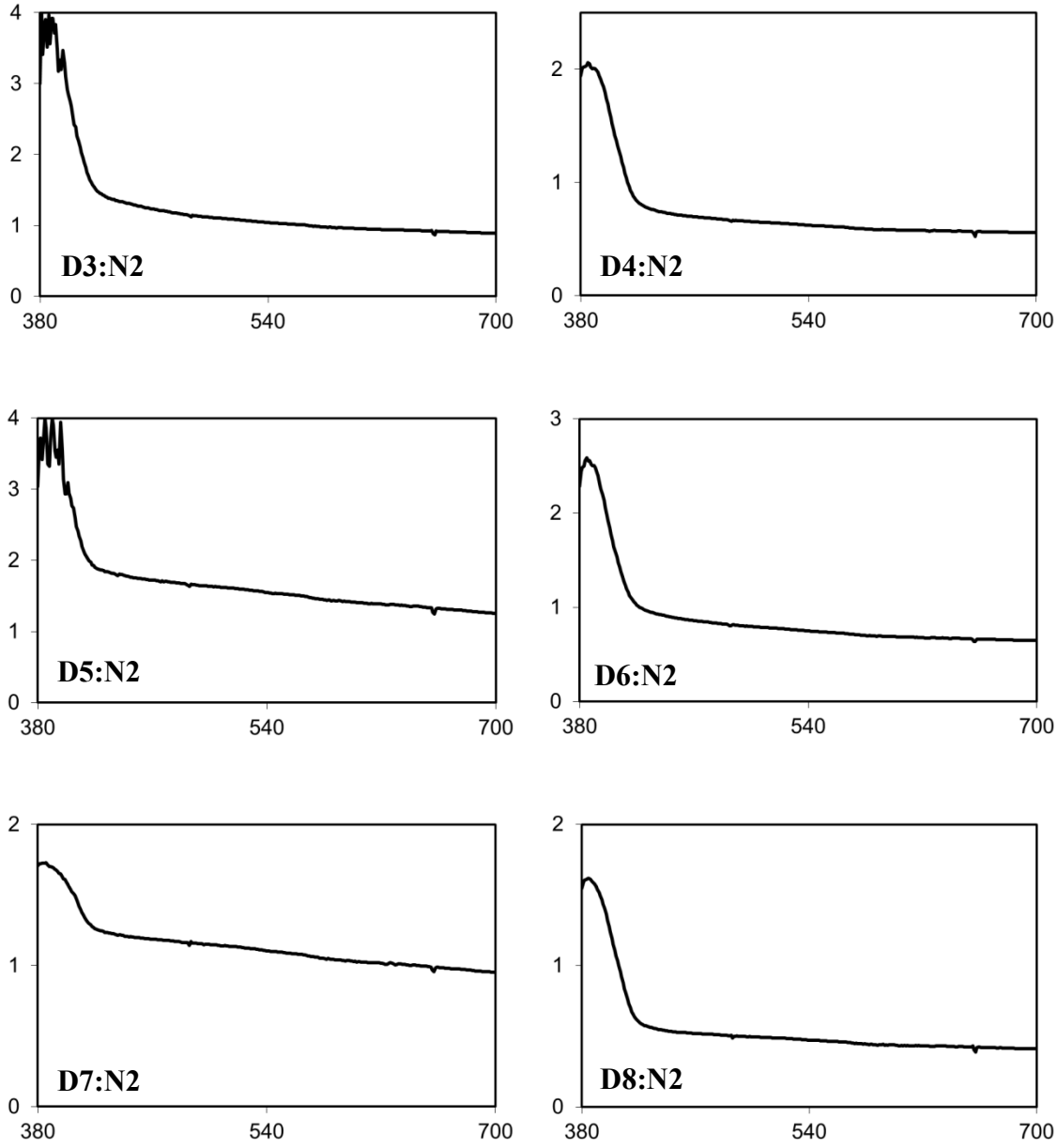
D3:N2
D4:N2
D5:N2
D6:N2
D7:N2
D8:N2
380
540
700

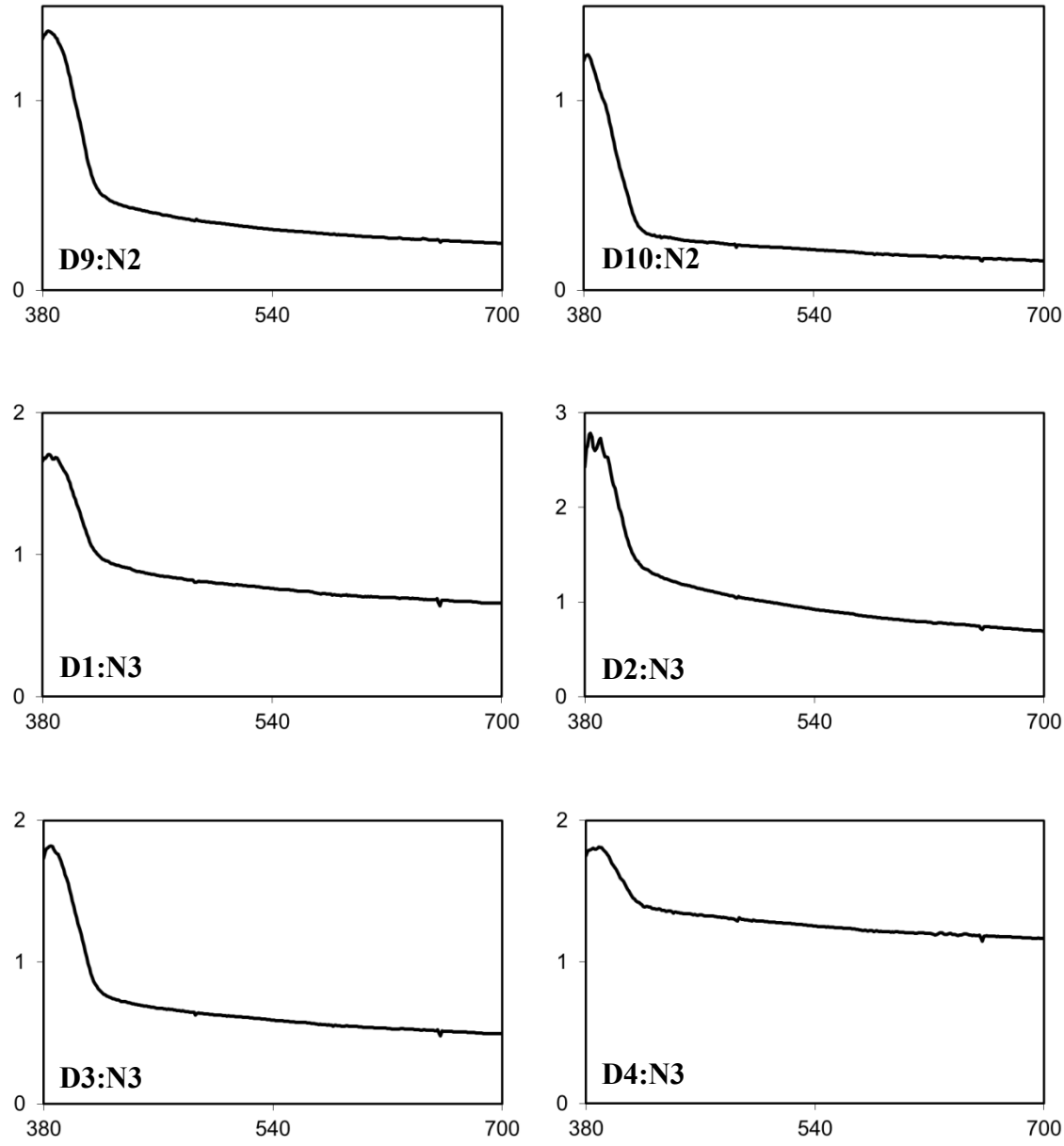
D9:N2
D10:N2
D1:N3
D2:N3
D3:N3
D4:N3
380
540
700

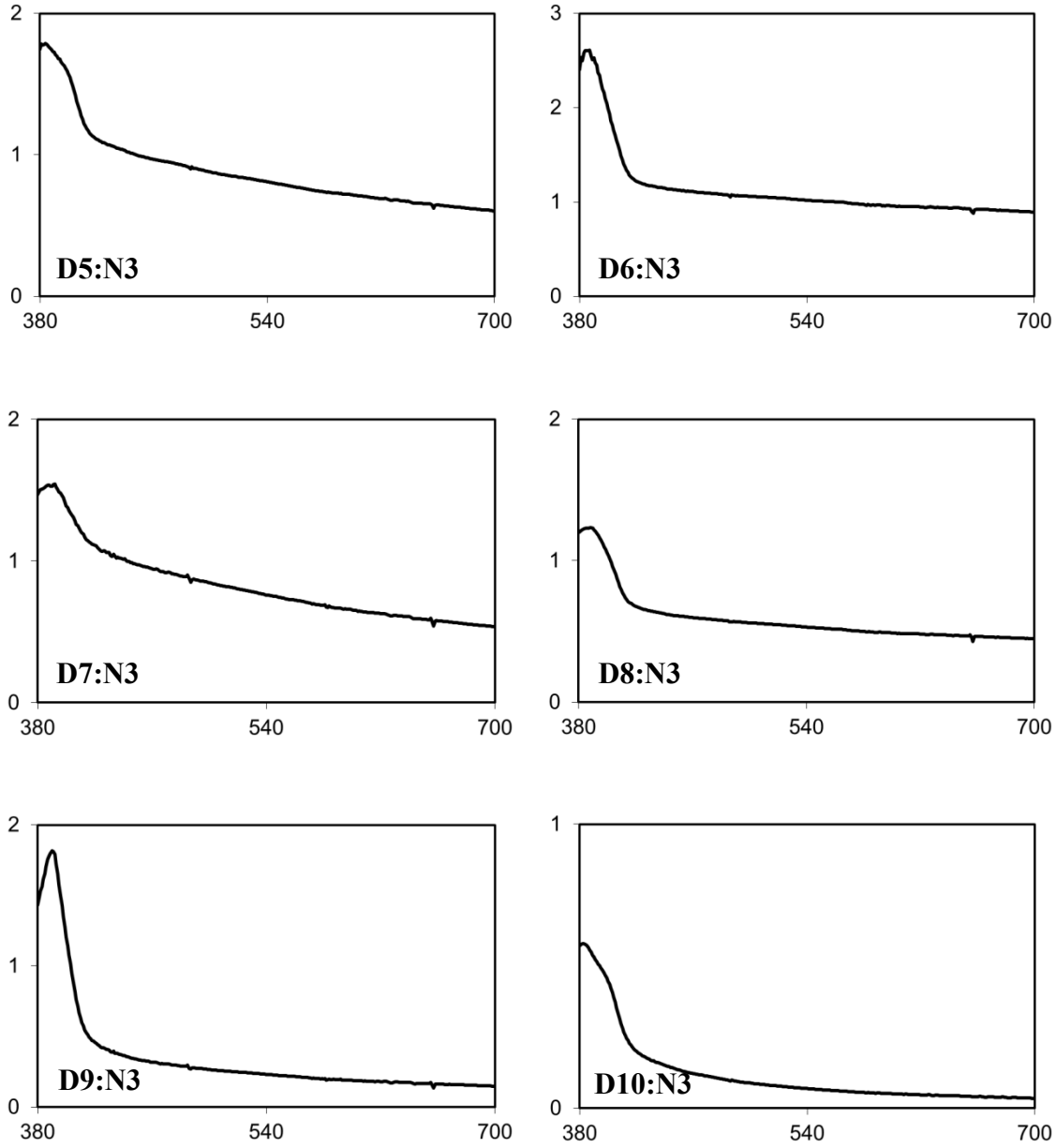
D5:N3
D6:N3
D7:N3
D8:N3
D9:N3
D10:N3
380
540
700

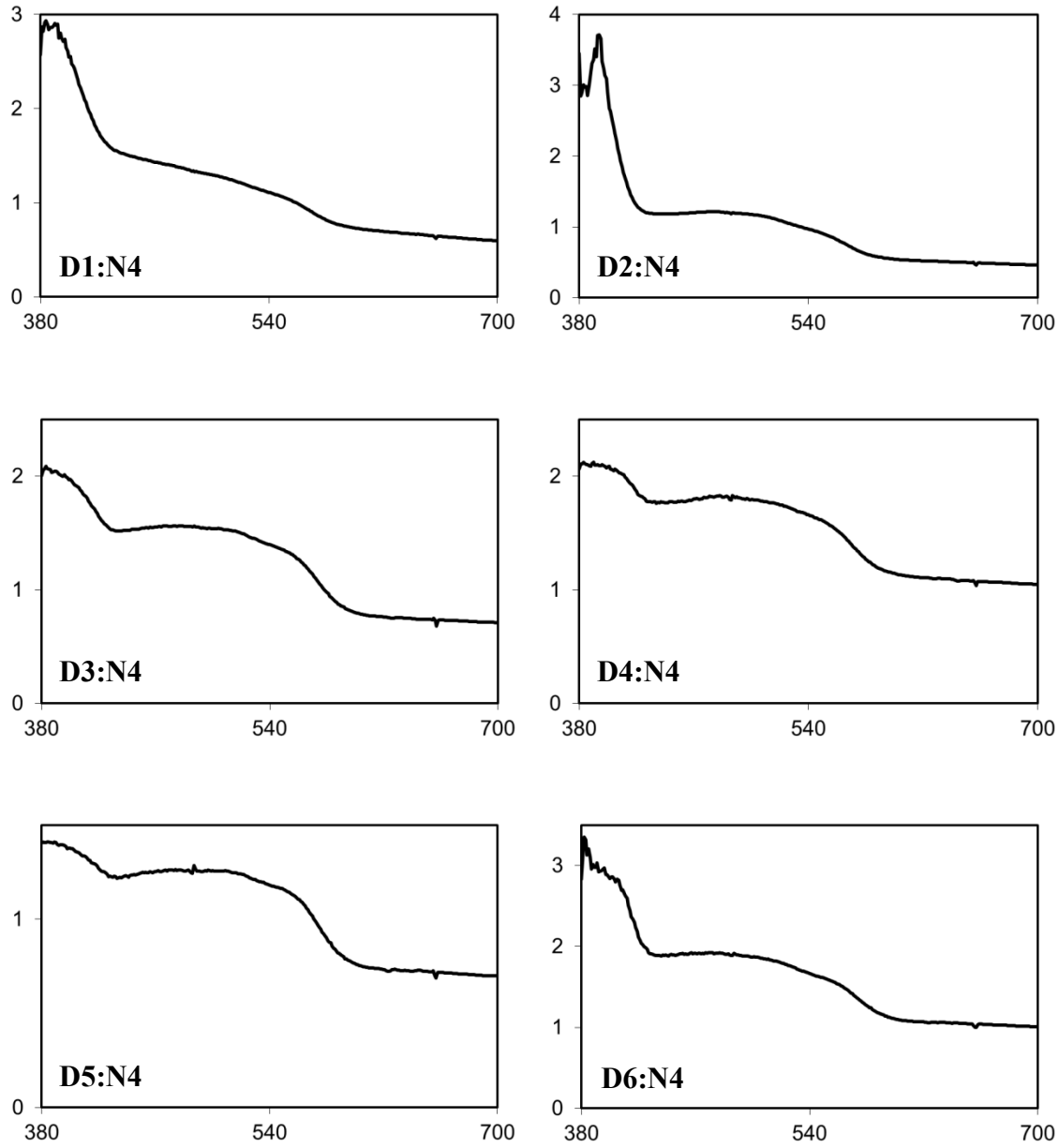
D1:N4
D2:N4
D3:N4
D4:N4
D5:N4
D6:N4
380
540
700

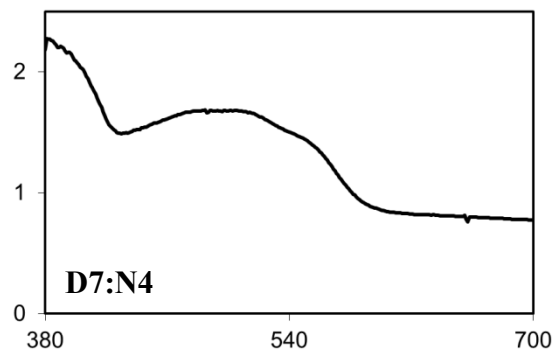
2
1
0
D7:N4
380
540
700

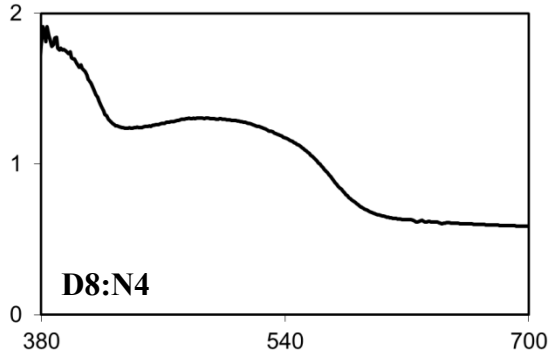
2
1
0
D8:N4
380
540
700

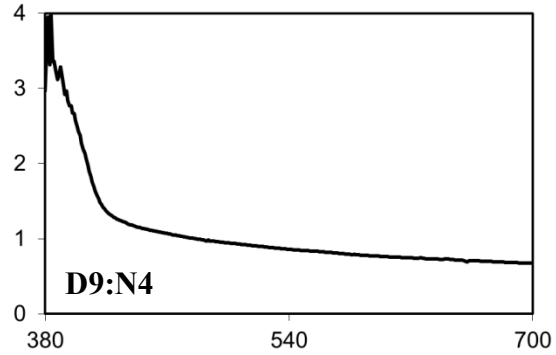
4
3
2
1
0
D9:N4
380
540
700

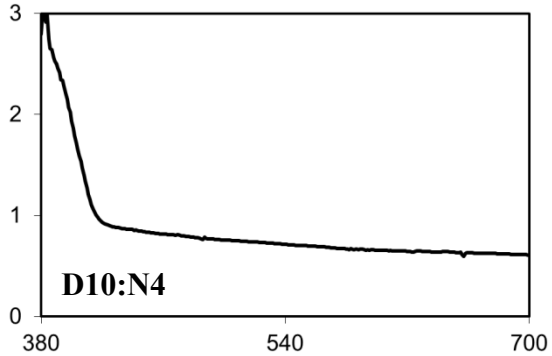
3
2
1
0
D10:N4
380
540
700

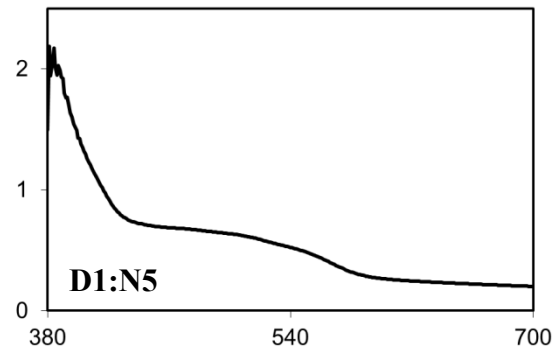
2
1
0
D1:N5
380
540
700

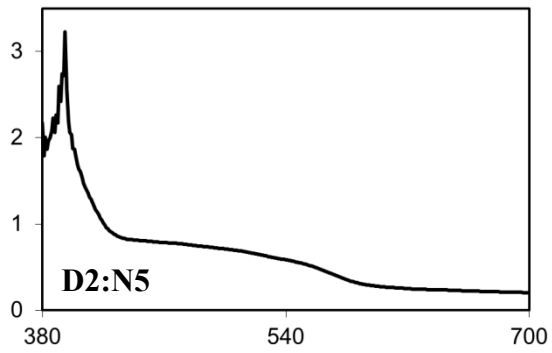
3
2
1
0
D2:N5
380
540
700

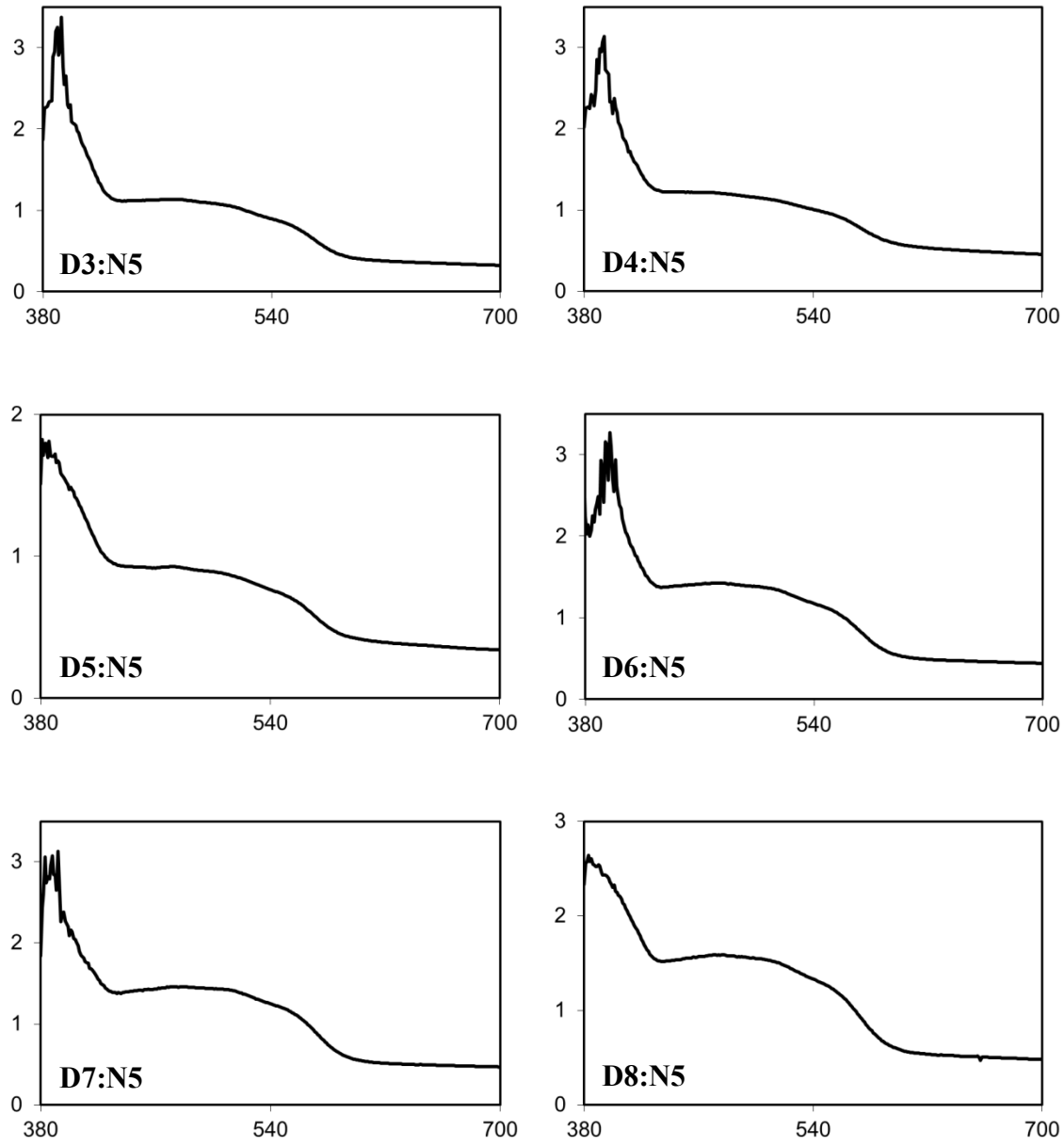
D3:N5
D4:N5
D5:N5
D6:N5
D7:N5
D8:N5
380
540
700

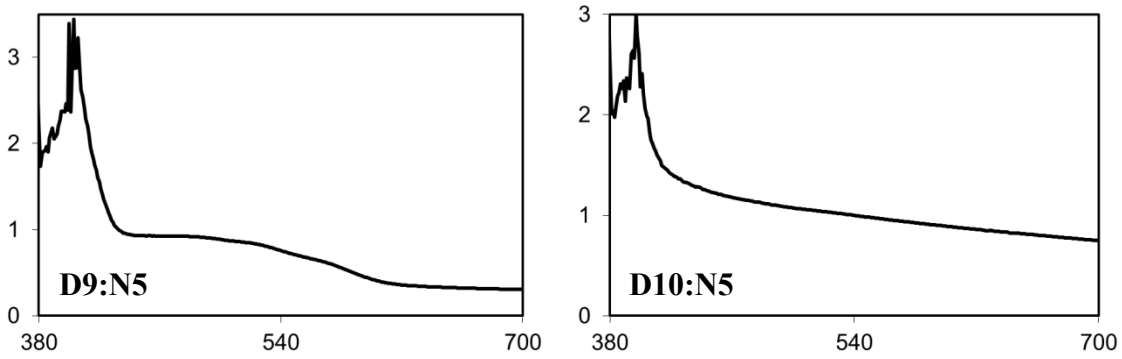

Figure 2.15 UV-vis spectra of all DAN:NDI mixtures in the crystalline state. The Y-axis is absorbance (a.u.) and the X-axis is wavelength (nm).

2.6.7 Crystal Structure Parameters

Space Group: P -1; Cell Lengths: **a** 6.436(2) **b** 7.537(2) **c** 7.554(3); Cell Angles: **α** 71.507(7) **β** 87.585(7) **γ** 71.475(8); Cell Volume: 328.801; Z, Z´: 1, 0; R-Factor (%): 4.04.

Atoms

Number	Label	Charge	SybylType	Xfrac + ESD	Yfrac + ESD	Zfrac + ESD	Symm. op.
1	O1	0	O.3	0.09459(15)	0.68056(14)	0.67276(13)	x,y,z
2	C1	0	C.2	0.8777(2)	0.2911(2)	0.6565(2)	x,y,z
3	C2	0	C.2	0.7417(2)	0.3376(2)	0.7979(2)	x,y,z
4	C3	0	C.2	0.5258(2)	0.4489(2)	0.7592(2)	x,y,z
5	C4	0	C.2	0.4339(2)	0.5223(2)	0.57300(19)	x,y,z
6	C5	0	C.2	0.2090(2)	0.6419(2)	0.52473(19)	x,y,z
7	C6	0	C.3	-0.1352(2)	0.7926(2)	0.6348(2)	x,y,z
8	C7	0	C.3	-0.2316(2)	0.8133(2)	0.8155(2)	x,y,z
9	C8	0	C.3	-0.4764(2)	0.9268(2)	0.7806(2)	x,y,z
10	H1	0	H	1.026(3)	0.215(2)	0.689(2)	x,y,z
11	H2	0	H	0.807(2)	0.290(2)	0.923(2)	x,y,z
12	H3	0	H	0.437(2)	0.476(2)	0.853(2)	x,y,z
13	H6A	0	H	-0.152(2)	0.927(2)	0.539(2)	x,y,z
14	H6B	0	H	-0.207(2)	0.723(2)	0.576(2)	x,y,z
15	H7B	0	H	-0.205(2)	0.680(2)	0.908(2)	x,y,z
16	H7A	0	H	-0.156(2)	0.884(2)	0.867(2)	x,y,z
17	H8C	0	H	-0.505(3)	1.065(3)	0.696(2)	x,y,z
18	H8B	0	H	-0.549(3)	0.861(2)	0.720(2)	x,y,z
19	H8A	0	H	-0.543(3)	0.929(2)	0.898(2)	x,y,z
20	O1	0	O.3	0.90541(15)	0.31944(14)	0.32724(13)	1-x,1-y,1-z
21	C1	0	C.2	0.1223(2)	0.7089(2)	0.3435(2)	1-x,1-y,1-z
22	C2	0	C.2	0.2583(2)	0.6624(2)	0.2021(2)	1-x,1-y,1-z
23	C3	0	C.2	0.4742(2)	0.5511(2)	0.2408(2)	1-x,1-y,1-z
24	C4	0	C.2	0.5661(2)	0.4777(2)	0.42700(19)	1-x,1-y,1-z
25	C5	0	C.2	0.7910(2)	0.3581(2)	0.47527(19)	1-x,1-y,1-z
26	C6	0	C.3	1.1352(2)	0.2074(2)	0.3652(2)	1-x,1-y,1-z
27	C7	0	C.3	1.2316(2)	0.1867(2)	0.1845(2)	1-x,1-y,1-z
28	C8	0	C.3	1.4764(2)	0.0732(2)	0.2194(2)	1-x,1-y,1-z
29	H1	0	H	-0.026(3)	0.785(2)	0.311(2)	1-x,1-y,1-z
30	H2	0	H	0.193(2)	0.710(2)	0.077(2)	1-x,1-y,1-z
31	H3	0	H	0.563(2)	0.524(2)	0.147(2)	1-x,1-y,1-z
32	H6A	0	H	1.152(2)	0.073(2)	0.461(2)	1-x,1-y,1-z
33	H6B	0	H	1.207(2)	0.277(2)	0.424(2)	1-x,1-y,1-z
34	H7B	0	H	1.205(2)	0.320(2)	0.092(2)	1-x,1-y,1-z
35	H7A	0	H	1.156(2)	0.116(2)	0.133(2)	1-x,1-y,1-z
36	H8C	0	H	1.505(3)	-0.065(3)	0.304(2)	1-x,1-y,1-z
37	H8B	0	H	1.549(3)	0.139(2)	0.280(2)	1-x,1-y,1-z
38	H8A	0	H	1.543(3)	0.071(2)	0.102(2)	1-x,1-y,1-z

Bonds

Number	Atom1	Atom2	Type	Polymeric	Length	SybylType
1	O1	C5	Unknown	no	1.371(2)	1
2	O1	C6	Unknown	no	1.439(1)	1
3	C1	C2	Unknown	no	1.412(2)	un
4	C1	H1	Unknown	no	0.94(2)	1
5	C1	C5	Unknown	no	1.374(2)	un
6	C2	C3	Unknown	no	1.363(2)	un
7	C2	H2	Unknown	no	0.96(1)	1
8	C3	C4	Unknown	no	1.415(2)	un
9	C3	H3	Unknown	no	0.92(1)	1
10	C4	C5	Unknown	no	1.431(2)	un
11	C4	C4	Unknown	no	1.424(2)	un
12	C5	C1	Unknown	no	1.374(2)	un
13	C6	C7	Unknown	no	1.508(2)	1
14	C6	H6A	Unknown	no	1.02(1)	1
15	C6	H6B	Unknown	no	1.00(2)	1
16	C7	C8	Unknown	no	1.523(2)	1
17	C7	H7B	Unknown	no	0.99(1)	1
18	C7	H7A	Unknown	no	0.99(2)	1
19	C8	H8C	Unknown	no	1.00(2)	1
20	C8	H8B	Unknown	no	0.99(2)	1
21	C8	H8A	Unknown	no	0.97(2)	1
22	O1	C5	Unknown	no	1.371(2)	1
23	O1	C6	Unknown	no	1.439(1)	1
24	C1	C2	Unknown	no	1.412(2)	un
25	C1	H1	Unknown	no	0.94(2)	1
26	C2	C3	Unknown	no	1.363(2)	un
27	C2	H2	Unknown	no	0.96(1)	1
28	C3	C4	Unknown	no	1.415(2)	un
29	C3	H3	Unknown	no	0.92(1)	1
30	C4	C5	Unknown	no	1.431(2)	un
31	C6	C7	Unknown	no	1.508(2)	1
32	C6	H6A	Unknown	no	1.02(1)	1
33	C6	H6B	Unknown	no	1.00(2)	1
34	C7	C8	Unknown	no	1.523(2)	1
35	C7	H7B	Unknown	no	0.99(1)	1
36	C7	H7A	Unknown	no	0.99(2)	1
37	C8	H8C	Unknown	no	1.00(2)	1
38	C8	H8B	Unknown	no	0.99(2)	1
39	C8	H8A	Unknown	no	0.97(2)	1

Figure 2.16 Crystal structure parameters for **D1**.

Space Group: P -1; Cell Lengths: **a** 6.849(2) **b** 8.040(3) **c** 8.248(4); Cell Angles: **α** 70.981(9) **β** 67.810(10) **γ** 68.179(12); Cell Volume: 381.215; Z, Z´: 1, 0; R-Factor (%): 7.2.

Atoms

Number	Label	Charge	SybylType	Xfrac + ESD	Yfrac + ESD	Zfrac + ESD	Symm. op.
1	O1	0	O.3	0.7570(3)	0.6060(2)	0.6535(2)	x,y,z
2	C1	0	C.2	0.4456(3)	0.5074(3)	0.4389(3)	x,y,z
3	C2	0	C.2	0.4415(4)	0.6585(3)	0.2868(3)	x,y,z
4	H2	0	H	0.3695	0.6695	0.2052	x,y,z
5	C3	0	C.2	0.5419(4)	0.7851(3)	0.2619(3)	x,y,z
6	H3	0	H	0.5395	0.8833	0.1615	x,y,z
7	C4	0	C.2	0.6506(4)	0.7741(3)	0.3826(3)	x,y,z
8	H4	0	H	0.7179	0.8646	0.3626	x,y,z
9	C5	0	C.2	0.6571(3)	0.6303(3)	0.5290(3)	x,y,z
10	C6	0	C.3	0.8590(4)	0.7418(3)	0.6299(3)	x,y,z
11	H6A	0	H	0.7504	0.8627	0.6287	x,y,z
12	H6B	0	H	0.9758	0.7473	0.5155	x,y,z
13	C7	0	C.3	0.9541(4)	0.6899(3)	0.7832(3)	x,y,z
14	H7A	0	H	1.0619	0.5686	0.7832	x,y,z
15	H7B	0	H	0.8364	0.6821	0.8968	x,y,z
16	C8	0	C.3	1.0646(4)	0.8287(3)	0.7697(3)	x,y,z
17	H8A	0	H	0.9545	0.9484	0.7757	x,y,z
18	H8B	0	H	1.1763	0.8414	0.6529	x,y,z
19	C9	0	C.3	1.1728(4)	0.7750(4)	0.9171(3)	x,y,z
20	H9A	0	H	1.0622	0.7669	1.033	x,y,z
21	H9B	0	H	1.2423	0.867	0.9009	x,y,z
22	H9C	0	H	1.2828	0.657	0.9114	x,y,z
23	O1	0	O.3	0.2430(3)	0.3940(2)	0.3465(2)	1-x,1-y,1-z
24	C1	0	C.2	0.5544(3)	0.4926(3)	0.5611(3)	1-x,1-y,1-z
25	C2	0	C.2	0.5585(4)	0.3415(3)	0.7132(3)	1-x,1-y,1-z
26	H2	0	H	0.6305	0.3305	0.7948	1-x,1-y,1-z
27	C3	0	C.2	0.4581(4)	0.2149(3)	0.7381(3)	1-x,1-y,1-z
28	H3	0	H	0.4605	0.1167	0.8385	1-x,1-y,1-z
29	C4	0	C.2	0.3494(4)	0.2259(3)	0.6174(3)	1-x,1-y,1-z
30	H4	0	H	0.2821	0.1354	0.6374	1-x,1-y,1-z
31	C5	0	C.2	0.3429(3)	0.3697(3)	0.4710(3)	1-x,1-y,1-z
32	C6	0	C.3	0.1410(4)	0.2582(3)	0.3701(3)	1-x,1-y,1-z
33	H6A	0	H	0.2496	0.1373	0.3713	1-x,1-y,1-z
34	H6B	0	H	0.0242	0.2527	0.4845	1-x,1-y,1-z
35	C7	0	C.3	0.0459(4)	0.3101(3)	0.2168(3)	1-x,1-y,1-z
36	H7A	0	H	-0.0619	0.4314	0.2168	1-x,1-y,1-z
37	H7B	0	H	0.1636	0.3179	0.1032	1-x,1-y,1-z
38	C8	0	C.3	-0.0646(4)	0.1713(3)	0.2303(3)	1-x,1-y,1-z
39	H8A	0	H	0.0455	0.0516	0.2243	1-x,1-y,1-z
40	H8B	0	H	-0.1763	0.1586	0.3471	1-x,1-y,1-z
41	C9	0	C.3	-0.1728(4)	0.2250(4)	0.0829(3)	1-x,1-y,1-z
42	H9A	0	H	-0.0622	0.2331	-0.033	1-x,1-y,1-z
43	H9B	0	H	-0.2423	0.133	0.0991	1-x,1-y,1-z
44	H9C	0	H	-0.2828	0.343	0.0886	1-x,1-y,1-z

Bonds

Number	Atom1	Atom2	Type	Polymeric	Length	SybylType
1	O1	C5	Unknown	no	1.364(4)	1
2	O1	C6	Unknown	no	1.430(4)	1
3	C1	C2	Unknown	no	1.435(3)	un
4	C1	C1	Unknown	no	1.417(4)	un
5	C1	C5	Unknown	no	1.427(4)	un
6	C2	H2	Unknown	no	0.940(3)	1
7	C2	C3	Unknown	no	1.352(4)	un
8	C3	H3	Unknown	no	0.940(2)	1
9	C3	C4	Unknown	no	1.417(4)	un
10	C4	H4	Unknown	no	0.940(3)	1
11	C4	C5	Unknown	no	1.374(3)	un
12	C5	C1	Unknown	no	1.427(4)	un
13	C6	H6A	Unknown	no	0.980(2)	1
14	C6	H6B	Unknown	no	0.980(2)	1
15	C6	C7	Unknown	no	1.508(4)	1
16	C7	H7A	Unknown	no	0.980(2)	1
17	C7	H7B	Unknown	no	0.980(2)	1
18	C7	C8	Unknown	no	1.521(4)	1
19	C8	H8A	Unknown	no	0.980(2)	1
20	C8	H8B	Unknown	no	0.980(2)	1
21	C8	C9	Unknown	no	1.521(4)	1
22	C9	H9A	Unknown	no	0.970(2)	1
23	C9	H9B	Unknown	no	0.970(4)	1
24	C9	H9C	Unknown	no	0.970(3)	1
25	O1	C5	Unknown	no	1.364(4)	1
26	O1	C6	Unknown	no	1.430(4)	1
27	C1	C2	Unknown	no	1.435(3)	un
28	C2	H2	Unknown	no	0.940(3)	1
29	C2	C3	Unknown	no	1.352(4)	un
30	C3	H3	Unknown	no	0.940(2)	1
31	C3	C4	Unknown	no	1.417(4)	un
32	C4	H4	Unknown	no	0.940(3)	1
33	C4	C5	Unknown	no	1.374(3)	un
34	C6	H6A	Unknown	no	0.980(2)	1
35	C6	H6B	Unknown	no	0.980(2)	1
36	C6	C7	Unknown	no	1.508(4)	1
37	C7	H7A	Unknown	no	0.980(2)	1
38	C7	H7B	Unknown	no	0.980(2)	1
39	C7	C8	Unknown	no	1.521(4)	1
40	C8	H8A	Unknown	no	0.980(2)	1
41	C8	H8B	Unknown	no	0.980(2)	1
42	C8	C9	Unknown	no	1.521(4)	1
43	C9	H9A	Unknown	no	0.970(2)	1
44	C9	H9B	Unknown	no	0.970(4)	1
45	C9	H9C	Unknown	no	0.970(3)	1

Figure 2.17 Crystal structure parameters for **D2**.

Space Group: P $2_1/n$; Cell Lengths: **a** 7.2003(4) **b** 14.2320(12) **c** 8.4409(5); Cell Angles: **α** 90.00 **β** 102.960(9) **γ** 90.00; Cell Volume: 842.945; Z, Z′: 2, 0; R-Factor (%): 4.44

Atoms

Number	Label	Charge	SybylType	Xfrac + ESD	Yfrac + ESD	Zfrac + ESD	Symm. op.
1	O1	0	O.3	0.10537(11)	0.57047(6)	0.36487(10)	x,y,z
2	C1	0	C.2	0.57862(15)	0.46866(8)	0.51017(13)	x,y,z
3	C2	0	C.2	0.56199(16)	0.38392(8)	0.41931(14)	x,y,z
4	C3	0	C.2	0.39451(17)	0.36298(9)	0.31290(14)	x,y,z
5	C4	0	C.2	0.23558(16)	0.42356(9)	0.29109(13)	x,y,z
6	C5	0	C.2	0.24877(16)	0.50616(8)	0.37708(13)	x,y,z
7	C6	0	C.3	-0.07324(16)	0.54695(9)	0.25805(14)	x,y,z
8	C7	0	C.3	-0.21077(16)	0.62749(9)	0.25514(15)	x,y,z
9	C8	0	C.3	-0.40010(16)	0.60560(9)	0.13838(14)	x,y,z
10	C9	0	C.3	-0.54787(17)	0.68362(9)	0.12435(15)	x,y,z
11	C10	0	C.3	-0.73423(17)	0.65687(10)	0.00752(15)	x,y,z
12	H2	0	H	0.671(2)	0.3425(11)	0.4346(17)	x,y,z
13	H3	0	H	0.3837(19)	0.3052(10)	0.2527(17)	x,y,z
14	H4	0	H	0.1212(19)	0.4064(10)	0.2168(17)	x,y,z
15	H6A	0	H	-0.0526(18)	0.5351(9)	0.1471(16)	x,y,z
16	H6B	0	H	-0.1235(18)	0.4902(10)	0.3000(15)	x,y,z
17	H7A	0	H	-0.2285(19)	0.6372(10)	0.3658(18)	x,y,z
18	H7B	0	H	-0.156(2)	0.6840(11)	0.2197(17)	x,y,z
19	H8A	0	H	-0.3767(19)	0.5924(10)	0.0311(18)	x,y,z
20	H8B	0	H	-0.4523(19)	0.5475(10)	0.1779(16)	x,y,z
21	H9A	0	H	-0.5734(19)	0.6953(10)	0.2327(18)	x,y,z
22	H9B	0	H	-0.496(2)	0.7423(11)	0.0871(19)	x,y,z
23	H10A	0	H	-0.834(2)	0.7066(12)	-0.0012(19)	x,y,z
24	H10B	0	H	-0.714(2)	0.6456(10)	-0.1004(18)	x,y,z
25	H10C	0	H	-0.787(2)	0.6010(13)	0.048(2)	x,y,z
26	O1	0	O.3	0.89463(11)	0.42953(6)	0.63513(10)	1-x,1-y,1-z
27	C1	0	C.2	0.42138(15)	0.53134(8)	0.48983(13)	1-x,1-y,1-z
28	C2	0	C.2	0.43801(16)	0.61608(8)	0.58069(14)	1-x,1-y,1-z
29	C3	0	C.2	0.60549(17)	0.63702(9)	0.68710(14)	1-x,1-y,1-z
30	C4	0	C.2	0.76442(16)	0.57644(9)	0.70891(13)	1-x,1-y,1-z
31	C5	0	C.2	0.75123(16)	0.49384(8)	0.62292(13)	1-x,1-y,1-z
32	C6	0	C.3	1.07324(16)	0.45305(9)	0.74195(14)	1-x,1-y,1-z
33	C7	0	C.3	1.21077(16)	0.37251(9)	0.74486(15)	1-x,1-y,1-z
34	C8	0	C.3	1.40010(16)	0.39440(9)	0.86162(14)	1-x,1-y,1-z
35	C9	0	C.3	1.54787(17)	0.31638(9)	0.87565(15)	1-x,1-y,1-z
36	C10	0	C.3	1.73423(17)	0.34313(10)	0.99248(15)	1-x,1-y,1-z
37	H2	0	H	0.329(2)	0.6575(11)	0.5654(17)	1-x,1-y,1-z
38	H3	0	H	0.6163(19)	0.6948(10)	0.7473(17)	1-x,1-y,1-z
39	H4	0	H	0.8788(19)	0.5936(10)	0.7832(17)	1-x,1-y,1-z
40	H6A	0	H	1.0526(18)	0.4649(9)	0.8529(16)	1-x,1-y,1-z
41	H6B	0	H	1.1235(18)	0.5098(10)	0.7000(15)	1-x,1-y,1-z
42	H7A	0	H	1.2285(19)	0.3628(10)	0.6342(18)	1-x,1-y,1-z
43	H7B	0	H	1.156(2)	0.3160(11)	0.7803(17)	1-x,1-y,1-z
44	H8A	0	H	1.3767(19)	0.4076(10)	0.9689(18)	1-x,1-y,1-z
45	H8B	0	H	1.4523(19)	0.4525(10)	0.8221(16)	1-x,1-y,1-z
46	H9A	0	H	1.5734(19)	0.3047(10)	0.7673(18)	1-x,1-y,1-z
47	H9B	0	H	1.496(2)	0.2577(11)	0.9129(19)	1-x,1-y,1-z
48	H10A	0	H	1.834(2)	0.2934(12)	1.0012(19)	1-x,1-y,1-z
49	H10B	0	H	1.714(2)	0.3544(10)	1.1004(18)	1-x,1-y,1-z
50	H10C	0	H	1.787(2)	0.3990(13)	0.952(2)	1-x,1-y,1-z

Bonds

Number	Atom1	Atom2	Type	Polymeric	Length	SybylType
1	O1	C5	Unknown	no	1.366(1)	1
2	O1	C6	Unknown	no	1.435(1)	1
3	C1	C2	Unknown	no	1.420(2)	un
4	C1	C1	Unknown	no	1.421(2)	un
5	C1	C5	Unknown	no	1.431(1)	un
6	C2	C3	Unknown	no	1.365(2)	un
7	C2	H2	Unknown	no	0.97(1)	1
8	C3	C4	Unknown	no	1.411(2)	un
9	C3	H3	Unknown	no	0.96(1)	1
10	C4	C5	Unknown	no	1.374(2)	un
11	C4	H4	Unknown	no	0.95(1)	1
12	C5	C1	Unknown	no	1.431(1)	un
13	C6	C7	Unknown	no	1.511(2)	1
14	C6	H6A	Unknown	no	0.99(1)	1
15	C6	H6B	Unknown	no	0.98(1)	1
16	C7	C8	Unknown	no	1.525(1)	1
17	C7	H7A	Unknown	no	0.98(2)	1
18	C7	H7B	Unknown	no	0.97(2)	1
19	C8	C9	Unknown	no	1.524(2)	1
20	C8	H8A	Unknown	no	0.98(2)	1
21	C8	H8B	Unknown	no	1.00(1)	1
22	C9	C10	Unknown	no	1.525(2)	1
23	C9	H9A	Unknown	no	0.99(2)	1
24	C9	H9B	Unknown	no	0.99(2)	1
25	C10	H10A	Unknown	no	1.00(2)	1
26	C10	H10B	Unknown	no	0.97(2)	1
27	C10	H10C	Unknown	no	0.98(2)	1
28	O1	C5	Unknown	no	1.366(1)	1
29	O1	C6	Unknown	no	1.435(1)	1
30	C1	C2	Unknown	no	1.420(2)	un
31	C2	C3	Unknown	no	1.365(2)	un
32	C2	H2	Unknown	no	0.97(1)	1
33	C3	C4	Unknown	no	1.411(2)	un
34	C3	H3	Unknown	no	0.96(1)	1
35	C4	C5	Unknown	no	1.374(2)	un
36	C4	H4	Unknown	no	0.95(1)	1
37	C6	C7	Unknown	no	1.511(2)	1
38	C6	H6A	Unknown	no	0.99(1)	1
39	C6	H6B	Unknown	no	0.98(1)	1
40	C7	C8	Unknown	no	1.525(1)	1
41	C7	H7A	Unknown	no	0.98(2)	1
42	C7	H7B	Unknown	no	0.97(2)	1
43	C8	C9	Unknown	no	1.524(2)	1
44	C8	H8A	Unknown	no	0.98(2)	1
45	C8	H8B	Unknown	no	1.00(1)	1
46	C9	C10	Unknown	no	1.525(2)	1
47	C9	H9A	Unknown	no	0.99(2)	1
48	C9	H9B	Unknown	no	0.99(2)	1
49	C10	H10A	Unknown	no	1.00(2)	1
50	C10	H10B	Unknown	no	0.97(2)	1
51	C10	H10C	Unknown	no	0.98(2)	1

Figure 2.18 Crystal structure parameters for **D3**.

Space Group: P -1; Cell Lengths: **a** 7.2228(4) **b** 9.2274(6) **c** 9.3317(6); Cell Angles: **α** 63.944(3) **β** 89.954(4) **γ** 89.959(3); Cell Volume: 558.725; Z, Z′: 1, 0; R-Factor (%): 4.63.

Atoms

Number	Label	Charge	SybylType	Xfrac + ESD	Yfrac + ESD	Zfrac + ESD	Symm. op.
1	O1	0	O.3	0.85889(17)	0.67710(13)	0.39634(14)	x,y,z
2	C1	0	C.2	0.4238(2)	0.46337(18)	0.5513(2)	x,y,z
3	C2	0	C.2	0.4158(3)	0.46276(19)	0.7037(2)	x,y,z
4	C3	0	C.2	0.5536(3)	0.5351(2)	0.7491(2)	x,y,z
5	C4	0	C.2	0.7062(3)	0.60915(19)	0.6491(2)	x,y,z
6	C5	0	C.2	0.7178(3)	0.60987(19)	0.5020(2)	x,y,z
7	C6	0	C.3	1.0085(3)	0.7472(2)	0.4461(2)	x,y,z
8	C7	0	C.3	1.1461(3)	0.8164(2)	0.3108(2)	x,y,z
9	C8	0	C.3	1.3049(3)	0.9007(2)	0.3511(2)	x,y,z
10	C9	0	C.3	1.4463(3)	0.9727(2)	0.2170(2)	x,y,z
11	C10	0	C.3	1.6036(3)	1.0608(2)	0.2546(2)	x,y,z
12	C11	0	C.3	1.7421(3)	1.1358(2)	0.1185(2)	x,y,z
13	C12	0	C.3	1.8993(3)	1.2253(2)	0.1541(2)	x,y,z
14	C13	0	C.3	2.0393(3)	1.2953(3)	0.0189(3)	x,y,z
15	H2	0	H	0.310(3)	0.4183(19)	0.766(2)	x,y,z
16	H3	0	H	0.544(2)	0.5298(19)	0.854(2)	x,y,z
17	H4	0	H	0.803(3)	0.659(2)	0.689(2)	x,y,z
18	H6A	0	H	1.066(2)	0.662(2)	0.545(2)	x,y,z
19	H6B	0	H	0.959(2)	0.8349(19)	0.471(2)	x,y,z
20	H7A	0	H	1.077(3)	0.898(2)	0.213(2)	x,y,z
21	H7B	0	H	1.191(3)	0.728(2)	0.288(2)	x,y,z
22	H8A	0	H	1.252(2)	0.9875(18)	0.373(2)	x,y,z
23	H8B	0	H	1.370(3)	0.825(2)	0.449(3)	x,y,z
24	H9A	0	H	1.381(3)	1.055(2)	0.117(3)	x,y,z
25	H9B	0	H	1.494(3)	0.886(2)	0.194(2)	x,y,z
26	H10A	0	H	1.549(2)	1.1458(19)	0.2791(19)	x,y,z
27	H10B	0	H	1.669(3)	0.985(2)	0.350(3)	x,y,z
28	H11A	0	H	1.671(3)	1.212(2)	0.025(3)	x,y,z
29	H11B	0	H	1.791(2)	1.050(2)	0.090(2)	x,y,z
30	H12A	0	H	1.844(3)	1.313(2)	0.178(2)	x,y,z
31	H12B	0	H	1.964(3)	1.151(2)	0.252(3)	x,y,z
32	H13A	0	H	2.092(3)	1.209(2)	-0.001(2)	x,y,z
33	H13B	0	H	2.145(3)	1.350(3)	0.041(3)	x,y,z
34	H13C	0	H	1.979(3)	1.374(2)	-0.074(3)	x,y,z
35	O1	0	O.3	0.14111(17)	0.32290(13)	0.60366(14)	1-x,1-y,1-z
36	C1	0	C.2	0.5762(2)	0.53663(18)	0.4487(2)	1-x,1-y,1-z
37	C2	0	C.2	0.5842(3)	0.53724(19)	0.2963(2)	1-x,1-y,1-z
38	C3	0	C.2	0.4464(3)	0.4649(2)	0.2509(2)	1-x,1-y,1-z
39	C4	0	C.2	0.2938(3)	0.39085(19)	0.3509(2)	1-x,1-y,1-z
40	C5	0	C.2	0.2822(3)	0.39013(19)	0.4980(2)	1-x,1-y,1-z
41	C6	0	C.3	-0.0085(3)	0.2528(2)	0.5539(2)	1-x,1-y,1-z
42	C7	0	C.3	-0.1461(3)	0.1836(2)	0.6892(2)	1-x,1-y,1-z
43	C8	0	C.3	-0.3049(3)	0.0993(2)	0.6489(2)	1-x,1-y,1-z
44	C9	0	C.3	-0.4463(3)	0.0273(2)	0.7830(2)	1-x,1-y,1-z
45	C10	0	C.3	-0.6036(3)	-0.0608(2)	0.7454(2)	1-x,1-y,1-z
46	C11	0	C.3	-0.7421(3)	-0.1358(2)	0.8815(2)	1-x,1-y,1-z
47	C12	0	C.3	-0.8993(3)	-0.2253(2)	0.8459(2)	1-x,1-y,1-z
48	C13	0	C.3	-1.0393(3)	-0.2953(3)	0.9811(3)	1-x,1-y,1-z
49	H2	0	H	0.690(3)	0.5817(19)	0.234(2)	1-x,1-y,1-z
50	H3	0	H	0.456(2)	0.4702(19)	0.146(2)	1-x,1-y,1-z
51	H4	0	H	0.197(3)	0.341(2)	0.311(2)	1-x,1-y,1-z
52	H6A	0	H	-0.066(2)	0.338(2)	0.455(2)	1-x,1-y,1-z
53	H6B	0	H	0.041(2)	0.1651(19)	0.529(2)	1-x,1-y,1-z
54	H7A	0	H	-0.077(3)	0.102(2)	0.787(2)	1-x,1-y,1-z
55	H7B	0	H	-0.191(3)	0.272(2)	0.712(2)	1-x,1-y,1-z
56	H8A	0	H	-0.252(2)	0.0125(18)	0.627(2)	1-x,1-y,1-z
57	H8B	0	H	-0.370(3)	0.175(2)	0.551(3)	1-x,1-y,1-z
58	H9A	0	H	-0.381(3)	-0.055(2)	0.883(3)	1-x,1-y,1-z
59	H9B	0	H	-0.494(3)	0.114(2)	0.806(2)	1-x,1-y,1-z
60	H10A	0	H	-0.549(2)	-0.1458(19)	0.7209(19)	1-x,1-y,1-z
61	H10B	0	H	-0.669(3)	0.015(2)	0.650(3)	1-x,1-y,1-z
62	H11A	0	H	-0.671(3)	-0.212(2)	0.975(3)	1-x,1-y,1-z
63	H11B	0	H	-0.791(2)	-0.050(2)	0.910(2)	1-x,1-y,1-z
64	H12A	0	H	-0.844(3)	-0.313(2)	0.822(2)	1-x,1-y,1-z
65	H12B	0	H	-0.964(3)	-0.151(2)	0.748(3)	1-x,1-y,1-z
66	H13A	0	H	-1.092(3)	-0.209(2)	1.001(2)	1-x,1-y,1-z
67	H13B	0	H	-1.145(3)	-0.350(3)	0.959(3)	1-x,1-y,1-z
68	H13C	0	H	-0.979(3)	-0.374(2)	1.074(3)	1-x,1-y,1-z

Bonds

Number	Atom1	Atom2	Type	Polymeric	Length	SybylType
1	O1	C5	Unknown	no	1.363(2)	1
2	O1	C6	Unknown	no	1.438(3)	1
3	C1	C2	Unknown	no	1.421(3)	un
4	C1	C1	Unknown	no	1.420(2)	un
5	C1	C5	Unknown	no	1.431(3)	un
6	C2	C3	Unknown	no	1.366(3)	un
7	C2	H2	Unknown	no	0.94(2)	1
8	C3	C4	Unknown	no	1.411(3)	un
9	C3	H3	Unknown	no	0.96(2)	1
10	C4	C5	Unknown	no	1.372(3)	un
11	C4	H4	Unknown	no	1.00(2)	1
12	C5	C1	Unknown	no	1.431(3)	un
13	C6	C7	Unknown	no	1.510(3)	1
14	C6	H6A	Unknown	no	1.00(1)	1
15	C6	H6B	Unknown	no	1.00(2)	1
16	C7	C8	Unknown	no	1.523(3)	1
17	C7	H7A	Unknown	no	1.02(2)	1
18	C7	H7B	Unknown	no	0.98(2)	1
19	C8	C9	Unknown	no	1.523(3)	1
20	C8	H8A	Unknown	no	0.99(2)	1
21	C8	H8B	Unknown	no	0.99(2)	1
22	C9	C10	Unknown	no	1.526(3)	1
23	C9	H9A	Unknown	no	1.02(2)	1
24	C9	H9B	Unknown	no	0.98(2)	1
25	C10	C11	Unknown	no	1.523(3)	1
26	C10	H10A	Unknown	no	0.99(2)	1
27	C10	H10B	Unknown	no	0.98(2)	1
28	C11	C12	Unknown	no	1.525(3)	1
29	C11	H11A	Unknown	no	0.99(2)	1
30	C11	H11B	Unknown	no	1.00(2)	1
31	C12	C13	Unknown	no	1.521(3)	1
32	C12	H12A	Unknown	no	1.01(2)	1
33	C12	H12B	Unknown	no	0.99(2)	1
34	C13	H13A	Unknown	no	0.97(2)	1
35	C13	H13B	Unknown	no	0.99(3)	1
36	C13	H13C	Unknown	no	0.96(2)	1
37	O1	C5	Unknown	no	1.363(2)	1
38	O1	C6	Unknown	no	1.438(3)	1
39	C1	C2	Unknown	no	1.421(3)	un
40	C2	C3	Unknown	no	1.366(3)	un
41	C2	H2	Unknown	no	0.94(2)	1
42	C3	C4	Unknown	no	1.411(3)	un
43	C3	H3	Unknown	no	0.96(2)	1
44	C4	C5	Unknown	no	1.372(3)	un
45	C4	H4	Unknown	no	1.00(2)	1
46	C6	C7	Unknown	no	1.510(3)	1
47	C6	H6A	Unknown	no	1.00(1)	1
48	C6	H6B	Unknown	no	1.00(2)	1
49	C7	C8	Unknown	no	1.523(3)	1
50	C7	H7A	Unknown	no	1.02(2)	1
51	C7	H7B	Unknown	no	0.98(2)	1
52	C8	C9	Unknown	no	1.523(3)	1
53	C8	H8A	Unknown	no	0.99(2)	1
54	C8	H8B	Unknown	no	0.99(2)	1
55	C9	C10	Unknown	no	1.526(3)	1
56	C9	H9A	Unknown	no	1.02(2)	1
57	C9	H9B	Unknown	no	0.98(2)	1
58	C10	C11	Unknown	no	1.523(3)	1
59	C10	H10A	Unknown	no	0.99(2)	1
60	C10	H10B	Unknown	no	0.98(2)	1
61	C11	C12	Unknown	no	1.525(3)	1
62	C11	H11A	Unknown	no	0.99(2)	1
63	C11	H11B	Unknown	no	1.00(2)	1
64	C12	C13	Unknown	no	1.521(3)	1
65	C12	H12A	Unknown	no	1.01(2)	1
66	C12	H12B	Unknown	no	0.99(2)	1
67	C13	H13A	Unknown	no	0.97(2)	1
68	C13	H13B	Unknown	no	0.99(3)	1
69	C13	H13C	Unknown	no	0.96(2)	1

Figure 2.19 Crystal structure parameters for **D6**.

Space Group: P -1; Cell Lengths: **a** 7.385(5) **b** 9.430(6) **c** 10.698(7); Cell Angles: **α** 67.731(13) **β** 78.411(14) **γ** 88.388(13); Cell Volume: 674.445; Z, Z': 1, 0; R-Factor (%): 6.11.

Atoms

Number	Label	Charge	SybylType	Xfrac + ESD	Yfrac + ESD	Zfrac + ESD	Symm. op.
1	O1	0	O.3	0.81097(16)	0.41348(13)	0.65199(12)	x,y,z
2	C1	0	C.2	0.4332(2)	0.54830(18)	0.46783(15)	x,y,z
3	C2	0	C.2	0.4204(2)	0.69954(18)	0.46515(17)	x,y,z
4	H2A	0	H	0.3326	0.7636	0.4221	x,y,z
5	C3	0	C.2	0.5357(2)	0.75237(19)	0.52519(17)	x,y,z
6	H3A	0	H	0.5253	0.8526	0.5235	x,y,z
7	C4	0	C.2	0.6697(2)	0.65974(19)	0.58957(17)	x,y,z
8	H4A	0	H	0.748	0.6985	0.6298	x,y,z
9	C5	0	C.2	0.6856(2)	0.51330(19)	0.59342(16)	x,y,z
10	C6	0	C.3	0.9383(2)	0.4687(2)	0.71192(18)	x,y,z
11	H6A	0	H	0.8697	0.5003	0.7847	x,y,z
12	H6B	0	H	1.0136	0.5575	0.6411	x,y,z
13	C7	0	C.3	1.0611(2)	0.3402(2)	0.77143(18)	x,y,z
14	H7A	0	H	1.1328	0.3125	0.6971	x,y,z
15	H7B	0	H	0.984	0.2498	0.8376	x,y,z
16	C8	0	C.3	1.1935(2)	0.3869(2)	0.84383(18)	x,y,z
17	H8A	0	H	1.2697	0.4777	0.7774	x,y,z
18	H8B	0	H	1.1211	0.415	0.9176	x,y,z
19	C9	0	C.3	1.3200(2)	0.2602(2)	0.90528(18)	x,y,z
20	H9A	0	H	1.3952	0.2346	0.8309	x,y,z
21	H9B	0	H	1.2436	0.1683	0.9692	x,y,z
22	C10	0	C.3	1.4486(2)	0.3034(2)	0.98209(19)	x,y,z
23	H10A	0	H	1.5243	0.3958	0.9184	x,y,z
24	H10B	0	H	1.3734	0.3282	1.057	x,y,z
25	C11	0	C.3	1.5757(2)	0.1772(2)	1.04245(19)	x,y,z
26	H11A	0	H	1.6515	0.1531	0.9674	x,y,z
27	H11B	0	H	1.4999	0.0846	1.1054	x,y,z
28	C12	0	C.3	1.7038(2)	0.2192(2)	1.12076(19)	x,y,z
29	H12A	0	H	1.7814	0.3107	1.0573	x,y,z
30	H12B	0	H	1.6281	0.2453	1.1946	x,y,z
31	C13	0	C.3	1.8282(2)	0.0921(2)	1.18341(18)	x,y,z
32	H13A	0	H	1.9031	0.0655	1.1096	x,y,z
33	H13B	0	H	1.7505	0.001	1.2473	x,y,z
34	C14	0	C.3	1.9573(3)	0.1337(2)	1.26063(19)	x,y,z
35	H14A	0	H	2.0331	0.2263	1.1976	x,y,z
36	H14B	0	H	1.8827	0.1574	1.3364	x,y,z
37	C15	0	C.3	2.0843(3)	0.0062(2)	1.3193(2)	x,y,z
38	H15A	0	H	2.1645	0.0396	1.3655	x,y,z
39	H15B	0	H	2.1591	-0.0176	1.2449	x,y,z
40	H15C	0	H	2.0103	-0.0846	1.3848	x,y,z
41	O1	0	O.3	0.18903(16)	0.58652(13)	0.34801(12)	1-x,1-y,1-z
42	C1	0	C.2	0.5668(2)	0.45170(18)	0.53217(15)	1-x,1-y,1-z
43	C2	0	C.2	0.5796(2)	0.30046(18)	0.53485(17)	1-x,1-y,1-z
44	H2A	0	H	0.6674	0.2364	0.5779	1-x,1-y,1-z
45	C3	0	C.2	0.4643(2)	0.24763(19)	0.47481(17)	1-x,1-y,1-z
46	H3A	0	H	0.4747	0.1474	0.4765	1-x,1-y,1-z
47	C4	0	C.2	0.3303(2)	0.34026(19)	0.41043(17)	1-x,1-y,1-z
48	H4A	0	H	0.252	0.3015	0.3702	1-x,1-y,1-z
49	C5	0	C.2	0.3144(2)	0.48670(19)	0.40658(16)	1-x,1-y,1-z
50	C6	0	C.3	0.0617(2)	0.5313(2)	0.28808(18)	1-x,1-y,1-z
51	H6A	0	H	0.1303	0.4997	0.2153	1-x,1-y,1-z
52	H6B	0	H	-0.0136	0.4425	0.3589	1-x,1-y,1-z
53	C7	0	C.3	-0.0611(2)	0.6598(2)	0.22857(18)	1-x,1-y,1-z
54	H7A	0	H	-0.1328	0.6875	0.3029	1-x,1-y,1-z
55	H7B	0	H	0.016	0.7502	0.1624	1-x,1-y,1-z
56	C8	0	C.3	-0.1935(2)	0.6131(2)	0.15617(18)	1-x,1-y,1-z
57	H8A	0	H	-0.2697	0.5223	0.2226	1-x,1-y,1-z
58	H8B	0	H	-0.1211	0.585	0.0824	1-x,1-y,1-z
59	C9	0	C.3	-0.3200(2)	0.7398(2)	0.09472(18)	1-x,1-y,1-z
60	H9A	0	H	-0.3952	0.7654	0.1691	1-x,1-y,1-z
61	H9B	0	H	-0.2436	0.8317	0.0308	1-x,1-y,1-z
62	C10	0	C.3	-0.4486(2)	0.6966(2)	0.01791(19)	1-x,1-y,1-z
63	H10A	0	H	-0.5243	0.6042	0.0816	1-x,1-y,1-z
64	H10B	0	H	-0.3734	0.6718	-0.057	1-x,1-y,1-z
65	C11	0	C.3	-0.5757(2)	0.8228(2)	-0.04245(19)	1-x,1-y,1-z
66	H11A	0	H	-0.6515	0.8469	0.0326	1-x,1-y,1-z
67	H11B	0	H	-0.4999	0.9154	-0.1054	1-x,1-y,1-z
68	C12	0	C.3	-0.7038(2)	0.7808(2)	-0.12076(19)	1-x,1-y,1-z
69	H12A	0	H	-0.7814	0.6893	-0.0573	1-x,1-y,1-z
70	H12B	0	H	-0.6281	0.7547	-0.1946	1-x,1-y,1-z
71	C13	0	C.3	-0.8282(2)	0.9079(2)	-0.18341(18)	1-x,1-y,1-z
72	H13A	0	H	-0.9031	0.9345	-0.1096	1-x,1-y,1-z
73	H13B	0	H	-0.7505	0.999	-0.2473	1-x,1-y,1-z
74	C14	0	C.3	-0.9573(3)	0.8663(2)	-0.26063(19)	1-x,1-y,1-z
75	H14A	0	H	-1.0331	0.7737	-0.1976	1-x,1-y,1-z
76	H14B	0	H	-0.8827	0.8426	-0.3364	1-x,1-y,1-z
77	C15	0	C.3	-1.0843(3)	0.9938(2)	-0.3193(2)	1-x,1-y,1-z
78	H15A	0	H	-1.1645	0.9604	-0.3655	1-x,1-y,1-z
79	H15B	0	H	-1.1591	1.0176	-0.2449	1-x,1-y,1-z
80	H15C	0	H	-1.0103	1.0846	-0.3848	1-x,1-y,1-z

Bonds

Number	Atom1	Atom2	Type	Polymeric	Length	SybylType
1	O1	C5	Unknown	no	1.369(2)	1
2	O1	C6	Unknown	no	1.445(3)	1
3	C1	C2	Unknown	no	1.416(3)	un
4	C1	C1	Unknown	no	1.423(2)	un
5	C1	C5	Unknown	no	1.444(3)	un
6	C2	H2A	Unknown	no	0.940(2)	1
7	C2	C3	Unknown	no	1.368(3)	un
8	C3	H3A	Unknown	no	0.940(2)	1
9	C3	C4	Unknown	no	1.409(2)	un
10	C4	H4A	Unknown	no	0.940(2)	1
11	C4	C5	Unknown	no	1.368(3)	un
12	C5	C1	Unknown	no	1.444(3)	un
13	C6	H6A	Unknown	no	0.980(2)	1
14	C6	H6B	Unknown	no	0.980(1)	1
15	C6	C7	Unknown	no	1.510(2)	1
16	C7	H7A	Unknown	no	0.981(2)	1
17	C7	H7B	Unknown	no	0.980(2)	1
18	C7	C8	Unknown	no	1.529(3)	1
19	C8	H8A	Unknown	no	0.980(2)	1
20	C8	H8B	Unknown	no	0.980(2)	1
21	C8	C9	Unknown	no	1.524(2)	1
22	C9	H9A	Unknown	no	0.980(2)	1
23	C9	H9B	Unknown	no	0.980(2)	1
24	C9	C10	Unknown	no	1.527(3)	1
25	C10	H10A	Unknown	no	0.980(2)	1
26	C10	H10B	Unknown	no	0.980(2)	1
27	C10	C11	Unknown	no	1.521(2)	1
28	C11	H11A	Unknown	no	0.980(2)	1
29	C11	H11B	Unknown	no	0.980(2)	1
30	C11	C12	Unknown	no	1.531(3)	1
31	C12	H12A	Unknown	no	0.980(2)	1
32	C12	H12B	Unknown	no	0.979(2)	1
33	C12	C13	Unknown	no	1.519(2)	1
34	C13	H13A	Unknown	no	0.979(2)	1
35	C13	H13B	Unknown	no	0.980(2)	1
36	C13	C14	Unknown	no	1.526(3)	1
37	C14	H14A	Unknown	no	0.980(2)	1
38	C14	H14B	Unknown	no	0.981(2)	1
39	C14	C15	Unknown	no	1.523(3)	1
40	C15	H15A	Unknown	no	0.970(3)	1
41	C15	H15B	Unknown	no	0.970(2)	1
42	C15	H15C	Unknown	no	0.970(2)	1
43	O1	C5	Unknown	no	1.369(2)	1
44	O1	C6	Unknown	no	1.445(3)	1
45	C1	C2	Unknown	no	1.416(3)	un
46	C2	H2A	Unknown	no	0.940(2)	1
47	C2	C3	Unknown	no	1.368(3)	un
48	C3	H3A	Unknown	no	0.940(2)	1
49	C3	C4	Unknown	no	1.409(2)	un
50	C4	H4A	Unknown	no	0.940(2)	1
51	C4	C5	Unknown	no	1.368(3)	un
52	C6	H6A	Unknown	no	0.980(2)	1
53	C6	H6B	Unknown	no	0.980(1)	1
54	C6	C7	Unknown	no	1.510(2)	1
55	C7	H7A	Unknown	no	0.981(2)	1
56	C7	H7B	Unknown	no	0.980(2)	1
57	C7	C8	Unknown	no	1.529(3)	1
58	C8	H8A	Unknown	no	0.980(2)	1
59	C8	H8B	Unknown	no	0.980(2)	1
60	C8	C9	Unknown	no	1.524(2)	1
61	C9	H9A	Unknown	no	0.980(2)	1
62	C9	H9B	Unknown	no	0.980(2)	1
63	C9	C10	Unknown	no	1.527(3)	1
64	C10	H10A	Unknown	no	0.980(2)	1
65	C10	H10B	Unknown	no	0.980(2)	1
66	C10	C11	Unknown	no	1.521(2)	1
67	C11	H11A	Unknown	no	0.980(2)	1
68	C11	H11B	Unknown	no	0.980(2)	1
69	C11	C12	Unknown	no	1.531(3)	1
70	C12	H12A	Unknown	no	0.980(2)	1
71	C12	H12B	Unknown	no	0.979(2)	1
72	C12	C13	Unknown	no	1.519(2)	1
73	C13	H13A	Unknown	no	0.979(2)	1
74	C13	H13B	Unknown	no	0.980(2)	1
75	C13	C14	Unknown	no	1.526(3)	1
76	C14	H14A	Unknown	no	0.980(2)	1
77	C14	H14B	Unknown	no	0.981(2)	1
78	C14	C15	Unknown	no	1.523(3)	1
79	C15	H15A	Unknown	no	0.970(3)	1
80	C15	H15B	Unknown	no	0.970(2)	1
81	C15	H15C	Unknown	no	0.970(2)	1

Figure 2.20 Crystal structure parameters for **D8**.

Space Group: P $2_1/c$; Cell Lengths: **a** 9.2006(2) **b** 8.5041(2) **c** 8.6679(2); Cell Angles: **α** 90.00 **β** 94.442(1) **γ** 90.00; Cell Volume: 676.164; Z, Z′: 2, 0; R-Factor (%): 3.44.

Atoms

Number	Label	Charge	SybylType	Xfrac + ESD	Yfrac + ESD	Zfrac + ESD	Symm. op.
1	C1	0	C.2	0.42683(10)	0.49968(11)	0.52076(10)	x,y,z
2	C2	0	C.2	0.39324(11)	0.41211(11)	0.65447(11)	x,y,z
3	C3	0	C.2	0.50036(11)	0.33067(12)	0.73980(12)	x,y,z
4	C4	0	C.2	0.64443(11)	0.33219(12)	0.69566(12)	x,y,z
5	C5	0	C.2	0.68162(11)	0.41439(12)	0.56912(11)	x,y,z
6	O6	0	O.3	0.24932(7)	0.41622(8)	0.68368(8)	x,y,z
7	C7	0	C.3	0.20516(12)	0.34137(13)	0.82295(12)	x,y,z
8	C8	0	C.3	0.04239(12)	0.31812(16)	0.79549(15)	x,y,z
9	C9	0	C.3	0.24608(14)	0.44343(15)	0.96271(13)	x,y,z
10	H3	0	H	0.4794(13)	0.2738(14)	0.8296(14)	x,y,z
11	H4	0	H	0.7180(13)	0.2706(14)	0.7589(14)	x,y,z
12	H5	0	H	0.7814(13)	0.4154(13)	0.5399(13)	x,y,z
13	H7	0	H	0.2535(13)	0.2376(15)	0.8336(13)	x,y,z
14	H8A	0	H	0.0054(15)	0.2641(17)	0.8869(16)	x,y,z
15	H8B	0	H	-0.0090(16)	0.4207(18)	0.7828(17)	x,y,z
16	H8C	0	H	0.0177(16)	0.2530(17)	0.7003(17)	x,y,z
17	H9A	0	H	0.1951(15)	0.5458(18)	0.9513(15)	x,y,z
18	H9B	0	H	0.3553(16)	0.4649(16)	0.9752(15)	x,y,z
19	H9C	0	H	0.2183(15)	0.3906(17)	1.0573(17)	x,y,z
20	C1	0	C.2	0.57317(10)	0.50032(11)	0.47924(10)	1-x,1-y,1-z
21	C2	0	C.2	0.60676(11)	0.58789(11)	0.34553(11)	1-x,1-y,1-z
22	C3	0	C.2	0.49964(11)	0.66933(12)	0.26020(12)	1-x,1-y,1-z
23	C4	0	C.2	0.35557(11)	0.66781(12)	0.30434(12)	1-x,1-y,1-z
24	C5	0	C.2	0.31838(11)	0.58561(12)	0.43088(11)	1-x,1-y,1-z
25	O6	0	O.3	0.75068(7)	0.58378(8)	0.31632(8)	1-x,1-y,1-z
26	C7	0	C.3	0.79484(12)	0.65863(13)	0.17705(12)	1-x,1-y,1-z
27	C8	0	C.3	0.95761(12)	0.68188(16)	0.20451(15)	1-x,1-y,1-z
28	C9	0	C.3	0.75392(14)	0.55657(15)	0.03729(13)	1-x,1-y,1-z
29	H3	0	H	0.5206(13)	0.7262(14)	0.1704(14)	1-x,1-y,1-z
30	H4	0	H	0.2820(13)	0.7294(14)	0.2411(14)	1-x,1-y,1-z
31	H5	0	H	0.2186(13)	0.5846(13)	0.4601(13)	1-x,1-y,1-z
32	H7	0	H	0.7465(13)	0.7624(15)	0.1664(13)	1-x,1-y,1-z
33	H8A	0	H	0.9946(15)	0.7359(17)	0.1131(16)	1-x,1-y,1-z
34	H8B	0	H	1.0090(16)	0.5793(18)	0.2172(17)	1-x,1-y,1-z
35	H8C	0	H	0.9823(16)	0.7470(17)	0.2997(17)	1-x,1-y,1-z
36	H9A	0	H	0.8049(15)	0.4542(18)	0.0487(15)	1-x,1-y,1-z
37	H9B	0	H	0.6447(16)	0.5351(16)	0.0248(15)	1-x,1-y,1-z
38	H9C	0	H	0.7817(15)	0.6094(17)	-0.0573(17)	1-x,1-y,1-z

Bonds

Number	Atom1	Atom2	Type	Polymeric	Length	SybylType
1	C1	C2	Unknown	no	1.431(1)	un
2	C1	C1	Unknown	no	1.420(1)	un
3	C1	C5	Unknown	no	1.420(1)	un
4	C2	C3	Unknown	no	1.373(1)	un
5	C2	O6	Unknown	no	1.368(1)	1
6	C3	C4	Unknown	no	1.408(1)	un
7	C3	H3	Unknown	no	0.95(1)	1
8	C4	C5	Unknown	no	1.366(1)	un
9	C4	H4	Unknown	no	0.99(1)	1
10	C5	H5	Unknown	no	0.97(1)	1
11	C5	C1	Unknown	no	1.420(1)	un
12	O6	C7	Unknown	no	1.450(1)	1
13	C7	C8	Unknown	no	1.511(2)	1
14	C7	C9	Unknown	no	1.514(2)	1
15	C7	H7	Unknown	no	0.99(1)	1
16	C8	H8A	Unknown	no	1.00(1)	1
17	C8	H8B	Unknown	no	0.99(2)	1
18	C8	H8C	Unknown	no	1.01(1)	1
19	C9	H9A	Unknown	no	0.99(1)	1
20	C9	H9B	Unknown	no	1.02(1)	1
21	C9	H9C	Unknown	no	0.99(1)	1
22	C1	C2	Unknown	no	1.431(1)	un
23	C2	C3	Unknown	no	1.373(1)	un
24	C2	O6	Unknown	no	1.368(1)	1
25	C3	C4	Unknown	no	1.408(1)	un
26	C3	H3	Unknown	no	0.95(1)	1
27	C4	C5	Unknown	no	1.366(1)	un
28	C4	H4	Unknown	no	0.99(1)	1
29	C5	H5	Unknown	no	0.97(1)	1
30	O6	C7	Unknown	no	1.450(1)	1
31	C7	C8	Unknown	no	1.511(2)	1
32	C7	C9	Unknown	no	1.514(2)	1
33	C7	H7	Unknown	no	0.99(1)	1
34	C8	H8A	Unknown	no	1.00(1)	1
35	C8	H8B	Unknown	no	0.99(2)	1
36	C8	H8C	Unknown	no	1.01(1)	1
37	C9	H9A	Unknown	no	0.99(1)	1
38	C9	H9B	Unknown	no	1.02(1)	1
39	C9	H9C	Unknown	no	0.99(1)	1

Figure 2.21 Crystal structure parameters for **D9**.

Space Group: P -1; Cell Lengths: **a** 5.2230(10) **b** 7.840(2) **c** 11.132(3); Cell Angles: **α** 103.716(2) **β** 94.279(2) **γ** 93.858(3); Cell Volume: 439.901; Z, Z′: 1, 0; R-Factor (%): 4.04

Atoms

Number	Label	Charge	SybylType	Xfrac + ESD	Yfrac + ESD	Zfrac + ESD	Symm. op.
1	O1	0	O.2	0.6658(2)	0.95343(14)	0.37171(10)	x,y,z
2	O2	0	O.2	-0.0492(2)	0.57406(15)	0.22696(10)	x,y,z
3	N1	0	N.am	0.3111(3)	0.76166(17)	0.29649(12)	x,y,z
4	C1	0	C.2	0.5380(4)	0.8191(2)	0.37445(14)	x,y,z
5	C2	0	C.2	0.6140(3)	0.7095(2)	0.46148(14)	x,y,z
6	C3	0	C.2	0.4620(3)	0.5523(2)	0.45913(14)	x,y,z
7	C4	0	C.2	0.2369(4)	0.4977(2)	0.37680(14)	x,y,z
8	C5	0	C.2	0.1515(4)	0.6098(2)	0.29416(14)	x,y,z
9	C6	0	C.2	0.8315(4)	0.7607(2)	0.54319(15)	x,y,z
10	C7	0	C.2	0.0937(4)	0.3425(2)	0.37541(14)	x,y,z
11	C8	0	C.3	0.2218(4)	0.8717(2)	0.21248(15)	x,y,z
12	C9	0	C.3	0.2635(4)	0.7941(2)	0.07702(14)	x,y,z
13	C10	0	C.3	0.5441(4)	0.7888(2)	0.05117(14)	x,y,z
14	C11	0	C.3	0.5759(4)	0.7142(2)	-0.08591(15)	x,y,z
15	H10B	0	H	0.629(4)	0.718(2)	0.1006(17)	x,y,z
16	H6	0	H	0.930(4)	0.866(2)	0.5443(16)	x,y,z
17	H11C	0	H	0.761(5)	0.715(3)	-0.1003(18)	x,y,z
18	H8B	0	H	0.323(4)	0.985(3)	0.2448(16)	x,y,z
19	H11A	0	H	0.494(4)	0.594(3)	-0.1143(18)	x,y,z
20	H9A	0	H	0.179(4)	0.867(2)	0.0282(16)	x,y,z
21	H9B	0	H	0.176(4)	0.677(3)	0.0523(17)	x,y,z
22	H7	0	H	-0.063(4)	0.307(2)	0.3192(18)	x,y,z
23	H8A	0	H	0.040(4)	0.883(2)	0.2239(16)	x,y,z
24	H10A	0	H	0.635(4)	0.909(3)	0.0783(16)	x,y,z
25	H11B	0	H	0.491(5)	0.787(3)	-0.1390(19)	x,y,z
26	O1	0	O.2	0.3342(2)	0.04657(14)	0.62829(10)	1-x,1-y,1-z
27	O2	0	O.2	1.0492(2)	0.42594(15)	0.77304(10)	1-x,1-y,1-z
28	N1	0	N.am	0.6889(3)	0.23834(17)	0.70351(12)	1-x,1-y,1-z
29	C1	0	C.2	0.4620(4)	0.1809(2)	0.62555(14)	1-x,1-y,1-z
30	C2	0	C.2	0.3860(3)	0.2905(2)	0.53852(14)	1-x,1-y,1-z
31	C3	0	C.2	0.5380(3)	0.4477(2)	0.54087(14)	1-x,1-y,1-z
32	C4	0	C.2	0.7631(4)	0.5023(2)	0.62320(14)	1-x,1-y,1-z
33	C5	0	C.2	0.8485(4)	0.3902(2)	0.70584(14)	1-x,1-y,1-z
34	C6	0	C.2	0.1685(4)	0.2393(2)	0.45681(15)	1-x,1-y,1-z
35	C7	0	C.2	0.9063(4)	0.6575(2)	0.62459(14)	1-x,1-y,1-z
36	C8	0	C.3	0.7782(4)	0.1283(2)	0.78752(15)	1-x,1-y,1-z
37	C9	0	C.3	0.7365(4)	0.2059(2)	0.92298(14)	1-x,1-y,1-z
38	C10	0	C.3	0.4559(4)	0.2112(2)	0.94883(14)	1-x,1-y,1-z
39	C11	0	C.3	0.4241(4)	0.2858(2)	1.08591(15)	1-x,1-y,1-z
40	H10B	0	H	0.371(4)	0.282(2)	0.8994(17)	1-x,1-y,1-z
41	H6	0	H	0.070(4)	0.134(2)	0.4557(16)	1-x,1-y,1-z
42	H11C	0	H	0.239(5)	0.285(3)	1.1003(18)	1-x,1-y,1-z
43	H8B	0	H	0.677(4)	0.015(3)	0.7552(16)	1-x,1-y,1-z
44	H11A	0	H	0.506(4)	0.406(3)	1.1143(18)	1-x,1-y,1-z
45	H9A	0	H	0.821(4)	0.133(2)	0.9718(16)	1-x,1-y,1-z
46	H9B	0	H	0.824(4)	0.323(3)	0.9477(17)	1-x,1-y,1-z
47	H7	0	H	1.063(4)	0.693(2)	0.6808(18)	1-x,1-y,1-z
48	H8A	0	H	0.960(4)	0.117(2)	0.7761(16)	1-x,1-y,1-z
49	H10A	0	H	0.365(4)	0.091(3)	0.9217(16)	1-x,1-y,1-z
50	H11B	0	H	0.509(5)	0.213(3)	1.1390(19)	1-x,1-y,1-z

Bonds

Number	Atom1	Atom2	Type	Polymeric	Length	SybylType
1	O1	C1	Unknown	no	1.216(2)	2
2	O2	C5	Unknown	no	1.217(2)	2
3	N1	C1	Unknown	no	1.396(2)	un
4	N1	C5	Unknown	no	1.401(2)	un
5	N1	C8	Unknown	no	1.486(2)	1
6	C1	C2	Unknown	no	1.489(2)	un
7	C2	C3	Unknown	no	1.414(2)	un
8	C2	C6	Unknown	no	1.375(2)	un
9	C3	C4	Unknown	no	1.411(2)	un
10	C3	C3	Unknown	no	1.415(2)	un
11	C4	C5	Unknown	no	1.481(3)	un
12	C4	C7	Unknown	no	1.381(2)	un
13	C6	H6	Unknown	no	0.94(2)	1
14	C6	C7	Unknown	no	1.402(3)	un
15	C7	H7	Unknown	no	0.97(2)	1
16	C7	C6	Unknown	no	1.402(3)	un
17	C8	C9	Unknown	no	1.524(2)	1
18	C8	H8B	Unknown	no	0.98(2)	1
19	C8	H8A	Unknown	no	0.97(2)	1
20	C9	C10	Unknown	no	1.516(3)	1
21	C9	H9A	Unknown	no	0.98(2)	1
22	C9	H9B	Unknown	no	0.97(2)	1
23	C10	C11	Unknown	no	1.525(2)	1
24	C10	H10B	Unknown	no	0.97(2)	1
25	C10	H10A	Unknown	no	0.99(2)	1
26	C11	H11C	Unknown	no	0.99(3)	1
27	C11	H11A	Unknown	no	0.98(2)	1
28	C11	H11B	Unknown	no	1.01(3)	1
29	O1	C1	Unknown	no	1.216(2)	2
30	O2	C5	Unknown	no	1.217(2)	2
31	N1	C1	Unknown	no	1.396(2)	un
32	N1	C5	Unknown	no	1.401(2)	un
33	N1	C8	Unknown	no	1.486(2)	1
34	C1	C2	Unknown	no	1.489(2)	un
35	C2	C3	Unknown	no	1.414(2)	un
36	C2	C6	Unknown	no	1.375(2)	un
37	C3	C4	Unknown	no	1.411(2)	un
38	C4	C5	Unknown	no	1.481(3)	un
39	C4	C7	Unknown	no	1.381(2)	un
40	C6	H6	Unknown	no	0.94(2)	1
41	C7	H7	Unknown	no	0.97(2)	1
42	C8	C9	Unknown	no	1.524(2)	1
43	C8	H8B	Unknown	no	0.98(2)	1
44	C8	H8A	Unknown	no	0.97(2)	1
45	C9	C10	Unknown	no	1.516(3)	1
46	C9	H9A	Unknown	no	0.98(2)	1
47	C9	H9B	Unknown	no	0.97(2)	1
48	C10	C11	Unknown	no	1.525(2)	1
49	C10	H10B	Unknown	no	0.97(2)	1
50	C10	H10A	Unknown	no	0.99(2)	1
51	C11	H11C	Unknown	no	0.99(3)	1
52	C11	H11A	Unknown	no	0.98(2)	1
53	C11	H11B	Unknown	no	1.01(3)	1

Figure 2.22 Crystal structure parameters for **N1**.

Space Group: P -1; Cell Lengths: **a** 4.6101(11) **b** 6.5900(15) **c** 27.733(7); Cell Angles: **α** 93.316(9) **β** 94.533(8) **γ** 104.5980(14); Cell Volume: 810.15; Z, Z': 1, 0; R-Factor (%): 5.41.

Atoms

Number	Label	Charge	SybylType	Xfrac + ESD	Yfrac + ESD	Zfrac + ESD	Symm. op.
1	O1	0	O.2	0.5704(3)	0.6039(2)	0.65097(5)	x,y,z
2	O2	0	O.2	0.9641(3)	0.1237(2)	0.57430(5)	x,y,z
3	N1	0	N.am	0.7704(4)	0.3657(3)	0.61283(6)	x,y,z
4	C1	0	C.2	0.6112(5)	0.5207(3)	0.61298(7)	x,y,z
5	C2	0	C.2	0.5009(4)	0.5766(3)	0.56552(7)	x,y,z
6	C3	0	C.2	0.5529(4)	0.4722(3)	0.52257(7)	x,y,z
7	C4	0	C.2	0.7088(4)	0.3143(3)	0.52414(7)	x,y,z
8	C5	0	C.2	0.8246(5)	0.2575(3)	0.57134(7)	x,y,z
9	C6	0	C.2	0.3474(5)	0.7303(3)	0.56312(8)	x,y,z
10	C7	0	C.2	0.7575(5)	0.2154(3)	0.48189(8)	x,y,z
11	C8	0	C.3	0.8846(5)	0.3113(3)	0.66017(7)	x,y,z
12	H8A	0	H	0.9652	0.442	0.6817	x,y,z
13	H8B	0	H	1.0529	0.2463	0.6555	x,y,z
14	C9	0	C.3	0.6457(5)	0.1609(3)	0.68500(7)	x,y,z
15	H9A	0	H	0.5219	0.2412	0.7015	x,y,z
16	H9B	0	H	0.5114	0.0582	0.6602	x,y,z
17	C10	0	C.3	0.7869(5)	0.0437(3)	0.72193(7)	x,y,z
18	H10A	0	H	0.9223	0.1471	0.7464	x,y,z
19	H10B	0	H	0.9109	-0.0358	0.7052	x,y,z
20	C11	0	C.3	0.5559(5)	-0.1080(3)	0.74769(7)	x,y,z
21	H11A	0	H	0.4588	-0.0264	0.7694	x,y,z
22	H11B	0	H	0.3977	-0.1938	0.7233	x,y,z
23	C12	0	C.3	0.6924(5)	-0.2535(3)	0.77729(7)	x,y,z
24	H12A	0	H	0.8475	-0.1673	0.8021	x,y,z
25	H12B	0	H	0.7943	-0.3319	0.7556	x,y,z
26	C13	0	C.3	0.4649(5)	-0.4104(3)	0.80249(7)	x,y,z
27	H13A	0	H	0.3075	-0.4952	0.7778	x,y,z
28	H13B	0	H	0.3662	-0.3324	0.8248	x,y,z
29	C14	0	C.3	0.6053(5)	-0.5578(3)	0.83112(8)	x,y,z
30	H14A	0	H	0.6977	-0.6392	0.8085	x,y,z
31	H14B	0	H	0.7682	-0.4725	0.8549	x,y,z
32	C15	0	C.3	0.3825(5)	-0.7105(3)	0.85804(7)	x,y,z
33	H15A	0	H	0.2185	-0.7951	0.8344	x,y,z
34	H15B	0	H	0.2917	-0.6293	0.8809	x,y,z
35	C16	0	C.3	0.5249(5)	-0.8583(3)	0.88611(7)	x,y,z
36	H16A	0	H	0.6137	-0.9407	0.8632	x,y,z
37	H16B	0	H	0.6904	-0.7737	0.9095	x,y,z
38	C17	0	C.3	0.3029(5)	-1.0095(3)	0.91348(8)	x,y,z
39	H17A	0	H	0.2227	-0.9273	0.9377	x,y,z
40	H17B	0	H	0.1317	-1.0884	0.8903	x,y,z
41	C18	0	C.3	0.4409(5)	-1.1651(3)	0.93925(8)	x,y,z
42	H18A	0	H	0.6086	-1.0865	0.9631	x,y,z
43	H18B	0	H	0.5258	-1.2449	0.9152	x,y,z
44	C19	0	C.3	0.2148(6)	-1.3190(4)	0.96540(8)	x,y,z
45	H19A	0	H	0.1351	-1.2412	0.9901	x,y,z
46	H19B	0	H	0.3145	-1.4165	0.981	x,y,z
47	H19C	0	H	0.0492	-1.3984	0.942	x,y,z
48	H6	0	H	0.315(5)	0.801(3)	0.5935(8)	x,y,z
49	H7	0	H	0.872(5)	0.111(4)	0.4824(7)	x,y,z
50	O1	0	O.2	0.4296(3)	0.3961(2)	0.34903(5)	1-x,1-y,1-z
51	O2	0	O.2	0.0359(3)	0.8763(2)	0.42570(5)	1-x,1-y,1-z
52	N1	0	N.am	0.2296(4)	0.6343(3)	0.38717(6)	1-x,1-y,1-z
53	C1	0	C.2	0.3888(5)	0.4793(3)	0.38702(7)	1-x,1-y,1-z
54	C2	0	C.2	0.4991(4)	0.4234(3)	0.43448(7)	1-x,1-y,1-z
55	C3	0	C.2	0.4471(4)	0.5278(3)	0.47743(7)	1-x,1-y,1-z
56	C4	0	C.2	0.2912(4)	0.6857(3)	0.47586(7)	1-x,1-y,1-z
57	C5	0	C.2	0.1754(5)	0.7425(3)	0.42866(7)	1-x,1-y,1-z
58	C6	0	C.2	0.6526(5)	0.2697(3)	0.43688(8)	1-x,1-y,1-z
59	C7	0	C.2	0.2425(5)	0.7846(3)	0.51811(8)	1-x,1-y,1-z
60	C8	0	C.3	0.1154(5)	0.6887(3)	0.33983(7)	1-x,1-y,1-z
61	H8A	0	H	0.0348	0.558	0.3183	1-x,1-y,1-z
62	H8B	0	H	-0.0529	0.7537	0.3445	1-x,1-y,1-z
63	C9	0	C.3	0.3543(5)	0.8391(3)	0.31500(7)	1-x,1-y,1-z
64	H9A	0	H	0.4781	0.7588	0.2985	1-x,1-y,1-z
65	H9B	0	H	0.4886	0.9418	0.3398	1-x,1-y,1-z
66	C10	0	C.3	0.2131(5)	0.9563(3)	0.27807(7)	1-x,1-y,1-z
67	H10A	0	H	0.0777	0.8529	0.2536	1-x,1-y,1-z
68	H10B	0	H	0.0891	1.0358	0.2948	1-x,1-y,1-z
69	C11	0	C.3	0.4441(5)	1.1080(3)	0.25231(7)	1-x,1-y,1-z
70	H11A	0	H	0.5412	1.0264	0.2306	1-x,1-y,1-z
71	H11B	0	H	0.6023	1.1938	0.2767	1-x,1-y,1-z
72	C12	0	C.3	0.3076(5)	1.2535(3)	0.22271(7)	1-x,1-y,1-z
73	H12A	0	H	0.1525	1.1673	0.1979	1-x,1-y,1-z
74	H12B	0	H	0.2057	1.3319	0.2444	1-x,1-y,1-z
75	C13	0	C.3	0.5351(5)	1.4104(3)	0.19751(7)	1-x,1-y,1-z
76	H13A	0	H	0.6925	1.4952	0.2222	1-x,1-y,1-z
77	H13B	0	H	0.6338	1.3324	0.1752	1-x,1-y,1-z
78	C14	0	C.3	0.3947(5)	1.5578(3)	0.16888(8)	1-x,1-y,1-z
79	H14A	0	H	0.3023	1.6392	0.1915	1-x,1-y,1-z
80	H14B	0	H	0.2318	1.4725	0.1451	1-x,1-y,1-z
81	C15	0	C.3	0.6175(5)	1.7105(3)	0.14196(7)	1-x,1-y,1-z
82	H15A	0	H	0.7815	1.7951	0.1656	1-x,1-y,1-z
83	H15B	0	H	0.7083	1.6293	0.1191	1-x,1-y,1-z
84	C16	0	C.3	0.4751(5)	1.8583(3)	0.11389(7)	1-x,1-y,1-z
85	H16A	0	H	0.3863	1.9407	0.1368	1-x,1-y,1-z
86	H16B	0	H	0.3096	1.7737	0.0905	1-x,1-y,1-z
87	C17	0	C.3	0.6971(5)	2.0095(3)	0.08652(8)	1-x,1-y,1-z
88	H17A	0	H	0.7773	1.9273	0.0623	1-x,1-y,1-z
89	H17B	0	H	0.8683	2.0884	0.1097	1-x,1-y,1-z
90	C18	0	C.3	0.5591(5)	2.1651(3)	0.06075(8)	1-x,1-y,1-z
91	H18A	0	H	0.3914	2.0865	0.0369	1-x,1-y,1-z
92	H18B	0	H	0.4742	2.2449	0.0848	1-x,1-y,1-z
93	C19	0	C.3	0.7852(6)	2.3190(4)	0.03460(8)	1-x,1-y,1-z
94	H19A	0	H	0.8649	2.2412	0.0099	1-x,1-y,1-z
95	H19B	0	H	0.6855	2.4165	0.019	1-x,1-y,1-z
96	H19C	0	H	0.9508	2.3984	0.058	1-x,1-y,1-z
97	H6	0	H	0.685(5)	0.199(3)	0.4065(8)	1-x,1-y,1-z
98	H7	0	H	0.128(5)	0.889(4)	0.5176(7)	1-x,1-y,1-z

Bonds

Number	Atom1	Atom2	Type	Polymeric	Length	SybylType
1	O1	C1	Unknown	no	1.209(2)	2
2	O2	C5	Unknown	no	1.218(3)	2
3	N1	C1	Unknown	no	1.400(3)	un
4	N1	C5	Unknown	no	1.391(3)	un
5	N1	C8	Unknown	no	1.473(3)	1
6	C1	C2	Unknown	no	1.474(3)	un
7	C2	C3	Unknown	no	1.408(3)	un
8	C2	C6	Unknown	no	1.376(3)	un
9	C3	C4	Unknown	no	1.407(3)	un
10	C3	C3	Unknown	no	1.409(3)	un
11	C4	C5	Unknown	no	1.478(3)	un
12	C4	C7	Unknown	no	1.369(3)	un
13	C6	H6	Unknown	no	0.98(2)	1
14	C6	C7	Unknown	no	1.401(3)	un
15	C7	H7	Unknown	no	0.97(3)	1
16	C7	C6	Unknown	no	1.401(3)	un
17	C8	H8A	Unknown	no	0.990(2)	1
18	C8	H8B	Unknown	no	0.990(2)	1
19	C8	C9	Unknown	no	1.523(3)	1
20	C9	H9A	Unknown	no	0.990(2)	1
21	C9	H9B	Unknown	no	0.991(2)	1
22	C9	C10	Unknown	no	1.519(3)	1
23	C10	H10A	Unknown	no	0.990(2)	1
24	C10	H10B	Unknown	no	0.991(2)	1
25	C10	C11	Unknown	no	1.520(3)	1
26	C11	H11A	Unknown	no	0.989(2)	1
27	C11	H11B	Unknown	no	0.989(2)	1
28	C11	C12	Unknown	no	1.517(3)	1
29	C12	H12A	Unknown	no	0.990(2)	1
30	C12	H12B	Unknown	no	0.990(2)	1
31	C12	C13	Unknown	no	1.520(3)	1
32	C13	H13A	Unknown	no	0.990(2)	1
33	C13	H13B	Unknown	no	0.990(2)	1
34	C13	C14	Unknown	no	1.522(3)	1
35	C14	H14A	Unknown	no	0.991(2)	1
36	C14	H14B	Unknown	no	0.990(2)	1
37	C14	C15	Unknown	no	1.521(3)	1
38	C15	H15A	Unknown	no	0.990(2)	1
39	C15	H15B	Unknown	no	0.989(2)	1
40	C15	C16	Unknown	no	1.521(3)	1
41	C16	H16A	Unknown	no	0.990(2)	1
42	C16	H16B	Unknown	no	0.990(2)	1
43	C16	C17	Unknown	no	1.521(3)	1
44	C17	H17A	Unknown	no	0.990(2)	1
45	C17	H17B	Unknown	no	0.990(2)	1
46	C17	C18	Unknown	no	1.519(3)	1
47	C18	H18A	Unknown	no	0.991(2)	1
48	C18	H18B	Unknown	no	0.989(2)	1
49	C18	C19	Unknown	no	1.521(3)	1
50	C19	H19A	Unknown	no	0.980(3)	1
51	C19	H19B	Unknown	no	0.980(3)	1
52	C19	H19C	Unknown	no	0.979(2)	1
53	O1	C1	Unknown	no	1.209(2)	2
54	O2	C5	Unknown	no	1.218(3)	2
55	N1	C1	Unknown	no	1.400(3)	un
56	N1	C5	Unknown	no	1.391(3)	un
57	N1	C8	Unknown	no	1.473(3)	1
58	C1	C2	Unknown	no	1.474(3)	un
59	C2	C3	Unknown	no	1.408(3)	un
60	C2	C6	Unknown	no	1.376(3)	un
61	C3	C4	Unknown	no	1.407(3)	un
62	C4	C5	Unknown	no	1.478(3)	un
63	C4	C7	Unknown	no	1.369(3)	un
64	C6	H6	Unknown	no	0.98(2)	1
65	C7	H7	Unknown	no	0.97(3)	1
66	C8	H8A	Unknown	no	0.990(2)	1
67	C8	H8B	Unknown	no	0.990(2)	1
68	C8	C9	Unknown	no	1.523(3)	1
69	C9	H9A	Unknown	no	0.990(2)	1
70	C9	H9B	Unknown	no	0.991(2)	1
71	C9	C10	Unknown	no	1.519(3)	1
72	C10	H10A	Unknown	no	0.990(2)	1
73	C10	H10B	Unknown	no	0.991(2)	1
74	C10	C11	Unknown	no	1.520(3)	1
75	C11	H11A	Unknown	no	0.989(2)	1
76	C11	H11B	Unknown	no	0.989(2)	1
77	C11	C12	Unknown	no	1.517(3)	1
78	C12	H12A	Unknown	no	0.990(2)	1
79	C12	H12B	Unknown	no	0.990(2)	1
80	C12	C13	Unknown	no	1.520(3)	1
81	C13	H13A	Unknown	no	0.990(2)	1
82	C13	H13B	Unknown	no	0.990(2)	1
83	C13	C14	Unknown	no	1.522(3)	1
84	C14	H14A	Unknown	no	0.991(2)	1
85	C14	H14B	Unknown	no	0.990(2)	1
86	C14	C15	Unknown	no	1.521(3)	1
87	C15	H15A	Unknown	no	0.990(2)	1
88	C15	H15B	Unknown	no	0.989(2)	1
89	C15	C16	Unknown	no	1.521(3)	1
90	C16	H16A	Unknown	no	0.990(2)	1
91	C16	H16B	Unknown	no	0.990(2)	1
92	C16	C17	Unknown	no	1.521(3)	1
93	C17	H17A	Unknown	no	0.990(2)	1
94	C17	H17B	Unknown	no	0.990(2)	1
95	C17	C18	Unknown	no	1.519(3)	1
96	C18	H18A	Unknown	no	0.991(2)	1
97	C18	H18B	Unknown	no	0.989(2)	1
98	C18	C19	Unknown	no	1.521(3)	1
99	C19	H19A	Unknown	no	0.980(3)	1
100	C19	H19B	Unknown	no	0.980(3)	1
101	C19	H19C	Unknown	no	0.979(2)	1

Figure 2.23 Crystal structure parameters for **N3**.

Space Group: C 2; Cell Lengths: **a** 41.893(2) **b** 6.8695(3) **c** 8.4203(3); Cell Angles: **α** 90.00 **β** 90.833(2) **γ** 90.00; Cell Volume: 2422.97; Z, Z′: 4, 0; R-Factor (%): 7.52.

Atoms

Number	Label	Charge	SybylType	Xfrac + ESD	Yfrac + ESD	Zfrac + ESD	Symm. op.
1	N1	0	N.am	0.33263(7)	0.1339(4)	0.1545(3)	x,y,z
2	C2	0	C.2	0.31057(9)	0.1487(5)	0.0294(4)	x,y,z
3	C3	0	C.2	0.27614(9)	0.1452(5)	0.0692(4)	x,y,z
4	C4	0	C.2	0.25325(9)	0.1668(6)	-0.0476(4)	x,y,z
5	H4	0	H	0.2597	0.191	-0.1547	x,y,z
6	C5	0	C.2	0.22051(9)	0.1566(5)	-0.0138(4)	x,y,z
7	H5	0	H	0.2046	0.1657	-0.0966	x,y,z
8	C6	0	C.2	0.21123(9)	0.1282(4)	0.1402(4)	x,y,z
9	C7	0	C.2	0.17674(9)	0.1153(4)	0.1786(4)	x,y,z
10	N8	0	N.am	0.16836(7)	0.1167(4)	0.3395(3)	x,y,z
11	C9	0	C.2	0.19030(9)	0.0861(5)	0.4641(4)	x,y,z
12	C10	0	C.2	0.22466(9)	0.0795(5)	0.4220(4)	x,y,z
13	C11	0	C.2	0.24771(9)	0.0518(6)	0.5388(4)	x,y,z
14	H11	0	H	0.2409	0.0252	0.645	x,y,z
15	C12	0	C.2	0.28022(9)	0.0597(6)	0.5039(4)	x,y,z
16	H12	0	H	0.2959	0.0443	0.5874	x,y,z
17	C13	0	C.2	0.29003(9)	0.0915(5)	0.3499(4)	x,y,z
18	C14	0	C.2	0.32448(9)	0.0982(5)	0.3123(4)	x,y,z
19	C15	0	C.2	0.26689(9)	0.1151(4)	0.2272(4)	x,y,z
20	C16	0	C.2	0.23399(9)	0.1103(4)	0.2629(4)	x,y,z
21	O17	0	O.2	0.31884(6)	0.1618(5)	-0.1081(3)	x,y,z
22	O18	0	O.2	0.15641(6)	0.1043(3)	0.0739(3)	x,y,z
23	O19	0	O.2	0.18181(6)	0.0652(5)	0.6007(3)	x,y,z
24	O20	0	O.2	0.34479(6)	0.0718(4)	0.4148(3)	x,y,z
25	C21	0	C.3	0.36742(8)	0.1460(5)	0.1150(4)	x,y,z
26	H21	0	H	0.3685	0.1782	0.0043	x,y,z
27	C22	0	C.3	0.38338(8)	-0.0510(6)	0.1348(4)	x,y,z
28	H22A	0	H	0.4056	-0.042	0.1094	x,y,z
29	H22B	0	H	0.3813	-0.0934	0.2428	x,y,z
30	H22C	0	H	0.3731	-0.143	0.065	x,y,z
31	C23	0	C.3	0.38442(8)	0.3098(5)	0.2053(4)	x,y,z
32	H23A	0	H	0.3904	0.2658	0.3098	x,y,z
33	H23B	0	H	0.3698	0.4167	0.216	x,y,z
34	C24	0	C.3	0.41415(8)	0.3789(6)	0.1198(4)	x,y,z
35	H24A	0	H	0.4078	0.4405	0.022	x,y,z
36	H24B	0	H	0.4271	0.268	0.0946	x,y,z
37	C25	0	C.3	0.43367(8)	0.5227(5)	0.2173(4)	x,y,z
38	H25A	0	H	0.4421	0.4564	0.3091	x,y,z
39	H25B	0	H	0.42	0.6254	0.2535	x,y,z
40	C26	0	C.3	0.46081(10)	0.6150(6)	0.1274(5)	x,y,z
41	H26A	0	H	0.4524	0.676	0.0332	x,y,z
42	H26B	0	H	0.4749	0.5127	0.0954	x,y,z
43	C27	0	C.3	0.47995(10)	0.7615(6)	0.2225(5)	x,y,z
44	H27A	0	H	0.4969	0.8119	0.1586	x,y,z
45	H27B	0	H	0.4662	0.8661	0.2539	x,y,z
46	H27C	0	H	0.4889	0.7001	0.3154	x,y,z
47	C28	0	C.3	0.13400(9)	0.1288(5)	0.3820(4)	x,y,z
48	H28	0	H	0.1329	0.1562	0.4936	x,y,z
49	C29	0	C.3	0.11793(8)	-0.0677(6)	0.3569(4)	x,y,z
50	H29A	0	H	0.0958	-0.0608	0.3836	x,y,z
51	H29B	0	H	0.1199	-0.1028	0.2471	x,y,z
52	H29C	0	H	0.1283	-0.1641	0.422	x,y,z
53	C30	0	C.3	0.11654(8)	0.2950(5)	0.2953(4)	x,y,z
54	H30A	0	H	0.1098	0.2517	0.1918	x,y,z
55	H30B	0	H	0.1313	0.4004	0.282	x,y,z
56	C31	0	C.3	0.08734(8)	0.3671(6)	0.3856(4)	x,y,z
57	H31A	0	H	0.0944	0.4297	0.4817	x,y,z
58	H31B	0	H	0.0743	0.2581	0.4139	x,y,z
59	C32	0	C.3	0.06768(8)	0.5111(5)	0.2893(4)	x,y,z
60	H32A	0	H	0.0586	0.4439	0.1994	x,y,z
61	H32B	0	H	0.0814	0.6115	0.2502	x,y,z
62	C33	0	C.3	0.04131(10)	0.6101(6)	0.3817(5)	x,y,z
63	H33A	0	H	0.0503	0.6705	0.475	x,y,z
64	H33B	0	H	0.0268	0.5105	0.4153	x,y,z
65	C34	0	C.3	0.02257(10)	0.7573(6)	0.2843(5)	x,y,z
66	H34A	0	H	0.0062	0.8125	0.3488	x,y,z
67	H34B	0	H	0.0367	0.8585	0.2498	x,y,z
68	H34C	0	H	0.013	0.695	0.1933	x,y,z

Bonds

Number	Atom1	Atom2	Type	Polymeric	Length	SybylType
1	N1	C2	Unknown	no	1.395(4)	un
2	N1	C14	Unknown	no	1.398(4)	un
3	N1	C21	Unknown	no	1.502(4)	1
4	C2	C3	Unknown	no	1.486(5)	un
5	C2	O17	Unknown	no	1.217(4)	2
6	C3	C4	Unknown	no	1.372(5)	un
7	C3	C15	Unknown	no	1.406(5)	un
8	C4	H4	Unknown	no	0.960(3)	1
9	C4	C5	Unknown	no	1.407(5)	un
10	C5	H5	Unknown	no	0.960(4)	1
11	C5	C6	Unknown	no	1.373(5)	un
12	C6	C7	Unknown	no	1.488(5)	un
13	C6	C16	Unknown	no	1.401(5)	un
14	C7	N8	Unknown	no	1.405(4)	un
15	C7	O18	Unknown	no	1.219(4)	2
16	N8	C9	Unknown	no	1.401(4)	un
17	N8	C28	Unknown	no	1.491(5)	1
18	C9	C10	Unknown	no	1.488(5)	un
19	C9	O19	Unknown	no	1.217(4)	2
20	C10	C11	Unknown	no	1.381(5)	un
21	C10	C16	Unknown	no	1.417(5)	un
22	C11	H11	Unknown	no	0.960(3)	1
23	C11	C12	Unknown	no	1.399(5)	un
24	C12	H12	Unknown	no	0.961(4)	1
25	C12	C13	Unknown	no	1.383(5)	un
26	C13	C14	Unknown	no	1.483(5)	un
27	C13	C15	Unknown	no	1.416(5)	un
28	C14	O20	Unknown	no	1.217(4)	2
29	C15	C16	Unknown	no	1.415(5)	un
30	C21	H21	Unknown	no	0.960(3)	1
31	C21	C22	Unknown	no	1.518(5)	1
32	C21	C23	Unknown	no	1.528(5)	1
33	C22	H22A	Unknown	no	0.960(3)	1
34	C22	H22B	Unknown	no	0.960(3)	1
35	C22	H22C	Unknown	no	0.961(4)	1
36	C23	H23A	Unknown	no	0.960(3)	1
37	C23	H23B	Unknown	no	0.961(3)	1
38	C23	C24	Unknown	no	1.523(5)	1
39	C24	H24A	Unknown	no	0.960(4)	1
40	C24	H24B	Unknown	no	0.961(4)	1
41	C24	C25	Unknown	no	1.516(5)	1
42	C25	H25A	Unknown	no	0.960(3)	1
43	C25	H25B	Unknown	no	0.961(3)	1
44	C25	C26	Unknown	no	1.514(5)	1
45	C26	H26A	Unknown	no	0.960(4)	1
46	C26	H26B	Unknown	no	0.959(4)	1
47	C26	C27	Unknown	no	1.509(6)	1
48	C27	H27A	Unknown	no	0.962(4)	1
49	C27	H27B	Unknown	no	0.960(4)	1
50	C27	H27C	Unknown	no	0.960(4)	1
51	C28	H28	Unknown	no	0.960(3)	1
52	C28	C29	Unknown	no	1.522(5)	1
53	C28	C30	Unknown	no	1.535(5)	1
54	C29	H29A	Unknown	no	0.958(3)	1
55	C29	H29B	Unknown	no	0.960(3)	1
56	C29	H29C	Unknown	no	0.960(4)	1
57	C30	H30A	Unknown	no	0.959(3)	1
58	C30	H30B	Unknown	no	0.960(3)	1
59	C30	C31	Unknown	no	1.532(5)	1
60	C31	H31A	Unknown	no	0.959(4)	1
61	C31	H31B	Unknown	no	0.959(4)	1
62	C31	C32	Unknown	no	1.515(5)	1
63	C32	H32A	Unknown	no	0.960(3)	1
64	C32	H32B	Unknown	no	0.959(3)	1
65	C32	C33	Unknown	no	1.521(5)	1
66	C33	H33A	Unknown	no	0.961(4)	1
67	C33	H33B	Unknown	no	0.961(4)	1
68	C33	C34	Unknown	no	1.514(6)	1
69	C34	H34A	Unknown	no	0.959(4)	1
70	C34	H34B	Unknown	no	0.961(4)	1
71	C34	H34C	Unknown	no	0.960(4)	1

Figure 2.24 Crystal structure parameters for **N4**.

Space Group: P -1; Cell Lengths: **a** 8.1677(15) **b** 14.211(3) **c** 20.027(4); Cell Angles: **α** 87.000(6) **β** 88.742(5) **γ** 86.499(6); Cell Volume: 2316.63; Z, Z′: 2, 0; R-Factor (%): 13.47.

Atoms

Number	Label	Charge	SybylType	Xfrac + ESD	Yfrac + ESD	Zfrac + ESD	Symm. op.
1	O1A	0	O.3	0.8481(5)	0.4504(4)	0.6333(2)	x,y,z
2	C1A	0	C.2	0.9944(8)	0.4925(5)	0.5354(3)	x,y,z
3	C2A	0	C.2	0.8443(8)	0.4643(5)	0.5658(4)	x,y,z
4	C3A	0	C.2	0.7143(8)	0.4476(5)	0.5266(3)	x,y,z
5	H3A	0	H	0.6159	0.4263	0.5467	x,y,z
6	C4A	0	C.2	0.7262(8)	0.4620(5)	0.4573(4)	x,y,z
7	H4A	0	H	0.6339	0.4522	0.4311	x,y,z
8	C5A	0	C.2	0.8694(8)	0.4903(5)	0.4254(4)	x,y,z
9	H5AA	0	H	0.8756	0.498	0.3781	x,y,z
10	C6A	0	C.3	0.6969(8)	0.4312(6)	0.6668(4)	x,y,z
11	H6A1	0	H	0.6588	0.3704	0.653	x,y,z
12	H6A2	0	H	0.612	0.4816	0.6548	x,y,z
13	C7A	0	C.3	0.7234(9)	0.4266(6)	0.7408(4)	x,y,z
14	H7A1	0	H	0.8075	0.3752	0.7515	x,y,z
15	H7A2	0	H	0.62	0.4094	0.7637	x,y,z
16	C8A	0	C.3	0.7763(9)	0.5157(6)	0.7694(4)	x,y,z
17	H8A1	0	H	0.6959	0.5682	0.7567	x,y,z
18	H8A2	0	H	0.8836	0.5309	0.7489	x,y,z
19	C9A	0	C.3	0.7917(10)	0.5098(6)	0.8443(4)	x,y,z
20	H9A1	0	H	0.8692	0.4557	0.8567	x,y,z
21	H9A2	0	H	0.6835	0.4958	0.8644	x,y,z
22	C10A	0	C.3	0.8501(10)	0.5980(7)	0.8760(4)	x,y,z
23	H10A	0	H	0.8722	0.5825	0.9239	x,y,z
24	H10B	0	H	0.9544	0.6154	0.854	x,y,z
25	C11A	0	C.3	0.7282(9)	0.6813(6)	0.8704(4)	x,y,z
26	H11A	0	H	0.6208	0.663	0.889	x,y,z
27	H11B	0	H	0.7138	0.7013	0.8227	x,y,z
28	C12A	0	C.3	0.7867(11)	0.7643(7)	0.9086(5)	x,y,z
29	H12A	0	H	0.8024	0.7442	0.9557	x,y,z
30	H12B	0	H	0.7041	0.8172	0.9054	x,y,z
31	H12C	0	H	0.8907	0.7842	0.8889	x,y,z
32	O1A	0	O.3	1.1519(5)	0.5496(4)	0.3667(2)	2-x,1-y,1-z
33	C1A	0	C.2	1.0056(8)	0.5075(5)	0.4646(3)	2-x,1-y,1-z
34	C2A	0	C.2	1.1557(8)	0.5357(5)	0.4342(4)	2-x,1-y,1-z
35	C3A	0	C.2	1.2857(8)	0.5524(5)	0.4734(3)	2-x,1-y,1-z
36	H3A	0	H	1.3841	0.5737	0.4533	2-x,1-y,1-z
37	C4A	0	C.2	1.2738(8)	0.5380(5)	0.5427(4)	2-x,1-y,1-z
38	H4A	0	H	1.3661	0.5478	0.5689	2-x,1-y,1-z
39	C5A	0	C.2	1.1306(8)	0.5097(5)	0.5746(4)	2-x,1-y,1-z
40	H5AA	0	H	1.1244	0.502	0.6219	2-x,1-y,1-z
41	C6A	0	C.3	1.3031(8)	0.5688(6)	0.3332(4)	2-x,1-y,1-z
42	H6A1	0	H	1.3412	0.6296	0.347	2-x,1-y,1-z
43	H6A2	0	H	1.388	0.5184	0.3452	2-x,1-y,1-z
44	C7A	0	C.3	1.2766(9)	0.5734(6)	0.2592(4)	2-x,1-y,1-z
45	H7A1	0	H	1.1925	0.6248	0.2485	2-x,1-y,1-z
46	H7A2	0	H	1.38	0.5906	0.2363	2-x,1-y,1-z
47	C8A	0	C.3	1.2237(9)	0.4843(6)	0.2306(4)	2-x,1-y,1-z
48	H8A1	0	H	1.3041	0.4318	0.2433	2-x,1-y,1-z
49	H8A2	0	H	1.1164	0.4691	0.2511	2-x,1-y,1-z
50	C9A	0	C.3	1.2083(10)	0.4902(6)	0.1557(4)	2-x,1-y,1-z
51	H9A1	0	H	1.1308	0.5443	0.1433	2-x,1-y,1-z
52	H9A2	0	H	1.3165	0.5042	0.1356	2-x,1-y,1-z
53	C10A	0	C.3	1.1499(10)	0.4020(7)	0.1240(4)	2-x,1-y,1-z
54	H10A	0	H	1.1278	0.4175	0.0761	2-x,1-y,1-z
55	H10B	0	H	1.0456	0.3846	0.146	2-x,1-y,1-z
56	C11A	0	C.3	1.2718(9)	0.3187(6)	0.1296(4)	2-x,1-y,1-z
57	H11A	0	H	1.3792	0.337	0.111	2-x,1-y,1-z
58	H11B	0	H	1.2862	0.2987	0.1773	2-x,1-y,1-z
59	C12A	0	C.3	1.2133(11)	0.2357(7)	0.0914(5)	2-x,1-y,1-z
60	H12A	0	H	1.1976	0.2558	0.0443	2-x,1-y,1-z
61	H12B	0	H	1.2959	0.1828	0.0946	2-x,1-y,1-z
62	H12C	0	H	1.1093	0.2158	0.1111	2-x,1-y,1-z
63	O1	0	O.2	0.5841(6)	0.2005(4)	0.3858(3)	x,y,z
64	O2	0	O.2	1.0674(6)	0.2843(4)	0.2866(3)	x,y,z
65	O3	0	O.2	0.9345(5)	0.2190(4)	0.7023(3)	x,y,z
66	O4	0	O.2	1.4168(6)	0.3017(4)	0.6038(2)	x,y,z
67	N1	0	N.am	0.8231(6)	0.2434(4)	0.3366(3)	x,y,z
68	N2	0	N.am	1.1796(6)	0.2540(4)	0.6542(3)	x,y,z
69	C1	0	C.2	0.7280(9)	0.2204(5)	0.3934(4)	x,y,z
70	C2	0	C.2	0.8039(8)	0.2212(5)	0.4580(4)	x,y,z
71	C3	0	C.2	0.7150(8)	0.1984(5)	0.5163(4)	x,y,z
72	H3	0	H	0.6058	0.1798	0.5129	x,y,z
73	C4	0	C.2	0.7819(8)	0.2020(5)	0.5792(4)	x,y,z
74	H4	0	H	0.7201	0.1861	0.6184	x,y,z
75	C5	0	C.2	0.9426(8)	0.2298(5)	0.5832(4)	x,y,z
76	C6	0	C.2	1.0134(8)	0.2347(5)	0.6501(4)	x,y,z
77	C7	0	C.2	1.2747(9)	0.2807(5)	0.5962(4)	x,y,z
78	C8	0	C.2	1.1981(8)	0.2804(5)	0.5318(4)	x,y,z
79	C9	0	C.2	1.2873(8)	0.3043(6)	0.4740(4)	x,y,z
80	H9	0	H	1.3964	0.3229	0.4774	x,y,z

Bonds

Number	Atom1	Atom2	Type	Polymeric	Length	SybylType
1	O1A	C2A	Unknown	no	1.357(9)	1
2	O1A	C6A	Unknown	no	1.427(8)	1
3	C1A	C2A	Unknown	no	1.427(9)	un
4	C1A	C1A	Unknown	no	1.425(8)	un
5	C1A	C5A	Unknown	no	1.42(1)	un
6	C2A	C3A	Unknown	no	1.37(1)	un
7	C3A	H3A	Unknown	no	0.950(7)	1
8	C3A	C4A	Unknown	no	1.39(1)	un
9	C4A	H4A	Unknown	no	0.949(7)	1
10	C4A	C5A	Unknown	no	1.39(1)	un
11	C5A	H5AA	Unknown	no	0.948(8)	1
12	C5A	C1A	Unknown	no	1.42(1)	un
13	C6A	H6A1	Unknown	no	0.991(9)	1
14	C6A	H6A2	Unknown	no	0.990(7)	1
15	C6A	C7A	Unknown	no	1.50(1)	1
16	C7A	H7A1	Unknown	no	0.990(8)	1
17	C7A	H7A2	Unknown	no	0.990(8)	1
18	C7A	C8A	Unknown	no	1.51(1)	1
19	C8A	H8A1	Unknown	no	0.990(8)	1
20	C8A	H8A2	Unknown	no	0.991(8)	1
21	C8A	C9A	Unknown	no	1.51(1)	1
22	C9A	H9A1	Unknown	no	0.990(8)	1
23	C9A	H9A2	Unknown	no	0.990(8)	1
24	C9A	C10A	Unknown	no	1.54(1)	1
25	C10A	H10A	Unknown	no	0.991(8)	1
26	C10A	H10B	Unknown	no	0.989(8)	1
27	C10A	C11A	Unknown	no	1.50(1)	1
28	C11A	H11A	Unknown	no	0.990(8)	1
29	C11A	H11B	Unknown	no	0.990(8)	1
30	C11A	C12A	Unknown	no	1.54(1)	1
31	C12A	H12A	Unknown	no	0.98(1)	1
32	C12A	H12B	Unknown	no	0.979(9)	1
33	C12A	H12C	Unknown	no	0.980(9)	1
34	O1A	C2A	Unknown	no	1.357(9)	1
35	O1A	C6A	Unknown	no	1.427(8)	1
36	C1A	C2A	Unknown	no	1.427(9)	un
37	C2A	C3A	Unknown	no	1.37(1)	un
38	C3A	H3A	Unknown	no	0.950(7)	1
39	C3A	C4A	Unknown	no	1.39(1)	un
40	C4A	H4A	Unknown	no	0.949(7)	1
41	C4A	C5A	Unknown	no	1.39(1)	un
42	C5A	H5AA	Unknown	no	0.948(8)	1
43	C6A	H6A1	Unknown	no	0.991(9)	1
44	C6A	H6A2	Unknown	no	0.990(7)	1
45	C6A	C7A	Unknown	no	1.50(1)	1
46	C7A	H7A1	Unknown	no	0.990(8)	1
47	C7A	H7A2	Unknown	no	0.990(8)	1
48	C7A	C8A	Unknown	no	1.51(1)	1
49	C8A	H8A1	Unknown	no	0.990(8)	1
50	C8A	H8A2	Unknown	no	0.991(8)	1
51	C8A	C9A	Unknown	no	1.51(1)	1
52	C9A	H9A1	Unknown	no	0.990(8)	1
53	C9A	H9A2	Unknown	no	0.990(8)	1
54	C9A	C10A	Unknown	no	1.54(1)	1
55	C10A	H10A	Unknown	no	0.991(8)	1
56	C10A	H10B	Unknown	no	0.989(8)	1
57	C10A	C11A	Unknown	no	1.50(1)	1
58	C11A	H11A	Unknown	no	0.990(8)	1
59	C11A	H11B	Unknown	no	0.990(8)	1
60	C11A	C12A	Unknown	no	1.54(1)	1
61	C12A	H12A	Unknown	no	0.98(1)	1
62	C12A	H12B	Unknown	no	0.979(9)	1
63	C12A	H12C	Unknown	no	0.980(9)	1
64	O1	C1	Unknown	no	1.240(9)	2
65	O2	C12	Unknown	no	1.22(1)	2
66	O3	C6	Unknown	no	1.233(9)	2
67	O4	C7	Unknown	no	1.230(9)	2
68	N1	C1	Unknown	no	1.40(1)	un
69	N1	C12	Unknown	no	1.413(9)	un
70	N1	C15	Unknown	no	1.53(1)	1
71	N2	C6	Unknown	no	1.406(8)	un
72	N2	C7	Unknown	no	1.43(1)	un
73	N2	C22	Unknown	no	1.49(1)	1
74	C1	C2	Unknown	no	1.45(1)	un
75	C2	C3	Unknown	no	1.40(1)	un
76	C2	C14	Unknown	no	1.42(1)	un
77	C3	H3	Unknown	no	0.950(7)	1
78	C3	C4	Unknown	no	1.39(1)	un
79	C4	H4	Unknown	no	0.949(7)	1
80	C4	C5	Unknown	no	1.40(1)	un

81	C10	0	C.2	1.2174(8)	0.3011(5)	0.4101(4)	x,y,z	81	C5	C6	Unknown	no	1.48(1)	un
82	H10	0	H	1.2785	0.3183	0.3709	x,y,z	82	C5	C13	Unknown	no	1.41(1)	un
83	C11	0	C.2	1.0577(8)	0.2725(5)	0.4054(4)	x,y,z	83	C7	C8	Unknown	no	1.45(1)	un
84	C12	0	C.2	0.9871(9)	0.2695(5)	0.3380(4)	x,y,z	84	C8	C9	Unknown	no	1.39(1)	un
85	C13	0	C.2	1.0339(8)	0.2533(5)	0.5246(4)	x,y,z	85	C8	C13	Unknown	no	1.43(1)	un
86	C14	0	C.2	0.9667(8)	0.2500(5)	0.4632(4)	x,y,z	86	C9	H9	Unknown	no	0.950(7)	1
87	C15	0	C.3	0.7478(9)	0.2434(6)	0.2675(4)	x,y,z	87	C9	C10	Unknown	no	1.42(1)	un
88	H15B	0	H	0.8307	0.2661	0.2371	x,y,z	88	C10	H10	Unknown	no	0.950(7)	1
89	H15A	0	H	0.6382	0.2257	0.2778	x,y,z	89	C10	C11	Unknown	no	1.40(1)	un
90	C16	0	C.3	0.719(2)	0.3419(8)	0.2386(6)	x,y,z	90	C11	C12	Unknown	no	1.48(1)	un
91	H16A	0	H	0.6335	0.3433	0.2048	x,y,z	91	C11	C14	Unknown	no	1.40(1)	un
92	H16B	0	H	0.8204	0.3634	0.2179	x,y,z	92	C13	C14	Unknown	no	1.36(1)	un
93	H16C	0	H	0.6826	0.3836	0.2743	x,y,z	93	C15	H15B	Unknown	no	0.960(8)	1
94	C17	0	C.3	0.8125(18)	0.1677(9)	0.2242(8)	x,y,z	94	C15	H15A	Unknown	no	0.960(8)	1
95	H17A	0	H	0.8346	0.1098	0.253	x,y,z	95	C15	C16	Unknown	no	1.49(1)	1
96	H17B	0	H	0.9192	0.1864	0.205	x,y,z	96	C15	C17	Unknown	no	1.48(2)	1
97	C18	0	C.3	0.709(3)	0.1430(13)	0.1679(9)	x,y,z	97	C16	H16A	Unknown	no	0.98(1)	1
98	H18A	0	H	0.6001	0.1269	0.1863	x,y,z	98	C16	H16B	Unknown	no	0.98(2)	1
99	H18B	0	H	0.6921	0.1994	0.1371	x,y,z	99	C16	H16C	Unknown	no	0.98(1)	1
100	C19	0	C.3	0.7767(18)	0.0650(13)	0.1298(8)	x,y,z	100	C17	H17A	Unknown	no	0.99(1)	1
101	H19A	0	H	0.833	0.0185	0.1613	x,y,z	101	C17	H17B	Unknown	no	0.99(1)	1
102	H19B	0	H	0.8615	0.0896	0.0986	x,y,z	102	C17	C18	Unknown	no	1.49(3)	1
103	C20	0	C.3	0.654(2)	0.0102(14)	0.0876(10)	x,y,z	103	C18	H18A	Unknown	no	0.99(2)	1
104	H20A	0	H	0.5452	0.0198	0.1098	x,y,z	104	C18	H18B	Unknown	no	0.99(2)	1
105	H20B	0	H	0.6459	0.0456	0.0437	x,y,z	105	C18	C19	Unknown	no	1.45(3)	1
106	C21	0	C.3	0.669(2)	-0.0873(13)	0.0727(10)	x,y,z	106	C19	H19A	Unknown	no	0.99(2)	1
107	H21A	0	H	0.7853	-0.1084	0.07	x,y,z	107	C19	H19B	Unknown	no	0.99(2)	1
108	H21B	0	H	0.6175	-0.0957	0.0299	x,y,z	108	C19	C20	Unknown	no	1.59(3)	1
109	H21C	0	H	0.6144	-0.1247	0.1082	x,y,z	109	C20	H20A	Unknown	no	0.99(2)	1
110	C22	0	C.3	1.2547(9)	0.2479(6)	0.7214(4)	x,y,z	110	C20	H20B	Unknown	no	0.99(2)	1
111	H22B	0	H	1.3687	0.2565	0.7118	x,y,z	111	C20	C21	Unknown	no	1.43(3)	1
112	H22A	0	H	1.1774	0.2174	0.7507	x,y,z	112	C21	H21A	Unknown	no	0.98(2)	1
113	C23	0	C.3	1.4085(13)	0.1891(9)	0.7270(6)	x,y,z	113	C21	H21B	Unknown	no	0.98(2)	1
114	H23A	0	H	1.4999	0.2255	0.7098	x,y,z	114	C21	H21C	Unknown	no	0.98(2)	1
115	H23B	0	H	1.4014	0.1332	0.7008	x,y,z	115	C22	H22B	Unknown	no	0.960(7)	1
116	H23C	0	H	1.4267	0.1694	0.774	x,y,z	116	C22	H22A	Unknown	no	0.960(8)	1
117	C24	0	C.3	1.2602(16)	0.3518(8)	0.7453(8)	x,y,z	117	C22	C23	Unknown	no	1.47(1)	1
118	H24A	0	H	1.1554	0.3882	0.7356	x,y,z	118	C22	C24	Unknown	no	1.58(2)	1
119	H24B	0	H	1.3504	0.3845	0.722	x,y,z	119	H22B	C23	Unknown	no	1.03(1)	1
120	C25	0	C.3	1.2897(9)	0.3428(7)	0.8234(4)	x,y,z	120	C23	H23A	Unknown	no	0.98(1)	1
121	H25C	0	H	1.2473	0.2992	0.8567	x,y,z	121	C23	H23B	Unknown	no	0.98(1)	1
122	H25D	0	H	1.4034	0.3243	0.816	x,y,z	122	C23	H23C	Unknown	no	0.98(1)	1
123	H25A	0	H	1.3963	0.3126	0.8315	x,y,z	123	C24	H24A	Unknown	no	0.99(1)	1
124	H25B	0	H	1.2089	0.3045	0.8449	x,y,z	124	C24	H24B	Unknown	no	0.99(1)	1
125	C26	0	C.3	1.2793(10)	0.4379(7)	0.8524(4)	x,y,z	125	C24	C25	Unknown	no	1.59(2)	1
126	H26A	0	H	1.1684	0.4681	0.8445	x,y,z	126	C25	H25C	Unknown	no	0.960(9)	1
127	H26B	0	H	1.3595	0.4778	0.8286	x,y,z	127	C25	H25D	Unknown	no	0.960(7)	1
128	C27	0	C.3	1.3127(10)	0.4351(7)	0.9272(4)	x,y,z	128	C25	H25A	Unknown	no	0.960(8)	1
129	H27A	0	H	1.2336	0.3949	0.9513	x,y,z	129	C25	H25B	Unknown	no	0.961(8)	1
130	H27B	0	H	1.4244	0.4064	0.9353	x,y,z	130	C25	C26	Unknown	no	1.50(1)	1
131	C28	0	C.3	1.2983(10)	0.5329(7)	0.9547(4)	x,y,z	131	C26	H26A	Unknown	no	0.991(8)	1
132	H28A	0	H	1.3814	0.5718	0.9331	x,y,z	132	C26	H26B	Unknown	no	0.991(9)	1
133	H28B	0	H	1.3153	0.5278	1.003	x,y,z	133	C26	C27	Unknown	no	1.53(1)	1
134	H28C	0	H	1.1888	0.5623	0.9456	x,y,z	134	C27	H27A	Unknown	no	0.990(9)	1
135	O1B	0	O.3	0.8550(5)	-0.0496(4)	0.6355(3)	x,y,z	135	C27	H27B	Unknown	no	0.990(8)	1
136	C1B	0	C.2	1.0003(8)	-0.0079(5)	0.5355(3)	x,y,z	136	C27	C28	Unknown	no	1.52(1)	1
137	C2B	0	C.2	0.8479(8)	-0.0361(5)	0.5675(4)	x,y,z	137	C28	H28A	Unknown	no	0.980(9)	1
138	C3B	0	C.2	0.7146(9)	-0.0536(5)	0.5304(4)	x,y,z	138	C28	H28B	Unknown	no	0.979(8)	1
139	H3B	0	H	0.6171	-0.074	0.5518	x,y,z	139	C28	H28C	Unknown	no	0.980(8)	1
140	C4B	0	C.2	0.7243(8)	-0.0408(5)	0.4603(4)	x,y,z	140	O1B	C2B	Unknown	no	1.37(1)	1
141	H4B	0	H	0.6311	-0.0531	0.4354	x,y,z	141	O1B	C6B	Unknown	no	1.410(8)	1
142	C5B	0	C.2	0.8626(8)	-0.0111(5)	0.4257(4)	x,y,z	142	C1B	C2B	Unknown	no	1.456(9)	un
143	H5BA	0	H	0.8656	-0.0039	0.3782	x,y,z	143	C1B	C1B	Unknown	no	1.428(8)	un
144	C6B	0	C.3	0.7073(8)	-0.0701(6)	0.6694(4)	x,y,z	144	C1B	C5B	Unknown	no	1.42(1)	un
145	H6B1	0	H	0.6737	-0.1331	0.6582	x,y,z	145	C2B	C3B	Unknown	no	1.37(1)	un
146	H6B2	0	H	0.6189	-0.0224	0.6564	x,y,z	146	C3B	H3B	Unknown	no	0.950(7)	1
147	C7B	0	C.3	0.7387(10)	-0.0684(6)	0.7439(4)	x,y,z	147	C3B	C4B	Unknown	no	1.41(1)	un
148	H7B1	0	H	0.643	-0.0919	0.7693	x,y,z	148	C4B	H4B	Unknown	no	0.949(7)	1
149	H7B2	0	H	0.8355	-0.1112	0.7552	x,y,z	149	C4B	C5B	Unknown	no	1.39(1)	un
150	C8B	0	C.3	0.7687(11)	0.0303(7)	0.7646(5)	x,y,z	150	C5B	H5BA	Unknown	no	0.951(8)	1
151	H8B1	0	H	0.6754	0.0736	0.7499	x,y,z	151	C5B	C1B	Unknown	no	1.42(1)	un
152	H8B2	0	H	0.8686	0.0517	0.741	x,y,z	152	C6B	H6B1	Unknown	no	0.990(9)	1
153	C9B	0	C.3	0.7899(12)	0.0381(7)	0.8407(5)	x,y,z	153	C6B	H6B2	Unknown	no	0.989(7)	1
154	H9B1	0	H	0.893	0.003	0.8545	x,y,z	154	C6B	C7B	Unknown	no	1.52(1)	1
155	H9B2	0	H	0.6979	0.0085	0.8651	x,y,z	155	C7B	H7B1	Unknown	no	0.989(8)	1
156	C10B	0	C.3	0.7944(14)	0.1435(9)	0.8603(5)	x,y,z	156	C7B	H7B2	Unknown	no	0.990(8)	1
157	H10C	0	H	0.8889	0.1719	0.8369	x,y,z	157	C7B	C8B	Unknown	no	1.52(1)	1
158	H10D	0	H	0.6934	0.1788	0.8442	x,y,z	158	C8B	H8B1	Unknown	no	0.990(9)	1
159	C11B	0	C.3	0.8070(15)	0.1551(9)	0.9301(6)	x,y,z	159	C8B	H8B2	Unknown	no	0.990(9)	1
160	H11C	0	H	0.9059	0.1178	0.9463	x,y,z	160	C8B	C9B	Unknown	no	1.55(1)	1

161	H11D	0	H	0.7107	0.1282	0.9531	x,y,z
162	C12B	0	C.3	0.8167(15)	0.2525(9)	0.9502(6)	x,y,z
163	H12D	0	H	0.9186	0.2579	0.9743	x,y,z
164	H12E	0	H	0.7226	0.2692	0.9793	x,y,z
165	H12F	0	H	0.8154	0.2955	0.9103	x,y,z
166	O1B	0	O.3	1.1450(5)	0.0496(4)	0.3645(3)	2-x,-y,1-z
167	C1B	0	C.2	0.9997(8)	0.0079(5)	0.4645(3)	2-x,-y,1-z
168	C2B	0	C.2	1.1521(8)	0.0361(5)	0.4325(4)	2-x,-y,1-z
169	C3B	0	C.2	1.2854(9)	0.0536(5)	0.4696(4)	2-x,-y,1-z
170	H3B	0	H	1.3829	0.074	0.4482	2-x,-y,1-z
171	C4B	0	C.2	1.2757(8)	0.0408(5)	0.5397(4)	2-x,-y,1-z
172	H4B	0	H	1.3689	0.0531	0.5646	2-x,-y,1-z
173	C5B	0	C.2	1.1374(8)	0.0111(5)	0.5743(4)	2-x,-y,1-z
174	H5BA	0	H	1.1344	0.0039	0.6218	2-x,-y,1-z
175	C6B	0	C.3	1.2927(8)	0.0701(6)	0.3306(4)	2-x,-y,1-z
176	H6B1	0	H	1.3263	0.1331	0.3418	2-x,-y,1-z
177	H6B2	0	H	1.3811	0.0224	0.3436	2-x,-y,1-z
178	C7B	0	C.3	1.2613(10)	0.0684(6)	0.2561(4)	2-x,-y,1-z
179	H7B1	0	H	1.357	0.0919	0.2307	2-x,-y,1-z
180	H7B2	0	H	1.1645	0.1112	0.2448	2-x,-y,1-z
181	C8B	0	C.3	1.2313(11)	-0.0303(7)	0.2354(5)	2-x,-y,1-z
182	H8B1	0	H	1.3246	-0.0736	0.2501	2-x,-y,1-z
183	H8B2	0	H	1.1314	-0.0517	0.259	2-x,-y,1-z
184	C9B	0	C.3	1.2101(12)	-0.0381(7)	0.1593(5)	2-x,-y,1-z
185	H9B1	0	H	1.107	-0.003	0.1455	2-x,-y,1-z
186	H9B2	0	H	1.3021	-0.0085	0.1349	2-x,-y,1-z
187	C10B	0	C.3	1.2056(14)	-0.1435(9)	0.1397(5)	2-x,-y,1-z
188	H10C	0	H	1.1111	-0.1719	0.1631	2-x,-y,1-z
189	H10D	0	H	1.3066	-0.1788	0.1558	2-x,-y,1-z
190	C11B	0	C.3	1.1930(15)	-0.1551(9)	0.0699(6)	2-x,-y,1-z
191	H11C	0	H	1.0941	-0.1178	0.0537	2-x,-y,1-z
192	H11D	0	H	1.2893	-0.1282	0.0469	2-x,-y,1-z
193	C12B	0	C.3	1.1833(15)	-0.2525(9)	0.0498(6)	2-x,-y,1-z
194	H12D	0	H	1.0814	-0.2579	0.0257	2-x,-y,1-z
195	H12E	0	H	1.2774	-0.2692	0.0207	2-x,-y,1-z
196	H12F	0	H	1.1846	-0.2955	0.0897	2-x,-y,1-z
197	C16'	0	C.3	0.6082(14)	0.3105(10)	0.2573(7)	x,y,z
198	H16D	0	H	0.5717	0.3092	0.2111	x,y,z
199	H16E	0	H	0.6402	0.374	0.2659	x,y,z
200	H16F	0	H	0.5185	0.2935	0.2881	x,y,z
201	C17'	0	C.3	0.7382(17)	0.1403(9)	0.2520(7)	x,y,z
202	H17C	0	H	0.8418	0.1057	0.266	x,y,z
203	H17D	0	H	0.6483	0.1138	0.2796	x,y,z
204	C18'	0	C.3	0.711(3)	0.1219(10)	0.1810(7)	x,y,z
205	H18C	0	H	0.6035	0.1535	0.1683	x,y,z
206	H18D	0	H	0.7959	0.153	0.1535	x,y,z
207	C19'	0	C.3	0.7107(19)	0.0245(11)	0.1621(7)	x,y,z
208	H19C	0	H	0.6154	-0.0051	0.184	x,y,z
209	H19D	0	H	0.8113	-0.0102	0.1792	x,y,z
210	C20'	0	C.3	0.703(2)	0.0129(13)	0.0835(8)	x,y,z
211	H20C	0	H	0.5899	0.0351	0.0716	x,y,z
212	H20D	0	H	0.7745	0.0613	0.0636	x,y,z
213	C21'	0	C.3	0.738(2)	-0.0670(14)	0.0452(9)	x,y,z
214	H21D	0	H	0.7341	-0.1245	0.0743	x,y,z
215	H21E	0	H	0.8478	-0.0638	0.0247	x,y,z
216	H21F	0	H	0.6566	-0.0681	0.0102	x,y,z
217	C23'	0	C.3	1.2572(18)	0.1509(8)	0.7543(6)	x,y,z
218	H23D	0	H	1.2791	0.104	0.7205	x,y,z
219	H23E	0	H	1.1507	0.141	0.7761	x,y,z
220	H23F	0	H	1.3435	0.144	0.7877	x,y,z
221	C24'	0	C.3	1.202(2)	0.3306(9)	0.7608(10)	x,y,z
222	H24C	0	H	1.2124	0.3883	0.7316	x,y,z
223	H24D	0	H	1.0839	0.3264	0.7723	x,y,z

161	C9B	H9B1	Unknown	no	0.99(1)	1
162	C9B	H9B2	Unknown	no	0.99(1)	1
163	C9B	C10B	Unknown	no	1.57(2)	1
164	C10B	H10C	Unknown	no	0.99(1)	1
165	C10B	H10D	Unknown	no	0.99(1)	1
166	C10B	C11B	Unknown	no	1.42(2)	1
167	C11B	H11C	Unknown	no	0.99(1)	1
168	C11B	H11D	Unknown	no	0.99(1)	1
169	C11B	C12B	Unknown	no	1.47(2)	1
170	C12B	H12D	Unknown	no	0.98(1)	1
171	C12B	H12E	Unknown	no	0.98(1)	1
172	C12B	H12F	Unknown	no	0.98(1)	1
173	O1B	C2B	Unknown	no	1.37(1)	1
174	O1B	C6B	Unknown	no	1.410(8)	1
175	C1B	C2B	Unknown	no	1.456(9)	un
176	C2B	C3B	Unknown	no	1.37(1)	un
177	C3B	H3B	Unknown	no	0.950(7)	1
178	C3B	C4B	Unknown	no	1.41(1)	un
179	C4B	H4B	Unknown	no	0.949(7)	1
180	C4B	C5B	Unknown	no	1.39(1)	un
181	C5B	H5BA	Unknown	no	0.951(8)	1
182	C6B	H6B1	Unknown	no	0.990(9)	1
183	C6B	H6B2	Unknown	no	0.989(7)	1
184	C6B	C7B	Unknown	no	1.52(1)	1
185	C7B	H7B1	Unknown	no	0.989(8)	1
186	C7B	H7B2	Unknown	no	0.990(8)	1
187	C7B	C8B	Unknown	no	1.52(1)	1
188	C8B	H8B1	Unknown	no	0.990(9)	1
189	C8B	H8B2	Unknown	no	0.990(9)	1
190	C8B	C9B	Unknown	no	1.55(1)	1
191	C9B	H9B1	Unknown	no	0.99(1)	1
192	C9B	H9B2	Unknown	no	0.99(1)	1
193	C9B	C10B	Unknown	no	1.57(2)	1
194	C10B	H10C	Unknown	no	0.99(1)	1
195	C10B	H10D	Unknown	no	0.99(1)	1
196	C10B	C11B	Unknown	no	1.42(2)	1
197	C11B	H11C	Unknown	no	0.99(1)	1
198	C11B	H11D	Unknown	no	0.99(1)	1
199	C11B	C12B	Unknown	no	1.47(2)	1
200	C12B	H12D	Unknown	no	0.98(1)	1
201	C12B	H12E	Unknown	no	0.98(1)	1
202	C12B	H12F	Unknown	no	0.98(1)	1

Figure 2.25 Crystal structure parameters for **D5**:**N4**.

Chapter 3

Rigid DAN–NDI Dyads That Retain Electrostatic Complementarity

3.1 CHAPTER SUMMARY

3.1.1 Introduction

Chapter 2 explores the subtle interactions that affect the assembly of separate DAN and NDI molecules in the bulk phase. This chapter describes the synthetic progress towards a rigid, non-conjugated DAN–NDI molecule that retains electrostatic complementarity and the relative stacking geometry of the individual molecules. Ultimately we would like to explore the interactions that affect the assembly of tethered DAN–NDI molecules in the bulk phase.

3.1.2 Goals

The "big picture" goal of this study is to answer the question: *How will a rigid, non-conjugated DAN–NDI dyad stack in the meso- or crystalline phase*? These results should be of interest to the development of NDI-based materials for optoelectronic applications. The short term goal is to determine if it is *possible to append DAN onto the imide position of NDI through an ethynyl linker using current carbon–nitrogen (C–N) bond formation chemistry*.

3.1.3 Approach

This chapter presents successful approaches to synthesize both DAN and NDI derivatives that may serve as suitable precursors to a tethered molecule. The primary focus of the chapter is to report the results of catalytic C–N bond formation and

elimination-based reactions as a method to create an ethynyl moiety on the NDI N-imide position.

3.2 BACKGROUND

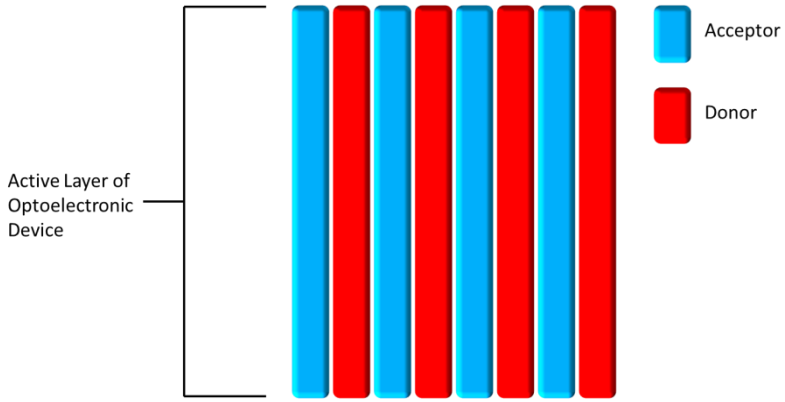

Figure 3.1 The proposed bicontinuous array of donor and acceptor units for optimal performance and efficiency in optoelectronic devices.

An efficient organic optoelectronic device requires a well-ordered active layer that can sufficiently absorb visible light, undergo charge separation to form electron–hole pairs, resist charge recombination, and transport these electron and holes to the device electrodes (82). Blends of electron donor and electron acceptor moieties have been incorporated to fulfill some of these design criteria. Specifically, these blends rely on sufficient self-organization to form an active layer morphology that will facilitate charge generation and a bicontinuous (Figure 3.1) route for the charge carriers. While blends of independent donor and acceptor monomers can lead to interesting morphologies, these systems lack the precise control over the self-assembly and their phase separation can

lead to defects within the active layer. Incorporation of a covalent link between the donor and acceptor units offers an alternative approach that can yield increased control over the organization between the donor and acceptor units (82).

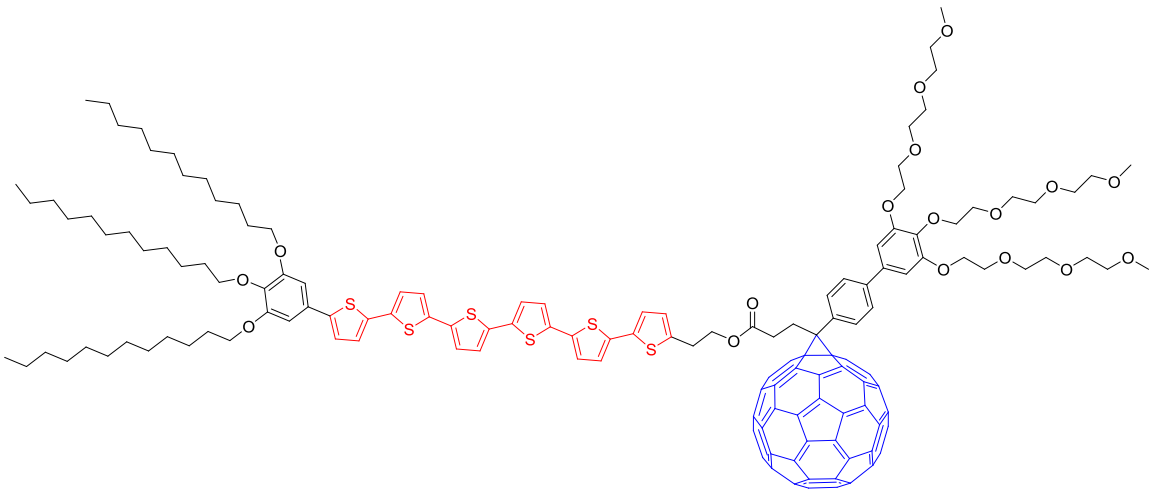

Figure 3.2 Oligothiophene–C_{60} dyad that forms a bicontinuous D–A array.

There are numerous examples of donor–acceptor (D–A) dyads, many of which incorporate oligothiophene donors and fullerene (C_{60}) acceptors. Aida *et al*. developed an amphiphilic D–A dyad (Figure 3.2) that forms bicontinuous arrays of donors and acceptors while in the liquid crystalline phase (83). The dyad tethers together an oligothiophene donor with a fullerene acceptor using a flexible linker. The amphiphilic nature afforded by the hydrophilic and hydrophobic side chains drives the liquid crystalline assembly. The bicontinuous nature of the resultant morphology is promising for charge transport in optoelectronic devices. In addition, the material can be fashioned into thin films and its liquid crystalline properties yield self-healing ability.

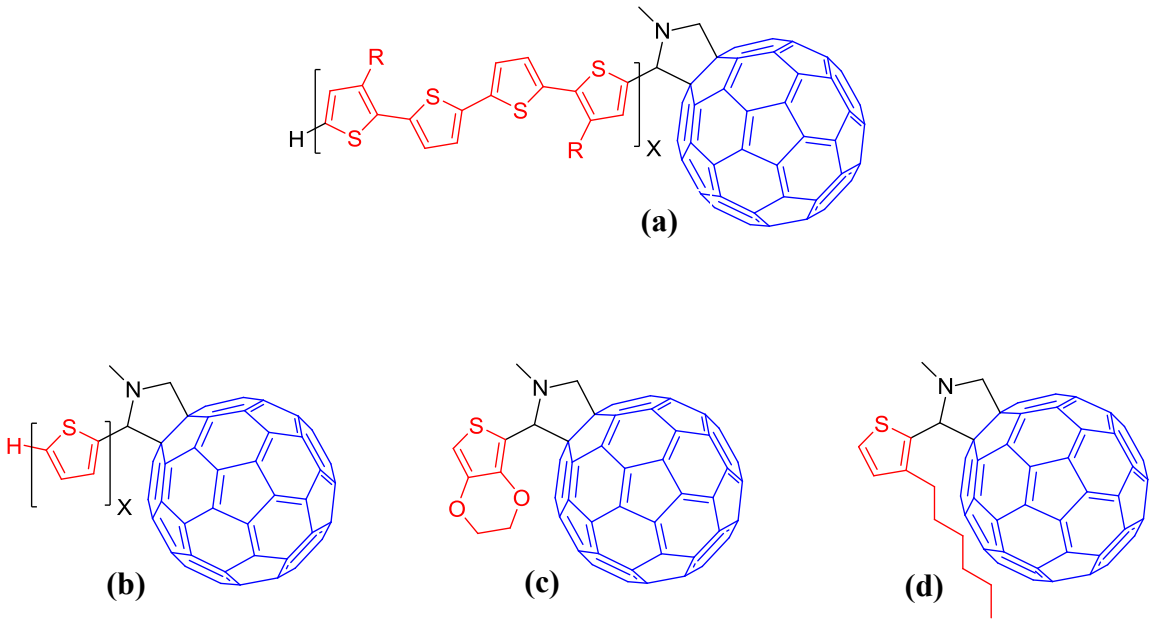

Figure 3.3 Additional dyads containing thiophene or oligothiophene and C_{60}.

Other C_{60}-based dyads of interest are shown in Figure 3.3. Otsubo *et al.* incorporated oligothiophene–C_{60} dyads (Figure 3.3a) as single component materials in photovoltaic devices to produce relatively high incident photon-to-current efficiencies (84). Additional thiophene–C_{60} (Figure 3.3b-d) dyads also exhibit promising electronic photocurrent generation characteristics for photovoltaic devices (85; 86). It has also been shown that small molecule thiophene–C_{60} dyads can behave as compatibilizers in P3HT–PCBM mixtures to suppress macrophase separation of the active layer during thermal annealing (87).

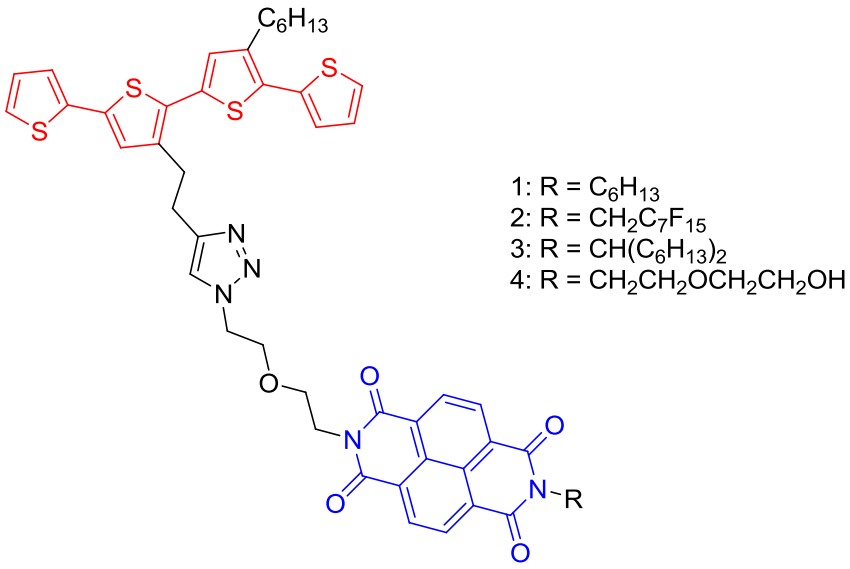

Figure 3.4 NDI– oligothiophene dyads with pairs of miscible and immiscible side chains.

A growing interest in C_{60} alternatives has led to recent D–A dyads that now incorporate different acceptor moieties. In particular, NDI–oligothiophene dyads (Figure 3.4) were synthesized by a click reaction of an NDI–azide and oligothiophene with a terminal alkyne (88). These dyads from Venkataraman *et al*. were created to study dyad organization using D–A interactions and pairs of miscible and or immiscible side chains. Although their study was performed in solution, it supports the notion that incompatible side chains can drive the solid–state packing of future dyads to achieve separate stacks of donors and acceptors while preventing intramolecular D–A stacking.

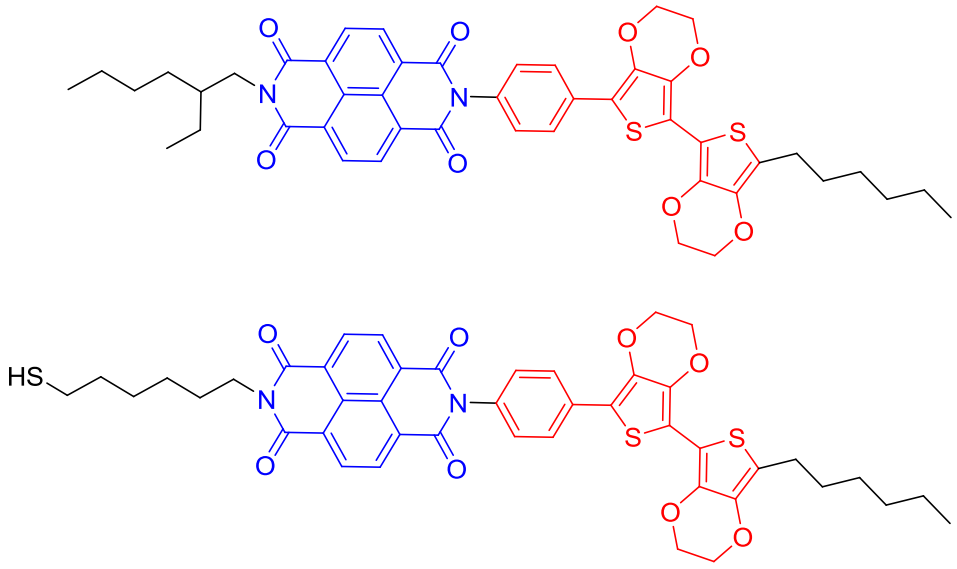

Figure 3.5 Two NDI– EDOT dyads without (top) and with (bottom) thiol functionality.

In addition, a series of NDI–oligo(3,4-ethylenedioxy)thiophene (NDI–EDOT) dyads connected through a phenylene linker were synthesized by Perepichka *et al*. (Figure 3.5) (89). It was reported that complete separation of the EDOT HOMO and NDI LUMO resulted from the twisted, perpendicular orientation of the phenylene linker with respect to the plane of NDI. Thiol functionalities were further appended onto either the EDOT or the NDI alkyl chain to attach these molecules onto gold electrodes, imparting different monolayer junction orientation.

We wish to study the intermolecular stacking behavior of a rigid, tethered DAN–NDI dyad that retains the electrostatic complementarity and relative stacking geometry of the individual molecules. A rigid linker between DAN and the *N*-imide position of NDI will prohibit possible intramolecular D–A interactions arising from DAN and NDI within the same dyad. While a phenylene linker (Figure 3.5) will prohibit the dyad from folding onto itself, the out-of-plane nature of the phenyl group could prohibit an accurate assessment of DAN and NDI contributions on the intermolecular stacking nature of these dyads. Rather, an ethynyl linker will eliminate steric issues and allow us to explore the electronic effects of such a linker on HOMO and LUMO orbital mixing from the DAN and NDI, respectively.

3.3 DESIGN AND SYNTHETIC APPROACH

3.3.1 Ideal Dyad Design

For our purposes, a DAN–NDI dyad must satisfy several design criteria. The molecule must be rigid to prohibit intramolecular self-stacking. The linker must preserve the electrostatic complementarity of DAN and NDI while maintaining a completely planar structure. DAN and NDI must retain an orientation within the dyad that reflects the orientation of DAN and NDI monomers stacked in an alternating fashion. Finally, the molecule must possess side chain tunability to impart solubility as well as explore possible liquid crystalline phases and the effects of side chains versus aromatic D–A interactions on the overall stacking behavior of the dyad.

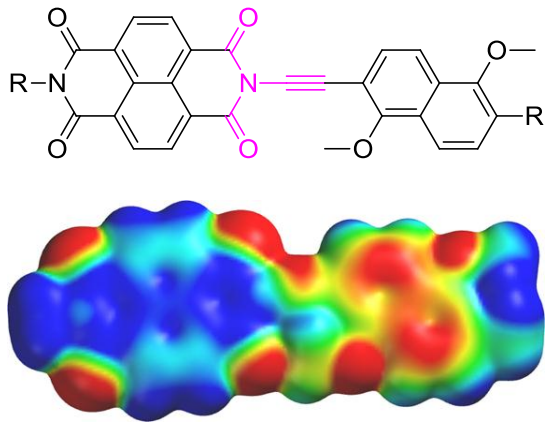

Figure 3.6 The target DAN–NDI dyad (ynimide functionality highlighted in pink) and its corresponding electrostatic potential map. The electrostatic potential map was generated in Spartan using the DFT B3LTP G-31* method.

The ideal DAN–NDI dyad and its electrostatic potential map is shown in Figure 3.6. Functionalization limitations of DAN mean that the relative orientation of DAN and NDI is approximately the same in the dyad as the orientation observed between stacked DAN and NDI monomers. The calculated electrostatic potential map shows satisfactory electrostatic separation with DAN and NDI and each retains their electron rich and electron deficient character, respectively. Importantly, local electrostatics (DAN oxygen and NDI carbonyl groups) are still present which is currently believed to have a dominant role in aromatic D–A stacking (19). The structure does present one significant synthetic challenge. The ethynyl linker requires the formation of an *N*-alkynyl imide or ynimide functionality (Figure 3.6).

3.3.2 Ynimides and Similar C–N Bonds

Nitrogen-substituted alkynes serve as important functionalities and intermediates in organic chemistry. The literature is full of *N*-alkynyl amine (ynamine) and *N*-alkynyl amide (ynamide) examples and their formation, electronics, and reactivity are well understood (90; 91; 92; 93). Yet there are few examples of ynimides. Besides one report of a slight ynimide byproduct (94), the *only* synthetic protocol to form an ynimide was recently developed by Sueda *et al*. using a copper-catalyzed reaction between alkynyl(triaryl)bismuthonium salts and five-membered imides (Figure 3.7d) (95).

C–N bonds, including those in the single set of ynimide examples, are often directly accessed through copper-mediated coupling reactions between nitrogen and substituted alkynes, alkenes, or arenes. Several of these conditions are shown in Figure 3.7 (96; 97; 98; 99). Non-direct methods of *N*-alkynyl formation typically involve elimination, substitution, or isomerization. Examples of these non-direct methods for the production of ynamines and ynamides are shown in Figure 3.8 (100; 101; 102; 103; 104).

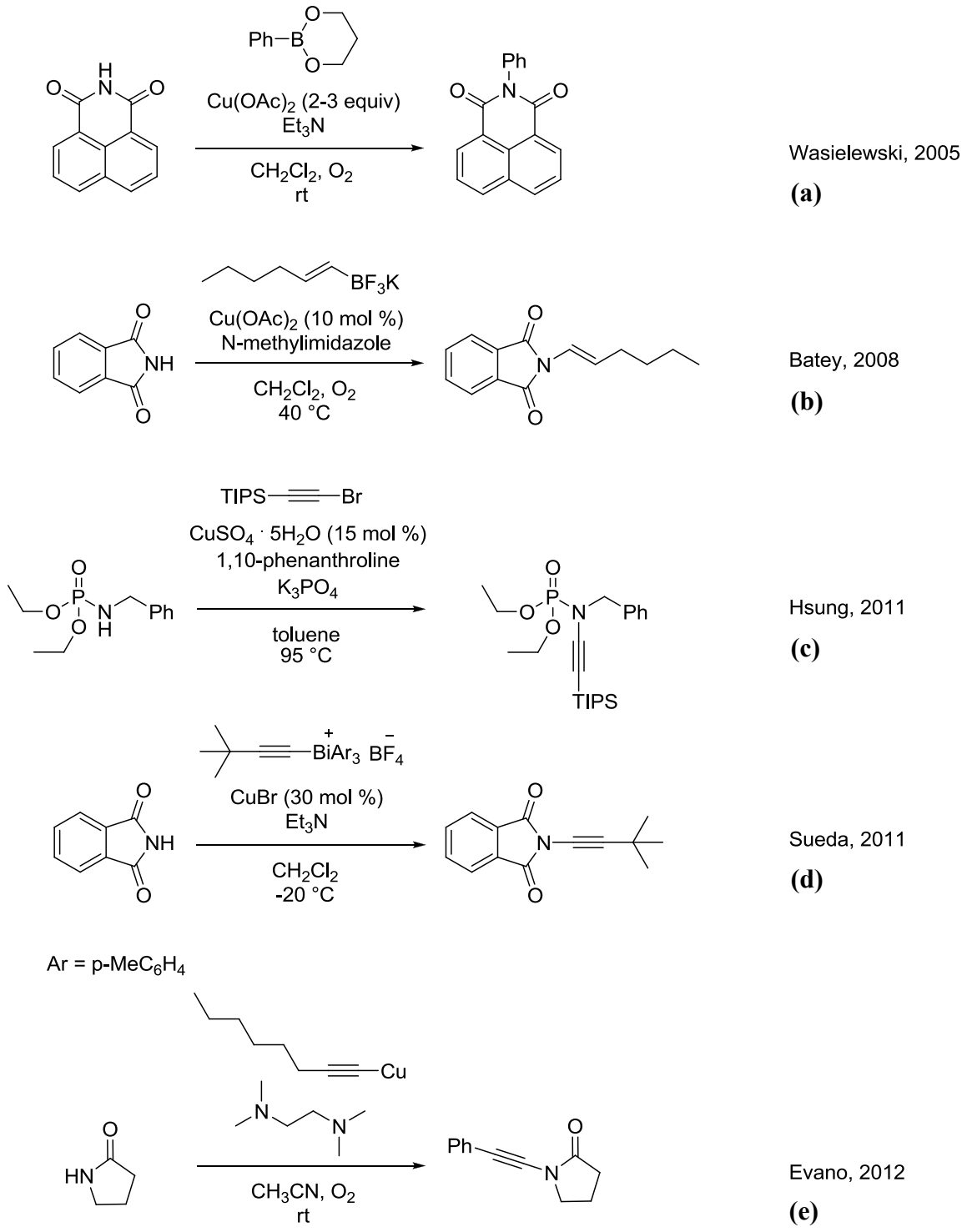

Figure 3.7 Common routes to directly form a C–N bond.

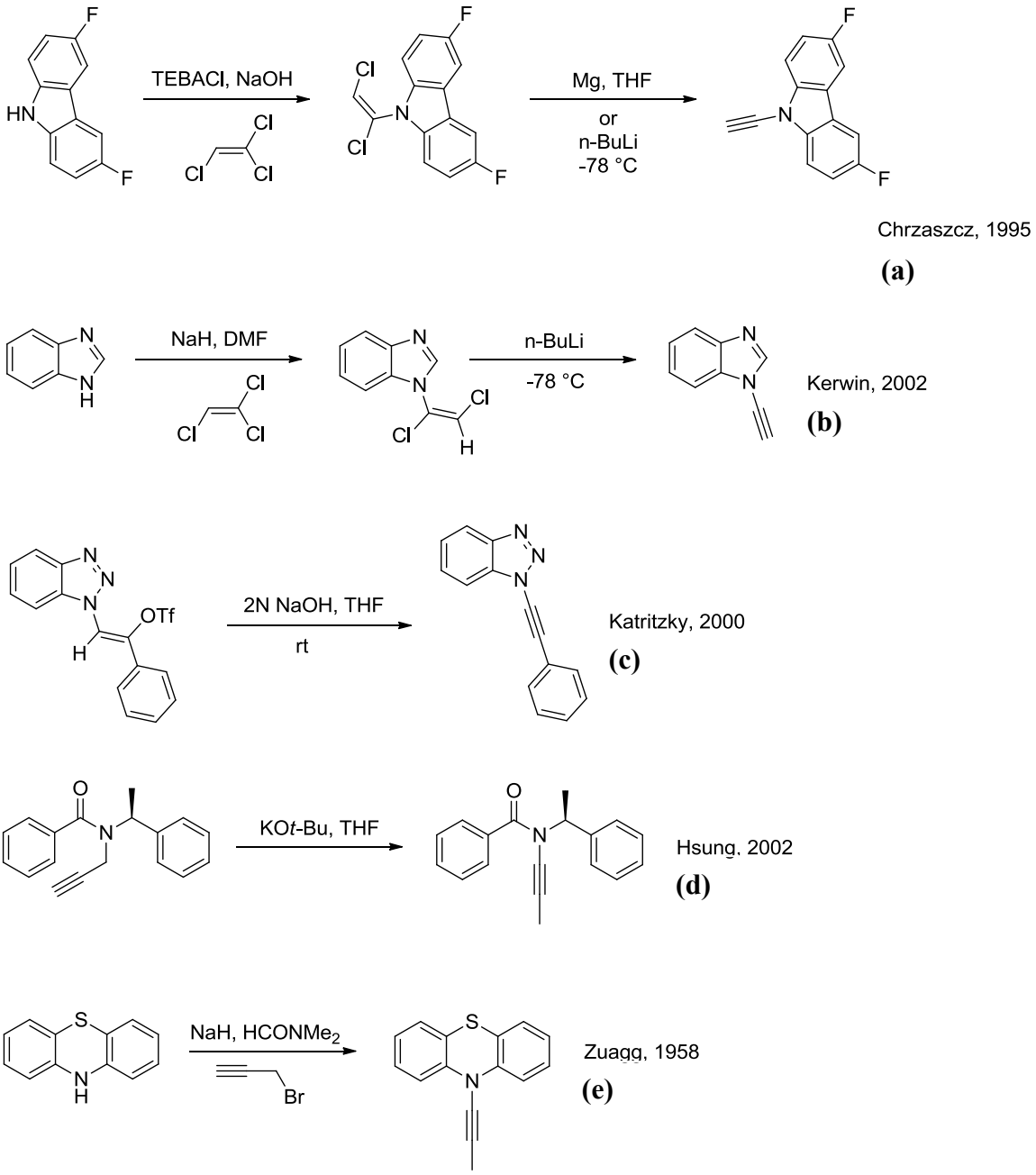

Figure 3.8 Common routes to non-directly form an ynamine or ynamide.

3.3.3 NDI Ynimide Prerequisites

There are some prerequisites that reaction conditions must satisfy to make an NDI ynimide. Many NDI derivatives are poorly soluble, particularly at low temperatures. Suitable conditions require an appropriate solvent and possibly high temperature conditions. Since many of the non-direct methods that are typically employed to produce an ynamine or ynamide require the use of a strong base, caution should be taken when adapting these protocols for an NDI ynimide in order to avoid anion-induced charge-transfer and electron-transfer between NDI and the base (105).

3.3.4 Synthetic Approach

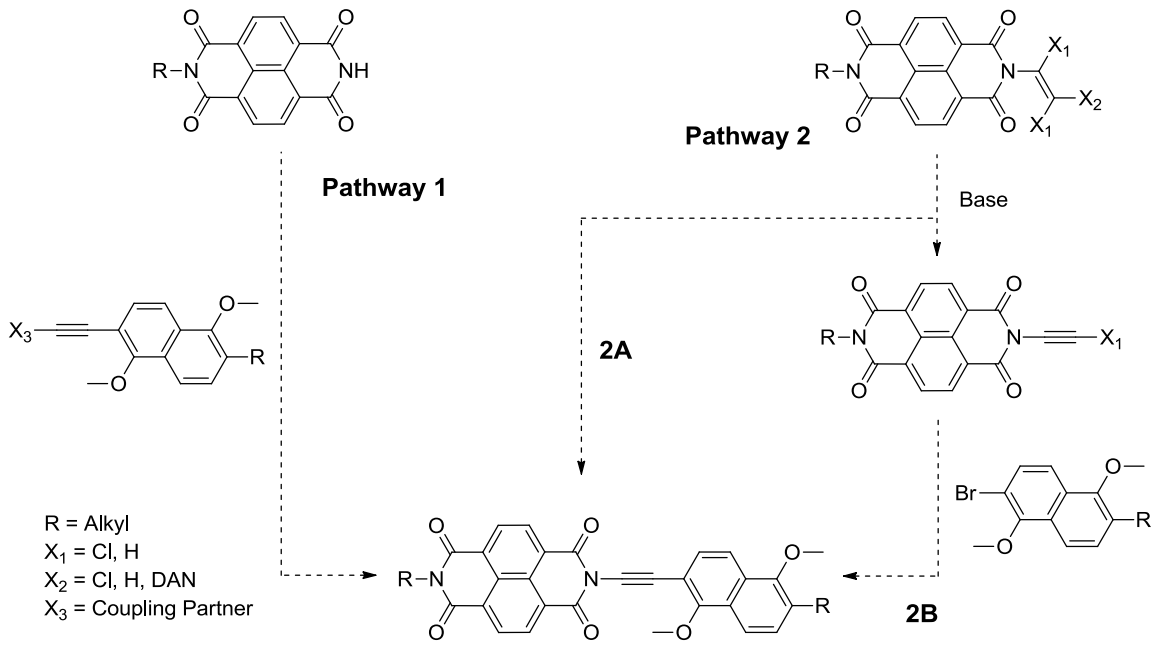

Figure 3.9 Proposed synthetic pathways for a DAN–NDI dyad with ynimide linker.

Keeping the existing synthetic methods for ynamines and ynamides in mind, a direct (Pathway 1) and a non-direct (Pathway 2) route were envisioned to construct the

DAN–NDI dyad through an ynimide linker (Figure 3.9). Pathway 1 proposes to use existing C–N coupling reactions to directly link an appropriately functionalized DAN alkyne to the N–H position of the NDI imide. Pathway 2 proposes to append an ethenyl moiety with leaving groups onto NDI. If one of the ethenyl substituents is DAN, base elimination can directly yield the dyad with ynimide linker (Pathway 2A). Otherwise, base elimination can yield an ynimide that can further undergo a coupling reaction with a DAN halide to yield the dyad (Pathway 2B).

The following sections detail the synthetic steps used to produce DAN and NDI precursors to incorporate into the proposed scheme of Figure 3.9. Representative reactions were performed to test the validity of the two possible pathways to form an ynimide. These reactions include metal-mediated coupling reactions and elimination-based approaches. The results of these direct and non-direct modes of ynimide formation are presented in the following sections.

3.4 RESULTS

3.4.1 Synthesis of DAN and NDI Precursors

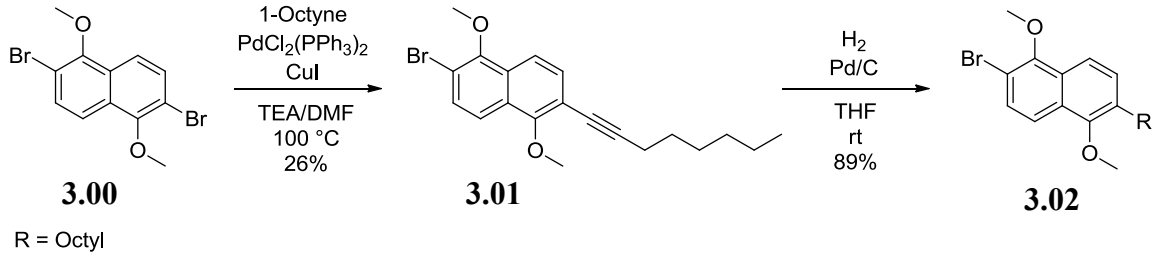

Scheme 3.1 Synthesis of a DAN derivative with a synthetic handle for metal mediated coupling reactions.

The ideal DAN monomer **3.02** and its synthesis are shown in Scheme 3.1. **3.02** has methyl groups on the DAN oxygen atoms to eliminate unnecessary steric issues and to maintain the electronic contribution that the DAN aromatic core receives from its two alkoxy substituents. An alkyl group was appended onto **3.00** using standard Sonogashira coupling protocol and subsequent hydrogenation to yield **3.02**. Another Sonogashira reaction and subsequent deprotection could add a terminal alkyne to give a derivative that can undergo further functionalization for metal-mediated reactions as presented in Pathway 1 of Figure 3.9. The intermediate **3.02** can also be used to synthesize derivatives for reactions in Pathway 2 of Figure 3.9.

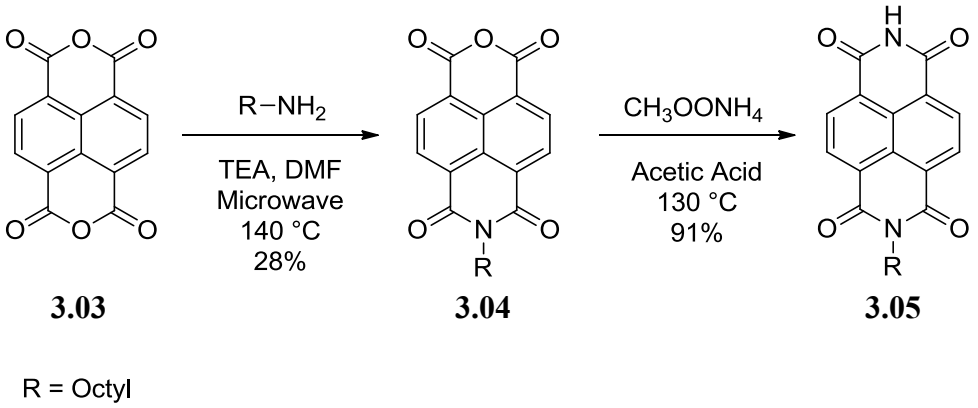

Scheme 3.2 Synthesis of NDI precursors.

An asymmetric NDI with an N-H imide (**3.05**) was prepared through two successive imidization reactions as shown in Scheme 3.2. The first reaction was carried out with **3.03** and octylamine under microwave conditions to give the mono-substituted intermediate **3.04**. **3.04** was also used in reactions to make derivatives for the investigation of methods laid out in Pathway 2 of Figure 3.9 (*vide infra*). Excess ammonium acetate in acetic acid successfully converted **3.04** into **3.05** which exhibited low solubility in common organic solvents. **3.05** was used to investigate metal-mediated coupling reactions (Pathway 1, Figure 3.9) between functionalized alkynes and the imide N-H position (*vide infra*).

3.4.2 Direct Ynimide Formation

Unable to reliably synthesize alkynyl(triaryl)bismuthonium salts, low reaction temperatures and the insoluble nature of NDI under these conditions resulted in unsuccessful attempts to reproduce the copper-catalyzed ynimide reactions by Sueda (Figure 3.7d). The next step was to screen other metal-mediated coupling reactions that have been successful in synthesizing C–N bonds. These reactions are less sensitive to

solvents and are often performed at higher temperatures which were expected to aid in solubilizing NDI. Several coupling methodologies were applied to **3.05** (Scheme 3.3) and the specific alkyne in each case was based on commercially available or literature protocol.

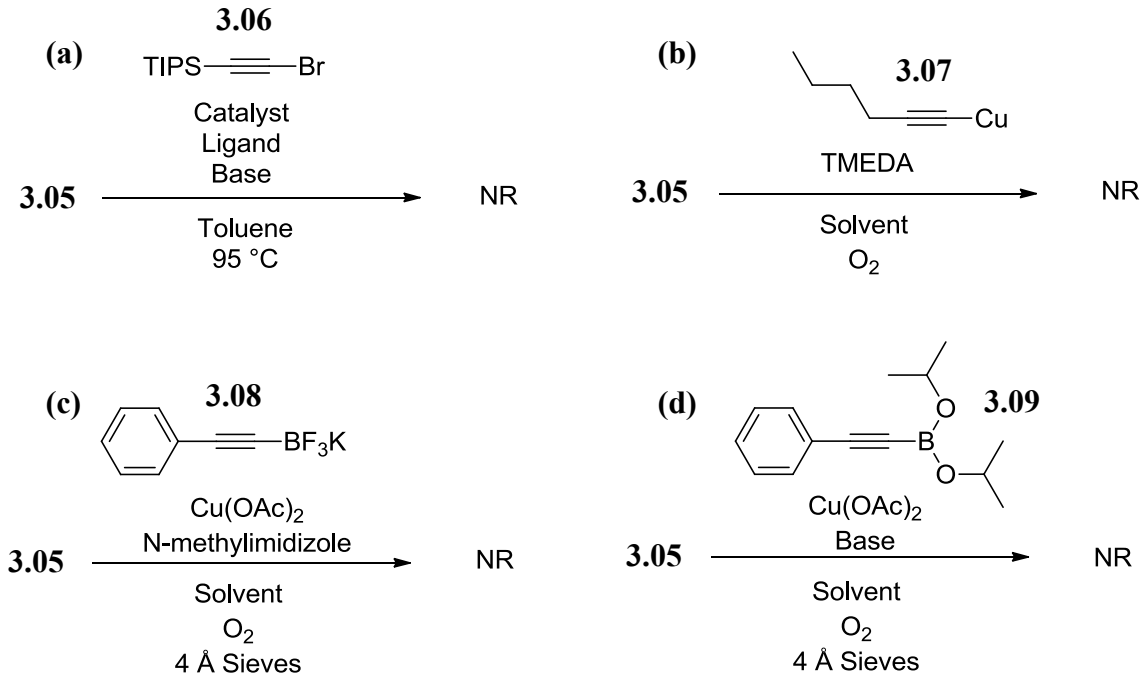

Scheme 3.3 Four coupling reactions that were attempted with **3.05**.

Entry	Catalyst (15 mol %)	Ligand (30 mol %)	Base (2 equiv.)	Yield (%)
1	$CuSO_4•5H_2O$	1,10-phenanthroline	K_2CO_3	0
2	$CuSO_4•5H_2O$	1,10-phenanthroline	K_3PO_4	0
3	$CuSO_4•5H_2O$	1,10-phenanthroline	NaH	0
4	CuI	TMEDA	–	0
5	$CuSO_4•5H_2O$	TMEDA	K_3PO_4	0
6	CuI	1,10-phenanthroline	K_3PO_4	0
7	CuI	DMEDA	K_3PO_4	0

Table 3.1 Coupling conditions for the reaction shown in Scheme 3.3a.

Hsung *et al*. (98) described the synthesis of a series of *N*-phosphoryl ynamides through a copper-catalyzed cross-coupling reaction between phosphoramidates and alkynyl bromides (Figure 3.7c). The reaction was found to be particularly sensitive to the base and ligand. Their reaction optimization involved testing various copper catalysts, ligands, and bases. The same conditions were tested with **3.05** (Table 3.1). $CuSO_4•5H_2O$ and CuI were employed as catalysts while 1,10-phenanthroline, tetramethylethylenediamine (TMEDA), and *N*,*N*′-dimethylethylenediamine (DMEDA) were used as ligands. The bases used in this study were K_2CO_3, K_3PO_4, and NaH. **3.05** (1 equiv.), copper catalyst (15 mol %), ligand (30 mol %), and base (2 equiv.) were added to a dry vial under argon. Toluene (0.1 M) and the alkynyl bromide **3.06** (1.3 equiv., Scheme 3.3a) were added to the vial and the reaction mixture was brought to 95 °C. TLC indicated the presence of starting material (and homo-coupled diyne) only and no ynimide product was observed after 24 h (Table 3.1).

Entry	Temp (°C)	Base (equiv.)	Solvent	Yield (%)
1	rt	–	MeCN	0
2	rt	K_2CO_3 (8)	MeCN	0
3	rt	–	Toluene	0
4	rt	KOH (2)	Toluene/EtOH	0
5	rt	–	DMF	0
6	rt	K_2CO_3 (8)	DMF	0
7	rt	–	THF	0
8	rt	KOH (2)	THF/EtOH	0

Table 3.2 Coupling conditions for the reaction shown in Scheme 3.3b.

Evano *et al*. (99) synthesized a series of ynamides using a cross-coupling reaction between amides and alkynyl organocopper reagents (Figure 3.7e). Optimized literature conditions showed that the reaction required a ligand and that TMEDA gave the best results. The solvent was found to have little effect on the overall reaction. The specific solvents were chosen to best solubilize **3.05** (Table 3.2). Literature protocol did not use a base as the amides were sufficiently nucleophilic. K_2CO_3 or KOH was added to four of the reactions to help compensate for the poor nucleophilicity of NDI. EtOH was added in entries 4 and 8 to help solubilize KOH and to avoid unwanted electron-transfer reactions with NDI. **3.05** (1 equiv.), the alkynyl organocopper reagent **3.07** (2 equiv., Scheme 3.3b), TMEDA (2 equiv.), base (if indicated), and solvent (0.1 M) were added to a vial purged with oxygen (Table 3.2). The mixture was stirred at room temperature to best prevent diyne side-products. TLC indicated the presence of starting material (and homo-coupled diyne) only and no ynimide product was observed after 24 h (Table 3.2).

Entry	Temp (°C)	$Cu(OAc)_2$ (Amount)	Ligand (20 mol %)	TEA (equiv.)	Solvent	Yield (%)
1	40	10 mol %	*N*-methylimidizole	–	CH_2Cl_2	0
2	40	10 mol %	*N*-methylimidizole	–	DMF	0
3	40	10 mol %	–	–	CH_2Cl_2/DMSO	0
4	130	10 mol %	*N*-methylimidizole	–	DMF	0
5	40	2-3 equiv	*N*-methylimidizole	Yes	DMF	0
6	40	10 mol %	*N*-methylimidizole	Yes	DMF	0
7	130	10 mol %	*N*-methylimidizole	Yes	DMF	0

Table 3.3 Coupling conditions for the reaction shown in Scheme 3.3c.

Batey *et al*. (97) used a copper-catalyzed coupling reaction between amides and potassium alkenyltrifluoroborate salts to yield a series of *N*-alkenyl amides (enamides) (Figure 3.7b). Phthalimide was the test substrate in their ligand optimization study for the cross-coupling of phthalimide with potassium hexenyltrifluoroborate. The screening process was modeled after a similar coupling between phthalimide and hexenylboronic acid using Cu^{II} salts and base. The study found that *N*-methylimidazole was the best choice of ligand and that additional base lowered reaction yields significantly. Optimized conditions included running the reactions in CH_2Cl_2 or 1:1 CH_2Cl_2/DMSO at 40 °C under oxygen with 10 mol % of $Cu(OAc)_2$. Test reactions with **3.05** were based off of these optimized conditions and incorporated various temperatures, amounts of $Cu(OAc)_2$, different solvents, and the presence or absence of *N*-methylimidazole and TEA (Table 3.3). **3.05** (1 equiv.), potassium alkynyltrifluoroborate **3.08** (2 equiv., Scheme 3.3c), $Cu(OAc)_2$ (10 mol % to 3 equiv.), solvent (0.1 M), *N*-methylimidazole, TEA (if indicated), and 4 Å molecular sieves were added to a dry vial purged with oxygen (Table

3.3). The mixture was stirred at the indicated temperature under an oxygen atmosphere. TLC indicated the presence of starting material (and homo-coupled diyne) only and no ynimide product was observed after 24 h (Table 3.3).

Entry	Temp (°C)	Equiv. $Cu(OAc)_2$	Equiv. **3.09**	Base (equiv.)	Solvent	Yield (%)
1	55	3	3	TEA (3)	CH_2Cl_2	0
2	55	3	3	TEA (3)	DMF	0
3	55	3	3	K_2CO_3 (3)	DMF	0
4[a]	55	3	6	TEA (6)	DMF	0
5[a]	55	3	6	K_2CO_3 (6)	DMF	0

Table 3.4 Coupling conditions for the reaction shown in Scheme 3.3d. [a]Three more equivalents of $Cu(OAc)_2$, six more equivalents of **3.09**, and six more equivalents of base were added after two days.

Wasielewski *et al*. (96) demonstrated a copper-promoted *N*-arylation of various cyclic imides (Figure 3.7a). Boronic acid and various boronic esters were suitable coupling partners. The most efficient reaction conditions included a slight excess of boronic acid, $Cu(OAc)_2$, and TEA dissolved in CH_2Cl_2 at 55 °C under an oxygen atmosphere. Test conditions with **3.05** were based on Wasielewski protocol using commercially available boronic ester **3.09** (Scheme 3.3d). While CH_2Cl_2 was used in entry 1 to replicate the Wasielewski protocol, DMF was used to better solubilize **3.05** in entries 2–5. **3.05** (1 equiv.), **3.09** (3 or 6 equiv.), $Cu(OAc)_2$ (3 equiv.), and base (3 or 6 equiv.) were suspended in the solvent (0.01 M) with 4 Å molecular sieves (Table 3.4). The reaction mixtures were purged with oxygen and stirred at 55 °C. Additional equivalents of $Cu(OAc)_2$, **3.09**, and base were added to the reaction mixtures in entries 4 and 5 after 48 h. These two reactions were then left to stir at 55 °C for another 48 h. TLC indicated the presence of starting material (and homo-coupled diyne) only and no ynimide product was observed after 24 h for entries 1–3. No ynimide product was

observed as well for entries 4 and 5 after 4 days and additional reagents. Again, only starting material and homo-coupled diyne was visible by TLC.

3.4.3 Non-direct Ynimide Formation

A promising NDI precursor contains leaving groups for an elimination or halide removal reaction to yield an ynimide. One issue is that the removal or elimination of most leaving groups requires strong bases which are problematic for the reasons mentioned in section 3.3.3. Two non-direct routes similar to those in Figure 3.8a and Figure 3.8c were pursued, nonetheless, while trying to implement reaction conditions that would alleviate side-reactions with NDI.

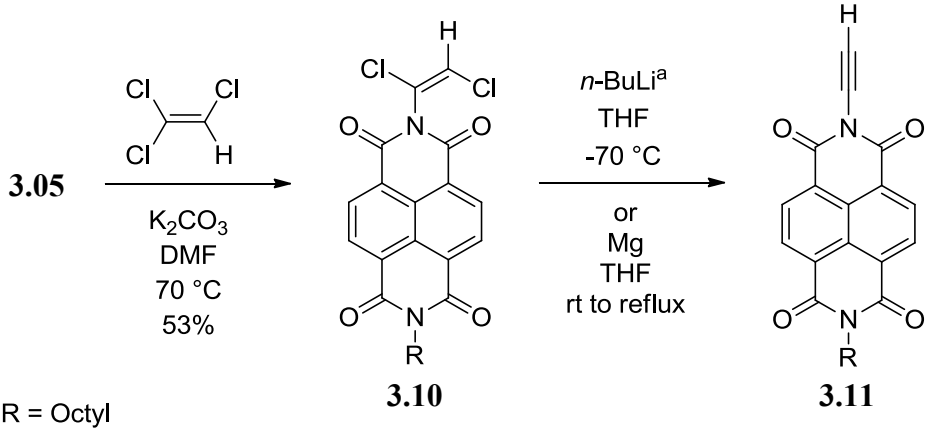

Scheme 3.4 Attempt to synthesize an NDI ynimide through the loss of chloride atoms. [a]Trace **3.11** was detected.

N-ethynyl carbazoles (Figure 3.8a) and *N*-ethynyl pyrroles (Figure 3.8b) were previously prepared by the method in Scheme 3.4. Scheme 3.4 shows the successful synthesis of the chloroethynyl precursor **3.10** and attempts to further convert it into the ynimide **3.11**. **3.10** was prepared by nucleophilic attack of an NDI anion on a dichloroethynyl electrophile formed *in situ* from trichloroethylene (100). An excess of potassium carbonate facilitated both the deprotonation of NDI and the hydrogen abstraction of trichloroethylene to yield the NDI anion and dichloroethynyl electrophile, respectively. Potassium carbonate was selected for its solubility in DMF and inability to

form radical anions with NDI in an aprotic solvent (105). The subsequent addition of 2 equivalents *n*-BuLi to **3.10** at –70 °C resulted in a black, viscous solution and many spots by TLC. A competition was expected under these basic conditions between the **3.11** and products formed through side-reactions. One particular reaction did have a group of TLC spots that appeared to contain a trace amount of **3.11** by ^{1}H NMR and low resolution mass spectrometry (LRMS) (Figure 3.10). Unfortunately, it was difficult to collect further trace amounts of product in other reaction batches and TLC patterns varied greatly during each attempt. Additional efforts to perform this same conversion under literature Grignard conditions (100) also failed.

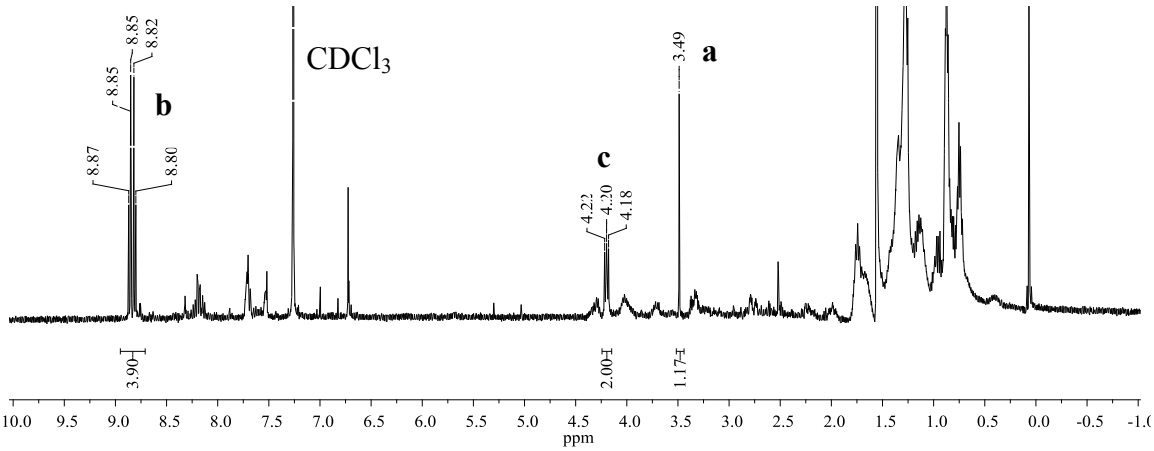

(a)

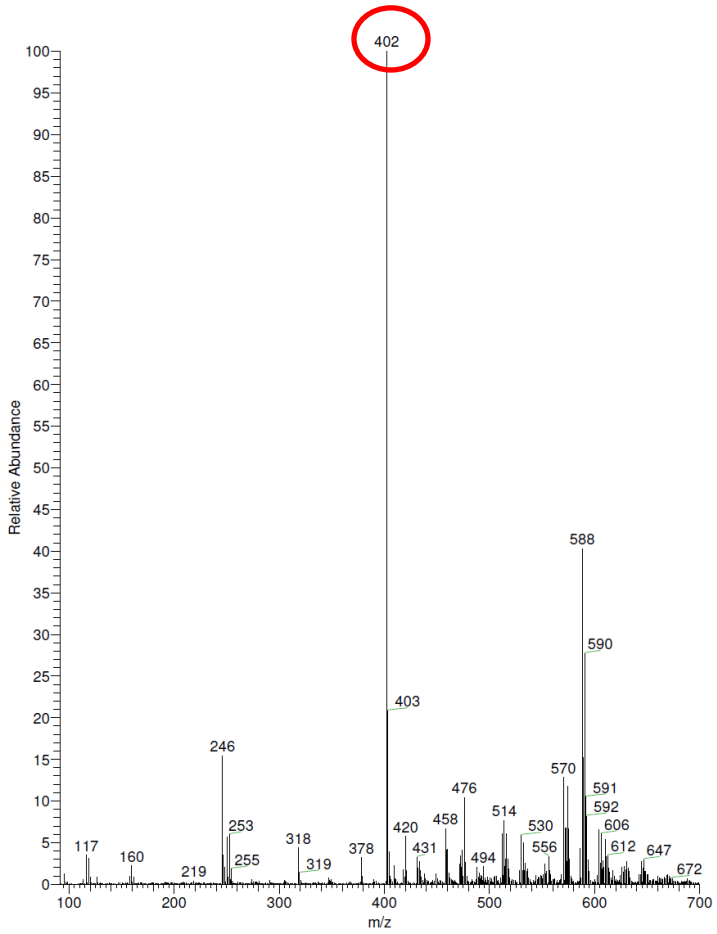

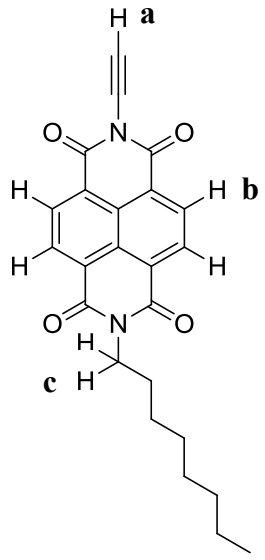

Exact Mass: 402.1580

(b)

Figure 3.10 (a) ^{1}H NMR and (b) LRMS that shows presence of **3.11**.

One way to avoid unwanted side-reactions between NDI and a strong base is to surround the base with a polar protic environment (105). Unlike **3.10**, the intermediate **3.15** in Scheme 3.5 may undergo a traditional E2 elimination to form an ynimide. The same approach was successful for ynamide formation (Figure 3.8c). More importantly, the elimination is performed with KOH in 50/50 H_2O/THF which should provide an environment to help prohibit side-reactions.

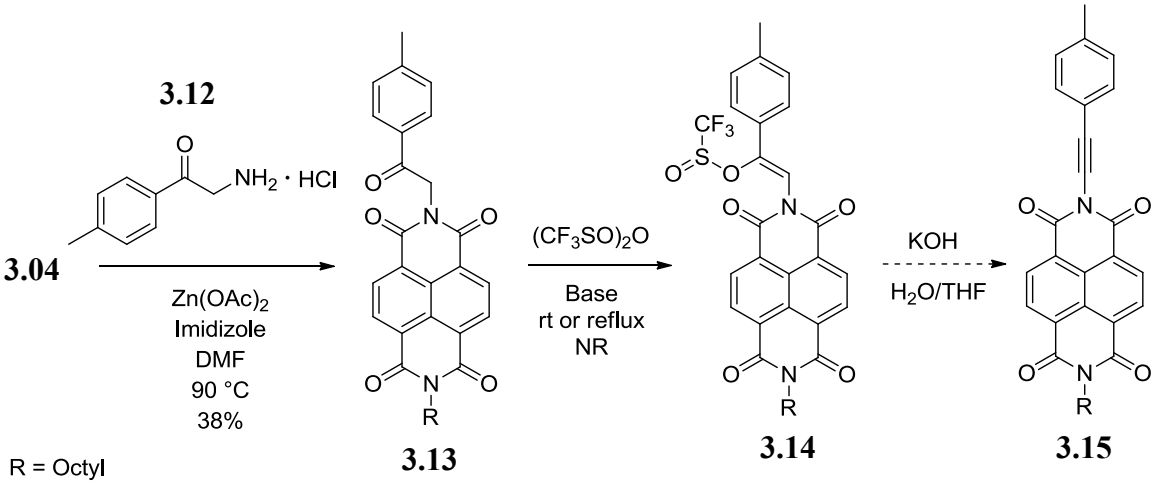

Scheme 3.5 Attempt to synthesize an NDI ynimide through a traditional E2 elimination route.

3.13 was synthesized using **3.06** and **3.12**. **3.12** was selected for the reaction in Scheme 3.5 due to its commercial availability and the phenyl group is an aromatic substituent like DAN. It is worth noting that a catalytic amount of $Zn(OAc)_2$ is necessary to promote the imidization reaction to yield **3.13**, otherwise only starting material is recovered. Yet all literature protocols failed to synthesize **3.14** with triflic anhydride and base (102; 106; 107). Only starting material was observed by TLC over the reaction course.

3.5 DISCUSSION

The formation of **3.10** demonstrates that bases such as K_2CO_3 are able to deprotonate **3.05** and that DMF is suitable for solubilizing NDI. The lack of coupling activity associated with the direct methods, therefore, must then be the result of other factors yet to be determined. The boronic acid or boronic ester route held promise as a similar protocol was used in a low yielding and time consuming reaction by Matile *et al*. for the *N*-arylation of NDI (Figure 3.11) (108) but attempts to perform a similar reaction using the alkynyl boronic ester were unsuccessful.

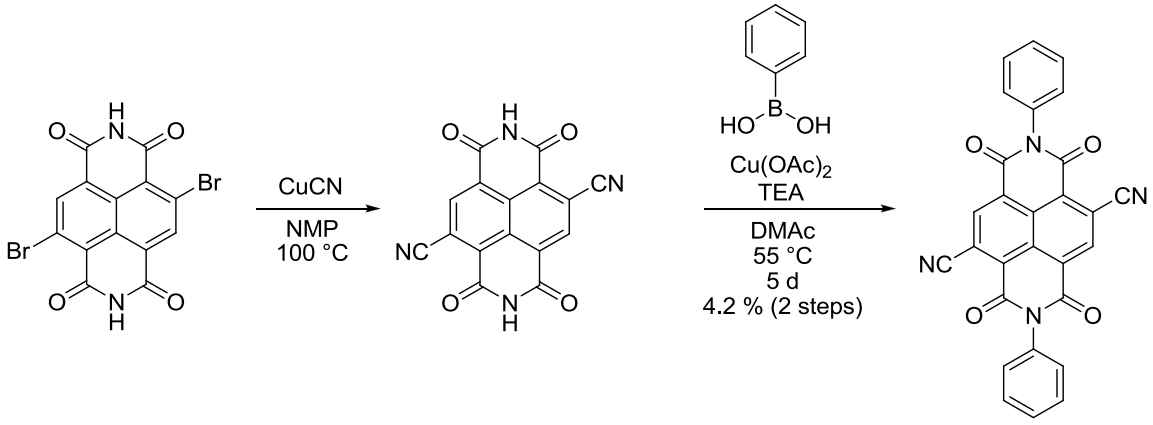

Figure 3.11 Copper-promoted *N*-arylation of NDI by Matile *et al*.

Until more reliable direct methods for ynimide formation are discovered, the most probable pathway at this time may be a non-direct method. The trace amount of **3.11** that was detected in some reactions indicates that a non-direct route might work if NDI–base interactions are attenuated. One method is to synthesize an NDI derivative that can undergo an elimination reaction to form an ynimide while in an organic/aqueous environment. Our synthesis of such a molecule failed while trying to create a vinyl triflate (**3.14**) and Stang *et al*. also reported that their attempts to synthesize a vinyl triflate from a carbonyl compound with an electron withdrawing group on the alpha

carbon also failed (109). They even reported that high temperatures (100 °C) and neat reagents resulted in unchanged starting material. NDI is a strong electron withdrawing substituent and it is possible that similar complications are prohibiting the conversion of **3.13** into **3.14**.

3.6 CONCLUSION

Besides what appears to be the occasional trace of an ynimide product during the conversion of **3.10** to **3.11**, all methods presented in this chapter to provide an accessible route for NDI ynimide formation have been unsuccessful. The lack of synthetic success shifted our focus towards more readily available rigid DAN–NDI systems. Specifically, reliable methods to functionalize the NDI aromatic core and a substantial interest in rigid NDI-containing systems inspired our investigation to explore the effects of aromatic D–A interactions on the solid state assembly of conjugated NDI–donor polymers. The results of such an investigation are the subject of chapter 4.

3.7 EXPERIMENTAL

3.7.1 General Methods

(2-bromoethynyl)triisopropylsilane (**3.06**) (110), hex-1-ynylcopper (**3.07**) (99), and 2,6-dibromo-1,5-dimethoxynaphthalene (**3.00**) (111) were synthesized according to literature procedure. Potassium phenylethynyltrifluoroborate (**3.08**) was purchased from Frontier Scientific, CuI and $Pd(PPh_3)_2Cl_2$ were purchased from STREM, and 2-amino-4′-tolylacetophenone hydrochloride (**3.12**) was purchased from APAC Pharmaceutical, LLC. 1,4,5,8-Naphthalenetetracarboxylic dianhydride (**3.03**), diisopropyl 3,3-dimethylbut-1-ynylboronate (**3.09**), and all other chemicals were purchased from Sigma Aldrich or Fisher Scientific. Dry solvents were stored over molecular sieves prior to use. All reactions were carried out under argon. NMR spectra were taken on a Varian Unity 400 spectrometer. Melting points were detected using a MEL-TEMP apparatus.

3.7.2 Synthesis and Characterization

2-bromo-1,5-dimethoxy-6-(oct-1-yn-1-yl)naphthalene (**3.01**). To a solution of **3.00** (0.1224 g, 0.35 mmol) in 50/50 DMF/TEA (4 ml) was added 1-octyne (0.052 ml, 0.35 mmol), $PdCl_2(PPh_3)$ (0.0242 g, 10 mol %), and CuI (0.0048, 7 mol %). The solution was stirred overnight at 100 °C. The solvent was removed by rotary evaporation and the solid was washed with water and extracted with CH_2Cl_2. The CH_2Cl_2 extracts were dried over Na_2SO_4, filtered and the CH_2Cl_2 was removed by rotary evaporation. The crude material was purified by column chromatography (5% to 7% CH_2Cl_2/Hex) to yield **3.01** (0.0347 g, 0.09 mmol, 26% yield) as a light yellow oil. ^{13}C NMR (400 MHz, $CDCl_3$) 157.99, 153.13, 131.05, 130.33, 129.61, 128.68, 119.69, 117.32, 113.88, 113.00, 96.84 (1 peak behind solvent), 61.54, 61.48, 31.38, 29.70, 28.66, 22.59, 19.82, 14.07 δ ppm; ^1H NMR

(400 MHz, $CDCl_3$) δ 7.81 (d, *J* = 8 Hz, 1H), 7.77 (d, *J* = 8 Hz, 1H), 7.58 (d, *J* = 12 Hz, 1H), 7.45 (d, *J* = 8 Hz, 1H), 4.11 (s, 3H), 3.98 (s, 3H), 2.51 (t, *J* = 8 Hz, 2H), 1.67 (m, 2H), 1.50 (m, 2H), 1.34 (m, 4H), 0.92 (t, *J* = 6 Hz, 3H) ppm; CI-HRMS (positve ion) calculated for $C_{20}H_{23}BrO_2$ (M^+), 374.0881; found 374.0878.

2-bromo-1,5-dimethyoxy-6-octylnaphthalene (**3.02**). To a solution of **3.01** (0.0347 g, 0.09 mmol) in THF (2 ml) was added Pd/C (20 weight %). The solution was purged with hydrogen and a balloon was used to maintain the hydrogen atmosphere. The solution stirred under hydrogen at room temperature for two days. Upon completion, the solution was passed through a short plug of celite to yield **3.02** (0.0316 g, 0.08 mmol, 89%) as a colorless oil. ^{13}C NMR (400 MHz, $CDCl_3$) 153.61, 153.34, 131.99, 129.89, 129.32, 129.23, 128.88, 119.58, 117.98, 112.23, 62.16, 61.44, 31.89, 30.81, 29.75, 29.66, 29.50, 29.26, 22.67, 14.11 δ ppm; ^1H NMR (400 MHz, $CDCl_3$) δ 7.84 (d, *J* = 8 Hz, 1H), 7.74 (d, *J* = 8 Hz, 1H), 7.57 (d, *J* = 8 Hz, 1H), 7.38 (d, *J* = 12 Hz, 1H), 4.00 (s, 3H), 3.90 (s, 3H), 2.78 (t, *J* = 8 Hz, 2H), 1.68 (m, 2H), 1.30 (m, 10H), 0.89 (t, *J* = 8 Hz, 3H) ppm; CI-HRMS (positve ion) calculated for $C_{20}H_{27}BrO_2$ (M+H), 380.1174; found 380.1191.

7-octyl-1*H*-isochromeno[6,5,4-*def*]isoquinoline-1,3,6,8(7*H*)-tetraone (**3.04**). A 1:1 molar mixture of **3.03** (10 g, 37 mmol) and 1-octylamine (4.8 g, 38 mmol) in DMF (375 ml) was reacted with TEA (3.8 g, 38 mmol) under previously described microwave conditions (79). After cooling to room temperature, the reaction mixture was refrigerated for several hours to precipitate the di-substituted byproduct. The solution was filtered and the mono-substituted product was collected from the filtrate by rotary evaporation. Clean product was obtained by taking up the crude material in acetone and slowly adding it to stirred glacial acetic acid. The mixture was stirred for 0.5 h and the product was

collected by vacuum filtration and thoroughly washed with H_2O to afford **3.04** (4.5 g, 12 mmol, 32% yield) as an off-white solid. Mp 175-177 °C; ^{13}C NMR (400 MHz, $CDCl_3$) δ 162.17, 158.83, 133.13, 131.18, 128.83, 127.90, 126.81, 122.76, 41.20, 31.77, 29.24, 29.16, 28.00, 27.04, 22.61, 14.08 ppm; ^1H NMR (400 MHz, $CDCl_3$) δ 8.80 (s, 4H), 4.17 (t, *J* = 7.2 Hz, 2H), 1.69 (q, 7.6 Hz, 2H), 1.25 (m, 10H), 0.85 (t, *J* = 7.2 Hz, 3H) ppm; CI-HRMS (positive ion) calculated $C_{22}H_{21}NO_5$ (M+H) 380.1498, found 380.1498.

2-octylbenzo[*lmn*][3,8]phenanthroline-1,3,6,8(2*H*,7*H*)-tetraone (**3.05**). To a solution of **3.04** (0.8895 g, 2.4 mmol) and glacial acetic acid (30 ml) was added excess ammonium acetate (2.9294 g, 38.0 mmol) and heated at 140 °C for 1 h. After cooling, the mixture was poured over ice and the solid product was collected by vacuum filtration. Poor solubility and streaking complicated purification by column chromatography. The product was washed with H_2O and any excess H_2O was removed by lyophilization to yield **3.07** (0.8265 g, 2.2 mmol, 91% yield) as a light brown solid. Decomposition 283 °C; ^{13}C NMR (500 MHz, 100 °C, DMF-d_7) δ 163.83, 163.59, 131.08, 130.38, 128.01, 127.71, 41.16, 32.20, 29.67, 29.51, 28.51, 27.55, 22.89, 14.00 ppm; ^1H NMR (500 MHz, 100 °C, DMF-d_7) δ 11.51 (br. s, 1H), 8.74 (d, *J* = 7.5 Hz, 2H), 8.69 (d, *J* = 7.5 Hz, 2H), 4.18 (t, *J* = 7.5 Hz, 2H), 1.79 (p, *J* = 7 Hz, 2H), 1.37 (m, 10H), 0.89 (t, *J* = 7 Hz, 3H) ppm; ^1H NMR (400 MHz, $CDCl_3$) δ 8.78 (dd, *J* = 8 Hz, 4H), 8.55 (br. s, 1H), 4.20 (t, *J* = 8 Hz, 2H), 1.74 (m, 2H), 1.46–1.22 (m, 10H), 0.88 (t, *J* = 6 Hz, 3H) ppm; CI-HRMS (positive ion, M + H) calculated 379.1658 for $C_{22}H_{23}N_2O_4$; found 379.1657.

(E)-2-(1,2-dichlorovinyl)-7-octylbenzo[lmn][3,8]phenanthroline-1,3,6,8(2H,7H)-tetraone (**3.10**). A DMF (0.1 M) solution of **3.05** (0.0500 g, 0.13 mmol) and excess K_2CO_3 (0.14 g, 1.01 mmol) was heated to 75 °C. To this solution was added

trichloroethylene (0.018 ml, 0.20 mmol) and it stirred at this temperature for 5 h. The DMF was removed by rotary evaporation and the crude material was taken up in CH_2Cl_2 and washed with H_2O. The organics were dried over Na_2SO_4 and the solvent was removed by rotary evaporation. Purification was accomplished by column chromatography (50/50 CH_2Cl_2/Hexane) to yield **3.12** as an off-white solid (0.0326 g, 0.07 mmol, 53% yields). Mp 138-141 °C; ^{13}C NMR (400 MHz, $CDCl_3$) δ 162.49, 160.10, 131.86, 130.99, 127.49, 127.25, 126.93, 125.64, 124.10, 121.05, 41.11, 31.78, 29.26, 29.17, 28.04, 27.05, 22.62, 14.09 ppm; ^{1}H NMR (400 MHz, $CDCl_3$) δ 8.85 (dd, *J* = 0.8 Hz, *J* = 10.8 Hz, 2H), 8.81 (dd, *J* = 0.8 Hz, *J* = 10.8 Hz, 2H), 6.82 (s, 1H), 4.20 (t, *J* = 8 Hz, 2H), 1.74 (m, 2H), 1.34 (m, 10H), 0.87 (t, *J* = 6 Hz, 3H) ppm; CI-HRMS (positive ion, M + H) calculated 473.1035 for $C_{24}H_{23}N_2O_4Cl_2$; found 473.1031.

2-octyl-7-(2-oxo-2-(p-tolyl)ethyl)benzo[lmn][3,8]phenanthroline-1,3,6,8(2H,7H)-tetraone (**3.13**). A solution of **3.04** (0.1205 g, 0.32 mmol), **3.12** (0.05 g, 0.34 mmol), imidazole (0.0550 g, 0.81 mmol), and a catalytic amount of zinc acetate were added to DMF (3 ml). The solution was stirred at 135 °C for 2 h. Upon cooling, the DMF was removed by rotary evaporation. The crude material was taken up in CH2CL2 and washed with H_2O. The organics were dried over Na_2SO_4 and the solvent was removed by rotary evaporation. Purification was accomplished by column chromatography (100% CH_2Cl_2) to yield **3.13** as an off-white solid (0.0592 g, 0.12 mmol, 38% yield). Mp 226-228 °C; ^{13}C NMR (400 MHz, $CDCl_3$) δ 190.78, 162.77, 162.66, 145.01, 132.20, 131.23, 130.91, 129.56, 128.29, 126.92, 126.75, 126.27, 46.66, 41.03, 31.79, 29.28, 29.18, 28.08, 27.09, 22.63, 21.81, 14.09 ppm; ^{1}H NMR (400 MHz, $CDCl_3$) δ 8.76 (s, 4H), 7.96 (d, *J* = 8 Hz, 2H), 7.33 (d, *J* = 8 Hz, 2H), 5.64 (s, 2H), 2.46 (s, 3H), 1.75 (p, *J* = 8 Hz, 2H), 1.28

(m, 10H), 0.88 (t, J = 6 Hz, 3H) ppm; ESI-HRMS (positive ion, $(M + Na)^+$) calculated 533.20470 for $C_{24}H_{23}N_2O_4Cl_2$; found 533.20410.

Chapter 4

Conjugated NDI–Donor Polymers: Exploration of Donor Size and Electrostatic Complementarity

4.1 CHAPTER SUMMARY

4.1.1 Introduction

Chapter 2 investigates DAN and NDI monomer association while in the solid state. Chapter 4 further explores aromatic donor–acceptor (D–A) interactions in the solid state by incorporating NDI and various aromatic donors into conjugated polymers. Conjugated D–A polymers are an important class of materials geared toward next generation organic electronic applications.

4.1.2 Goals

The goal of this chapter is to answer the question: *How will donors with different aromatic sizes and electrostatic potentials affect the overall stacking morphology of conjugated NDI–donor polymer chains?* The answer to this question will help build a working model for the interchain stacking behavior for this particular class of polymers which should aid in the development of next generation organic electronic materials.

4.1.3 Approach

Polymerizations were carried out between dibrominated NDI and four different diethynyl donor moieties using the Sonogashira coupling protocol. Polymers were characterized by GPC, UV-vis and fluorescence spectroscopy, IR spectroscopy, and CV. Polymer chain stacking morphology was investigated with fluorescence spectroscopy and XRD to develop a model that describes the interchain stacking behavior.

4.1.4 Results

Conjugated D–A copolymers comprised of electron-deficient NDI linked to a series of relatively electron-rich aromatics via ethynyl spacers were synthesized and characterized. While LUMO levels remained constant at –3.75 eV, HOMO levels were sensitive to the relatively electron rich aromatic donors and systematically tuned from –5.68 eV to –5.17 eV. Regardless of the electron-rich comonomer, fluorescence and XRD data were consistent with the polymer chains being assembled through the stacking of NDI moieties in an offset face-to-face fashion rather than alternating D–A stacks (112).

4.2 BACKGROUND

The unique electronic properties of conjugated polymers have rendered them desirable materials for applications that range from photovoltaic (PV) cells (113) to field effect transistors (114; 115) and electrochromic devices (116). Conjugation along the polymer backbone allows for extended π-delocalization that can result in a relatively high HOMO level, a relatively low LUMO level, or a small HOMO–LUMO band gap. As a result, certain electronic characteristics are attainable such as p-type or n-type behaviors, high charge carrier mobilities and, for photovoltaic purposes, a broad visible absorption spectrum (113; 114; 116).

As a practical material, semiconducting polymers should have tunable electronic and photovoltaic properties. One method to fine-tune the electronic properties of these materials has been to synthesize conjugated aromatic D–A polymers (113; 117; 118). Energy levels can be tuned through careful selections of monomer units, as D–A polymer HOMO–LUMO levels are well-approximated by the individual monomeric donor HOMO and acceptor LUMO orbitals (119; 120). Hence, progress in this area has

focused on developing new monomers and implementing appropriate combinations of these donor and acceptor moieties (121; 122).

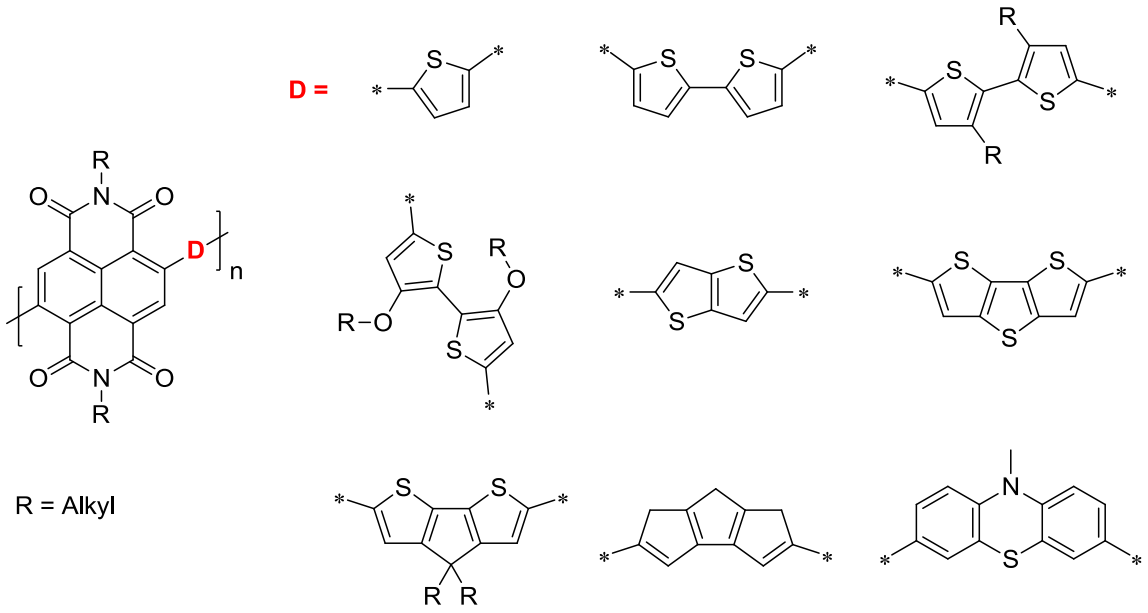

Figure 4.1 Structures of other literature conjugated NDI–donor polymers.

NDI has emerged as a popular acceptor moiety due to its electron deficient aromatic core, high electron carrier mobility (123; 124), and low lying LUMO (125). Recent synthetic advances have not only allowed for substitution through the imide positions, but direct substitution on the NDI aromatic core is now readily accessible (126; 36). In addition, solubility limitations have been addressed and the construction of large polymers with NDI is now possible (123; 124; 127; 128). Numerous donor monomers have been copolymerized with NDI (Figure 4.1) in a conjugated fashion to alter polymer electronic and photovoltaic properties. These groups have included thiophene-based (123; 124; 127; 128; 129; 130; 131; 132; 133; 134; 135), thiazole-based (136), and fluorene-based (137) donors.

Previously, our group has exploited the complementary size and electrostatics of the relatively electron-deficient NDI with electron-rich DAN to affect the macromolecular assembly of aqueous foldamers (24; 23; 21), self-assembling polymers (28) and tunable liquid crystals (38; 29). Although DAN polymers have been reported (138), to the best of our knowledge there has been no report of a conjugated, alternating polymer incorporating both DAN and NDI. We reasoned that the complementary nature of the DAN and NDI donor–acceptor units could facilitate interchain assembly, thereby leading to useful bulk properties. Alternatively, there are now theoretical arguments asserting that electrostatic complementarity between highly polarized groups on the periphery of aromatics, rather than overall aromatic electron density, can provide the dominant interactions between stacked aromatics (19). Such considerations and a number of recent experimental examples suggest that NDI units themselves may dominate the interchain assembly of NDI-containing polymers, favoring an offset face-centered stacking mode in which the strong NDI carbonyl dipole moments complement each other from one unit to the next (33; 34; 139; 140; 141). Herein, we report the synthesis and characterization of a series of conjugated alternating NDI-based aromatic D–A polymers linked by single alkynyl units and present evidence that NDI self-stacking dominates the intermolecular polymer chain assembly.

4.3 RESULTS

4.3.1. Design

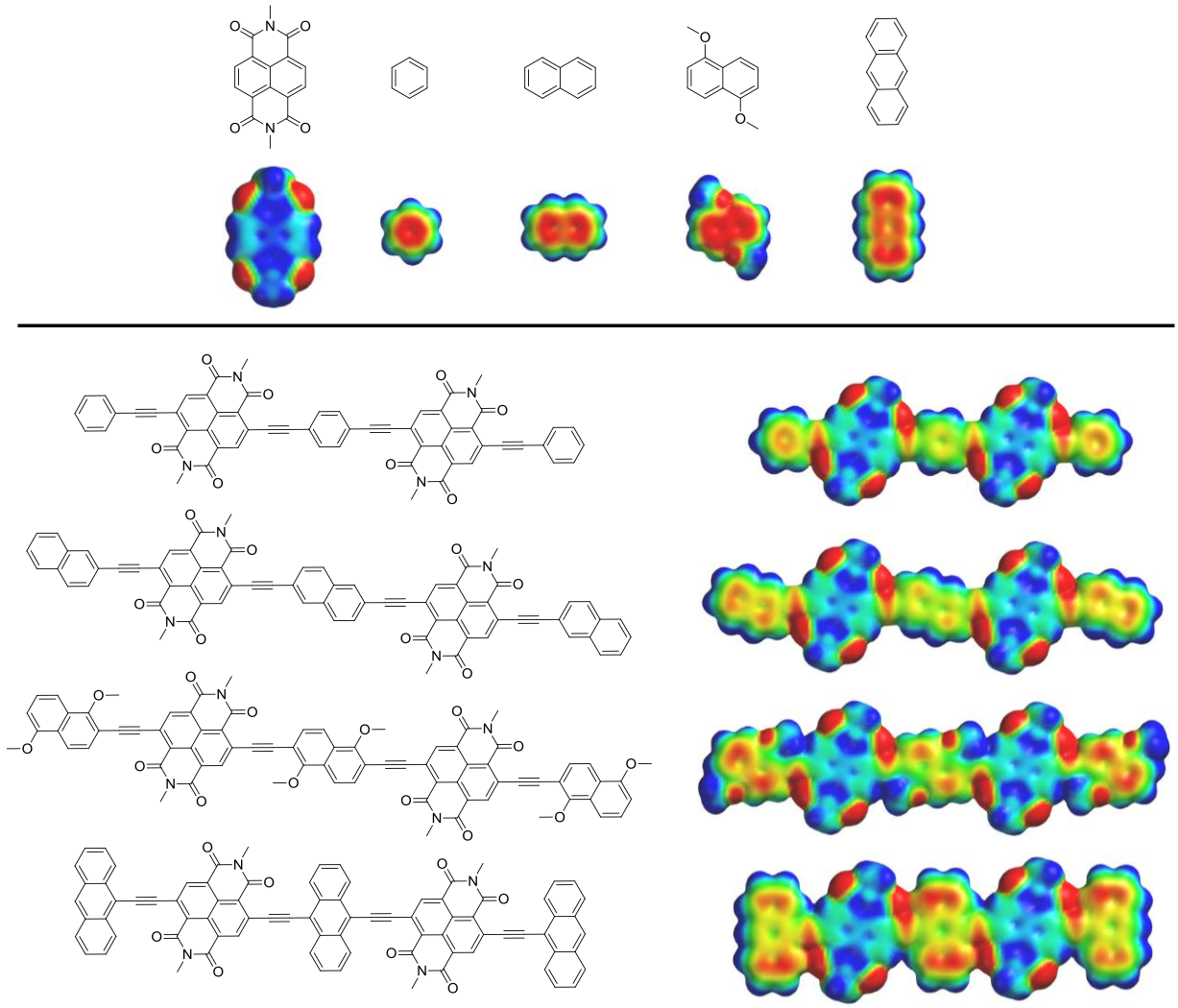

Figure 4.2 1) Figure shows the electrostatic potential maps of the individual monomers (top) and the monomers connected by alkyne linkages (bottom) 2) Models were generated with the same electrostatic potential color scale in Spartan using the DFT B3LYP G-31* method.

DAN, benzene, naphthalene, and anthracene were selected to explore how the physical size and donating properties influence the properties of conjugated NDI–donor

polymers. DAN and NDI are known to stack in an alternating fashion (21; 29) due to electrostatic complementarity that drives desolvation effects in polar media (142). Similar self-assembly has also been observed in a 1:1 complex of an anthracene-based host and NDI guest (143). On the contrary, benzene and naphthalene are not expected to stack as well with NDI due to a lesser degree of size and electrostatic complementarity, respectively. Although the differences are small, electrostatic potential maps (Figure 4.2) show that the area of electron density on the aromatic cores follows the following trend: anthracene > DAN > naphthalene > benzene. The electrostatic potential maps also show that the oxygen atoms on DAN strongly contribute to the increased electron density on the aromatic core when compared to naphthalene which lacks these oxygen atoms. In general, acene-based molecules form polycrystalline assemblies in which the aromatics exhibit some sort of stacked geometry facilitated by the rigid and planar acene structure. Several such derivatives have found use in devices such as OFETs (144). Note the strong local electron density on the DAN oxygen atoms. It is likely that these areas of localized high electron density on the DAN periphery can interact with the relative lack of electron density around the carbon atoms of the NDI carbonyl groups, an interaction that is not possible with the other donors.

Instead of directly connecting together the aromatic cores of NDI and the donors, an alkynyl linkage was selected to serve as the mode of conjugation in order to alleviate steric hindrance that would otherwise prevent coplanarity of aromatic donor and acceptor units. Thus, we anticipate that all of the aromatic units in the polymers **P4.2**, **P4.5**, **P4.8**, and **P4.11** (Scheme 4.1) can adopt a highly conjugated and coplanar conformation. The planar structure is expected to facilitate interchain assembly through some type of stacked arrangement. The minimized structures in Figure 4.2 indicate that, consistent with our design criteria, the donor moieties should be able to adopt a relatively planar arrangement

when connected to two NDI moieties through alkynyl linkages. The alkynyl linkages and subsequent conjugation are expected to result in strong delocalization and diminished electrostatic separation between the donor moieties and NDI, although some level of donor and acceptor properties should remain with the acene and NDI units, respectively.

4.3.2 Synthesis

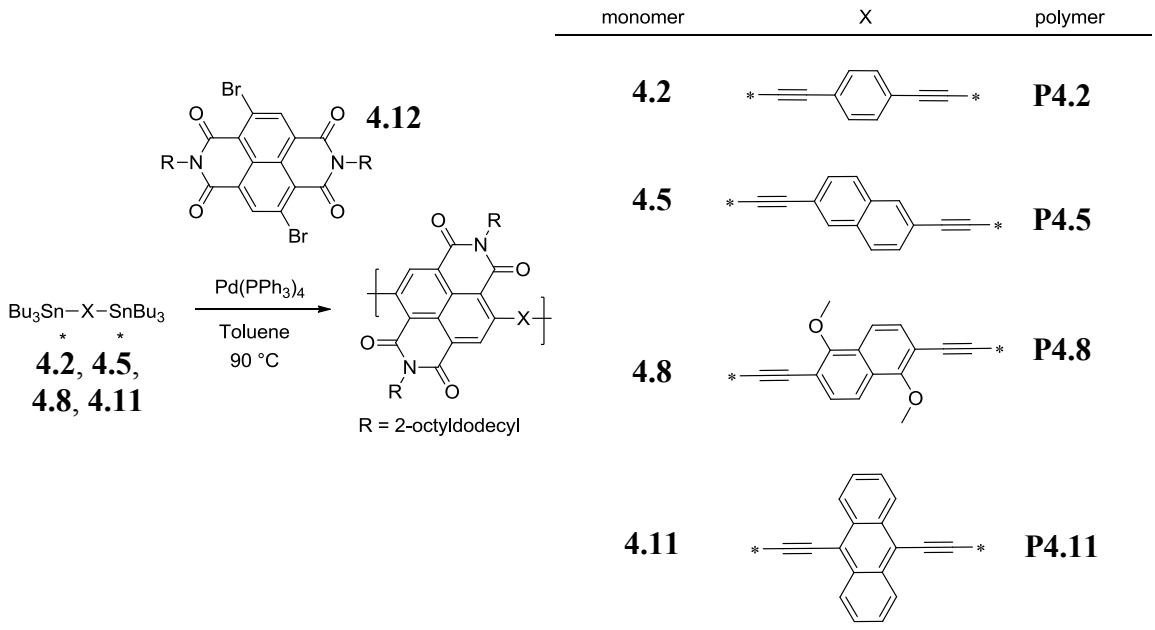

Scheme 4.1 Copolymerization of NDI **4.12** with donor monomers.

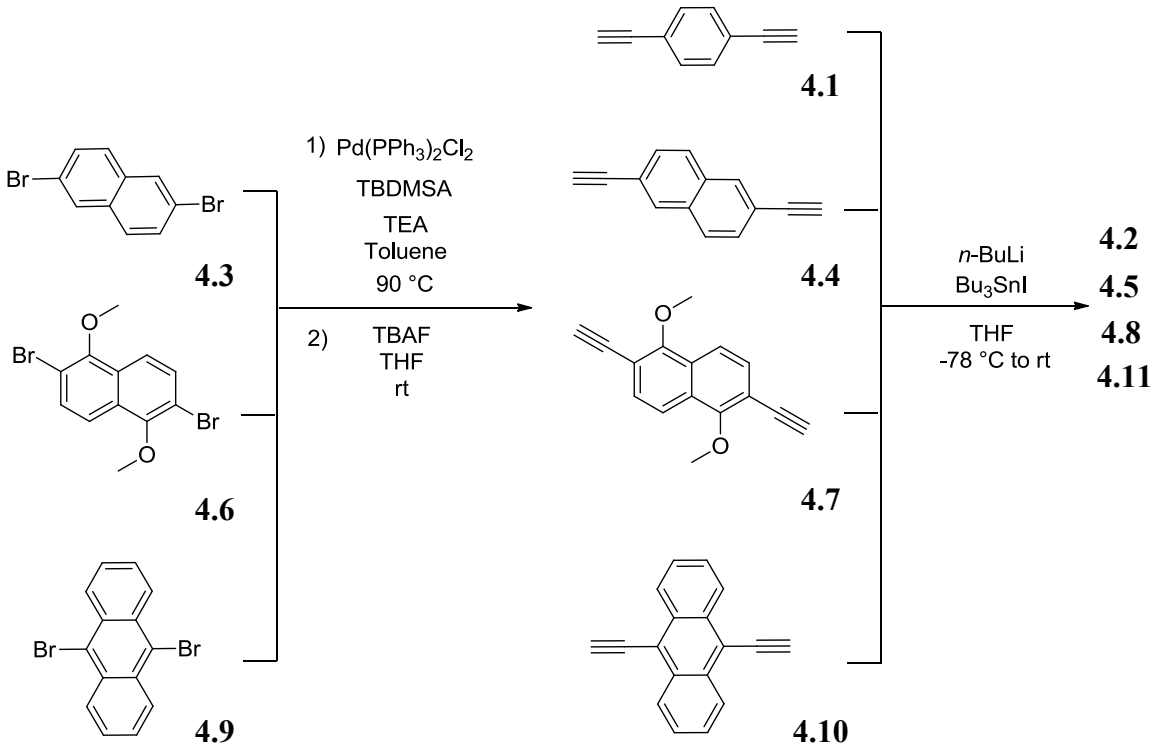

Scheme 4.2 General synthesis of donor monomers **4.2**, **4.5**, **4.8**, **4.11**.

NDI monomer **4.12** (136; 128) (Scheme 3.1) was prepared from dibrominated 1,4,5,8-naphthalenetetracarboxylic dianhydride (36) and 2-octyldodecylamine (145) using literature procedures. Synthesis of the donor monomers **4.2**, **4.5**, **4.8**, and **4.11** is shown in Scheme 4.2. Dibrominated naphthalene derivative **4.6** was synthesized by the deprotonation of 2,6-dibromonaphthalene-1,5-diol and its reaction with methyl iodide. Naphthalene **4.3** was commercially available and **4.9** was prepared by the direct bromination of anthracene according to literature procedures (146).

Next, (*tert*-butyldimethylsilyl)acetylene (TBDMSA) moieties were appended onto the aromatic cores of **4.3**, **4.6**, and **4.9** using standard Sonogashira conditions, followed by TBAF deprotection to afford terminal alkynes **4.4**, **4.7**, and **4.10** (Scheme 4.2). These intermediates, along with commercially available **4.1**, were subsequently stannylated with

tributyltin iodide to yield suitable electron-rich coupling partners (**4.2**, **4.5**, **4.8**, **4.11**). Due to its instability (147), **4.10** was stannylated immediately after deprotection and polymerized before significant decomposition occurred. To prevent loss of the stannyl groups on the silica column, **4.2**, **4.5**, **4.8**, and **4.11** were used without purification prior to polymerization.

D–A polymers (**P4.2**, **P4.5**, **P4.8**, **P4.11**) were synthesized through the copolymerization of dibrominated NDI **4.12** with diethynyl donor monomers **4.2**, **4.5**, **4.8**, **4.11** using the Stille protocol (148) (Scheme 4.1). An advantage of this route is that it permits precise control over polymer architecture. An analogous Sonogashira approach was successfully utilized by Guo and Watson to copolymerize substituted diethynyl benzene monomers with pyromellitic diimide (PMDI) (149).

The polymerization progress was monitored by UV-vis spectroscopy and reactions were stopped upon reaching the maximum bathochromic shift to provide solubility in common organic solvents such as tetrahydrofuran, methylene chloride, chloroform and toluene. Excess iodobenzene was added to the reaction mixture to cap the polymers. The reaction proceeded another 2 hours before the solvent was removed and crude polymers were collected by precipitation from methanol. Purification was achieved by successive Soxhlet extractions with methanol, acetone, and methylene chloride. The filtrate collected from the extraction with methylene chloride was then concentrated, and the polymers were isolated following two more precipitations from methanol. Reactions resulted in satisfactory yields with the exception of **P4.11**, which was isolated in 41% yield. Even with the short reaction period, a significant amount of insoluble material remained in the Soxhlet thimble. Therefore, the reported yields only represent the readily soluble fraction of each sample.

4.3.3 Characterization

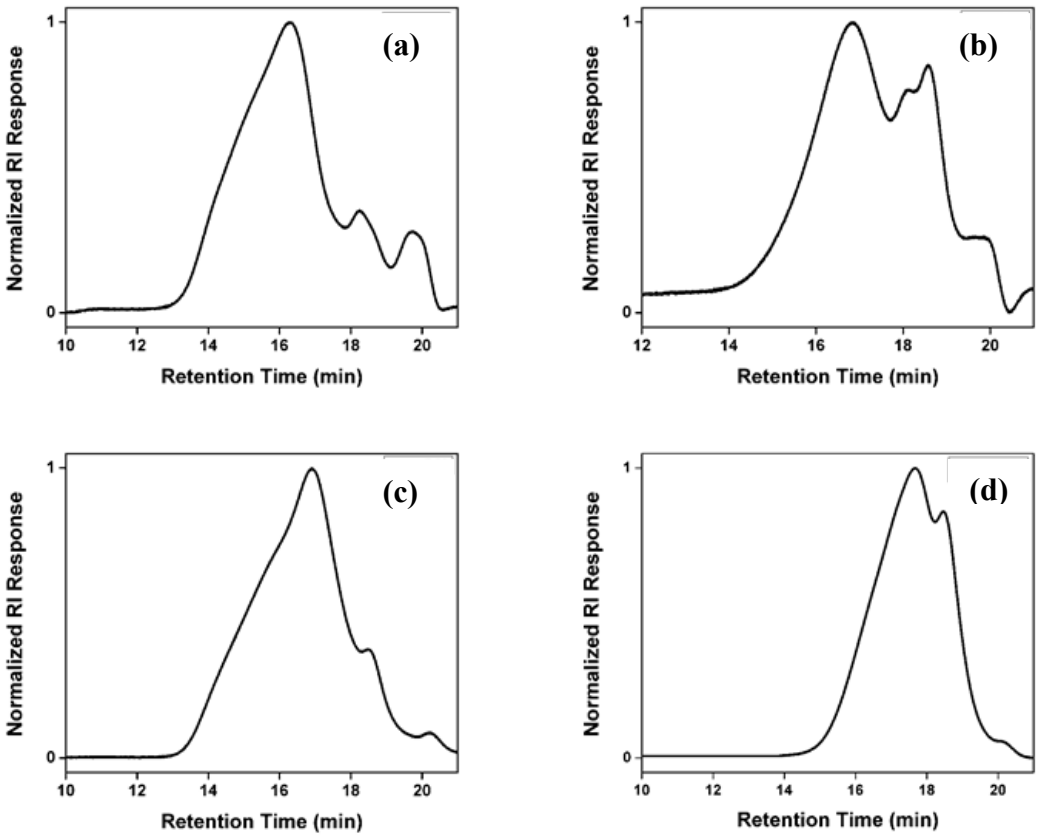

Figure 4.3 GPC traces of (a) **4.2**, (b) **4.5**, (c) **4.8**, and (d) **4.11**.

Number average (M_n) and weight average (M_w) molecular weights were determined by gel permeation chromatography (GPC) (Table 4.1). M_n values that ranged from 3.3 kDa to 18.7 kDa were observed with polydispersity indices (PDI) between 2.8 and 3.9. These values may be overestimated in analogy to previously reported GPC data for other rigid rod polymers (150).

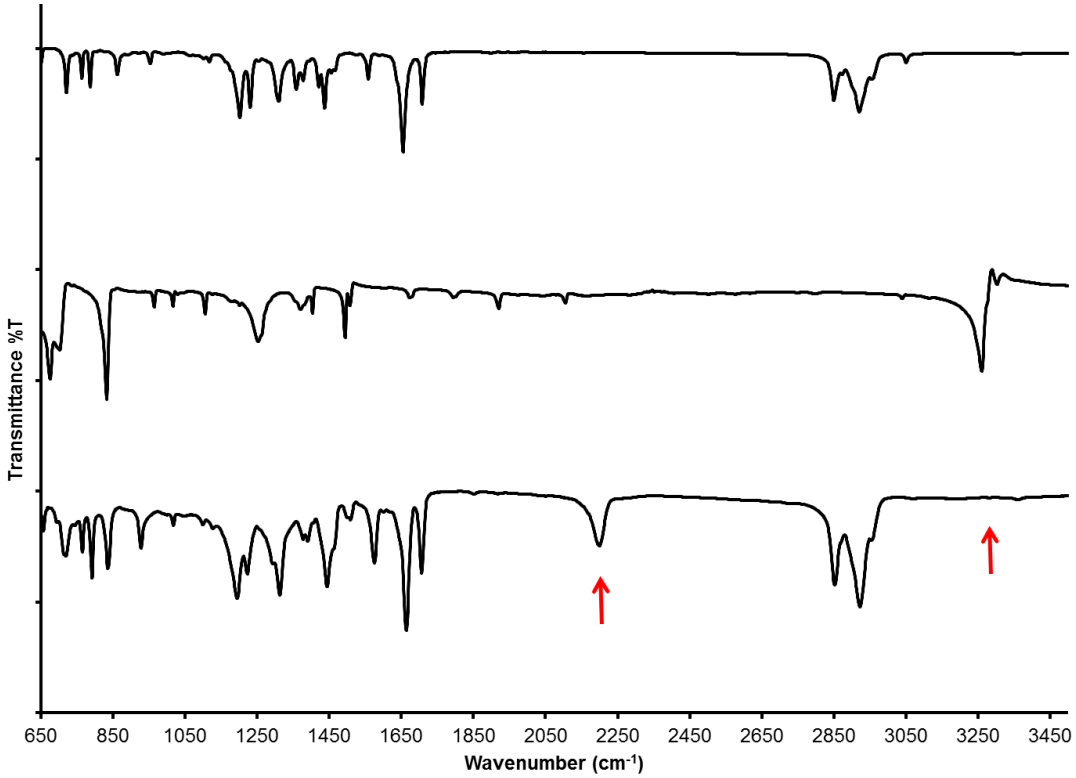

Figure 4.4 IR spectrum of **4.12** (top), **4.1** (middle), and **P4.2** (bottom). Red arrows indicate presence of asymmetric alkyne and absence of terminal alkyne.

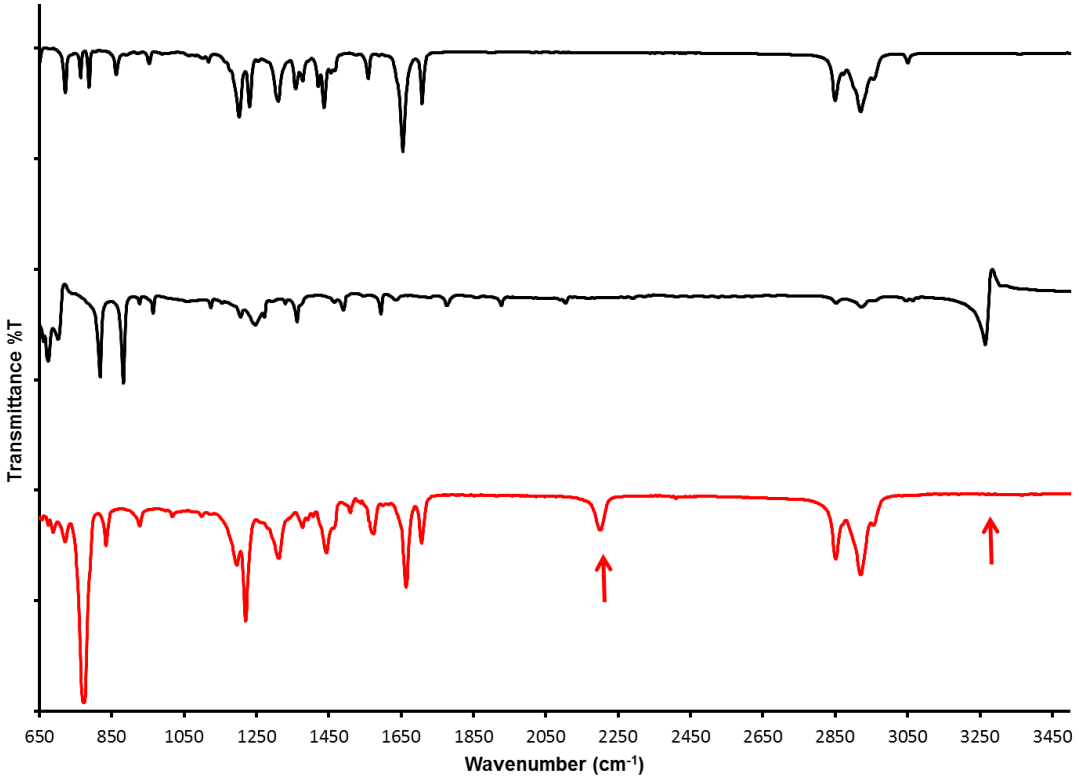

Figure 4.5 IR spectrum of **4.12** (top), **4.4** (middle), and **P4.5** (bottom). Red arrows indicate presence of asymmetric alkyne and absence of terminal alkyne.

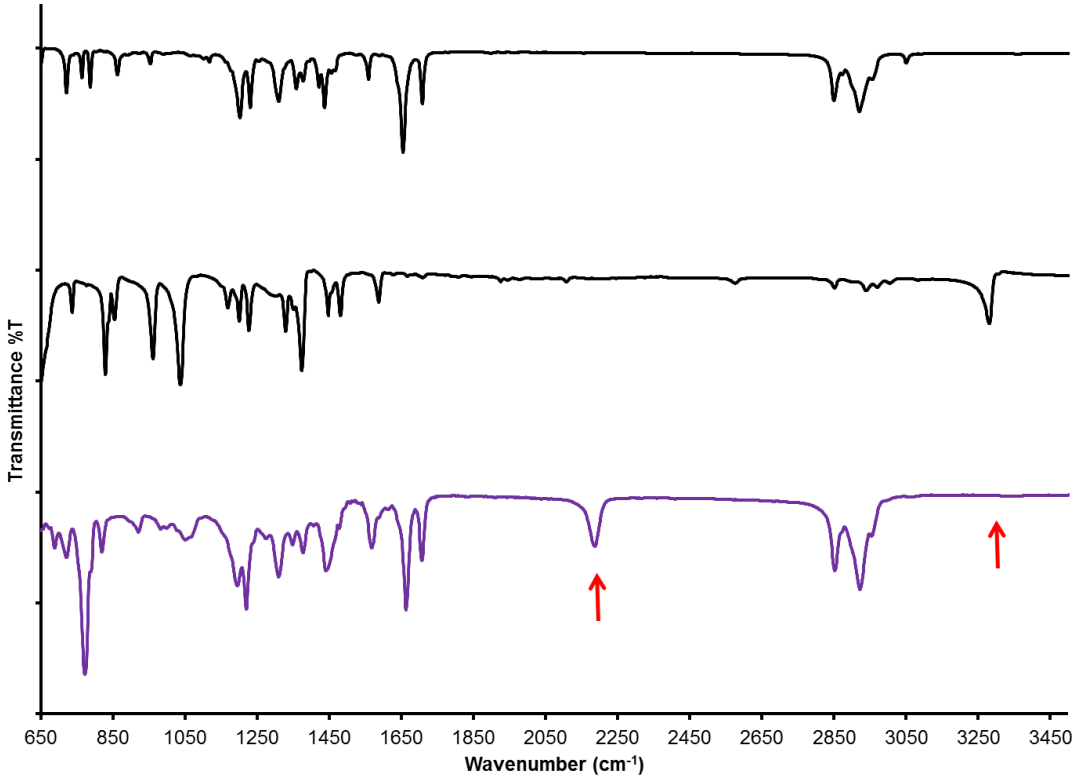

Figure 4.6 IR spectrum of **4.12** (top), **4.7** (middle), and **P4.8** (bottom). Red arrows indicate presence of asymmetric alkyne and absence of terminal alkyne.

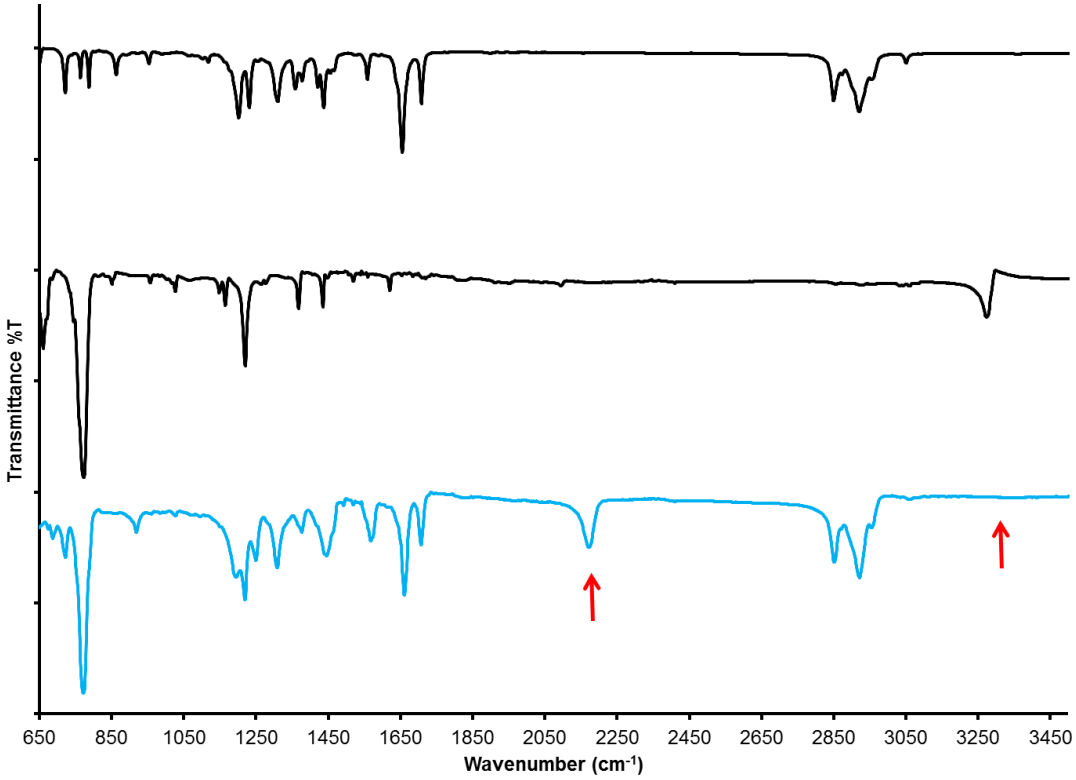

Figure 4.7 IR spectrum of **4.12** (top), **4.10** (middle), and **P4.11** (bottom). Red arrows indicate presence of asymmetric alkyne and absence of terminal alkyne.

The presence of aggregated polymers was supported by ^{1}H NMR spectroscopy, as resolved spectra of these polymers were unattainable even at 130 °C. Similar characterization problems were encountered with the conjugated PMDI–benzene polymers (149). In light of these NMR characterization complications, IR was used to structurally characterize the polymers (Figure 4.4 – Figure 4.7). The IR spectrum for **4.12** and the appropriate diyne donor are included for comparison in each polymer IR figure. For example (Figure 4.4), the IR spectrum of **4.12** exhibits strong signals from 2828 cm^{-1} to 3000 cm^{-1} (C–H stretching vibrations of the alkyl chains) and signals at 1656 cm^{-1} and 1710 cm^{-1} (carbonyl stretching vibrations) while the spectrum of **4.1** shows a signal at 3262 cm^{-1} (C–H stretching vibrations of the terminal alkyne). The IR

spectrum of **P4.2** maintains both the alkyl C–H and carbonyl stretching signals of **4.12** and lacks the C–H stretching vibration of a terminal alkyne as seen in **4.1**. The asymmetric, internal alkynes of **P4.2** result in a new stretching vibration at 2207 cm^{-1}.

4.3.4 Optical and Electrochemical Properties

	Soln Abs. λ_{max} nm	Film Abs. λ_{max} nm	Soln Flu. λ_{max} nm	E_g^{opt} eV	$^{a}E_{1/2}$ red1 V	$^{a}E_{1/2}$ red2 V	^{b}LUMO eV	^{c}HOMO eV
P4.2	558	561	646	1.89	–1.01	–1.31	–3.79	–5.68
P4.5	534	527	579	1.90	–1.05	–1.34	–3.75	–5.65
P4.8	576	583	677	1.82	–1.06	–1.42	–3.74	–5.56
P4.11	678	673	791	1.44	–1.07	–1.31	–3.73	–5.17

Table 4.1 A Summary of Optical and Electrochemical Properties. a) Values were estimated using the vacuum ferrocene reference value of –4.8 eV at 0.0 V. b) LUMO = – ($E_{1/2}$ red1 + 4.8) eV. c) HOMO = LUMO – E_g^{opt}.

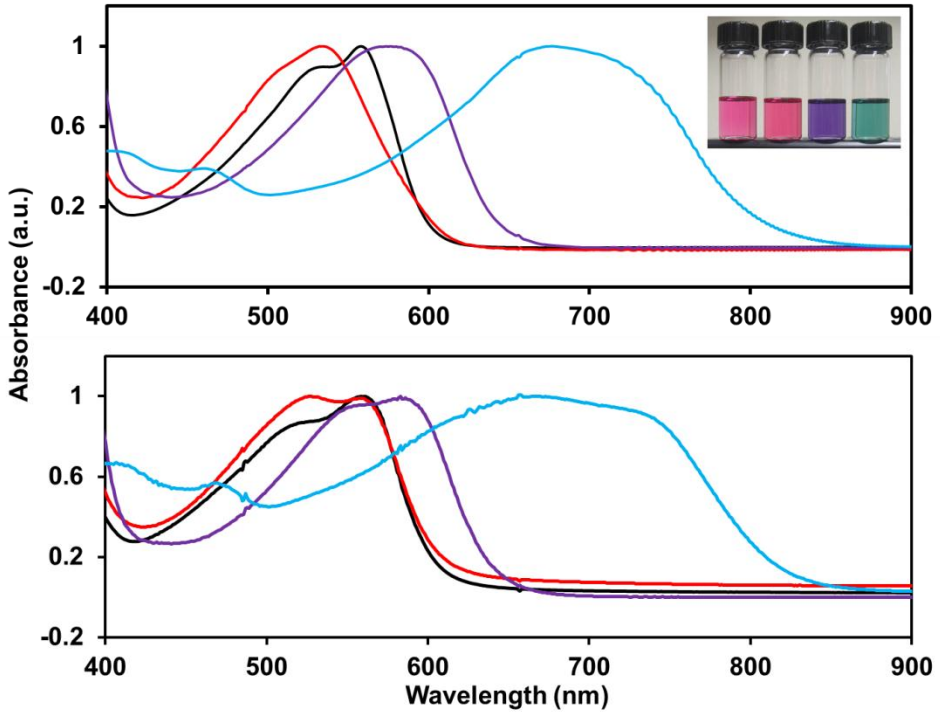

Figure 4.8 The normalized absorption spectra in chloroform (top) and as a thin film (bottom) of **P4.2** (black), **P4.5** (red), **P4.8** (purple), and **P4.11** (teal). The inset picture of the polymers dissolved in chloroform shows the bright red color of **P4.2**, **P4.5** and the purple and teal color of **P4.8** and **P4.11**, respectively.

The absorption spectra for all polymers in chloroform and as a thin film are shown in Figure 4.8. The polymer absorption maximum (λ_{max}) and the estimated optical band gap (E_g^{opt}) energies are listed in Table 4.1. Absorption maxima in solution were 558, 534, 576 and 678 nm for **P4.2**, **P4.5**, **P4.8**, and **P4.11**, respectively, and little change from these numbers was observed in the thin film measurements. In the thin films, peak broadening was clearly visible for **P4.11**, and **P4.5** appears to develop a shoulder much like the one present in **P4.2**. The maximum shift (blue or red) observed between the solution and thin film absorption maxima was only 7 nm, suggesting that the polymers adopt a similar structure in both solution and solid state.

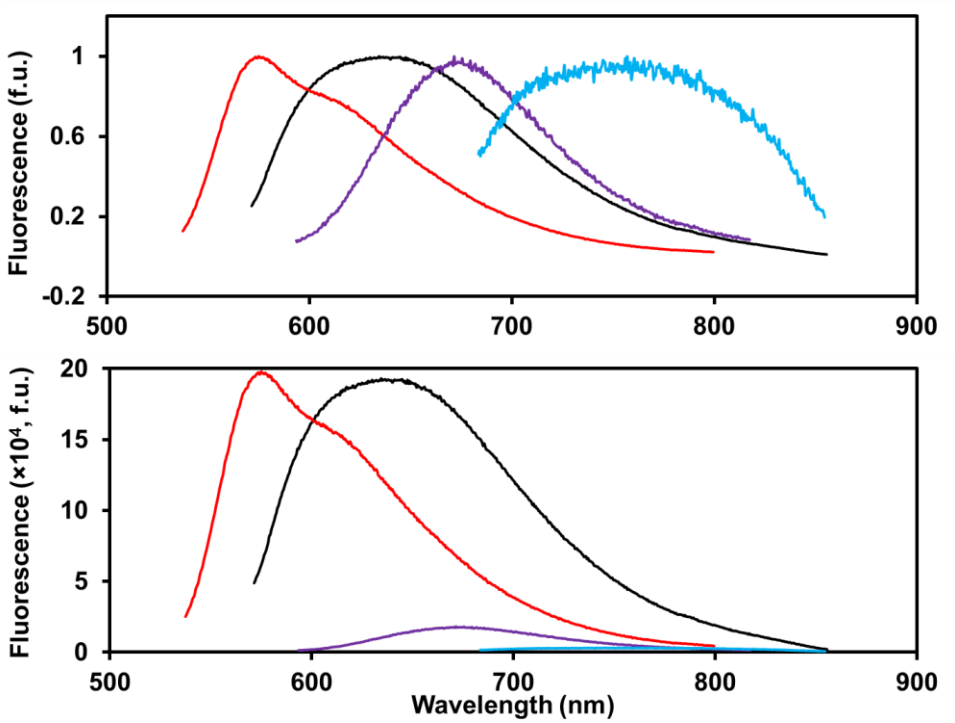

Figure 4.9 The normalized (top) and non-normalized (bottom) polymer fluorescence spectra in chloroform (4×10^{-6} M) of **P4.2** (black), **P4.5** (red), **P4.8** (purple), and **P4.11** (teal). Concentration is based on the molecular weight of the polymer repeat unit.

The normalized and non-normalized fluorescence spectra of the polymers in chloroform are shown in Figure 4.9. There was a dramatic decrease in fluorescence in **P4.8** and **P4.11**, amounting to approximately a 10-fold and 50-fold decrease of emission intensity in chloroform, respectively, when compared to that of **P4.2**. Two possible explanations could account for such a dramatic decrease in fluorescence. Since DAN and anthracene can stack with NDI, it is reasonable to assume that at least some of the dramatic fluorescence decrease seen with **P4.8** and **P4.11** could be due to interchain assembly through intermolecular donor–acceptor interactions. Alternatively, increased intramolecular charge-transfer could be playing a significant role in the fluorescence quenching of **P4.8** and **P4.11**.

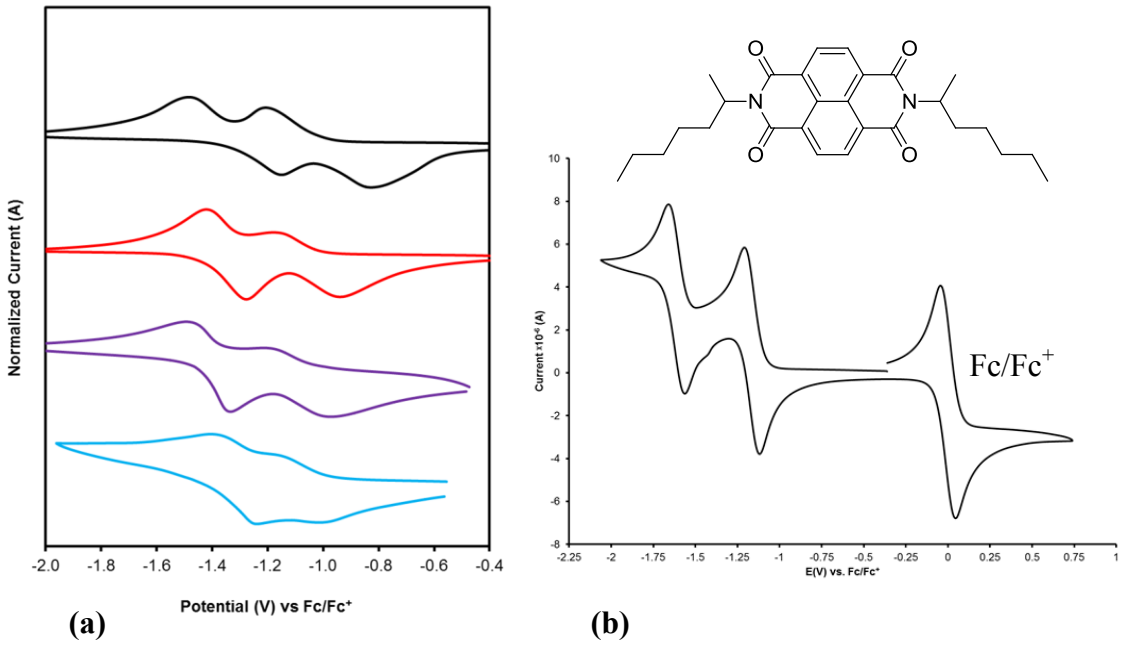

Figure 4.10 (a) The normalized cyclic voltammogram of **P4.2** (black), **P4.5** (red), **P4.8** (purple), and **P4.11** (teal) as a thin film on a platinum electrode in 0.1 M TBAP/MeCN at a scan rate of 50 mV s^{-1}. (b) The cyclic voltammogram of the NDI unit pictured above (1 mM) taken in a 0.1 M TBAP/CH_2Cl_2 solution at a scan rate was 50 mV s^{-1}.

Electrochemical data was collected by thin film CV using a standard three electrode cell with platinum working, tungsten counter and silver reference electrodes (Figure 4.10a). No oxidation peaks were observed within the solvent operating window during the anodic sweep, but two clear reduction peaks were observed for each polymer during the cathodic sweep (Table 4.1), results that are characteristic of n-type materials.

LUMO energy levels (Table 4.1) were determined from the $E_{1/2}$ values of the first reduction potentials. As previously reported (127), the $E_{1/2}$ from the first reduction potentials are around –1.0 V and resemble that of the parent NDI monomer (125) (Figure 4.10b). LUMO levels are relatively consistent among the four polymers with values between –3.73 eV and –3.79 eV, reflecting the dominant NDI contribution to the overall

polymer LUMO energy level. A likely explanation is that the LUMO is predominately localized on the NDI units, even in the conjugated systems. The HOMO energy levels were estimated from the calculated LUMO energies and the E_g^{opt}. As expected, the HOMO energies exhibited a strong dependence on the donor monomer used. **P4.2** and **P4.5**, possessing comparable visible absorbance onsets, have calculated HOMO levels of –5.68 eV and –5.65 eV, respectively. The acene units, which were expected to be stronger donor monomers, exhibited an increase of the HOMO level; the DAN-containing **P4.8** exhibited a HOMO of –5.56 eV, a 0.09 eV increase over the HOMO of **P4.5**. Incorporation of anthracene resulted in the highest HOMO energy level, as **P4.11** exhibited a HOMO energy of –5.17 eV.

Using the maximum thin film absorption edge for each polymer, the E_g^{opt} values for **P4.2**, **P4.5**, and **P4.8** were estimated at 1.89, 1.90 and 1.82 eV, respectively. The additional electron donation from the oxygen atoms on the naphthalene rings in **P4.8** resulted in a minimum band gap change (0.08 eV) when compared to **P4.5**, which lacks oxygen atoms on the naphthalene rings. Replacing naphthalene with anthracene, however, resulted in a significant lowering of the band gap; **P4.11** exhibited the lowest band gap of 1.44 eV.

4.3.5 Aggregation Assessment by Fluorescence Spectroscopy

The aggregation properties of the different polymers were investigated to probe the nature of interchain interactions. In particular, the dramatic loss of fluorescence seen with **P4.8** and **P4.11** could in part be the result of aromatic D–A stacking interactions between chains. Unfortunately, the strong absorbance associated with intramolecular charge transfer deterred detection of possible intermolecular donor–acceptor interactions

with UV-vis spectroscopy. Serial dilution fluorescence was instead conducted to investigate the interchain stacking behavior of the polymers (Figure 4.11). Although each polymer exhibited different fluorescence intensities (Figure 4.9), their serial dilution plots are presented as a normalized series to compare the overall fluorescence behavior of the polymers at various concentrations.

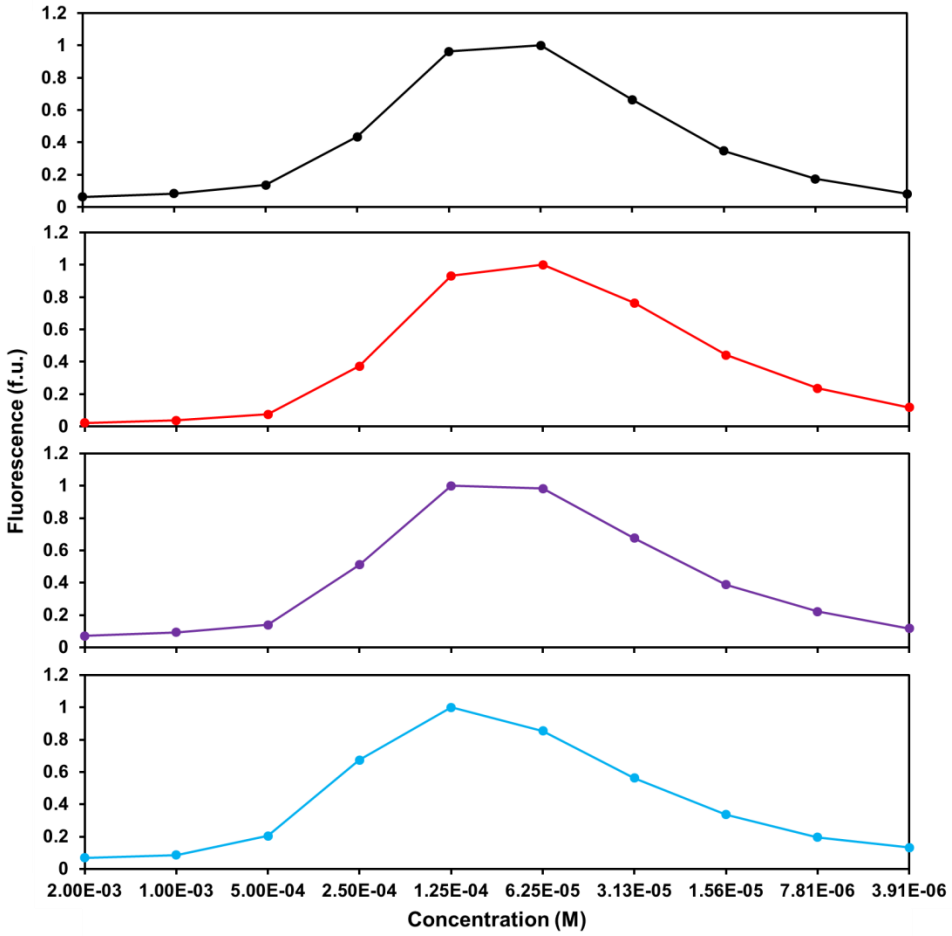

Figure 4.11 The normalized serial dilution fluorescence pattern of **P4.2** (black), **P4.5** (red), **P4.8** (purple), and **P4.11** (teal) in chloroform. Concentration is based on the molecular weight of the polymer repeat unit. The solutions were two-fold diluted in serial fashion and each point represents the maximum fluorescence at that particular concentration.

All of the polymers exhibited a similar dramatic decrease in fluorescence at high concentrations in chloroform. The fluorescence intensity for each polymer increased with decreasing concentration and a maximum signal was attained in the range of 125 μM to 62 μM before the fluorescence intensity again decreased with decreasing concentration.

4.3.6 Interchain Stacking Model by XRD

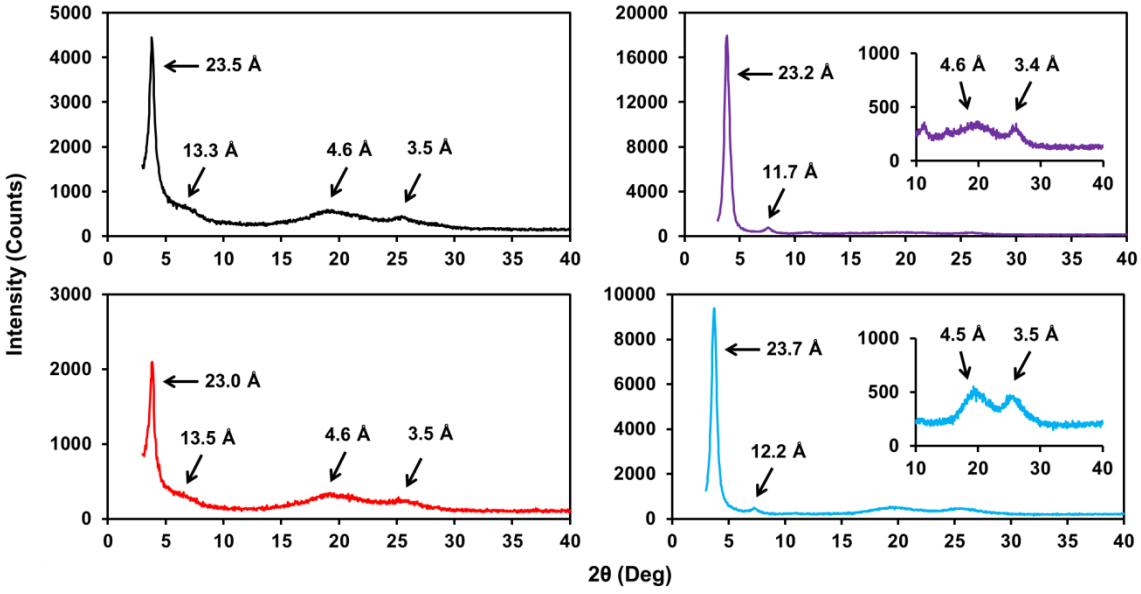

Figure 4.12 The XRD patterns of **P4.2** (black), **P4.5** (red), **P4.8** (purple), and **P4.11** (teal). Peaks are labeled with their corresponding *d*-spacing value and the inset plots represent an enlarged portion of the pattern.

Bulk polymers collected from methanol precipitation (slow evaporation from dichloromethane to form a film gave analogous results) were analyzed by XRD to determine the actual stacking mode of the polymer chains. Four peaks were consistent in all of the XRD patterns (Figure 4.12). These peaks corresponded to *d*-spacings of 23 Å,

12-13 Å, 4.6 Å, and 3.5 Å. In addition, the variation among peak intensities at 2θ ≈ 3.8° indicates that **P4.8** and **P4.11** possess a higher relative crystallinity than **P4.2** and **P4.5**.

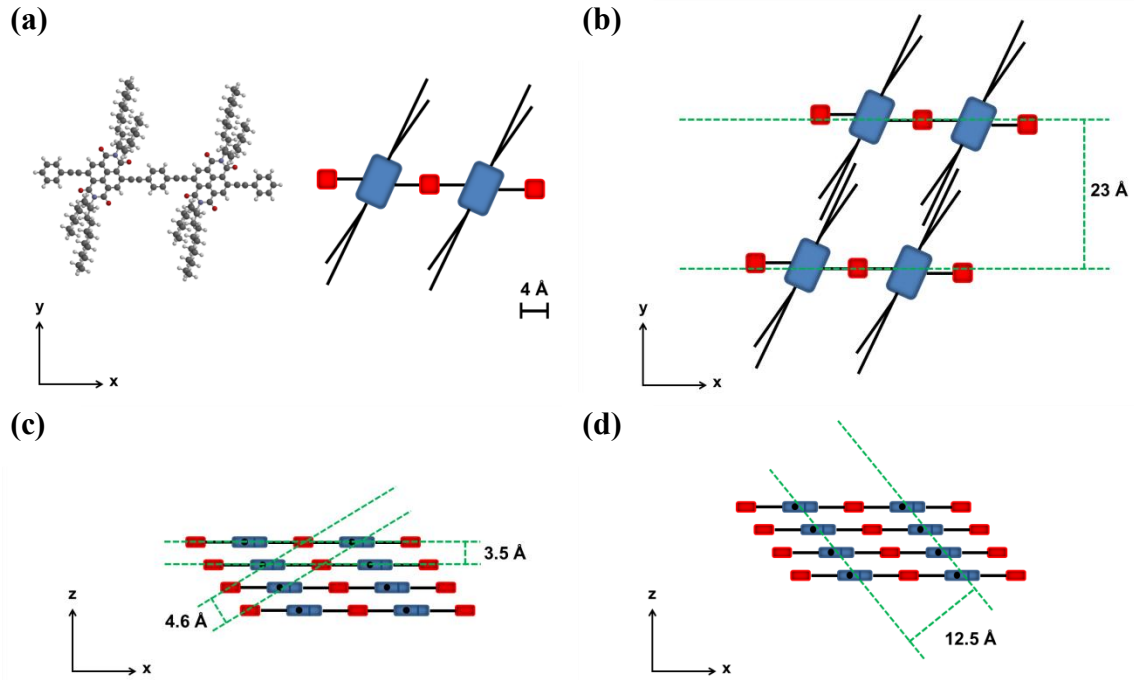

Figure 4.13 A scale representation (a) of **P4.2** and the proposed stacking (b, c, d) to account for the *d*-spacing values obtained by XRD. NDI = blue and benzene = red. Side chains were removed for clarity (c, d) and marked by a black dot on the blue NDI.

The *d*-spacing of 23 Å is representative of a lamellar structure with interdigitated side chains (130) as this distance is shorter than the extended length of the NDI moiety (~35 Å). A scale model of **P4.2** and the proposed packing mode (representative of **P4.5**, **P4.8**, and **P4.11** as well) is shown in Figure 4.13. The viewpoint of a single layer (Figure 4.13b) along the Y–X axis shows the 23 Å distance between two parallel polymer chains. The distance of 3.5 Å matches the characteristic distance between stacked aromatic units seen in numerous XRD studies of NDI-based or other aromatic systems (33; 34; 139).

The polymer chains were then separated by a distance of 3.5 Å along the Z-axis (Figure 4.13c) in the scale model. Importantly, the observed *d*-spacing of 4.6 Å closely resembles the reported centroid-to-centroid distance between adjacent NDI moieties stacked in an offset face-to-face fashion (140) and the polymer chains were adjusted as such in the model. It was then possible to draw parallel planes along the Y-axis that matched the 4.6 Å *d*-spacing (Figure 4.13c). In addition, another set of parallel planes could be drawn along the Y-axis that has a distance of ~12.5 Å (Figure 4.13d) which resembles the *d*-spacing of 13.3 Å. The difference may be due to the error associated with a broad XRD peak. It also seems plausible that the distance (12.5 Å) between these particular parallel planes would be sensitive to the donor size and could explain the small difference among the polymers at $2\theta \approx 7°$ (11.7 Å, 12.2 Å, 13.3 Å, 13.5 Å).

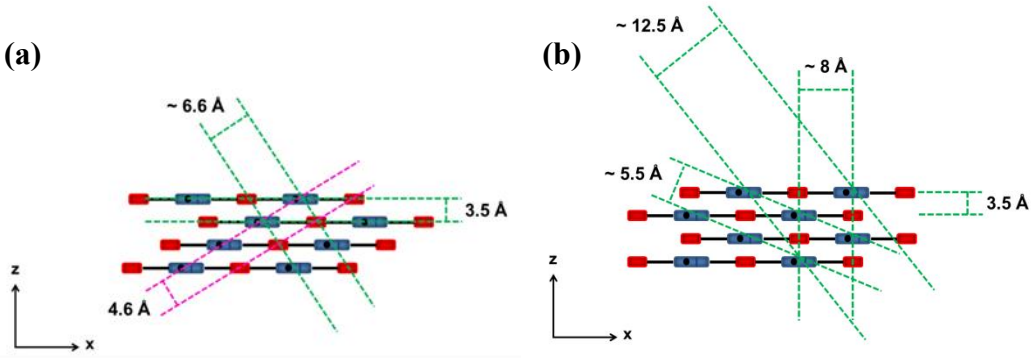

Figure 4.14 Scale representations (same scale as Figure 4.13a) of two more proposed stacking models that did not account for the XRD *d*-spacing values. NDI = blue and benzene = red. Side chains were removed for clarity and marked by a black dot on the blue NDI.

For the sake of completeness, two other scale models with **P4.2** were generated; one that set the centroid-to-centroid distance between NDI and benzene at 4.6 Å (Figure 4.14a) and another one that assumed a complete alternating D–A assembly along the Z-

axis (Figure 4.14b). Neither of these models accounted for all of the XRD peaks. The model in Figure 4.14a orients the polymer chains such that the benzene and NDI are stacked in an offset face-to-face fashion with a centroid-to-centroid distance of 4.6 Å. Polymer chains are separated by a distance of 3.5 Å. A set of two parallel planes separated by a distance of 4.6 Å is not supported in this particular orientation as the two planes drawn as a result of the centroid-to-centroid distance are not identical (pink dashed lines). Rather, these parallel planes exist at 9.2 Å (double 4.6 Å), but this is not supported by XRD. Additional sets of parallel planes can be drawn with *d*-spacing values of ~ 6.6 Å. Again, these distance values are not supported by XRD. The model in Figure 4.14b orients the polymer chains with benzene stacked in an alternating face-to-face fashion with NDI. Polymer chains are separated by a distance of 3.5 Å. With the exception of ~ 12.5 Å and 3.5 Å, the *d*-spacing values of ~ 5.5 Å and ~ 8 Å were not detected by XRD.

4.4 DISCUSSION

4.4.1 Optical and Electrochemical Properties

Four new conjugated aromatic D–A polymers incorporating NDI as the acceptor moiety were synthesized and characterized. A Stille coupling reaction between diethynyl aryl monomers and dibromo NDI yielded high molecular weight polymers that were readily soluble in organic solvents. As with previously reported conjugated NDI polymers, the NDI–aryl polymers reported herein also exhibited interesting electrochemical properties. LUMO levels remained around –3.75 eV for all polymers examined, a higher value than that of the commonly used PV acceptor PCBM (–4.3 eV), while the HOMO levels were sensitive to the aromatic donor groups and resembled those

of commonly employed thiophene or fluorene-based monomers (HOMO approximately –5.8 eV to –4.8 eV). Most notably, polymer **P4.11** possesses one of the smallest conjugated NDI–donor polymer band gaps to date as well as HOMO/LUMO levels that may be suitable for use in PV devices (151).

4.4.2 Aggregation Assessment by Fluorescence Spectroscopy

All of the polymers experienced a dramatically quenched fluorescence at high concentrations which is characteristic of all materials using standard 90° fluorescence measurements. In addition, polymers **P4.8** and **P4.11** displayed dramatically quenched fluorescence at all concentrations examined compared to **P4.2** and **P4.5**. NDI is known to quench fluorescence when stacked with a fluorophore (152; 139). A noticeable difference was expected in the fluorescence behavior of **P4.2**, **P4.5** and **P4.8**, **P4.11** during the dilution experiments if interchain assembly was driven by intermolecular D–A interactions because these units, representing a range of different sizes and donor capabilities, are expected to display different levels of interaction with NDI. In contrast to this expectation, the strong similarity among the concentration dependencies of the fluorescence patterns in Figure 4.11 can most easily be interpreted to indicate that all four polymers aggregate in a similar fashion. In other words, aggregation is apparently not dependent on the nature of the donor monomer, ruling out D–A interactions as the primary driver of aggregation behavior. A reasonable explanation is that interchain aggregation and, by inference, the concentration dependent fluorescence quenching, is the result of interactions between the NDI units common to all the polymers. To the extent that this is true, the diminished fluorescence of **P4.8** and **P4.11** is most likely the result of intramolecular charge-transfer and not interchain aromatic D–A interactions.

4.4.3 Interchain Stacking Model by XRD

XRD data was strikingly similar among all four polymers and combined with models to further refine the mode of interchain aggregation. The only model that was able to explain the observed XRD data for all of the polymers contained interdigitated side chains with the NDI moieties stacked in an offset face-to-face fashion (Figure 4.13). Although DAN and anthracene are known to form aromatic D–A interactions with NDI, none of the aromatic donor units investigated in this study was able to interrupt NDI self-stacking in these conjugated polymer chains. NDI is well-known to have a propensity for self-association in an offset face-centered stacking mode, presumably because such a stacking geometry provides for maximum complementary electrostatic interactions between the carbon and oxygen atoms of the highly polarized NDI carbonyl groups on adjacent NDI units. Taken together, our results are therefore consistent with more recent discussions of aromatic stacking dominated by interactions between highly polarized groups on the periphery of aromatic units rather than overall polarization of the aromatic ring itself (*i.e.* D–A interactions). Interestingly, the XRD patterns additionally suggest that **P4.8** and **P4.11** have a higher degree of crystallinity than **P4.2** or **P4.5**, possibly the result of larger acene donor moieties.

It is worth pointing out that the branched side chains, which are necessary to solubilize the polymers, might also drive the observed polymer assembly geometry as evidenced by an interdigitated side chain arrangement. We have previously shown that side chains can have a great impact on the solid state packing of donor–acceptor assemblies (38) and this influence should not be ruled out.

4.5 CONCLUSION

The electronic properties of conjugated D–A polymers containing NDI have been thoroughly investigated over the last few years. A common feature of these systems is the ability to tune the HOMO/LUMO energy levels, making these polymers popular candidates for electronic materials investigations. However, a thorough understanding of the polymer chain organization is necessary to take these systems past the investigation level and on to application. The ideal material will exhibit both suitable electronic properties and predictable self-assembly into well-organized architectures. The results reported here have shed considerable light on the interchain stacking behavior of a set of NDI D–A polymer systems and have brought into sharp focus the apparent dominance of NDI–NDI interactions.

4.6 EXPERIMENTAL

4.6.1 General Methods

1,4-bis(ethynyl)benzene **(4.1)** was purchased from Aldrich and 2,6-dibromonaphthalene **(4.3)** was purchased from Alfa Aesar. $Pd(PPh_3)_2Cl_2$, $Pd(Ph_3)_4$, and CuI were purchased from STREM. Dry toluene and TEA were obtained by distillation over CaH. Dry NMP was purchased from Fisher Scientific and stored over molecular sieves prior to use. All other chemicals were acquired from Aldrich and used without further purification. All reactions were carried out under argon. NMR spectra were taken on a Varian Unity 400 spectrometer. Melting points were detected using a MEL-TEMP apparatus. GPC analyses were performed on polymer solutions in THF using a Waters Model 510 HPLC pump, two fluorinated polystyrene columns (IMBHW -3078 and I-MBLMW-03078) arranged in series, and a Waters 486 Tunable Absorbance Detector (λ =450 nm). Calibration was based on polystyrene standards in THF. Absorption spectra were obtained on an Agilent 8453 UV-vis spectrometer. Fluorescence measurements were made on a PTI fluorimeter (4 nm slits) with an 814 photomultiplier detection system using a 75W xenon short arc lamp. IR spectra were obtained using polymer solids on a PerkinElmer Spectrum 100 FT-IR equipped with a universal ATR (UATR) accessory. Electrochemical cyclic voltammetry was performed under a nitrogen atmosphere. The cell was equipped with platinum working, tungsten counter and silver electrodes. Thin films were measured in a 0.1 M tetrabutylammonium hexafluorophosphate (TBAP) MeCN solution at a scan rate of 50 mV s^{-1} and referenced to Fc/Fc^+ by shifting $(Fc^*)^{0/+}$ to 0.0 V (111). XRD patterns were obtained with a Scintag X1 theta-theta diffractometer equipped with a Cu x-ray tube and a solid state x-ray detector set to count Cu K-alpha radiation. Samples were prepared by smearing a small amount of polymer onto a zero background quartz plate sample holder. Suitable samples

were obtained by methanol precipitation or slow evaporation from CH_2Cl_2 to yield a powder and film, respectively. Both methods gave the same XRD pattern.

4.6.2 Synthesis and Characterization

2,6-dibromo-1,5-bis(methoxy)naphthalene (**4.6**) (111). To a solution of 2,6-dibromonaphthalene-1,5-diol (153) (5.90 g, 19.0 mmol) in dry, degassed NMP (85 ml) at 0 °C was added NaH (60% mineral oil dispersion, 1.70 g, 42.0 mmol). After allowing the solution to stir at 0 °C for 5 min, MeI (6.20 g, 44.0 mmol) was added and the solution warmed to room temperature while stirring overnight. The solution was poured onto ice (400 g), extracted with diethyl ether, and the organic fractions were poured through a short neutral alumina plug. The solvent was removed by rotary evaporation and the crude material was purified by recrystallization from acetone to yield a light brown solid (5.24 g, 15.0 mmol, 79% yield). Mp 149–156 °C; ^{13}C NMR (400 MHz, $CDCl_3$) δ 153.68, 131.32, 129.87, 119.68, 113.83, 61.76 ppm; ^{1}H NMR (400 MHz, $CDCl_3$) δ 7.78 (d, J = 8.0 Hz, 2H), 7.63 (d, J = 8.0 Hz, 2H), 3.99 (s, 6H) ppm; CI-HRMS (positive ion) calculated for $C_{12}H_{10}Br_2O_2$, 343.9048; found 343.9048.

2,6-diethynylnaphthalene (**4.4**). **4.3** (0.3258 g, 1.14 mmol) was dissolved in 11 ml of a 50/50 toluene/TEA solution. The solution was degassed with argon. $Pd(PPh_3)_2Cl_2$ (0.1145 g, 15 mol %), CuI (0.0105 g, 5 mol %), and (tert-butyldimethylsilyl)acetylene (0.3229 g, 2.30 mmol) were subsequently added and the solution was heated at reflux for 24 hours. The solvent was removed by rotary evaporation and the material was passed through a short silica column (Column 1: Hex) to yield a mixture of the di-substituted and mono-substituted protected alkyne intermediates. This mixture was taken up in 11

ml THF with TBAF (2.3 ml of 1.0 M in THF, 2.3 mmol) and stirred at room temperature for 1 hour. The solvent was removed by rotary evaporation and the crude material was purified by column chromatography (Column 2: Hex) to afford the desired product as a white solid (0.1508 g, 0.86 mmol, 75% yield). Mp 144–148 °C; ^{13}C NMR (400 MHz, $CDCl_3$) δ 132.37, 132.03, 129.33, 127.86, 120.45, 83.67, 78.23 ppm; ^{1}H NMR (400 MHz, $CDCl_3$) δ 7.99 (s, 2H), 7.74 (d, *J* = 12.0 Hz, 2H), 7.54 (dd, *J* = 1.3 Hz, *J* = 8.0 Hz, 2H), 3.18 (s, 2H) ppm; CI-HRMS (positive ion) calculated for $C_{14}H_8$, 176.0626; found 176.0626. IR: 678, 706, 819, 884, 1255, 1364, 1494, 1597, 3268 cm^{-1}.

2,6-diethynyl-1,5-bis(methoxy)naphthalene (**4.7**). **4.7** was synthesized in the same manner as that given for **4.4**, but with **4.6** as starting material. Column 1: 5% CH_2Cl_2/Hex; Column 2: 30% CH_2Cl_2/Hex; Collected as an off-white solid (0.1936 g, 0.82 mmol, 72% yield). Mp 142–147 °C; ^{13}C NMR (400 MHz, $CDCl_3$) δ 159.04, 130.27, 129.14, 117.85, 111.77, 83.18, 80.31, 61.94 ppm; ^{1}H NMR (400 MHz, $CDCl_3$) δ 7.86 (d, *J* = 8.0 Hz, 2H), 7.49 (d, *J* = 8.0 Hz, 2H), 4.13 (s, 6H), 3.45 (s, 2H) ppm; CI-HRMS (positive ion) calculated for $C_{16}H_{12}O_2$, 236.0837; found 236.0834. IR: 739, 831, 858, 963, 1041, 1174, 1203, 1229, 1332, 1376, 1449, 1484, 1590, 3284 cm^{-1}.

9,10-diethynylanthracene (**4.10**). **4.10** was synthesized in the same manner as that given for **4.4**, but with **4.9** as starting material with some modification explained below. Column 1: 100% Hex (further purified by recrystallization from ethanol to afford di-substituted material); purified product was stored as the silyl-protected intermediate. *Due to the instability of* **4.10***, this material was deprotected and immediately stannylated and polymerized.* The material was protected from light during deprotection and after a reaction period of 1 hour, the reaction mixture was quickly passed through a silica plug.

The solvent was removed by rotary evaporation and **4.10** was collected as a yellow solid (0.1571 g, 0.69 mmol, 61% yield) and immediately used in the next step. ^{13}C NMR (400 MHz, $CDCl_3$) δ 132.90, 127.49, 127.46, 118.23, 90.34, 80.64 ppm; ^{1}H NMR (400 MHz, $CDCl_3$) δ 8.61 (m, 4H), 7.62 (m, 4H), 4.07 (s, 2H) ppm. IR: 663, 776, 859, 980, 1029, 1170, 1167, 1222, 1370, 1435, 1623, 3280 cm^{-1}.

Polymer P4.2. A solution of **4.1** (0.0216 g, 0.17 mmol) and n-BuLi (0.43 ml of 1.6 M in Hex, 0.69 mmol) was allowed to stir in 2 ml of dry THF at -78 °C for 0.5 hours. To this solution was added tributyltin iodide (0.19 ml, 0.66 mmol) and the mixture temperature was allowed to reach room temperature while stirring for 2 hours. The solution was poured over water and extracted with CH_2Cl_2. The CH_2Cl_2 extracts were combined, dried over $NaSO_4$, and the solvent was removed by rotary evaporation. Proton NMR showed satisfactory conversion to **4.2** and this material was dissolved with **4.12** (0.1675 g, 0.17 mmol) in 2 ml of dry toluene. The mixture was subjected to 3 freeze, pump, and thaw cycles. $Pd(PPh_3)_4$ (0.0100 g, 5 mol %) was added and the solution was heated at 90 °C. The polymerization progress was monitored by UV-vis spectroscopy. Once the solution absorbance bathochromically shifted to its absorbance maximum, iodobenzene (0.19 ml, 1.7 mmol) was added to the solution and the reaction proceeded for an additional 2 hours. The toluene was concentrated to a minimal volume by rotary evaporation and the crude material was precipitated with MeOH/2N aqueous HCl (10/1 (v/v)). The solid was purified with a Soxhlet extraction apparatus using methanol, acetone, and CH_2Cl_2 in succession. The polymers were collected from the CH_2Cl_2 fraction and concentrated to a minimum volume by rotary evaporation. The polymers were precipitated two more times in MeOH/2N aqueous HCl (10/1 (v/v)) to yield a bright red solid (0.1037 g, 0.11 mmol, 64% yield). IR: 724, 767, 793, 839, 930, 1020, 1199,

1226, 1316, 1393, 1395, 1447, 1513, 1578, 1666, 1708, 2206, 2856, 2927, 2960 cm^{-1}. GPC: M_n 18.7, M_w 60.9, PDI 3.3.

Polymer P4.5. **P4.5** was synthesized using the same procedure and scale as that given for **P4.2**, but with **4.4** and **4.12** as starting materials. **P4.5** was collected as a red solid (0.1376 g, 0.14 mmol, 82% yield). IR: 693, 725, 776, 836, 931, 1201, 1222, 1316, 1382, 1447, 1514, 1577, 1666, 1709, 2207, 2855, 2925, 2963 cm^{-1}. GPC: M_n 8.2, M_w 23.0, PDI 2.8.

Polymer P4.8. **P4.8** was synthesized using the same procedure and scale as that given for **P4.2**, but with **4.7** and **4.12** as starting materials. **P4.8** was collected as a purple solid (0.1619 g, 0.15 mmol, 88% yield). IR: 693, 725, 775, 822, 926, 1062, 1200, 1222, 1314, 1352, 1381, 1451, 1573, 1666, 1709, 2191, 2856, 2926, 2960 cm^{-1}. GPC: M_n 14.9, M_w 58.4, PDI 3.9.

Polymer P4.11. **P4.11** was synthesized using the same procedure and scale as that given for **P4.2**, but with **4.10** and **4.12** as starting materials. **P4.11** was collected as a purple solid (0.0698 g, 0.07 mmol, 41% yield). IR: 694, 725, 775, 923, 1212, 1221, 1252, 1312, 1380, 1451, 1575, 1661, 1709, 2179, 2856, 2926, 2961 cm^{-1}. GPC: M_n 3.3, M_w 10.0, PDI 3.0.

Chapter 5

Reactions of Brominated NDI with *Bis*(tributylstannyl)acetylene

5.1 CHAPTER SUMMARY

5.1.1 Introduction

Chapter 4 describes our work with conjugated, alternating NDI–donor polymers. Those polymers were synthesized by a Stille coupling reaction between brominated NDI and a diyne donor moiety. Chapter 5 describes a similar approach to synthesize analogous conjugated NDI polymers, a method also used to develop useful polymers for chapter 6. It was also recognized that a diyne NDI can serve as an important intermediate. Synthesis, characterization and reaction scope of the NDI intermediate are described in this chapter.

5.1.2 Goals

The goal of this chapter is to answer the question: *Is there an easy synthetic method to create conjugated polymers composed of NDI through alkyne linkages?* An easy synthetic approach will allow us to create polymers composed of a single moiety connected through alkyne linkages for future polymer studies.

5.1.3 Approach

Polymerizations were carried out between brominated NDI and *bis*(tributylstannyl)acetylene or a diyne NDI using Sonogashira coupling protocol. Polymers were characterized by GPC, UV-vis, and IR spectroscopy. The diyne NDI intermediate was synthesized in a similar manner as the polymers but with adjustment to the *bis*(tributylstannyl)acetylene equivalents. The stability of the diyne NDI moiety

permitted characterization by NMR and further reaction with an electron-deficient coupling partner.

5.1.4 Results

A new synthetic approach to NDI containing materials and conjugates is described. A simple one-step Stille coupling procedure is used to create either novel alkyne-linked NDI polymers or a new stannylated diyne synthetic building block that provides a flexible approach to new NDI conjugates and polymers (154).

5.2 BACKGROUND

NDI has proven useful in a number of contexts ranging from highly ordered organic architectures and molecular recognition (155) to DNA intercalation (156). NDI has now become a promising material for organic electronics (155; 157; 158; 35) due to its respectable charge-carrier mobility (124; 123), electron deficient core and low lying, tunable LUMO (158; 125), tunable absorption spectrum (159; 160), and stable radical anion (35).

The widely used 2,6-dibromo NDI **5.1** (36; 126) has been assimilated into many conjugated small molecules and polymers by standard Stille coupling protocols (129; 128; 130; 131; 127; 132; 133; 134; 136; 137; 135; 148). For example, conjugated NDI-containing D–A polymers and small molecules are an important class of n-type materials that have exhibited efficiencies of 1.5% when paired with poly(3-hexylthiophene) as the p-type material in photovoltaic devices (151).

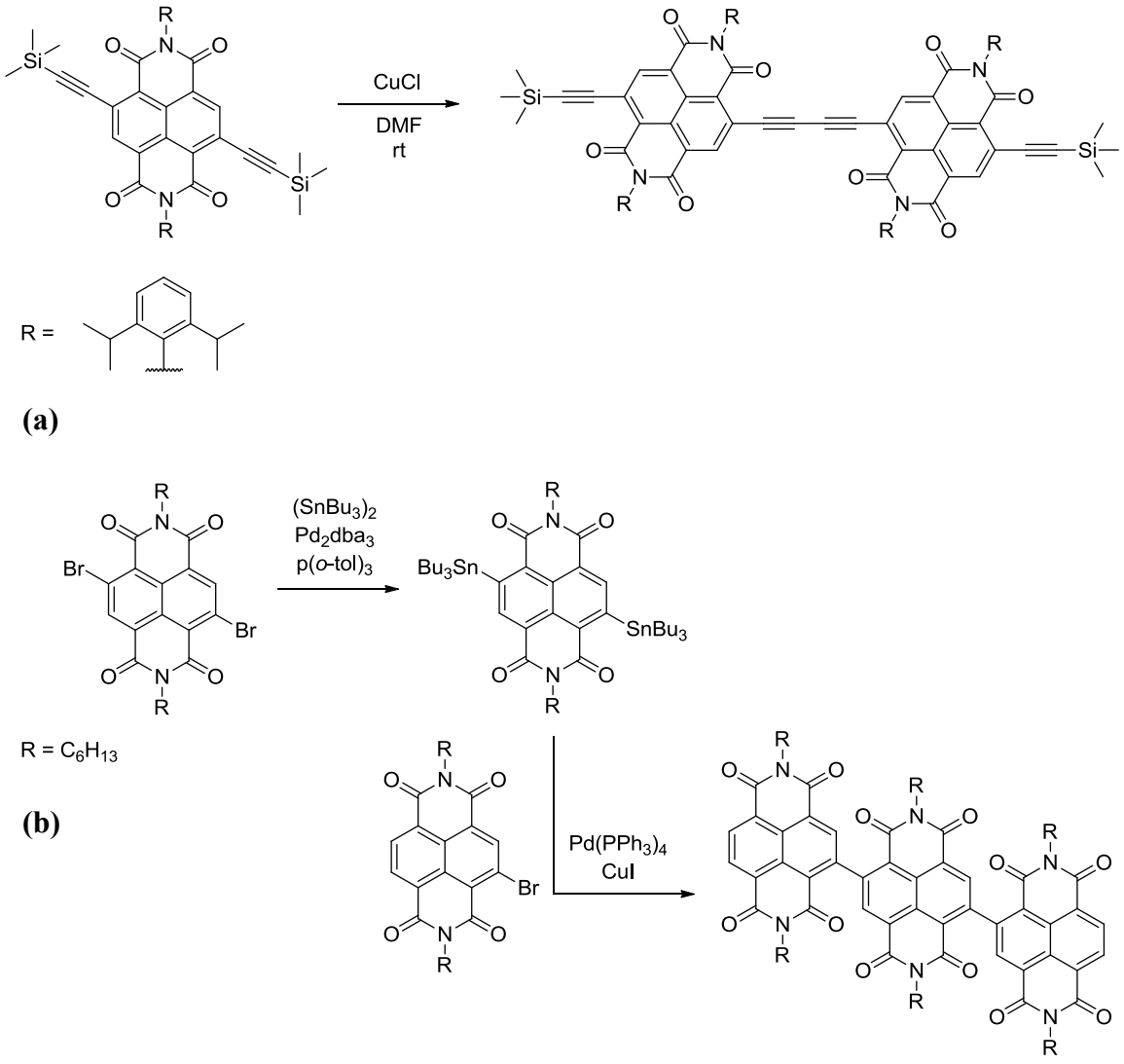

Figure 5.1 (a) Example of a conjugated NDI oligomer by Wang *et al*. (b) Example of tributylstannyl functionalized NDI and its Pd-catalyzed reaction with brominated NDI by Marder *et al*.

Current research now focuses on new methods to synthesize conjugated NDI-based materials. For instance, Wang *et al*., constructed conjugated butadiynylene-NDI oligomers through an oxidative coupling of 1,6-*bis*((trimethylsilyl)ethynyl)-NDI monomers (Figure 5.1a) (161). The Marder group was the first to append tributylstannyl

groups directly onto the aromatic core of NDI using a Pd-catalyzed reaction between brominated NDI and Sn_2Bu_6. Their stannyl functionalized NDIs should broaden the scope of NDI used in Stille coupling reactions and these workers demonstrated its utility by making short NDI oligomers (Figure 5.1b) (162).

We report here a simple method that utilizes the Stille coupling protocol and different substrate ratios for the synthesis of either alkyne-linked NDI containing polymers or the key stannyl functionalized diyne NDI monomer. The stannyl functionalized diyne NDI monomer is a versatile building block that can be used to produce NDI conjugates as well as polymeric materials.

5.3 RESULTS AND DISCUSSION

5.3.1 Synthesis of Conjugated NDI Polymers

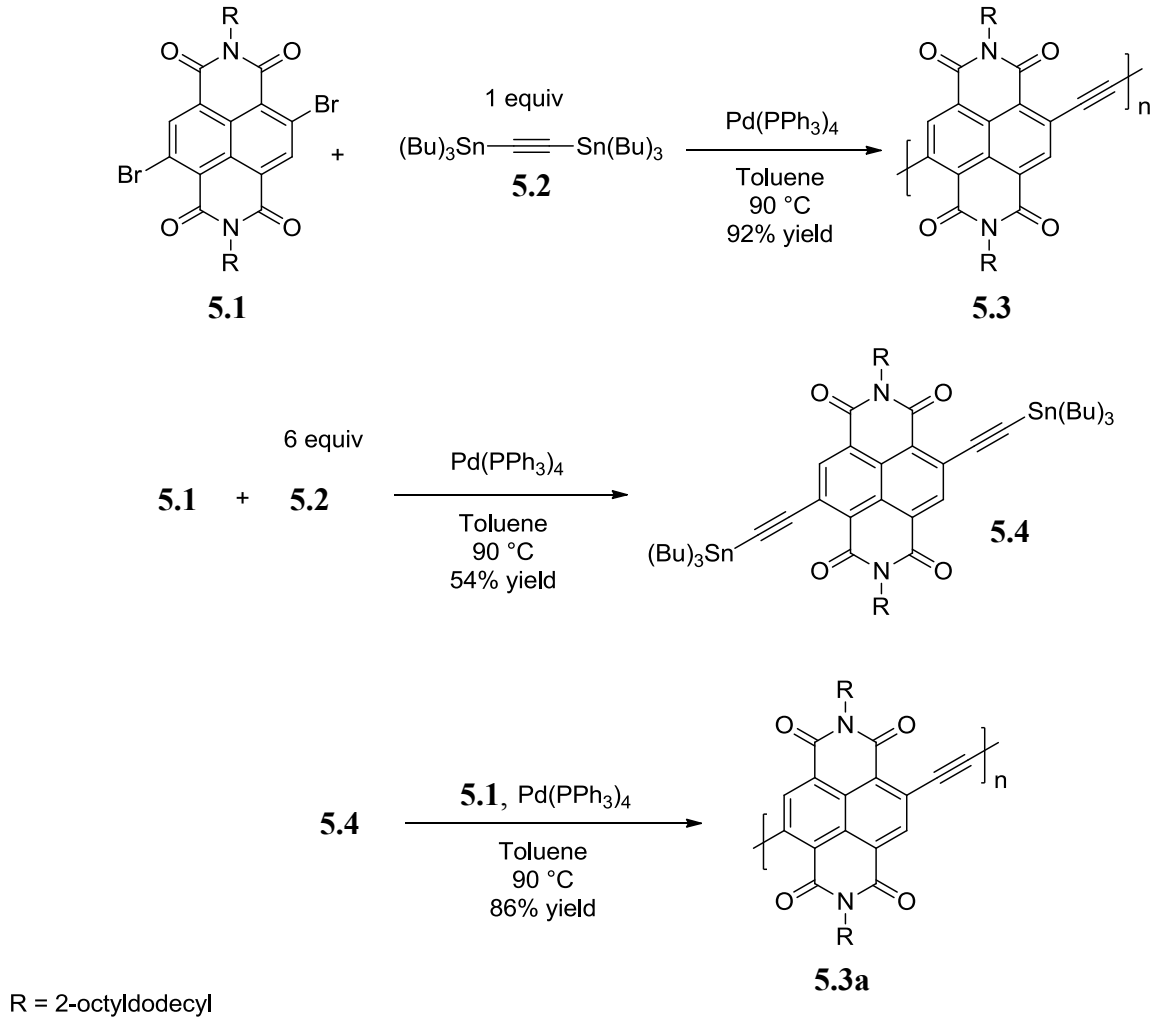

Scheme 5.1 Synthesis of NDI polymers **5.3** and **5.3a** and diyne intermediate **5.4**.

Conjugated NDI polymers were rapidly synthesized through the copolymerization of 2,6-dibromo NDI (**5.1**) with commercially available bis(tributylstannyl)acetylene (**5.2**) using the Stille protocol as shown in Scheme 5.1. A 1:1 molar mixture of **5.2** and **5.1**

with $Pd(PPh_3)_4$ was heated in toluene at 90 °C. The copolymerization was monitored by UV-vis spectroscopy and upon reaching the maximum bathochromic shift, stopped by removing the solvent. Crude polymers were collected by precipitation from methanol. Further purification was accomplished by successive Soxhlet extractions with methanol, acetone, and dichloromethane. The dichloromethane fraction was reduced in volume and polymer **5.3** was collected by precipitation from methanol.

Using a reaction time of 1 h provided polymers that were soluble in common organic solvents such as tetrahydrofuran, chloroform, and dichloromethane in 92% yield. Number average (M_n) and weight average (M_w) molecular weights were determined by gel permeation chromatography (GPC) against polystyrene standards in THF. Analysis using GPC (Figure 4.1a) yielded a M_n value of 4.5 kDa and an M_w value of 15.2 kDa with a polydispersity index (PDI) of 3.3 (Table 5.1). Increasing the polymerization time resulted in lower yields presumably due to the decreased solubility of larger polymers. For instance, a 2 h reaction period produced polymers with a M_n of 5.7 kDa and an M_w of 19.6 kDa (PDI 3.4) in only 28% yield.

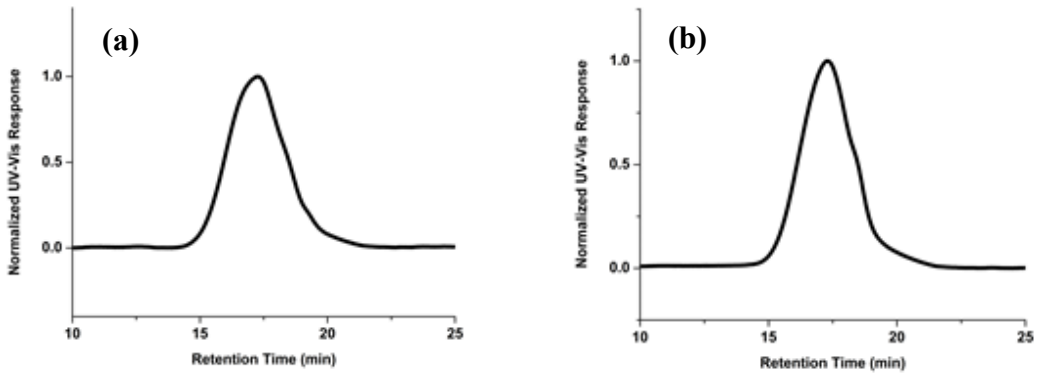

Figure 5.2 GPC trace of (a) **5.3** and (b) **5.3a**.

polymer **5.3**						polymer **5.3a**					
Rxn	**yield**	**M_n**	**M_w**	**M_w/M_n**	**λ_{max}**	**rxn**	**yield**	**M_n**	**M_w**	**M_w/M_n**	**λ_{max}**
h	%	kDa	kDa		nm	h	%	kDa	kDa		nm
1	92	4.5	15.2	3.3	557	1.5	86	4.3	14.0	3.2	557
2	28	5.7	19.6	3.4	557	2.5	36	4.5	13.5	3.0	557

Table 5.1 A summary of polymer molecular weights and optical properties.

Alternatively, an NDI polymer analogous to **5.3** was constructed through the copolymerization of **5.1** with distannyl NDI (**5.4**, vide infra) to make polymer **5.3a** (Scheme 5.1). The latter polymerization was carried out under the same reaction and purification conditions as for **5.3**, but required slightly longer reaction times (1.5 h) to adequately produce **5.3a** in 86% yield. Analysis by GPC (Figure 5.2b) yielded a M_n value of 4.3 kDa, an M_w of 14.0, and a PDI of 3.2 for this approach. Longer reaction times once again resulted in lower yields as 2.5 h provided similarly sized polymers but in only 36% isolated yield (Table 5.1). Several factors may account for the different reaction times required to obtain similar yields and chain lengths for the synthesis of **5.3** and **5.3a**. In particular, it is reasonable to suspect that the initial coupling to **5.1** will be faster with **5.2** than with **5.4** because **5.2** is expected to be the more electron rich of the two and an electron-rich organotin monomer typically facilitates the transmetalation step during a Stille coupling polymerization (163). The nature of the polymerization intermediates will also be different for the two approaches and may influence overall polymerization rates.

5.3.2 Structural Characterization of NDI Polymers

Structural characterization was accomplished with FT-IR as a well resolved ^{1}H NMR spectrum was not obtained. Figure 4.3 shows the IR spectrum of NDI **5.1**, polymer **5.3**, polymer **5.3a**, and polymer **5.3a** after three weeks. The spectra of **5.3** and **5.3a** appear consistent with each other and are different when compared to the starting monomer, **5.1**. The "fingerprint" region of **5.3** and **5.3a** (900-1300 cm^{-1}) are identical. A broad, weak peak in the range of 2000-2250 cm^{-1} was often observed in the polymer spectrum which is within the alkyne C-C stretch region. Since these internal alkynes are essentially symmetrical, a weak signal is expected. The very faint peak, for example, can be seen in the spectrum of **5.3a**. After several weeks, enhancements at 1094, 1124, 2000-2250, and 3381 cm^{-1} were observed for the polymers. These enhancements are marked with red arrows on the spectrum of **5.3a** after three weeks. The peak at 3381 cm^{-1} lies within the alkyne C-H stretching vibration region and the strong, broad absorption at 1094 cm^{-1} and 1124 cm^{-1} may be due to alkyne C-H bending vibrations (164). These absorptions are typically observed for monosubstituted alkynes, an observation that is consistent with the slow loss of terminal tributyltin groups.

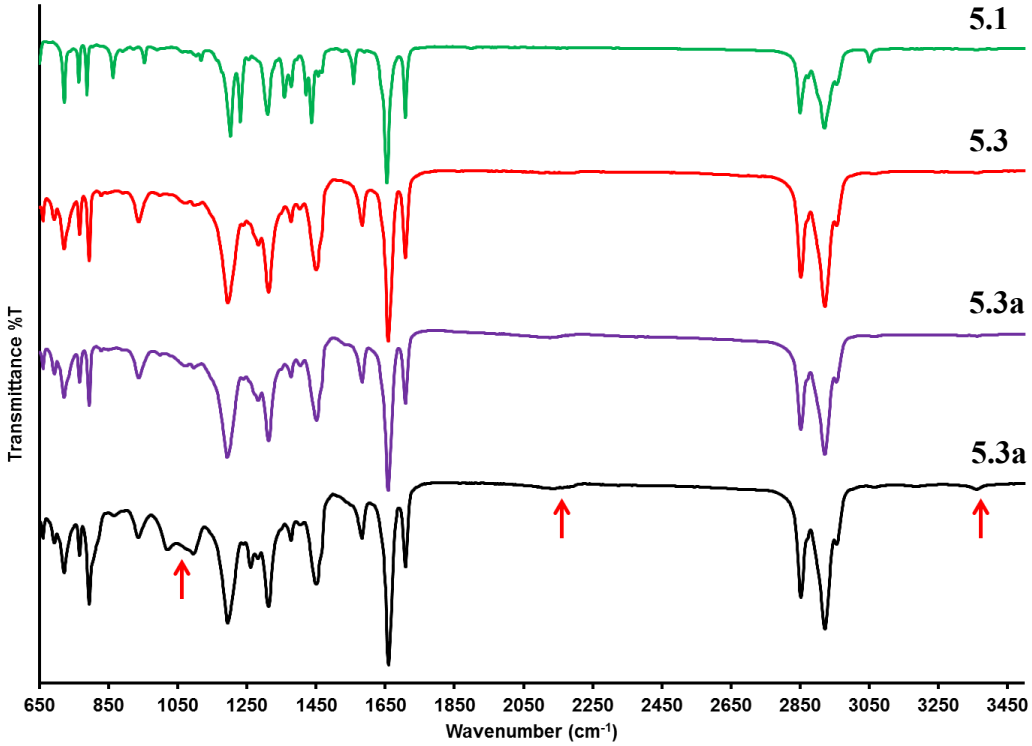

Figure 5.3 IR spectrum of NDI **5.1** (green), polymer **5.3** (red), polymer **5.3a** (purple), and polymer **5.3a** after three weeks (black).

5.3.3 Electronic Characterization of NDI Polymers

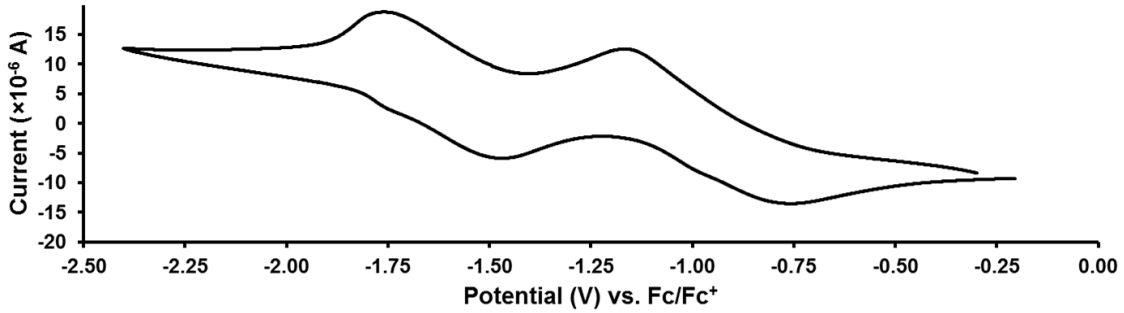

Figure 5.4 Representative CV trace of **5.3** and **5.3a**.

Polymers were characterized by cyclic voltammetry (CV) and UV-vis spectroscopy. Given the less desirable PDI values, both **5.3** and **5.3a** exhibited the same CV and UV-vis characteristics, indicating a saturation effect in terms of chain length for their electronic properties. Two half-wave reduction potentials ($E_{1/2}$) at –0.96 V and –1.61 V (referenced to Fc/Fc^+ at 0.0 V) were observed in the CV trace (Figure 5.4). These broad CV waves lack the distinct reduction peaks of individual NDI units but onset and redox potentials closely resemble those reported for poly-NDI (162). These two characteristic NDI reduction waves indicate initial radical anion and subsequent dianion formation. The UV-vis absorbance spectra in Figure 4.5 also show the strong bathochromic shift (λ_{max} of 557 nm) due to effective conjugation along the polymer backbone compared to monomer **5.1**.

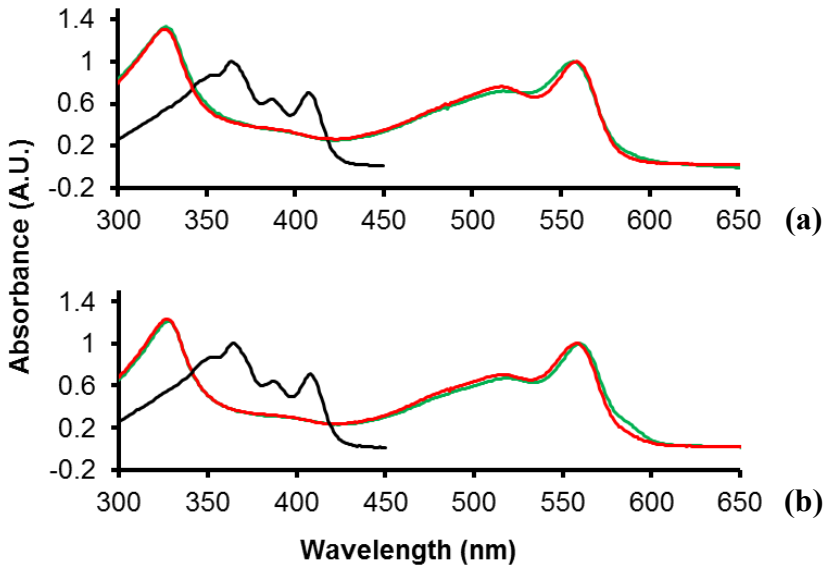

Figure 5.5 (a) Normalized UV-vis ($CHCl_3$) trace of monomer **5.1** (black) and polymer **5.3** after 1 h (red) and 2 h (green) (b) Normalized UV-vis ($CHCl_3$) trace of monomer **5.1** (black) and polymer **5.3a** after 1.5 h (red) and 2.5 h (green).

5.3.4 Synthesis and Characterization of Stannylated Diyne NDI

A common route to append stannylactylene moieties onto a molecule of interest can require up to three steps: coupling an unsaturated organohalide to a protected terminal alkyne, deprotection, and stannylation of the alkyne. Initial work to couple 2,6-dibromo NDI with a silyl-protected acetylene and subsequent deprotection using TBAF were frustrated by what we suspect was competing reactions as reported by Saha *et al*. (165; 166; 167). Reaction mixtures quickly turned black and NMR core ^1H signals were lost, an indication that radical NDI anions were generated. To eliminate the deprotection step and any interfering anions, we sought to synthesize **5.4** in a single step using **5.2**. Initial attempts to synthesize **5.4** by slowly adding **5.1** to a solution containing $Pd(PPh_3)_4$ and an excess of **5.2** proved ineffective. TLC typically showed multiple products and

the reaction required extended periods of time or additional equivalents of **5.2** to reach completion, presumably due to homo coupling of the excess tin reagent.

The more effective approach was to prepare **5.4** by saturating a toluene solution containing 5 mol% $Pd(PPh_3)_4$ and **5.1** at 90 °C with an excess of **5.2** in a single aliqout (Scheme 5.1). The solution was allowed to stir for 20 min before the reaction was stopped by removing the toluene. Monomer **5.4** was collected by reverse-phase (C-18) column chromatography in a 54% yield as tributyltin groups are often sensitive to silica gel (168), complicating the purification, and neutral alumina provided poorly resolved fractions.

The stability of **5.4** permitted full characterization by NMR and HRMS. The *sp* hybridized carbon peaks at 113.00 and 108.89 ppm presented in the ^{13}C spectrum (Figure 5.6) demonstrate that reverse-phase column chromatography cleanly yields **5.4** without contamination by acetylene-based side-products. Obtaining a clean monomer is critical because Stille coupling reactions are sensitive to monomer stoichiometry and purity (163).

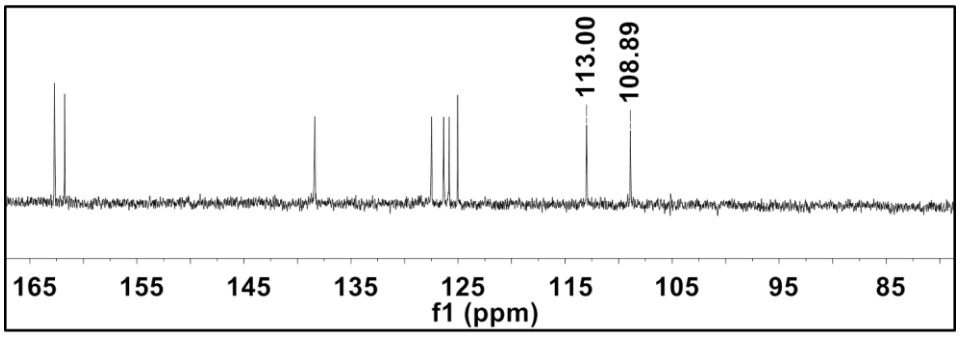

Figure 5.6 ^{13}C NMR ($CDCl_3$) spectrum of **5.4** showing the sp2 and sp region.

5.3.5 Reaction Scope of Stannylated Diyne NDI

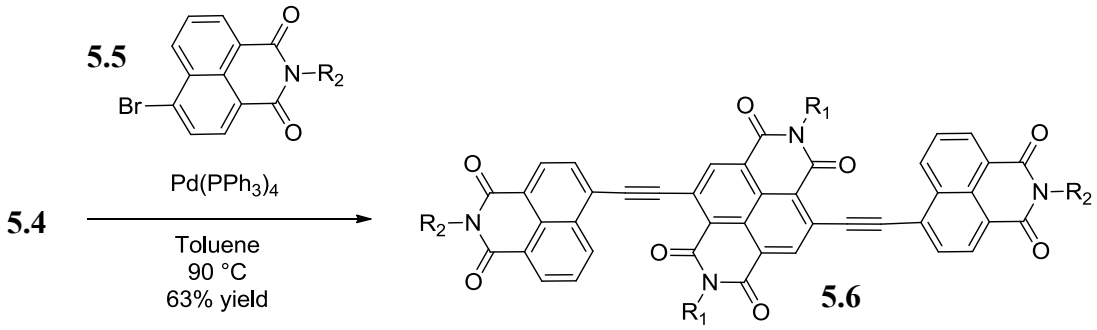

R_1 = 2-octyldodecyl
R_2 = *n*-octyl

Scheme 5.2 Representative Sonogashira coupling reaction of diyne **5.4**.

To further demonstrate its synthetic utility, **5.4** was also coupled with 2 equivalents of **5.5** to give **5.6** in 63% yield (Scheme 5.2). **5.5** was chosen for its similarly electron deficient nature and, unlike the NDI polymers, the product **5.6** was readily characterized with ^{1}H and ^{13}C NMR spectroscopy.

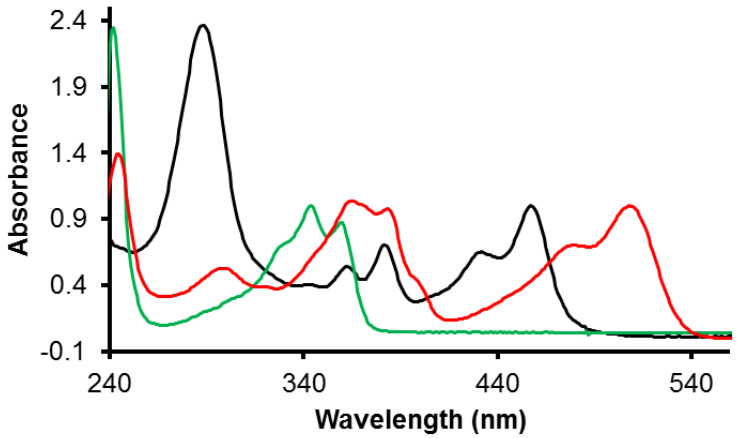

Figure 5.7 Normalized UV-vis ($CHCl_3$) trace of **5.4** (black), **5.5** (green), and **5.6** (red).

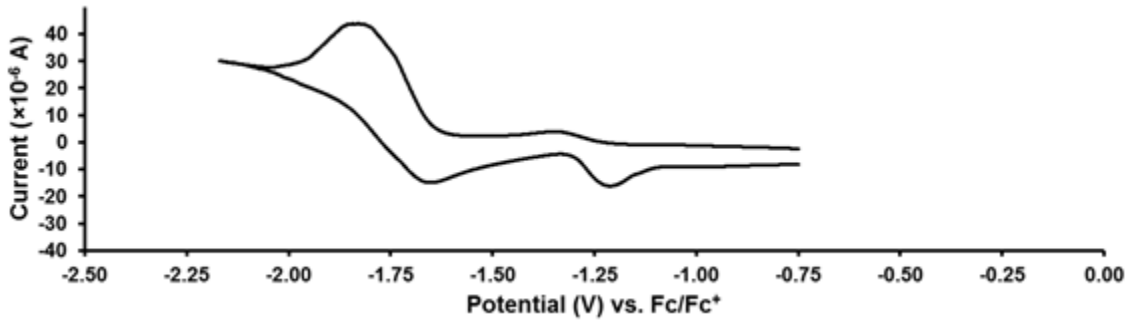

Figure 5.8 CV trace of **5.6**.

The UV-vis spectra in Figure 5.7 show that both the NDI and the naphthalene monoimide moieties of **5.6** are bathochromically shifted compared to the corresponding starting materials, **5.4** and **5.5**. Two reduction peaks were observed in the CV of **5.6** with $E_{1/2}$ values of –1.30 V and –1.74 V (Figure 5.8). The cathodic shift of these potentials compared to those observed for **5.3** and **5.3a** may be due to fewer electron withdrawing moieties on the small molecule **5.6** or that the naphthalene monoimide is a weaker electron withdrawing group than naphthalene diimide.

Stille coupling reactions are generally carried out with electron rich stannylated starting materials and relatively electron deficient unsaturated organohalides. Electron rich moieties are traditionally easier to stannylate and electron deficient unsaturated organohalides facilitate the initial oxidative insertion step (163). An advantage of using **5.4** is that different aryl halide monomers could be used in Stille coupling reactions to create a wide array of alkyne-linked, alternating polymer or small molecule architectures. For example, electron poor aromatic halides or electron rich units that are not readily stannylated could be combined with the relatively electron deficient NDI to create novel alkyne-linked alternating materials.

5.4 CONCLUSION

In summary, we have developed a very simple and versatile synthetic method that can be used for either the direct production of alkyne-linked NDI-containing polymers or, by adjusting conditions and relative stoichiometries, can yield the key synthetic intermediate **5.4**. Compound **5.4** will enable the synthesis of new NDI containing conjugates and alkyne-linked alternating polymers. It is worth noting that although the polymers accessible by this new approach do not have direct aryl-aryl linkages, an alkyne-linked NDI polymer maintains conjugation and may be of interest for applications that require more distance between aromatic units or would take advantage of alkyne chemistry.

5.5 EXPERIMENTAL

5.5.1 General Methods

NDI **5.1** (128; 136) was prepared from dibrominated 1,4,5,8-naphthalenetetracarboxylic dianhydride (36) and 2-octyldodecylamine (145) using literature procedures. **5.5** was also prepared according to literature procedure (169). $Pd(PPh_3)_4$ was purchased from STREM. Dry toluene was obtained by distillation over CaH. All reactions were carried out under argon. All other materials were purchased from Aldrich and used without further purification. Reverse phase chromatography was performed using C18 (carbon 23%) reverse phase silica gel from Silicycle. C18F reversed phase TLC plates were acquired from Whatman. NMR spectra were taken on a Varian Unity 400 spectrometer. Melting points were detected using a MEL-TEMP apparatus. Gel Permeation Chromatography (GPC) analyses were performed on polymer solutions in THF using a Waters Model 510 HPLC pump, two fluorinated polystyrene columns (IMBHW -3078 and I-MBLMW-03078) arranged in series, and a Waters 486 Tunable Absorbance Detector (λ =450 nm). Calibration was based on polystyrene standards in THF. UV-vis absorption spectra were obtained on an Agilent 8453 UV-vis spectrometer. IR spectra were obtained using polymer solids on a PerkinElmer Spectrum 100 FT-IR equipped with a universal ATR (UATR) accessory. Electrochemical cyclic voltammetry was performed under a nitrogen atmosphere. The cell was equipped with platinum working, tungsten counter and silver electrodes. Thin films were measured in a 0.1 M tetrabutylammonium hexafluorophosphate (TBAP) MeCN solution at a scan rate of 50 mV s^{-1} and referenced to Fc/Fc^+ by shifting (Fc*)0/+ to 0.0 V (170).

5.5.2 Synthesis and Characterization

NDI Polymer (**5.3**). A toluene (0.05 M) solution containing 50.0 mg of **5.1** (0.051 mmol) and 0.027 ml of **5.2** (0.051 mmol) was subjected to three freeze, pump, and thaw cycles. To this solution was added 2.9 mg of $Pd(PPh_3)_4$ (5 mol %) and the reaction mixture was heated at 90 °C for 1 h. The toluene was concentrated to a minimal volume by rotary evaporation and the crude material was precipitated in MeOH/2N aqueous HCl (10/1 (v/v)). The solid was purified with a Soxhlet extraction apparatus using methanol, acetone, and DCM in succession. The polymers were collected from the DCM fraction and concentrated to a minimum volume by rotary evaporation. The polymers were precipitated in MeOH/2N aqueous HCl (10/1 (v/v)) two more times to yield **5.3** as a bright red solid (40.2 mg, 0.047 mmol, 92% yield). M_n = 4.5 kDa, M_w = 15.2 KDa, M_w/M_n= 3.3; IR (cm^{-1}): 662, 713, 724, 790, 795, 943, 1094, 1124, 1200, 1299, 1316, 1380, 1426, 1455, 1586, 1661, 1710, 2000-2250 (very faint, may not see due to low polarity of alkyne spacers), 2854, 2926, 2959

NDI Polymer (**5.3a**). A toluene (0.05 M) solution containing 32.0 mg of **5.4** (0.022 mmol) and 21.3 mg of **5.1** (0.022 mmol) was subjected to three freeze, pump, and thaw cycles. To this solution was added 1.3 mg of $Pd(PPh_3)_4$ (5 mol %) and the reaction mixture was heated at 90 °C for 1.5 h. The toluene was concentrated to a minimal volume by rotary evaporation and the crude material was precipitated in MeOH/2N aqueous HCl (10/1 (v/v)). The solid was purified with a Soxhlet extraction apparatus using methanol, acetone, and DCM in succession. The polymers were collected from the DCM fraction and concentrated to a minimum volume by rotary evaporation. The polymers were precipitated in MeOH/2N aqueous HCl (10/1 (v/v)) two more times to yield **5.3a** as a bright red solid (33.2 mg, 0.019 mmol, 86% yield). M_n = 4.3 kDa, M_w =

14.0 KDa, M_w/M_n= 3.2; IR (cm^{-1}): 662, 713, 724, 790, 795, 943, 1094, 1124, 1200, 1299, 1316, 1380, 1426, 1455, 1586, 1661, 1710, 2000-2250 (very faint, may not see due to low polarity of alkyne spacers), 2854, 2926, 2959

2,7-bis(2-octyldodecyl)-4,9-bis((tributylstannyl)ethynyl)benzo[*lmn*][3,8]phenanthroline-1,3,6,8(*2H,7H*)-tetraone (**5.4**). A toluene (0.01 M) solution of 40.0 mg of **5.1** (0.041 mmol) and 2.3 mg of $Pd(PPh_3)_4$ (5 mol %) was subjected to three freeze, pump, and thaw cycles. The solution was placed in an oil bath at 90 °C and 0.13 ml of **5.2** (0.250 mmol) was added in a single aliquot. The reaction mixture continued to stir at 90 °C for another 20 min before the toluene was removed via rotary evaporation. The crude material was dissolved with CH_2Cl_2 and allowed to absorb onto reverse phase silica gel. The dry silica gel containing the crude material was purified by reverse phase column chromatography (short plug - 30/70 DCM/MeCN to elute excess **5.2** (stains under I_2 or with PMA) and 50/50 DCM/MeCN to elute **5.4** (stains silica bright yellow) as a dark red oil (32.0 mg, 0.022 mmol, 54% yield). ^{13}C NMR (400 MHz, $CDCl_3$) δ 162.69, 161.74, 138.39, 127.49, 126.34, 125.83, 125.04, 113.00, 108.89, 45.10, 36.62, 32.06, 31.77, 30.22, 29.79, 29.73, 29.50, 29.46, 29.18, 29.07, 28.95, 27.21, 26.91, 26.58, 22.82, 14.26, 13.87, 11.69 ppm; ^1H NMR (400 MHz, $CDCl_3$) δ 8.79 (s, 2H), 4.12 (d, J = 4.0 Hz, 4H), 2.01 (m, 2H), 1.69 (m, 12H), 1.48-1.12 (m, 88H), 0.95 (m, 18H), 0.86 (m, 12H) ppm; CI-HRMS (positive ion) calculated for ($C_{82}H_{139}N_2O_4Sn_2$)+1, 1455.8773; found 1455.8821.

4,9-bis((2-octyl-1,3-dioxo-2,3-dihydro-1*H*-benzo[*de*]isoquinolin-6-yl)ethynyl-2,7-bis(2-octyldodecyl)benzo[*lmn*][3,8]phenanthroline-1,3,6,8(*2H,7H*)-tetraone (**5.6**). A toluene (0.1 M) solution of 27.6 mg of **5.4** (0.019 mmol) and 15.5 mg of **5.5** (0.040

mmol) were subjected to three freeze, pump, and thaw cycles. To this solution was added 1.0 mg of $Pd(PPh_3)_4$ (5 mol %) and the reaction mixture was heated at 90 °C for 2 h. The toluene was removed via rotary evaporation and the crude material was purified by column chromatography (50/50 DCM/Hex to 80/20 DCM/Hex) to yield **5.6** as a red solid (18.0 mg, 0.012 mmol, 63% yield). MP 172-176°C; ^{13}C NMR (400 MHz, $CDCl_3$) δ 163.66, 163.34, 161.94, 161.45, 137.27, 132.96, 132.74, 132.32, 131.75, 130.03, 128.16, 127.94, 126.65, 126.22, 126.10, 125.56, 125.26, 123.83, 122.96, 99.30, 97.25, 45.19, 40.77, 37.05, 32.03, 31.98, 31.93, 30.29, 29.86, 29.84, 29.79, 29.51, 29.48, 29.40, 28.22, 27.32, 26.66, 22.80, 14.24 ppm; ^1H NMR (400 MHz, $CDCl_3$) δ 9.19 (d, *J* = 8.0 Hz, 2H), 8.82 (s, 2H), 8.60 (d, *J* = 8.0 Hz, 2H), 8.52 (d, *J* = 8.0 Hz, 2H), 8.06 (d, *J* = 8.0 Hz, 2H), 7.84 (t, *J* = 8.0 Hz, 2H), 4.26 (d, *J* = 4.0 Hz, 4H), 4.10 (t, *J* = 8.0 Hz, 4H), 2.04 (m, 2H), 1.71 (m, 4H), 1.55-1.05 (m, 84H), 0.88 (t, *J* = 8.0 Hz, 6H), 0.82 (m, 12H) ppm; CI-HRMS (positive ion) calculated for $(C_{98}H_{129}N_4O_8)+1$, 1489.9766; found 1489.9802.

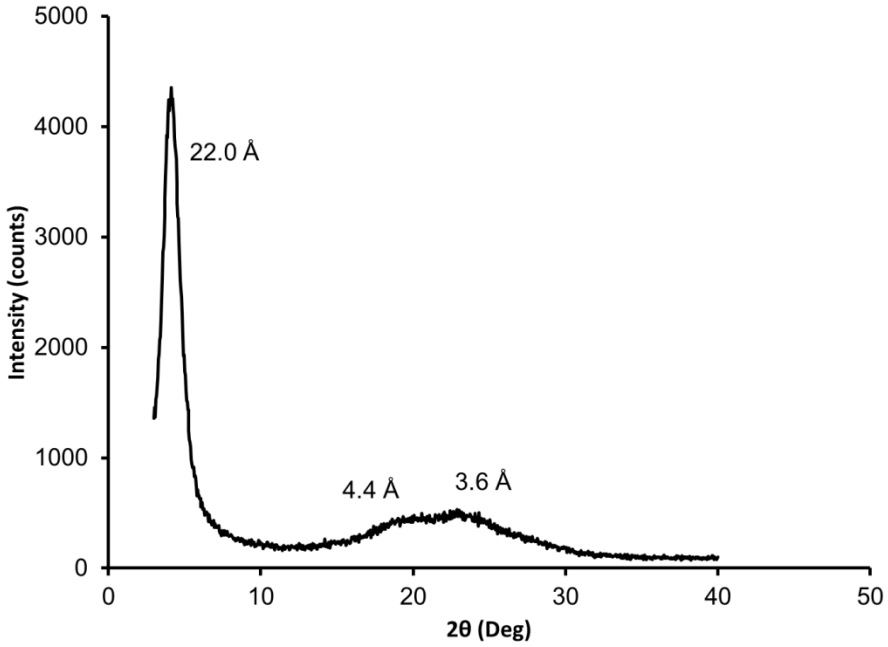

Figure 5.9 A reprentative XRD pattern of **5.3** and **5.3a**. Peaks are labeled with their corresponding *d*-spacing value. Note that a broad "hump" is often observed in the patterns of amorphous materials but the "hump" in this pattern (15–30 degrees) has a dip which suggests that these signals are the result of order. These *d*-spacing values are consistent with the patterns in Chapter 4 which indicate that the polymer chains are stacked through offset face-to-face NDI interactions.

Chapter 6

Association of Neutral DAN and NDI Polymers

6.1 CHAPTER SUMMARY

6.1.1 Introduction

The Iverson group has previously demonstrated the intermolecular recognition between charged aromatic donor and acceptor polymers in solution (Chapter 1). It was also shown that intermolecular aromatic interactions between neutral aromatic donor and acceptor monomers are present in the solid phase (Chapter 2). The work presented in this chapter seeks to test the feasibility of driving the association between neutral aromatic donor and acceptor polymer strands.

6.1.2 Goals

The goal of this chapter is to answer the question, "*Can neutral polymers that are connected in a linear fashion and composed of either flexible DAN or NDI units associate in a D–A fashion.*" The results have the potential to inspire materials that can self-assemble in a predictable fashion through aromatic D–A interactions.

6.1.3 Approach

Ethyl-linked polymers were prepared by the polymerization of brominated DAN or NDI derivatives with *bis*(tributylstannyl)acetylene and the subsequent hydrogenation of these conjugated polymers. Polymer films were analyzed with UV-vis spectroscopy to detect association between the separate DAN and NDI strands.

6.1.4 Results

Hydrogenated polymers were successfully synthesized after screening heterogeneous and homogeneous palladium catalyst conditions. DAN and NDI polymers were able to associate when slowly evaporated together from an organic solvent. UV-vis spectroscopy of a drop cast film showed a strong charge transfer (CT) absorbance for this mixture.

6.2 BACKGROUND

The Iverson group showed that intermolecular association between two complementary aromatic donor and acceptor oligomers can serve as a powerful tool for higher order structures in water (27). Most notably, the association between a donor and an acceptor oligomer increased with each additional aromatic unit along the linear oligomer backbone. The result directed the group's research towards a polymer system that could incorporate a large number of aromatic donor–acceptor (D−A) interactions and the possibility of a well-ordered material.

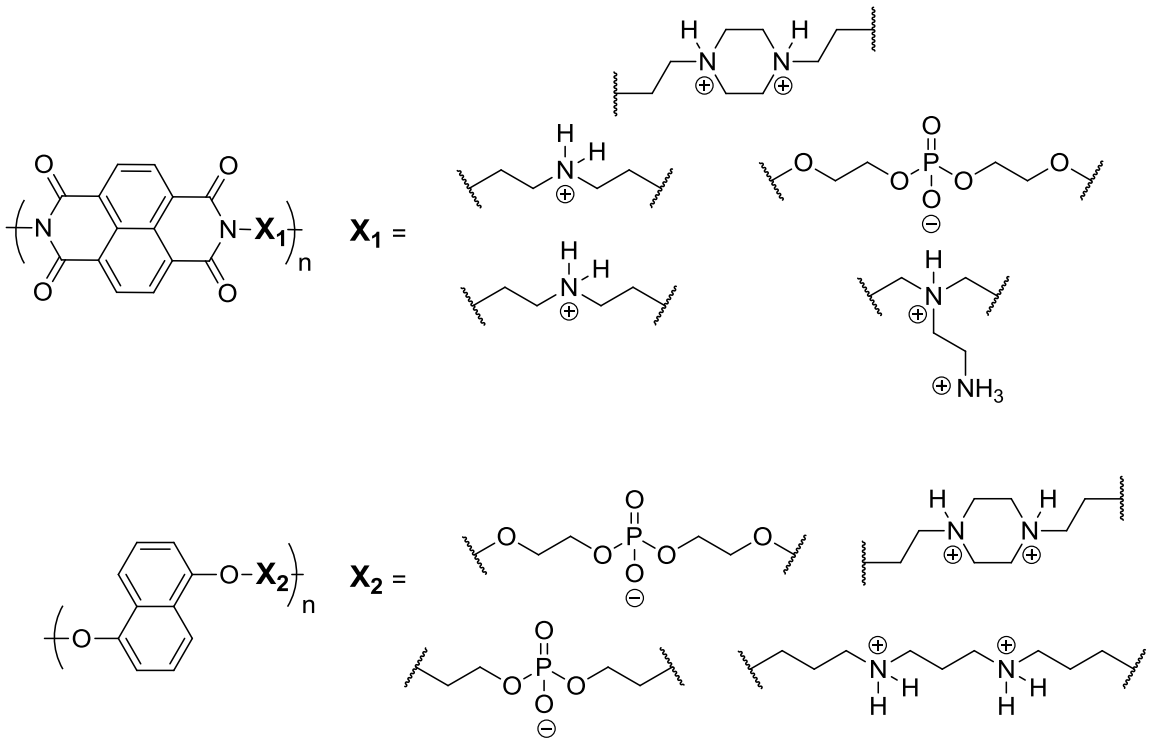

Figure 6.1 Linear polymers that were insoluble in aqueous solution.

Numerous linear polymer scaffolds were explored but solubility complications arose during their synthesis (171). These initial attempts sought to synthesize DAN and NDI polymers (polyDAN and polyNDI) through a step growth polymerization with various linker groups (Figure 6.1). The linkers contained amines or phosphate moieties to impart either a positive or negative charge to aid solubility in an aqueous solution. Unfortunately, neither system of charges afforded soluble polymers. These were surprising results as the Iverson group has traditionally used aspartic acid linkers with negative charges to solubilize DAN and/or NDI oligomers in water.

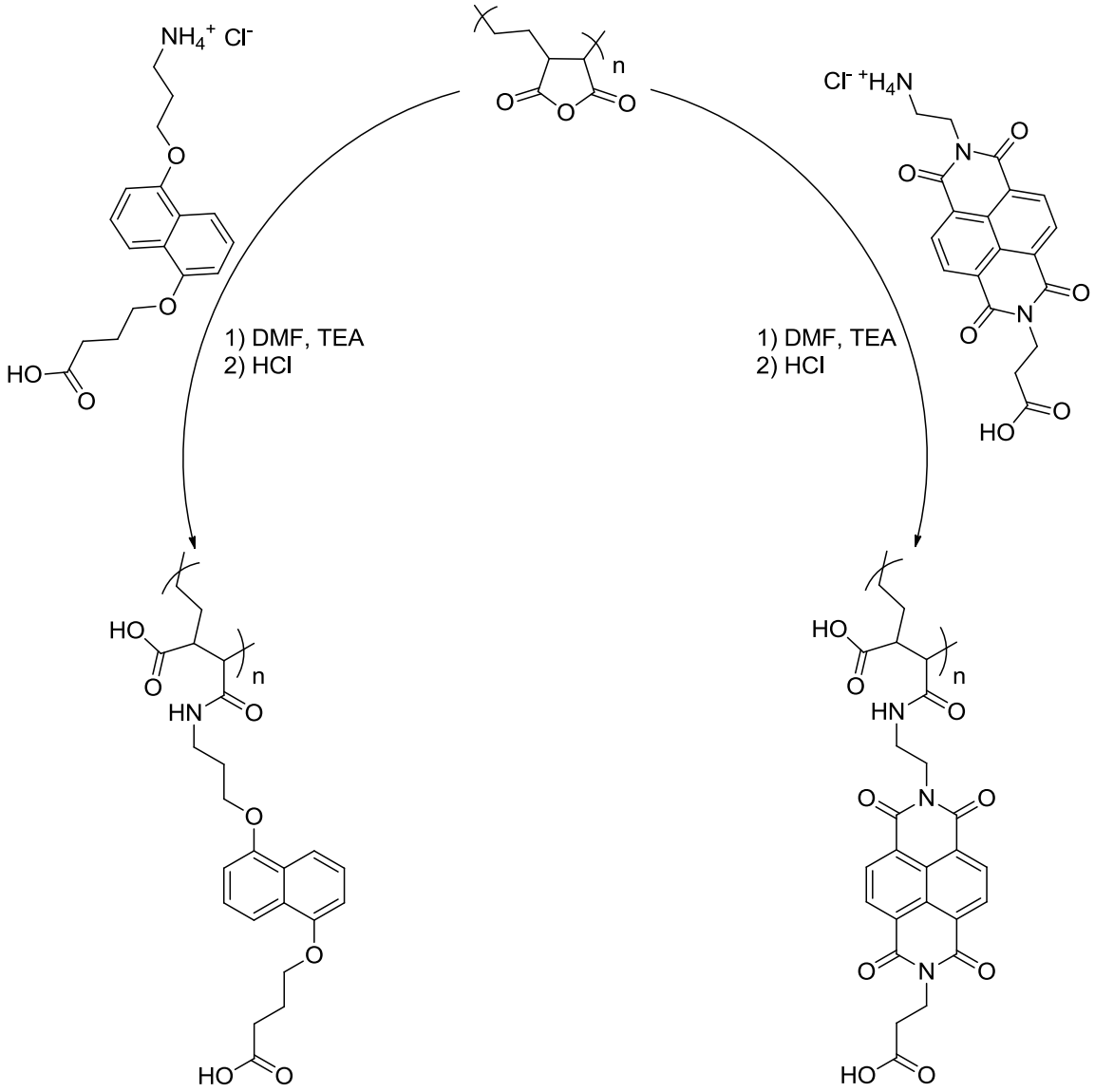

Figure 6.2 Successful synthesis of aqueous soluble branched polymers.

Aqueous soluble aromatic donor and acceptor polymers were synthesized by reacting DAN or NDI monomers with poly(ethylene-*alt*-maleic anhydride) (171) (Figure 6.2). The branched polymer scaffold placed charges along the backbone and on one side of the aromatic unit. The additional charges and branched nature facilitated polymer

solubility up to 3 weight percent in a basic media. The slight aqueous solubility was enough to initiate association studies between the polyDAN and polyNDI.

A weak charge transfer (CT) absorbance was observed in the UV-vis spectrum of a polyDAN–polyNDI mixture indicating some degree of association between the DAN and NDI units. Viscosity measurements and SEM images suggested that the components formed a network of associated polymer chains that interact through a few DAN−NDI interactions. This model was corroborated by the weak CT absorbance. Nonetheless, delicate fibers were formed when the mixture was injected into an acidic solution through a small aperture. Fiber formation was an exciting development as it actually resembled, in some small fashion, the formation of spider silk. These silk strands owe their infamous strength and flexibility to non-covalent intermolecular interactions that result in both crystalline β-sheet networks and amorphous regions.

The Iverson group now seeks the next generation of polyDAN and polyNDI that will display higher levels of association. The low level of association of the previous polymer mixture was attributed to poor solubility, the branched scaffold, and a close proximity of charges. In fact, calculations performed by Joe Reczek suggested that a neutral system can result in an association increase up to four orders in magnitude when compared to an analogous system with charges (171). Yet, attempts to synthesize neutral polymers that are soluble in water were once again thwarted due to solubility complications.

Before further efforts are made to address solubility, we believe it is necessary to determine if it is possible for two polymers that lack charges and whose aromatic units are connected in a linear fashion can associate through aromatic D–A interactions. It was realized that the hydrogenation of conjugated polymers prepared in the manner described in Chapter 5 can yield polyDAN and polyNDI for use in assessing these parameters. This

method of polymer preparation will also eliminate the branched scaffold and maintain a high level of flexibility within the polymer strand. Although these polymers will lack water solubility due to the absence of charges, any solid state interactions between these donor and acceptor polymers should still be relevant to the formation of D–A fibers for future systems. The work in this chapter describes the synthesis of linear DAN and NDI polymers and an assessment of their solid state interaction.

6.3 RESULTS

6.3.1 Polymer Synthesis

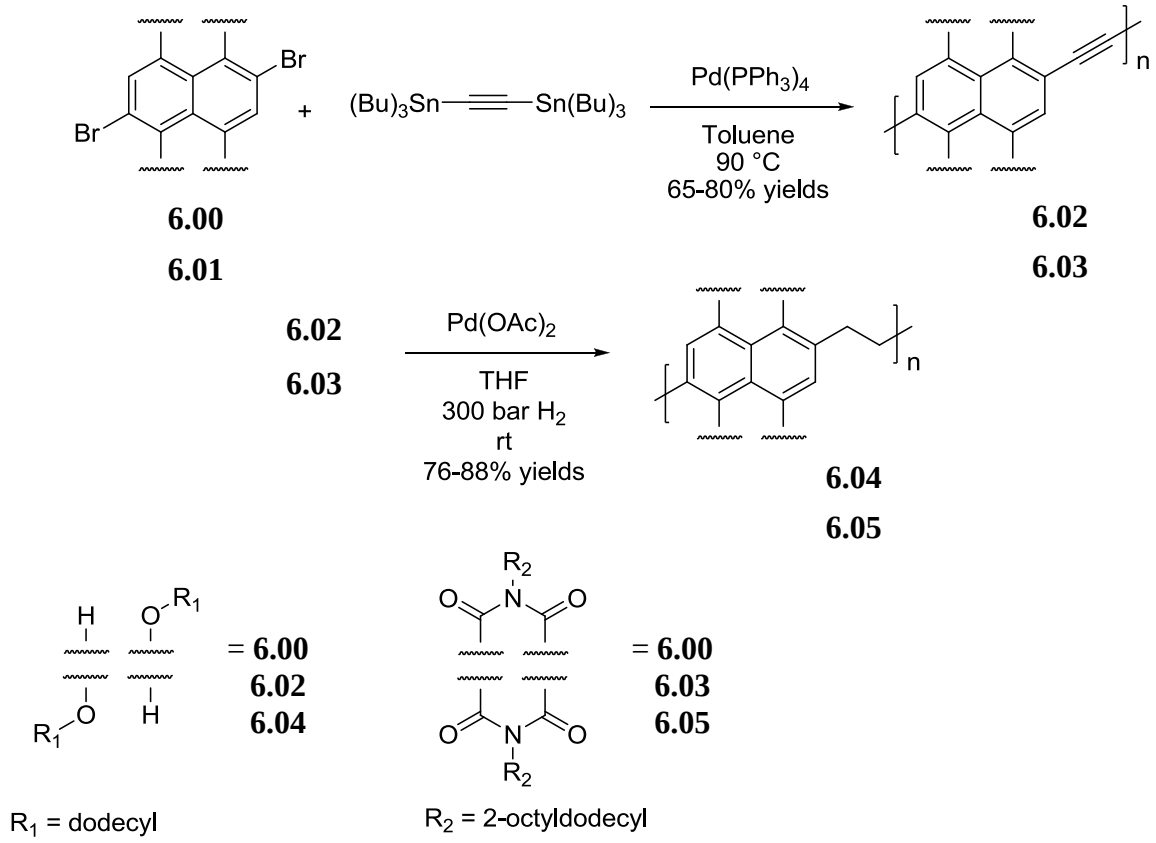

Scheme 6.1 Synthesis of flexible DAN or NDI polymers with aromatic units connected in a linear fashion.

Flexible polymers composed of DAN or NDI units connected in a linear fashion were synthesized in a two-step manner (Scheme 6.1) by the hydrogenation of conjugated polymers to yield polyDAN (**6.04**) and polyNDI (**6.05**). Brominated DAN or NDI monomer (**6.00** and **6.01**) was reacted with one equivalent of bis(tributylstannyl)acetylene using Stille coupling conditions (154) (Chapter 5) until the extent of conjugation reached its maximum visible absorbance. The polymerization

reaction was then quenched with excess iodobenzene to maintain solubility and to eliminate the stannyl groups.

Heterogeneous	Homogeneous
• palladium on carbon	• palladium (II) acetate
• palladium on calcium carbonate	• bis(triphenylphosphine) palladium (II) dichloride
• palladium hydroxide on carbon	• tetrakis (triphenylphosphine) palladium
• palladium on barium sulfate	• allylpalladium chloride dimer
• palladium on alumina	• tris(dibenzylidenacetone) dipalladium (0)
	• [1,1´-bis(diphenylphosphino)ferrocene] dichloropalladium (II) complex with dichloromethane
	• palladium chloride

Table 6.1 Palladium catalysts screened for the hydrogenation activity.

A number of palladium catalysts were screened (Table 6.1) to test their ability to hydrogenate **6.02**. Ruthenium hydrogenation catalysts were avoided due to reports of unwanted side reactions with alkene intermediates or solvent during the hydrogenation of acetylene-based polymers (172; 173; 174; 175). Hydrogenation progress was monitored using UV-vis spectroscopy. The hydrogenation progress correlated to the reduction of the maximum visible absorbance signal as the effective conjugation between DAN units was reduced. The heterogeneous catalysts (room temperature and 30 bar H_2) showed no

decrease in the visible absorbance spectrum of **6.02** after 24 h. It was inferred that phase incompatibility between the heterogeneous catalyst and the conjugated polymers of mediocre solubility resulted in the lack of hydrogenation activity. Alternatively, two homogeneous catalysts (palladium (II) acetate and bis(triphenylphosphine) palladium (II) dichloride) showed a dramatic decrease in the absorbance spectrum of **6.02** under the same reaction conditions. The most substantial change was associated with palladium acetate.

The hydrogenation progress of **6.02** appeared to cease after 48 h using palladium acetate. The reaction mixture was passed through a pad of celite to remove insoluble palladium products. The filtered solution was then shaken overnight with a palladium scavenger resin to ensure complete removal of the palladium catalyst. Methanol precipitation yielded **6.04**. The polymer was soluble in common organic solvents like $CHCl_3$, CH_2Cl_2, and toluene but a solid polymer was only obtained by methanol precipitation which took several hours. Otherwise, the polymer was an oil after solvent evaporation. Hydrogenation of the conjugated NDI polymer (**6.03**) was accomplished in the same manner to yield **6.05** (Scheme 6.1). Like **6.04**, solid **6.05** was only obtained by methanol precipitation which took several hours. Solvent evaporation always resulted in an oil for **6.05**.

6.3.2 Polymer Characterization

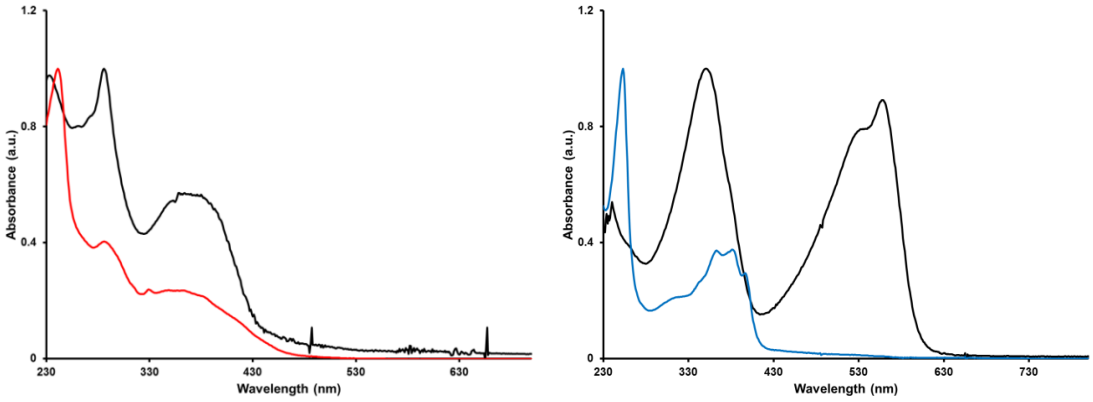

Figure 6.3 Normalized UV-vis spectrum of (a) **6.02** (black), (b) **6.04** (red), (b) **6.03** (black), and (b) **6.05** (blue) in chloroform.

The normalized UV-vis spectrum of **6.04** and **6.05** in chloroform is shown in Figure 6.3. The absorbance spectrum of the conjugated polymer is shown for comparison to highlight the dramatic change in absorbance after hydrogenation. The infrared (IR) spectrum of **6.04** and **6.05** showed that each polymer retained many of the same features of the parent conjugated polymer (Figure 6.4). Strong alkyne vibrational signals were not observed in the IR spectrum of the conjugated polymers due to the pseudo-symmetric nature of the molecules.

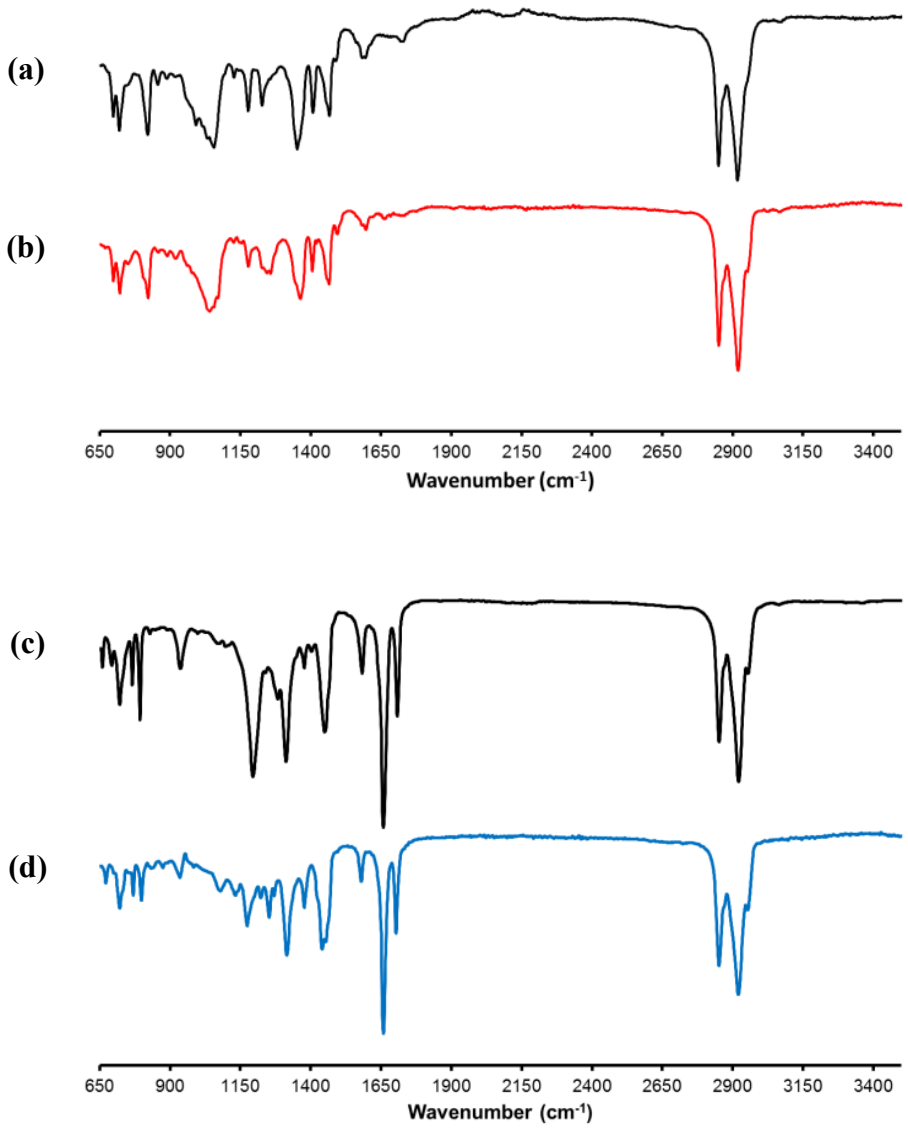

Figure 6.4 IR spectrum of (a) **6.02** (black), (b) **6.04** (red), (c) **6.03** (black), and (d) **6.05** (blue).

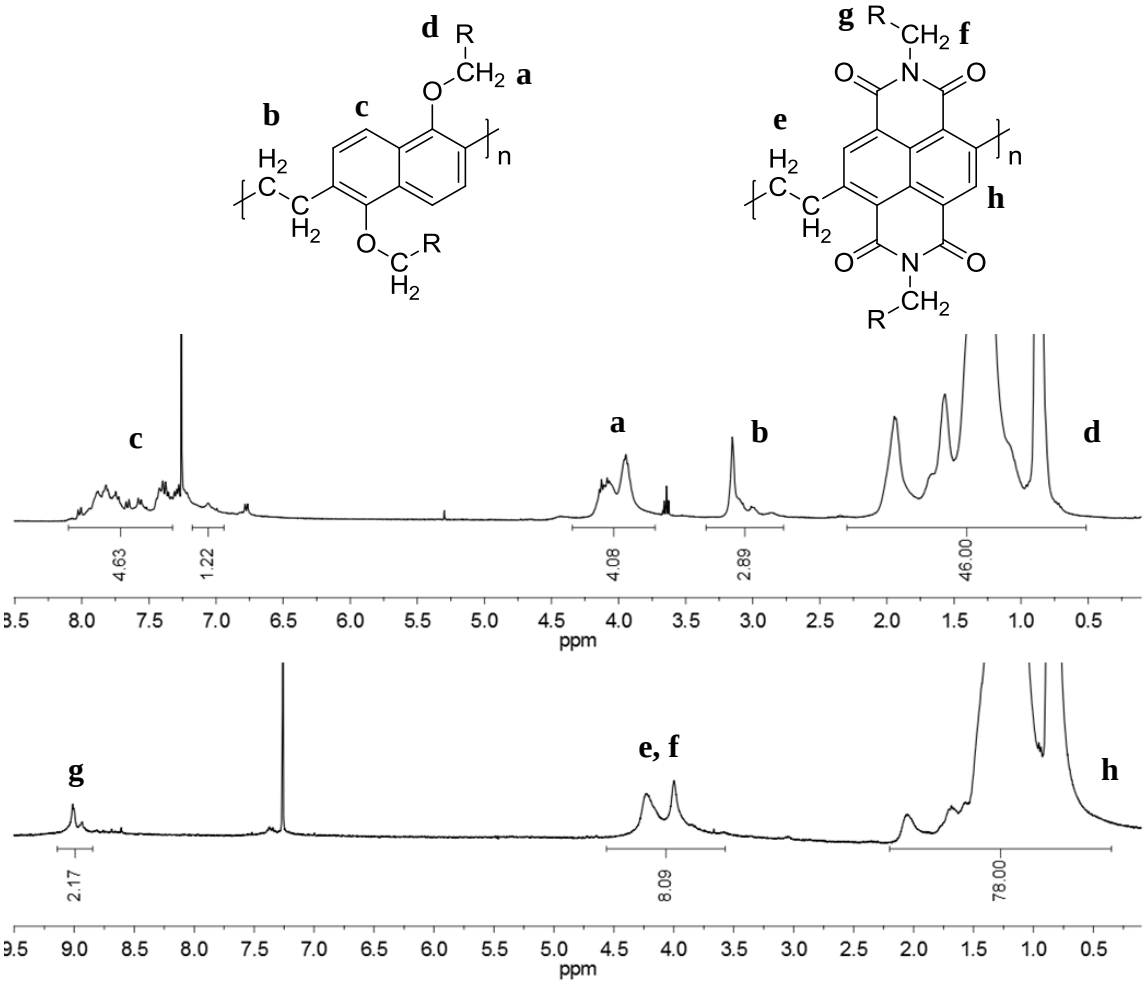

Figure 6.5 NMR spectrum of **6.04** (top) and **6.05** (bottom) in $CDCl_3$.

The hydrogenated polymers possessed an enhanced solubility compared to the conjugated ones which facilitated further characterization by ^{1}H NMR (Figure 6.5). Aromatic and alkyl hydrogen atoms were accounted for as broad signals in the spectrum of **6.04** and **6.05**. Signals from the hydrogen atoms on the side chain carbon adjacent to the DAN oxygen atoms of **6.04** were present at ≈ 4 ppm. The hydrogen atoms on the ethylene linkers were assigned to the broad singlet at ≈ 3 ppm for **6.04** (Figure 6.5a). This same signal appeared to shift downfield in the spectrum of the electron withdrawn

6.05. Integration of the broad doublet at ≈ 4 ppm integrates to eight hydrogen atoms which is consistent with hydrogen atoms on both the ethylene linker and those on the side chain carbon adjacent to the imide nitrogen (Figure 6.5b).

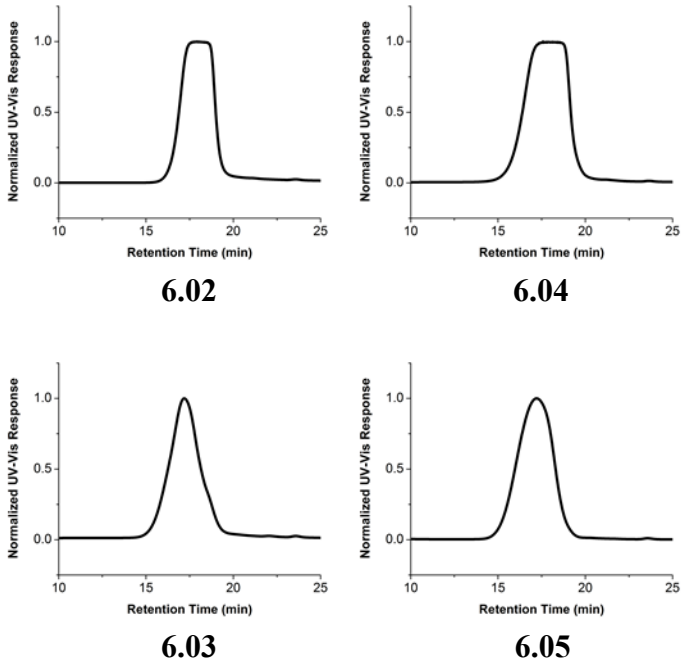

Figure 6.6 GPC traces of the conjugated and hydrogenated polymers.

Polymer	M_n (kDa)	M_w (kDa)	M_w/M_n
6.02	1,332	5,321	3.993
6.04	1,740	5,895	3.387
6.03	2,586	10,885	4.208
6.05	2,848	10,451	3.670

Table 6.2 Number average (M_n) and weight average (M_w) molecular weights determined by GPC.

Number average (M_n) and weight average (M_w) molecular weights were determined by gel permeation chromatography (GPC) (Table 6.2). The GPC traces are shown in Figure 6.6. GPC assigned M_n values of 1,332 kDa to **6.02** and 2,586 kDa to **6.03**. The hydrogenated polymers exhibited larger M_n values of 1,740 kDa and 2,848 kDa for **6.04** and **6.05**, respectively. The polydispersity index (PDI) of each hydrogenated polymer was also smaller than that of their conjugated analogue (Table 6.2).

6.3.3 Thin Film Characterization

Thin films were prepared by spin coating or drop casting a 10 weight percent chlorobenzene solution of polymer onto a glass plate. Films of **6.04**, **6.05** and a 50/50 mixture of these two polymer solutions were cast using each method. Spin cast films were prepared at 500 rpm for duration of 60 s and then baked at 120 °C for 5 min. The soft nature of the material made it difficult to acquire an accurate film thickness by stylus profilometry. Drop cast films were prepared by placing approximately 0.1 ml of solution onto a glass plate and then slowly evaporating the solvent at 65 °C. It was found that blowing a gentle stream of air over the material resulted in a thinner film for UV-vis spectroscopy.

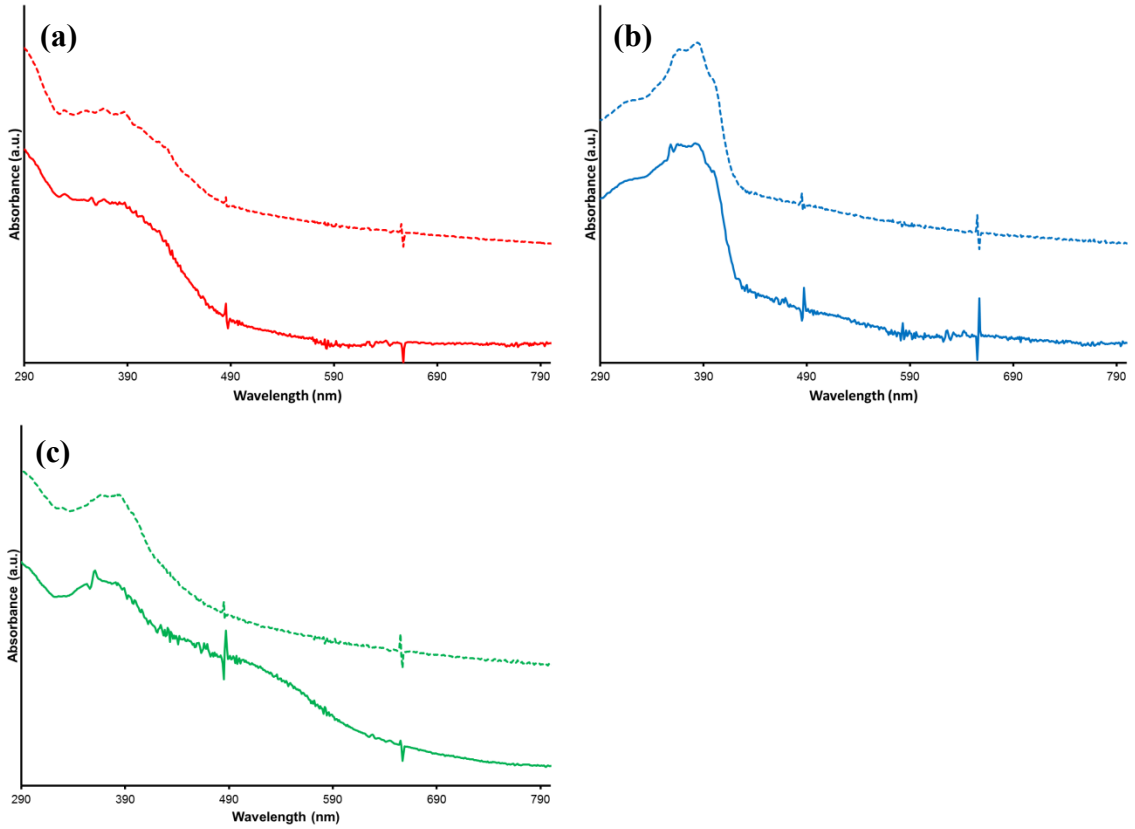

Figure 6.7 Normalized UV-vis spectrum of (a) spin coat **6.04** (red dash) and drop cast **6.04** (red solid), (b) spin coat **6.05** (blue dash) and drop cast **6.05** (blue solid), and (c) spin coat 50/50 mixture of **6.04**/**6.05** (green dash) and drop cast 50/50 mixture of **6.04**/**6.05** (green solid) from 10 weight percent chlorobenzene solutions onto a glass slide.

UV-vis spectra of the thin films are shown in Figure 6.7. The difference between the spin and drop cast films are minimal for the individual polymers (Figure 6.7a–b). The spin cast film from the 50/50 mixture did not show a CT absorbance but the drop cast film from the 50/50 mixture did exhibit a strong CT absorbance at 540 nm, characteristic of DAN–NDI interaction (Figure 6.7c–d) (Chapter 2).

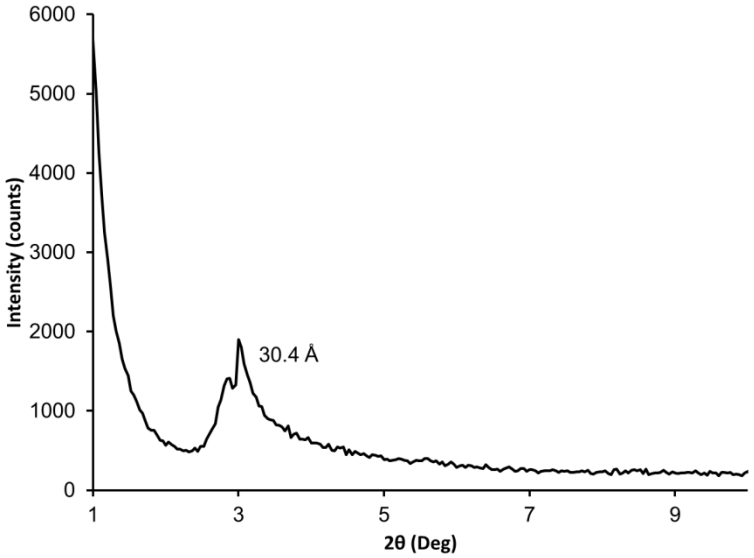

Figure 6.8 XRD pattern of a drop cast 50/50 mixture of **6.04**/**6.05** (on glass slide) from 10 weight percent chlorobenzene solutions.

X-ray diffraction (XRD) was used in an attempt to gain further structural details of the drop cast film from the 50/50 mixture. The lack of crystallinity resulted in poor diffraction and only a single low angle peak corresponding to a *d*-spacing of 30 Å was observed in the pattern.

6.4 DISCUSSION

6.4.1 Synthesis and Characterization

The ethyl linkers eliminate conjugation between aromatic units so that each DAN or NDI unit maintains its native electrostatic character. Electrostatic potential maps of the tethered aromatic units are shown in Figure 6.9. The ethyl linkers provide flexibility but are also short enough to prohibit intramolecular self-assembly.

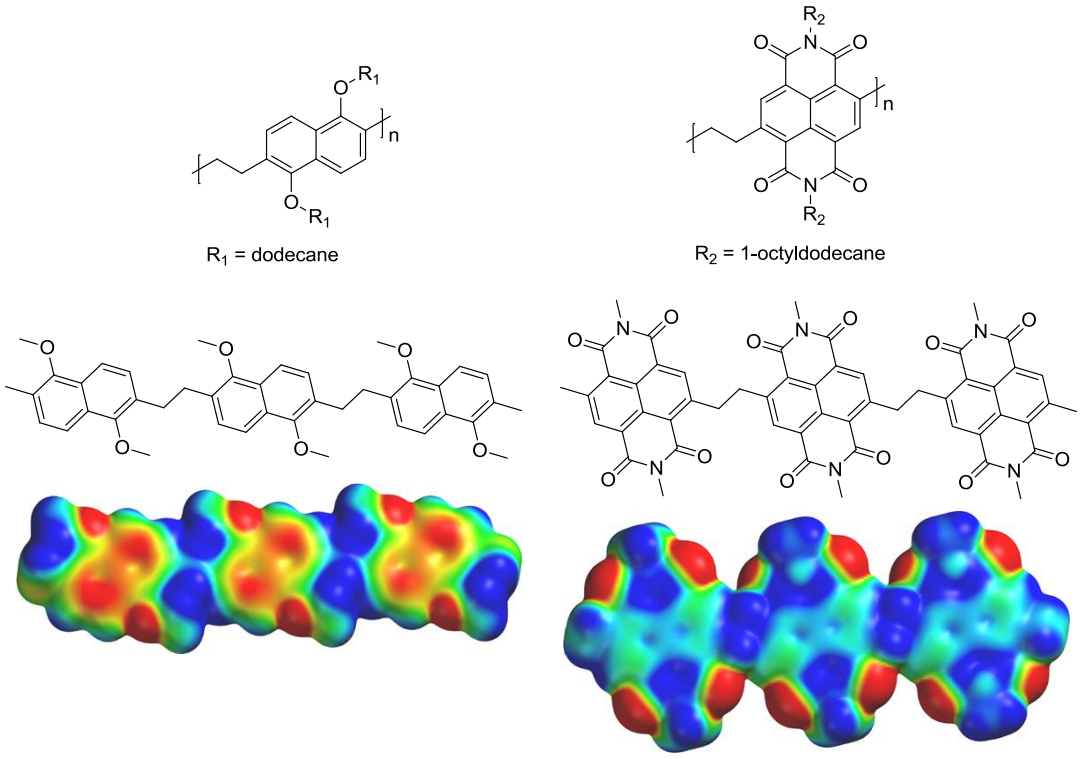

Figure 6.9 1) Figure shows the electrostatic potential maps of the individual polymers (top) 2) Models were generated with the same electrostatic potential color scale in Spartan using the DFT B3LYP G-31* method.

UV-vis and NMR spectroscopy supported a high degree of polymer hydrogenation. In particular, **6.05** completely lost the broad absorbance of **6.03 (**Figure 6.3b). The correct hydrogen ratio was also observed in the ^{1}H NMR spectrum of **6.05**. In addition, no alkene signals were observed in the spectrum and the benzene polymer caps could account for the weak signals between 7.25 and 7.5 ppm (Figure 6.5b).

There did appear to be some discrepancy in the hydrogen ratio of **6.04**. The observed ratio between the hydrogen atoms adjacent to oxygen and those hydrogen atoms on the ethane linker was 4.0:2.9 instead of the expected 4.0:4.0 (Figure 6.5a). The integration estimate suggested a hydrogenation completion of 72%. Signals from the solvent, the benzene polymer caps, and any residual alkene can appear in the same region

as the signals for aromatic hydrogen atoms on DAN, possibly skewing the integration values. An incomplete hydrogenation is corroborated by the UV-vis absorbance spectrum of **6.04** as it did not completely lose the broad absorbance of **6.02** (Figure 6.3a).

IR spectroscopy did not yield much information regarding the completion percentage of the polymer hydrogenation due to the pseudo-symmetric nature of the conjugated polymers. It did, however, show that the DAN and NDI units remained intact. **6.04** retained many of the same spectral features of **6.02**, especially in the fingerprint (1500–500 cm^{-1}) region (Figure 6.4a). **6.05** also retained many of the same spectral features of **6.03** (Figure 6.4b). The fingerprint region of **6.05** was more defined then that of **6.03**. This signal enhancement contrasted the DAN polymers and may indicate a more complete hydrogenation.

M_n values increased after hydrogenation, but the amount of change was much larger than expected. The M_n value rose ~31% for **6.04** (expected 0.8%) and ~10% for **6.05** (expected 0.5%) after hydrogenation from the conjugated species. The difference may be associated with overestimated M_n values which GPC often assigns to rigid-rod polymers (150). Hydrogenation ultimately transformed these polymers from a solid that readily forms thin films into an oil that was slow to precipitate from methanol. This change of state resulted from a drastic modification within the polymer that affected its flexibility in a manner that was consistent with a hydrogenated species.

6.4.2 Thin Film Characterization

The CT absorbance at 540 nm was consistent with the solid phase D–A interactions of Chapter 2. A CT absorbance was only observed in a 50/50 mixture of **6.04** and **6.05** when it was allowed to associate upon slow evaporation (Figure 6.7c). A

likely explanation is that the spin coat method did not afford the polymers enough time to associate before solvent evaporation and the subsequent mobility loss of the solvated polymers. Drop cast and spin coat methods did provide similar results for the individual polymers in the absence of intermolecular D–A association (Figure 6.7a–b).

The single peak in the XRD pattern with a *d*-spacing of 30 Å may represent the distance between some aromatic polymer chains (Figure 6.8), but this suggests little overlap of the side chains in an interdigitated manner when compared to the polymers in Chapter 4. It may be unlikely that an amorphous system with a high degree of flexibility would exhibit a substantial amount of interdigitated side chains. The extended length of the DAN and NDI moieties is ~35 Å. Therefore, the *d*-spacing of 30 Å could be attributed to the extended length of the aromatic units with the polymer flexibility causing the small discrepancy between these values. No other peaks were observed in the pattern which is characteristic of an amorphous material. The differences in polymer chain length (PDI) and the side chain identity (branched and linear) between **6.04** and **6.05** could contribute to this amorphous behavior.

6.5 CONCLUSION

The CT absorbance observed for a mixture of **6.04** and **6.05** shows that it is possible for neutral DAN and NDI polymers whose aromatic units are connected in a linear fashion to associate in the solid state. This study put forth new possibilities for future DAN and NDI polymers. The physical nature (thick oils) of these polymers suggests that they can tolerate longer chain lengths and still possess sufficient solubility. The limiting factor that dictates chain length using the method presented in this chapter is the solubility of the conjugated polymers. The efficiency of the hydrogenation process is yet another possible limitation. Since the mixture of **6.04** and **6.05** shows an intriguing level of association by UV-vis spectroscopy, the synthesis of new derivatives composed of the aromatic units connected in a linear fashion appears to be a worthwhile endeavor.

6.6 EXPERIMENTAL

6.6.1 General Methods

2,6-dibromo-1,5-bis(dodecyloxy)naphthalene (111) (**6.00**) and 4,9-dibromo-2,7-bis(2-octyldodecyl)benzo[*lmn*][3,8]phenanthroline-1,3,6,8(2*H*,7*H*)-tetraone (136) (**6.01**) were prepared as previously described. $Pd(Ph_3)_4$ was purchased from STREM. All other chemicals were acquired from Aldrich and used without further purification. All reactions were carried out under argon. NMR spectra were taken on a Varian Unity 400 spectrometer. Melting points were detected using a MEL-TEMP apparatus. GPC analyses were performed on polymer solutions in THF using a Waters Model 510 HPLC pump, two fluorinated polystyrene columns (IMBHW -3078 and I-MBLMW-03078) arranged in series, and a Waters 486 Tunable Absorbance Detector (λ =450 nm). Calibration was based on polystyrene standards in THF. Absorption spectra were obtained on an Agilent 8453 UV-vis spectrometer. IR spectra were obtained using a PerkinElmer Spectrum 100 FT-IR equipped with a universal ATR (UATR) accessory. XRD patterns were obtained with a Scintag X1 theta-theta diffractometer equipped with a Cu x-ray tube and a solid state x-ray detector set to count Cu K-alpha radiation.

6.6.2 Synthesis and Characterization

Polymerization: Conjugated polymers **6.02** and **6.03** were prepared according to the previously described method for **6.03** (Chapter 4). These polymerizations (100 mg scale) were halted with an excess of iodobenzene upon reaching suitable conjugation length by UV-vis spectroscopy (65–80% yields).

Conjugated DAN Polymer (**6.02**). **6.02** was collected as a dark red solid. IR: 716, 723, 1062, 1182, 1232, 1362, 1412, 1469, 1603, 1738, 2853, 2923 cm^{-1}. GPC: M_n 1,332, M_w 5,321, PDI 3.993.

Conjugated NDI Polymer (**6.03**). **6.03** was collected as a dark orange solid. IR: 662, 711, 725, 790, 795, 943, 1201, 1316, 1380, 1456, 1587, 1662, 1711, 2857, 2927 cm^{-1}. GPC: M_n 2,586, M_w 10,885, PDI 4.208.

Hydrogenation: **6.02** and **6.03** (5-10 mg) were dissolved in 0.5 ml THF. To this solution was added palladium acetate (10 weight %). The reaction was carried out in a bomb under 30 bar H_2. The reaction proceeded for 48 h before the reaction mixture was passed through a pad of celite to remove insoluble palladium impurities. Additional palladium acetate (10 weight %) was added to the solution after 24 h. The solvent was removed by rotary evaporation and the material was taken up in CH_2Cl_2 (0.05 M) then shaken for 24 h with QuadraPure^{TM} TU resin (5 g per 100 ml) to ensure complete removal of the palladium catalyst. The CH_2Cl_2 was concentrated to a minimal volume by rotary evaporation and the material was precipitated with MeOH/2N aqueous HCl (10/1 (v/v)). The polymers were slow to precipitate and eventually yielded solid **6.04** and **6.05** (76–88% yields).

Hydrogenated DAN Polymer (**6.04**). **6.04** was collected as an orange solid by methanol precipitation or an amber oil from solvent evaporation. ^1H NMR (400 MHz, $CDCl_3$) δ 8.16–6.90 (m, ~4H), 4.03 (br. d, 4H), 3.15 (br. s, ~4H), 1.94 (br. s, 4H), 1.77–1.00 (m, 36H), 0.88 (br. s, 6H) ppm. IR: 716, 723, 1062, 1182, 1232, 1362, 1412, 1469, 1603, 2853, 2923 cm^{-1}. GPC: M_n 1,740, M_w 5,895, PDI 3.387.

Hydrogenated NDI Polymer (**6.05**). **6.05** was collected as a colorless solid by methanol precipitation or an amber oil from solvent evaporation. ^{1}H NMR (400 MHz, $CDCl_3$) δ 9.01 (br. s, 2H), 4.24 (br. s, 4H), 4.12 (br. d, 4H), 2.04 (br. s, 2H), 1.86–0.93 (m, 64H), 0.84 (m, 12H) ppm. IR: 676, 726, 797, 801, 942, 1093, 1157, 1180, 1256, 1320, 1381, 1456, 1587, 1662, 1711, 2857, 2927 cm^{-1}. GPC: M_n 2,848, M_w 10,451, PDI 3.670.

APPENDIX A

Semiconductor Properties of Conjugated Polymers

A.1 INTRODUCTION

The work presented in this Appendix seeks to assess the semiconductor properties of the conjugated polymers from Chapter 4. Specifically, attempts were made to incorporate the polymers into an organic field-effect transistor and to benchmark their conductivity using four-point probe technique.

A.2 EXPERIMENTAL

A.2.1 Materials

The conjugated NDI–donor polymers in Figure A.1 (**A.1**, **A.2**, **A.3**, **A.4**) were synthesized as described in Chapter 4 (112). Conductive poly(3,4-ethylenedioxythiophene) poly(styrenesulfonate) (**A.5**) or PEDOT:PSS (Figure A.1, 3.0-4.0 weight percent in H_2O) was purchased from Sigma-Aldrich. Unless specified, all other reagents were purchased from Sigma-Aldrich and used without further purification.

Silicon wafers were purchased from NOVA Electronic Materials with the following specifications: heavily doped n-type wafers, 4" N/As <100> .001-.005 ohm-cm, 500-550 μm thick SSP prime grade Si wafers with two semi-standard flats, 4000 Å (400 nm) dry chlorinated thermal oxide on both sides & forming gas anneal (best effort basis due to swirls from arsenic doped wafer). The oxide layer was removed from one side of the wafer using a buffered oxide etch solution. To protect the other side during the oxide etch, a 10 weight percent solution of PMMA in chlorobenzene was applied by spin coating (500 rpm, 60 s, and soft bake at 150 °C for 10 min). After etching the exposed oxide layer, the PMMA layer was removed by successive washes (and

sonication) in acetone and dichloromethane to reveal a clean oxide layer. The dry wafers were then cleaned in a piranha solution for 0.5 h and the SiO_2 layer was immediately functionalized by slow evaporation with octadecyltrichlorosilane (OTS) for 24 h.

Shadow masks for the deposition of source/drain contacts were purchased from Ossila (item #E322). Gold wire for the deposition of source/drain contacts was purchased from Alfa Aesar. Evaporation boats were purchased from Kurt J Lesker.

A.2.2 Instruments

Transistors were tested using a Karl Suss PM 5 probe station with an Agilent 4156C precision semiconductor parameter analyzer. Four-point probe measurements were made on a Lucas Labs S-302 stand with SP4 four point probe head and Keithley 197A autoranging microvolt digital multimeter. Thermal evaporation of gold source/drain contacts was accomplished on a Denton thermal evaporation system. Film thickness measurements were performed with a J.A. Woollam M-2000 spectroscopic ellipsometer or a Veeco DEKTAK 6M profilometer.

A.2.3 Fabrication of Devices

Thin-film transistors: Bottom-contact organic field-effect transistors (OFETs) were constructed with **A.1** as the active layer. A 5 weight percent solution of **A.1** in chlorobenzene was passed through a 0.22 μm filter and spin coated (1500 rpm, 60 s, ~175 nm film) onto an OTS functionalized wafer. The wafer was heated at 150 °C for 10 min to remove residual solvent. Gold source/drain contacts (50 nm) were thermally evaporated through a shadow mask. Devices using **A.5** as the active layer were

constructed in an analogous manner to those with **A.1** (3.0-4.0 weight percent in H_2O, ~300 nm film).

Four-point probe: A 5 weight percent solution of **A.1**–**A.4** in chlorobenzene and a 3.0-4.0 weight percent solution of **A.5** in H_2O was spin coated (1500 rpm, 60 s) onto a glass slide (~300 nm film for **A.1**–**A.4** and ~900 nm film for **A.5**). The glass slide was heated at 150 °C for 10 min to remove residual solvent.

A.3 RESULTS

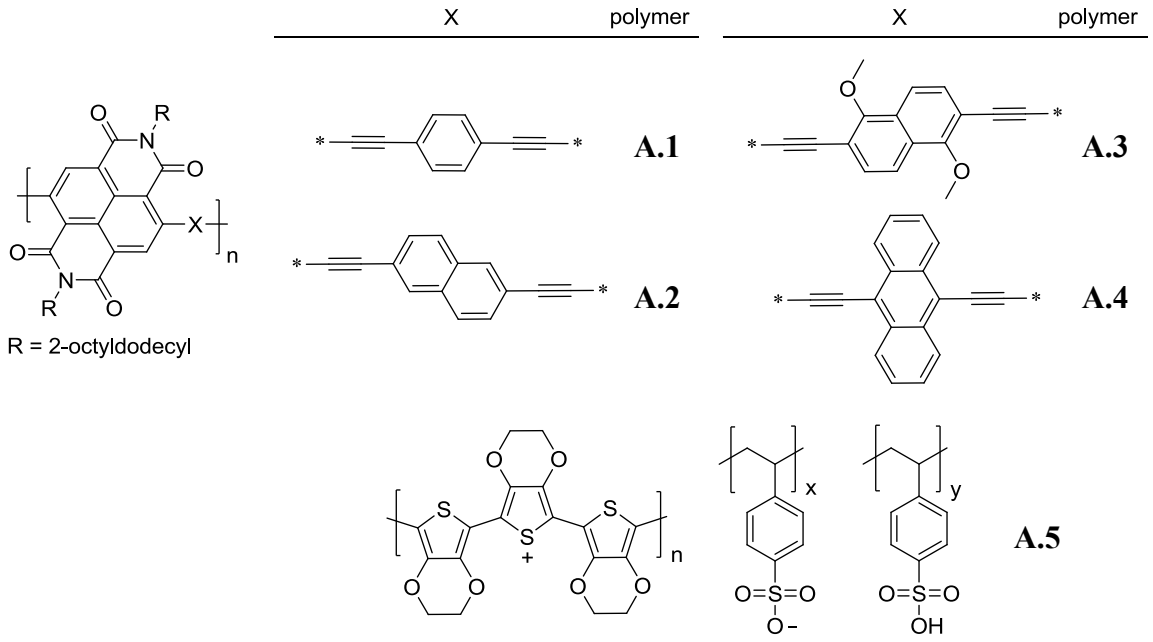

Figure A.1 The polymers from Chapter 4 and the commercially available PEDOT:PSS mixture used in OFETs and for four-point probe analysis.

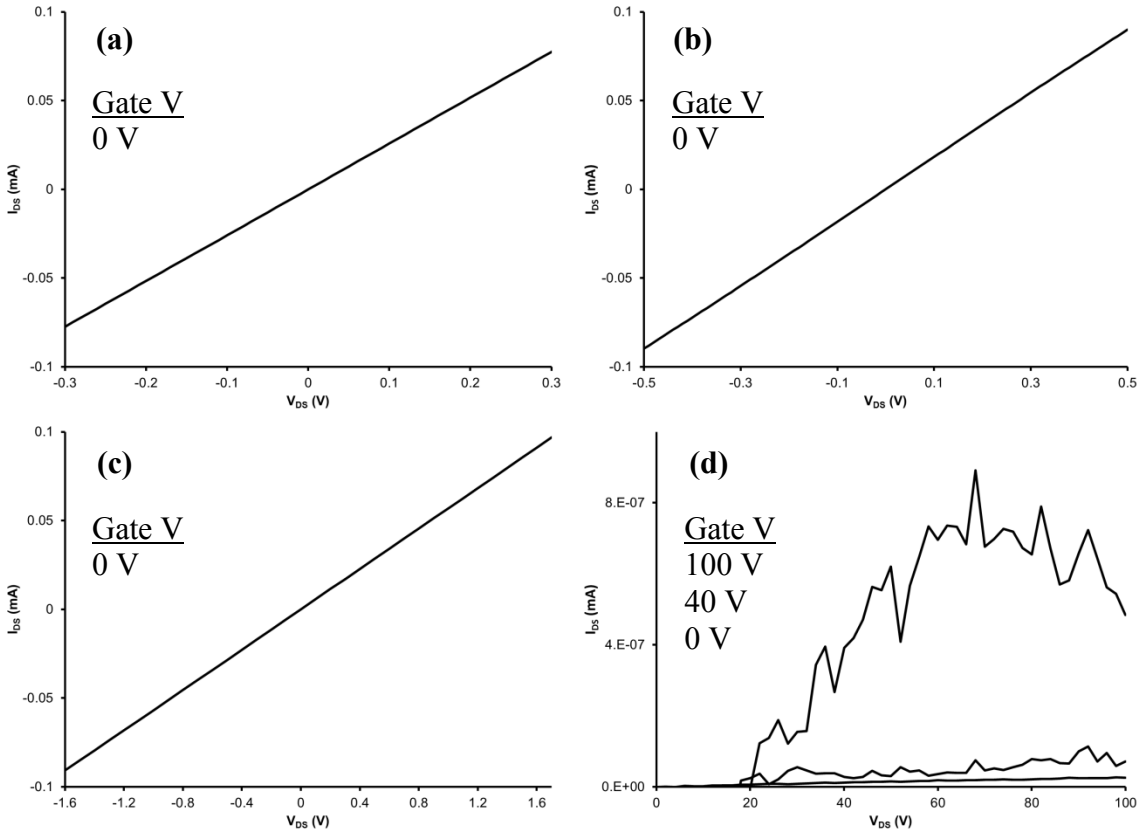

Figure A.2 I_{DS}–V_{DS} trace for (a) the contact of source/drain probes, (b) the source/drain probes on same gold contact, (c) the **A.5** device (30 μm channel width) as resistor standard, and (d) the **A.1** device (30 μm channel width) at three different gate voltages.

	A.1	**A.2**	**A.3**	**A.4**	**A.5**
Resistivity (Ω·m)	N/A	N/A	N/A	N/A	0.43
Conductivity (S/m)	N/A	N/A	N/A	N/A	2.3

Table A.1 The resistivity determined by four-point probe method. Resistivity = 4.532 × film thickness (m) × measured resistance (Ω). The resistance was an average of five measurements. NA = not available, exceeded maximum resistance range. Conductivity is the reciprocal of resistivity.

A.1 was selected as the representative polymer for OFET fabrication and testing. Devices were fabricated to replicate literature examples using NDI-based polymers (128; 176). Yet these devices often failed to exhibit current–voltage (I_{DS}–V_{DS}) curves that resemble an OFET device. On occasion, current (I_{DS}) curves did increase during a voltage (V_{DS}) sweep with higher gate voltages (Figure A.2d). But these observations were highly irreproducible and the I_{DS} intensity was several orders of magnitude lower than those typically observed for these types of NDI materials.

A.5 was incorporated into an OFET device in the same manner as **A.1**. **A.5** was selected as a fabrication standard because of its commercial availability and film application (spin coat). Although it is known that a device with **A.5** will not behave like an OFET (177), it does function as a resistor and yields some credence to the OFET fabrication process. The observed I_{DS}–V_{DS} curve for this resistor is shown in Figure A.2c.

The four-point probe method was used in an attempt to determine conductivity values for the polymers (Table A.1). The conductive **A.5** was also used as a standard for this technique. Four-point probe measurements provided a conductivity of approximately 2.3 S/m for **A.5**. The conductivity values for **A.1**–**A.4** were not obtained by this method as the sheet resistance for these materials exceeded the limit of the instrument.

A.4 DISCUSSION

The I_{DS}–V_{DS} curves in Figure A.2a–c demonstrate that the semiconductor parameter analyzer was functioning properly and the device with **A.5** yields some level of confidence in the fabrication process. Several different experimental conditions were implemented in an attempt to obtain reproducible OFET activity from a device with **A.1**.

Measurements were conducted under both nitrogen and air. A film of **A.1** was also cast by spin coating a dichlorobenzene solution in an analogous manner as described in the experimental section. Films were also baked at higher temperatures (200 °C) and cast with slower spin coating conditions (500 rpm, ~200 nm film). In addition, a device was constructed by drop casting a 5 weight percent solution of **A.1** in chlorobenzene directly onto the channel region of the source/drain contacts. After a slow evaporation, the wafer was baked at 150 °C for 10 min to remove residual solvent. None of these fabrication conditions resulted in a device with enhanced OFET activity.

It is unclear at this time if there are factors that are prohibiting the acquisition of semiconductor parameters that are representative of OFET materials. Success with the **A.5** device appears to indicate that any problem associated with the **A.1** device is attributed to the polymer itself or its physical application onto the wafer.

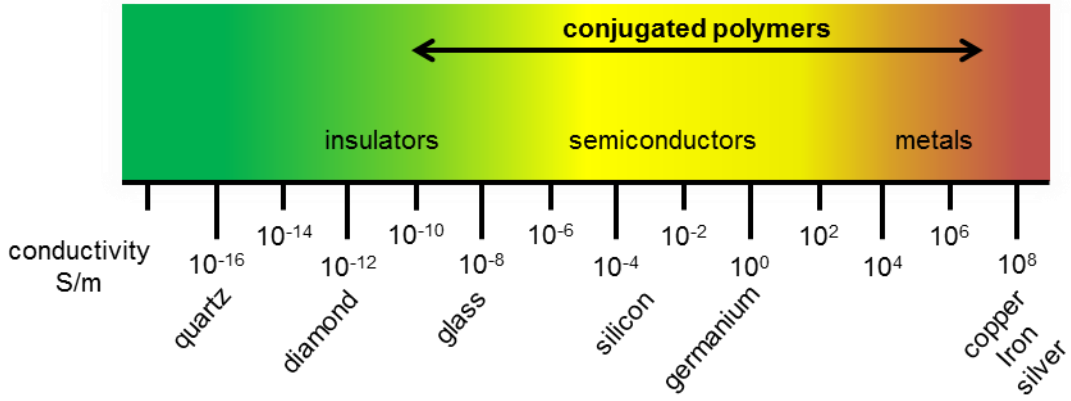

Figure A.3 Conductivity range of representative materials and conjugated polymers (178).

The observed conductivity of 2.3 S/m for **A.5** (Table A.1) is in relative agreement with the reported value by Hopkins and Reynolds (10.9 S/m) (179). It is also within the

conductivity range of typical semiconductors (Figure A.3). But resistance for **A.1**–**A.4** exceeded the working resistance range of the digital multimeter on the four-point probe setup (Table A.1). The maximum resistance is specified to be 200 MΩ which means that the instrument can measure a minimum conductivity of approximately 3.7×10^{-3} S/m for a film thickness of 300 nm. Therefore, the conductivity of **A.1**–**A.4** must be lower than 3.7×10^{-3} S/m which can still fall within the range of conjugated polymers (Figure A.3).

A.5 CONCLUSION

OFET devices were prepared with **A.1**, but literature protocol and numerous fabrication variations failed to produce a successful device. Four-point probe measurements suggested that **A.1**–**A.4** possess a native conductivity below 3.7×10^{-3} S/m which could still reflect semiconductor conductivity. At the very least, this Appendix has established a protocol for testing future materials and provided an estimate for a possible conductivity range of these conjugated polymers.

References

1. Vijay-Kumar, S.; Bugg, C. E.; Cook, W. J. *J. Mol. Biol.* **1987,** *194,* 531.
2. Julien, O.; Beadle, J. R.; Magee, W. C.; Chatterjee, S.; Hostetler, K. Y.; Evans, D. H.; Sykes, B. D. *J. Am. Chem. Soc.* **2011,** *133,* 2264.
3. Philip, D.; Stoddart, J. F. *Angew. Chem. Int. Ed. Engl.* **1996,** *35,* 1154.
4. Lehn, J.-M. *PNAS* **2002,** *99,* 4763.
5. Wilson, G. O.; Caruso, M. M.; Schelkopf, S. R.; Sottos, N. R.; White, S. R.; Moore, J. S. *ACS Appl. Mater. Interfaces* **2011,** *3,* 3072.
6. Dietrich-Buchecker, C. O.; Sauvage, J.-P. *Angew. Chem. Int. Ed. Engl.* **1989,** *28,* 189.
7. Collin, J.-P.; Frey, J.; Heitz, V.; Sakellariou, E.; Sauvage, J.-P.; Tock, C. *New J. Chem.* **2006,** *30,* 1386.
8. Burnworth, M.; Tang, L.; Kumpfer, J. R.; Duncan, A. J.; Beyer, F. L.; Fiore, G. L.; Rowan, S. J.; Weder, C. *Nature* **2011,** *472,* 334.
9. Cao, D.; Amelia, M.; Klivansky, L. M.; Koshkakaryan, G.; Khan, S. I.; Semeraro, M.; Silvi, S.; Venturi, M.; Credi, A.; Liu, Y. *J. Am. Chem. Soc.* **2009,** *132,* 1110.
10. Ye, T.; Kumar, A. S.; Saha, S.; Takami, T.; Huang, T. J.; Stoddart, J. F.; Weiss, P. S. *ACS Nano* **2010,** *4,* 3697.
11. Hunter, C. A.; Sanders, J. K. M. *J. Am. Chem. Soc.* **1990,** *112,* 5525.
12. Jeffery, G. A.; Ruble, J. R.; McCullan, R. K.; Pople, J. A. *Proc. R. Soc. Lond. A* **1987,** *414,* 47.
13. Janda, K. C.; Hemminger, J. C.; Novick, S. E.; Harra, S. E.; Klemperer, W. *J. Chem. Phys.* **1975,** *63,* 1419.
14. Sinnokrot, M. O.; Sherrill, C. D. *J. Phys. Chem. A* **2006,** *110,* 10656.
15. Headen, T. F.; Howard, C. A.; Skipper, N. T.; Wilkinson, M. A.; Bowron, D. T.; Soper, A. K. *J. Am. Chem. Soc.* **2010,** *132,* 5735.
16. Patrick, C. R.; Prosser, G. S. *Nature* **1960,** 1021.
17. Rashkin, M. J.; Waters, M. L. *J. Am. Chem. Soc.* **2002,** *124,* 1860.
18. Wheeler, S. E.; Houk, K. N. *J. Am. Chem. Soc.* **2008,** *130,* 10854.
19. Wheeler, S. E. *J. Am. Chem. Soc.* **2011,** *133,* 10262.
20. Cubberly, M. S.; Iverson, B. L. *J. Am. Chem. Soc.* **2001,** *123,* 7560.
21. Lokey, R. S.; Iverson, B. L. *Nature* **1995,** *375,* 303.
22. Zych, A.; Iverson, B. L. *J. Am. Chem. Soc.* **2000,** *122,* 8898.
23. Gabriel, G. J.; Sorey, S.; Iverson, B. L. *J. Am. Chem. Soc.* **2005,** *127,* 2637.
24. Bradford, V. J.; Iverson, B. L. *J. Am. Chem. Soc.* **2008,** *130,* 1517.
25. Nguyen, J. Q.; Iverson, B. L. *J. Am. Chem. Soc.* **1999,** *121,* 2639.

26. Dobson, C. M. *Sem. Cell Dev. Biol.* **2004,** *15,* 3.
27. Gabriel, G. J.; Iverson, B. L. *J. Am. Chem. Soc.* **2002,** *124,* 15174.
28. Reczek, J. J.; Iverson, B. L. *Macromolecules* **2006,** *39,* 5601.
29. Reczek, J. J.; Villazor, K. R.; Lynch, V.; Swager, T. M.; Iverson, B. L. *J. Am. Chem. Soc.* **2006,** *128,* 7995.
30. Talukdar, P.; Bollot, G.; Mareda, J.; Sakai, N.; Matile, S. *J. Am. Chem. Soc.* **2005,** *127,* 6528.
31. Koshkakaryan, G.; Klivansky, L.; Cao, D.; Snauko, M.; Teat, S.; Struppe, J.; Liu, Y. *J. Am. Chem. Soc.* **2009,** *131,* 2078.
32. Das, A.; Molla, M.; Maity, B.; Koley, D.; Ghosh, S. *Chem. Eur. J.* **2012,** *18,* 9849.
33. Shao, H.; Gao, M.; Kim, S.-H.; Jaroniec, C. P.; Parquette, J. R. *Chem. Eur. J.* **2011,** *17,* 12882.
34. Liu, K.; Yao, Y.; Wang, C.; Liu, Y.; Li, Z.; Zhang, X. *Chem. Eur. J.* **2012,** *18,* 8622.
35. Bhosale, S.; Jani, C.; Langford, S. *Chem. Soc. Rev.* **2008,** *37,* 331.
36. Thalacker, C.; Röger, C.; Würthner, F. *J. Org. Chem.* **2006,** *71,* 8098.
37. Bhosale, S.; Bhosale, S.; Bhargava, S. *Org. Biomol. Chem.* **2012,** *10,* 6455.
38. Alvey, P. M.; Reczek, J. J.; Lynch, V.; Iverson, B. L. *J. Org. Chem.* **2010,** *75,* 7682.
39. Wang, X.-Z.; Jiang, X.-K.; Li, Z.-T. *Youji Huaxue* **2004,** *24,* 753.
40. Zhao, X.; Jia, M.-X.; Jiang, X.-K.; Wu, L.-Z.; Li, Z.-T.; Chen, G.-J. *J. Org. Chem.* **2004,** *69,* 270.
41. Zhou, Q.-Z.; Jiang, X.-K.; Shao, X.-B.; Chen, G.-J.; Jia, M.-X.; Li, Z.-T. *Org. Lett.* **2003,** *5,* 1955.
42. De, S.; Ramakrishnan, S. *Macromolecules* **2009,** *42,* 8599.
43. Colquhoun, H. M.; Zhu, Z.; Cardin, C. J.; Gan, Y.; Drew, M. G. B. *J. Am. Chem. Soc.* **2007,** *129,* 16163.
44. Saraogi, I.; Hamilton, A. D. *Chem. Soc. Rev.* **2009,** *38,* 1726.
45. Zhou, Q.-Z.; Jia, M.-X.; Shao, X.-B.; Wu, L.-Z.; Jiang, X.-K.; Li, Z.-T.; Chen, G.-J. *Tetrahedron* **2005,** *61,* 7117.
46. Vignon, S. A.; Jarrosson, T.; Iijima, T.; Tseng, H.-R.; Sanders, J. K.; Stoddart, J. F. *J. Am. Chem. Soc.* **2004,** *126,* 9884.
47. Alcalde, E.; Pérez-García, L.; Ramos, S.; Stoddart, J. F.; White, A. J. P.; Williams, D. J. *Chem. Eur. J.* **2007,** *13,* 3964.
48. Waters, M. L. *Curr. Opin. Chem. Biol.* **2002,** *6,* 736.
49. Hunter, C. A.; Lawson, K. R.; Perkins, J.; Urch, C. J. *J. Chem. Soc., Perkin Trans. 2* **2001,** 651.
50. Hamilton, D. G.; Lynch, D. E.; Byriel, K. A.; Kennard, C. H. L. *Aust. J. Chem.* **1997,** *50,* 439.

51. Wang, C.; Yin, S.; Chen, S.; Xu, H.; Wang, Z.; Zhang, X. *Angew. Chem., Int. Ed.* **2008,** *47,* 9049.
52. Jonkheijm, P.; Stutzmann, N.; Chen, Z.; de Leeuw, D. M.; Meijer, E. W.; Schenning, A. P. H. J.; Würthner, F. *J. Am. Chem. Soc.* **2006,** *128,* 9535.
53. Koshkakaryan, G.; Klivansky, L. M.; Cao, D.; Snauko, M.; Teat, S. J.; Struppe, J. O.; Liu, Y. *J. Am. Chem. Soc.* **2009,** *131,* 2078.
54. Aprahamian, I.; Yasuda, T.; Ikeda, T.; Saha, S.; Dichtel, W. R.; Isoda, K.; Kato, T.; Stoddart, J. F. *Angew. Chem., Int. Ed.* **2007,** *46,* 4675.
55. Percec, V.; Glodde, M.; Bera, T. K.; Miura, Y.; Shiyanovskaya, I.; Singer, K. D.; Balagurusamy, V. S. K.; Heiney, P. A.; Schnell, I.; Rapp, A.; Spiess, H.-W.; Hudson, S. D.; Duan, H. *Nature* **2002,** *419,* 384.
56. Pisula, W.; Kastler, M.; Wasserfallen, D.; Robertson, J. W. F.; Nolde, F.; Kohl, C.; Muellen, K. *Angew. Chem., Int. Ed.* **2006,** *45,* 819.
57. Lee, S. J.; Change, J. Y. *Tetrahedron Lett.* **2003,** *44,* 7493.
58. Arikainen, E. O.; Boden, N.; Bushby, R. J.; Lozman, O. R.; Vinter, J. G.; Wood, A. *Angew. Chem., Int. Ed.* **2000,** *39,* 2333.
59. Weck, M.; Dunn, A. R.; Matsumoto, K.; Coates, G. W.; Lobkovsky, E. B.; Grubbs, R. H. *Angew. Chem., Int. Ed.* **1999,** *38,* 2741.
60. Praefcke, K.; Singer, D. In *Handbook of Liquid Crystals;* Demus, D., Goodby, J., Gary, G. W., Spiess, H. W., Vill, V., Eds.; Wiley-VCH: Weinheim, 1998; Vol. 2B, pp 945.
61. Bengs, H.; Ebert, M.; Karthaus, O.; Kohne, B.; Praefeke, K.; Ringsdorf, H.; Wendorff, J.; Wüstefeld, R. *Adv. Mater.* **1990,** *2,* 141.
62. Ringsdorff, H.; Wüstefeld, R.; Zerta, M.; Ebert, J.; Wendorff, J. *Angew. Chem.* **1989,** *101,* 934.
63. Goldmann, D.; Janietz, D.; Schmidt, C.; Wendorff, J. H. *Angew. Chem., Int. Ed.* **2000,** *39,* 1851.
64. Qu, S.; Chen, X.; Shao, X.; Li, F.; Zhang, H.; Wang, H.; Zhang, P.; Yu, Z.; Wu, K.; Wang, Y.; Li, M. *J. Mater. Chem.* **2008,** *18,* 3954.
65. Park, L. Y.; Hamilton, D. G.; McGehee, E. A.; McMenimen, K. A. *J. Am. Chem. Soc.* **2003,** *125,* 10586.
66. O'Neill, M.; Kelly, S. M. *Adv. Mater.* **2003,** *15,* 1135.
67. van Breemen, A. J. J. M.; Herwig, P. T.; Chlon, C. H. T.; Sweelssen, J.; Schoo, H. F. M.; Setayesh, S.; Hardeman, W. M.; Martin, C. A.; de Leeuw, D. M.; Valeton, J. J. P.; Bastiaansen, C. W. M.; Broer, D. J.; Popa-Merticaru, A. R.; Meskers, S. C. J. *J. Am. Chem. Soc.* **2006,** *128,* 2336.
68. Simpson, C. D.; Wu, J.; Watson, M. D.; Muellen, K. *J. Mater. Chem.* **2004,** *14,* 494.
69. An, Z.; Yu, J.; Jones, S. C.; Barlow, S.; Yoo, S.; Domercq, B.; Prins, P.; Siebbeles, L. D. A.; Kippelen, B.; Marder, S. R. *Adv. Mater.* **2005,** *17,* 2580.

70. Kato, T.; Mizoshita, N.; Kishimoto, K. *Angew. Chem., Int. Ed.* **2006,** *45,* 38-68.
71. Hoeben, F. J. M.; Jonkheijm, P.; Meijer, E. W.; Schenning, A. P. H. J. *Chem. Rev.* **2005,** *105,* 1491.
72. Leitch, A. A.; Reed, R. W.; Robertson, C. M.; Britten, J. F.; Yu, X.; Secco, R. A.; Oakley, R. T. *J. Am. Chem. Soc.* **2007,** *129,* 7903.
73. Shibahara, S.; Kitagawa, H.; Ozawa, Y.; Toriumi, K.; Kubo, T.; Nakasuji, K. *Inorg. Chem.* **2007,** *46,* 1162.
74. Okabe, A.; Fukushima, T.; Ariga, K.; Aida, T. *Angew. Chem., Int. Ed.* **2002,** *41,* 3414.
75. Wang, J.-Y.; Yan, J.; Ding, L.; Ma, Y.; Pei, J. *Adv. Funct. Mater.* **2009,** *19,* 1746.
76. Schmidt-Mende, L.; Fechtenkötter, A.; Müllen, K.; Moons, E.; Friend, R.; MacKenzie, J. *Science* **2001,** *293,* 1119.
77. Sergeyev, S.; Pisula, W.; Geerts, Y. H. *Chem. Soc. Rev.* **2007,** *36,* 1902.
78. Dierking, I. *Textures of Liquid Crystals;* Wiley-VCH: Weinheim, 2003.
79. Pengo, P.; Pantos, G. D.; Otto, S.; Sanders, J. K. M. *J. Org. Chem.* **2006,** *71,* 7063.
80. Aubuchon, S. R. Interpretation of the Crystallization Peak of Supercooled Liquids Using Tzero DSC. http://www.tainstruments.com.
81. Danley, R. L. *Thermochim. Acta* **2004,** *409,* 111.
82. Günes, S.; Neugebauer, H.; Sariciftci, N. S. *Chem. Rev.* **2007,** *107,* 1324.
83. Li, W.-S.; Yamamoto, Y.; Fukushima, T.; Saeki, A.; Seki, S.; Tagawa, S.; Masunaga, H.; Sasaki, S.; Takata, M.; Aida, T. *J. Am. Chem. Soc.* **2008,** *130,* 8886.
84. Negishi, N.; Yamada, K.; Takimiya, K.; Aso, Y.; Otsubo, T.; Harima, Y. *Chem. Lett.* **2003,** *32,* 404.
85. Lewandowska, K.; Bednarski, W.; Milczarek, G.; Waplak, S.; Graja, A.; Park, E. Y.; Kim, T.-D.; Lee, K.-S. *Synt. Met.* **2011,** *161,* 1640.
86. Barszcz, B.; Laskowska, B.; Graja, A.; Park, E. Y.; Kim, T.-D.; Lee, K.-S. *Synt. Met.* **2011,** *161,* 229.
87. Kim, J. B.; Allen, K.; Oh, S. J.; Lee, S.; Toney, M. F.; Kim, Y. S.; Kagan, C. R.; Nuckolls, C.; Loo, Y.-L. *Chem. Mater.* **2010,** *22,* 5762.
88. Bheemaraju, A.; Pourmand, M.; Yang, B.; Surampudi, S. K.; Benanti, T. L.; Achermann, M.; Barnes, M. D.; Venkataraman, D. *J. Macromol. Sci. A* **2011,** *48,* 986.
89. Kondratenko, M.; Moiseev, A. G.; Perepichka, D. F. *J. Mater. Chem.* **2011,** *21,* 1470.
90. Zificsak, C. A.; Mulder, J. A.; Hsung, R. P.; Rameshkumar, C.; Wei, L.-L. *Tetrahedron* **2001,** *57,* 7575.
91. Katritzky, A. R.; Jiang, R.; Singh, S. K. *Heterocycles* **2004,** *63,* 1455.
92. Dekorver, K. A.; Li, H.; Lohse, A. G.; Hayashi, R.; Lu, Z.; Zhang, Y.; Hsung, R. P.

Chem. Rev. **2010,** *110,* 5064.

93. Evano, G.; Coste, A.; Jouvin, K. *Angew. Chem., Int. Ed.* **2010,** *49,* 2840.
94. Eberson, L.; Lepistoe, M.; Finkelstein, M.; Hart, S. A.; Moore, W. M.; Ross, S. D. *Acta Chem. Scand.* **1988,** *B42,* 666.
95. Sueda, T.; Oshima, A.; Teno, N. *Org. Lett.* **2011,** *13,* 3996.
96. Chernick, E. T.; Ahrens, M. J.; Scheidt, K. A.; Wasielewski, M. R. *J. Org. Chem.* **2005,** *70,* 1486.
97. Bolshan, Y.; Batey, R. A. *Angew. Chem. Int. Ed.* **2008,** *47,* 2109.
98. DeKorver, K. A.; Walton, M. C.; North, T. D.; Hsung, R. P. *Org. Lett.* **2011,** *13,* 4862.
99. Jouvin, K.; Heimburger, J.; Evano, G. *Chem. Sci.* **2012,** *3,* 756.
100. Pielichowski, J.; Chrzaszcz, R. *B. S. C. Belg.* **1995,** *104,* 117.
101. Nadipuram, A. K.; David, W. M.; Kumar, D.; Kerwin, S. M. *Org. Lett.* **2002,** *4,* 4543.
102. Katritzky, A. R.; Zhang, S.; Fang, Y. *Org. Lett.* **2000,** *2,* 3789.
103. Huang, S.; Xiong, H.; Hsung, R. P.; Rameshkumar, C.; Mulder, J. A.; Grebe, T. P. *Org. Lett.* **2002,** *4,* 2417.
104. Zuagg, H. E.; Swett, L. R.; Stone, G. R. *J. Org. Chem.* **1958,** *23,* 1389.
105. Guha, S.; Goodson, F. S.; Corson, L. J.; Saha, S. *J. Am. Chem. Soc.* **2012,** *134,* 13679.
106. Hargrove, R. J.; Stang, P. J. *J. Org. Chem.* **1974,** *39,* 581.
107. Fearnley, S. P.; Funk, R. L.; Gregg, R. J. *Tetrahedron* **2000,** *56,* 10275.
108. Dawson, R. E.; Hennig, A.; Weimann, D. P.; Emery, D.; Ravikumar, V.; Montenegro, J.; Takeuchi, T.; Gabutti, S.; Mayor, M.; Mareda, J.; Schalley, C. A.; Matile, S. *Nature Chem.* **2010,** *2,* 533.
109. Stang, P. J.; Treptow, W. *Synthesis* **1980,** 283.
110. Kim, J. Y.; Kim, S. H.; Chang, S. *Tetrahedron Letters* **2008,** *49,* 1745.
111. Thomas, H.; Stuhr-Hansen, N.; Westerlund, F.; Laursen, B. W.; Magnussen, M.; Sørensen, H. O.; Bjørnholm, T.; Christensen, J. B. *Tetrahedron Lett.* **2009,** *50,* 7374.
112. Alvey, P. M.; Ono, R. J.; Bielawski, C. W.; Iverson, B. L. *Macromolecules* **2013,** *46,* 718.
113. Cheng, Y.-J.; Yang, S.-H.; Hsu, C.-S. *Chem. Rev.* **2009,** *109,* 5868.
114. Murphy, A. R.; Fréchet, J. M. J. *Chem. Rev.* **2007,** *107,* 1066.
115. Anthony, J. E.; Facchetti, A.; Heeney, M.; Marder, S. R.; Zhan, X. *Adv. Mater.* **2010,** *22,* 3876.
116. Beaujuge, P. M.; Reynolds, J. R. *Chem. Rev.* **2010,** *110,* 268.
117. Chen, J.; Cao, Y. *Acc. Chem. Res.* **2009,** *42,* 1709.

118. Havinga, E. E.; Hoeve, W.; Wynberg, H. *Polym. Bull.* **1992,** *29,* 119.
119. Thompson, B. C.; Kim, Y.-G.; McCarley, T. D.; Reynolds, J. R. *J. Am. Chem. Soc.* **2006,** *128,* 12714.
120. Blouin, N.; Michaud, A.; Gendron, D.; Wakim, S.; Blair, E.; Neagu-Plesu, R.; Belletête, M.; Durocher, G.; Tao, Y.; Leclerc, M. *J. Am. Chem. Soc.* **2007,** *130,* 732.
121. Abbotto, A.; Calderon, E. H.; Dangate, M. S.; De Angelis, F.; Manfredi, N.; Mari, C. M.; Marinzi, C.; Mosconi, E.; Muccini, M.; Ruffo, R.; Seri, M. *Macromolecules* **2010,** *43,* 9698.
122. Roncali, J. *Chem. Rev.* **1997,** *97,* 173.
123. Yan, H.; Chen, Z.; Zheng, Y.; Newman, C.; Quinn, J. R.; Dotz, F.; Kastler, M.; Facchetti, A. *Nature* **2009,** *457,* 679.
124. Katz, H. E.; Lovinger, A. J.; Johnson, J.; Kloc, C.; Siergrist, T.; Li, W.; Lin, Y. Y.; Dodabalapur, A. *Nature* **2000,** *404,* 478.
125. Chopin, S.; Chaignon, F.; Blart, E.; Odobel, F. *J. Mat.Chem.* **2007,** *4139,* 17.
126. Chaignon, F.; Falkenstrom, M.; Karlsson, S.; Blart, E.; Odobel, F.; Hammarstrom, L. *Chem. Comm.* **2007,** *42,* 64.
127. Guo, X.; Watson, M. D. *Org. Lett.* **2008,** *10,* 5333.
128. Chen, Z.; Zheng, Y.; Yan, H.; Facchetti, A. *J. Am. Chem. Soc.* **2009,** *131,* 8.
129. Chen, J.; Shi, M.-M.; Hu, X.-L.; Wang, M.; Chen, H.-Z. *Polymer* **2010,** *51,* 2897.
130. Durban, M. M.; Kazarinoff, P. D.; Luscombe, C. K. *Macromolecules* **2010,** *43,* 6348.
131. Durban, M. M.; Kazarinoff, P. D.; Segawa, Y.; Luscombe, C. K. *Macromolecules* **2011,** *44,* 4721.
132. Mohamad, K. A.; Yousuke, K.; Uesugi, K.; Fukuda, H. *Jpn. J. Appl. Phys.* **2011,** *50,* 091603.
133. Piyakulawat, P.; Keawprajak, A.; Chindaduang, A.; Hanusch, M.; Asawapirom, U. *Synth. Met.* **2009,** *159,* 467.
134. Polander, L. E.; Tiwari, S. P.; Pandey, L.; Seifried, B. M.; Zhang, Q.; Barlow, S.; Risko, C.; Brédas, J.-L.; Kippelen, B.; Marder, S. R. *Chem. Mater.* **2011,** *23,* 3408.
135. Wei, Y.; Zhang, Q.; Jiang, Y.; Yu, J. *Macromol. Chem. Phys.* **2009,** *210,* 769.
136. Kudla, C. J.; Dolfen, D.; Schottler, K. J.; Koenen, J.-M.; Breusov, D.; Allard, S.; Scherf, U. *Macromolecules* **2010,** *43,* 7864.
137. Piyakulawat, P.; Keawprajak, A.; Wlosnewski, J.; Forster, M.; Asawapirom, U. *Synth. Met.* **2011,** *161,* 1238.
138. Mori, T.; Kijima, M. *Opt. Mater.* **2007,** *30,* 545.
139. Shao, H.; Parquette, J. R. *Chem. Commun.* **2010,** *46,* 4285.
140. Tomasulo, M.; Naistat, D. M.; White, A. J. P.; Williams, D. J.; Raymo, F. M. *Tetrahedron Lett.* **2005,** *46,* 5695.

141. Avinash, M. B.; Govindaraju, T. *Adv. Funct. Mater.* **2011,** *21,* 3875.
142. Martinez, C. R.; Iverson, B. L. *Chem. Sci.* **2012,** *3,* 2191.
143. Jiang, W.; Han, M.; Zhang, H.-Y.; Zhang, Z.-J.; Liu, Y. *Chem. Eur. J.* **2009,** *15,* 9938.
144. Kymissis, I. *Organic Field Effect Transistors: Theory, Fabrication and Characterization;* Springer Science+Business Media, LLC: New York, 2009.
145. Letizia, J. A.; Salata, M. R.; Tribout, C. M.; Facchetti, A.; Ratner, M. A.; Marks, T. J. *J. Am. Chem. Soc.* **2008,** *130,* 9679.
146. Jones, S.; Atherton, J. C. C. *Synth. Commun.* **2001,** *31,* 1799.
147. Zhao, Z.; Yu, S.; Xu, L.; Wang, H.; Lu, P. *Tetrahedron* **2007,** *63,* 7809.
148. Würthner, F.; Suraru, S.-L. *Synthesis* **2009,** *2009,* 1841.
149. Guo, X.; Watson, M. D. *Macromolecules* **2011,** *44,* 6711.
150. Avila-Ortega, A.; Vázquez-Torres, H. *J. Polym. Sci., Part A: Polym. Chem.* **2007,** *45,* 1993.
151. Ahmed, E.; Ren, G.; Kim, F. S.; Hollenbeck, E. C.; Jenekhe, S. A. *Chem. Mater.* **2011,** *23,* 4563.
152. Alp, S.; Erten, S.; Karapire, C.; Köz, B.; Doroshenko, A. O.; Icli, S. J. *Photochem. Photobiol. A: Chem.* **2000,** *135,* 103.
153. Wheeler, A. S.; Ergle, D. R. *J. Am. Chem. Soc.* **1930,** *52,* 4872.
154. Alvey, P. M.; Iverson, B. L. *Org. Lett.* **2012,** *14,* 2706.
155. Sakai, N.; Mareda, J.; Vauthey, E.; Matile, S. **2010,** *46,* 4225.
156. Holman, G.; Zewail-Foote, M.; Smith, A.; Johnson, K.; Iverson, B. *Nature Chem.* **2011,** *3,* 875.
157. Usta, H.; Facchetti, A.; Marks, T. *Acc. Chem. Res.* **2011,** *44,* 501.
158. Würthner, F.; Stolte, M. *Chem. Commun.* **2011,** *47,* 5109.
159. Würthner, F.; Ashmed, S.; Thalacker, C.; Debaerdemaeker, T. *Chem.-Eur. J.* **2002,** *8,* 4742.
160. Kishore, R.; Kel, O.; Banerji, N.; Emery, D.; Bollot, G.; Mareda, J.; Gomez-Casado, A.; Jonkheijm, P.; Huskens, J.; Maroni, P.; Borkovec, M.; Vauthey, E.; Sakai, N.; Matile, S. *J. Am. Chem. Soc.* **2009,** *131,* 11106.
161. Yue, W.; Zhen, Y.; Li, Y.; Jiang, W.; Lv, A.; Wang, Z. *Org. Lett.* **2010,** *12,* 3460.
162. Polander, L.; Romanov, A.; Barlow, S.; Hwang, D.-K.; Kippelen, B.; Timofeeva, T.; Marder, S. *Org. Lett.* **2012,** *14,* 918.
163. Carsten, B.; He, F.; Jung Son, H.; Xu, T.; Yu, L. *Chem. Rev.* **2011,** *111,* 1493.
164. Silverstein, R.; Webster, F. *Spectrometric Identification of Organic Compounds, 6th ed.;* John Wiley and Sons: New York, 1998.
165. Guha, S.; Saha, S. *J. Am. Chem. Soc.* **2010,** *132,* 17674.

166. Guha, S.; Goodson, F.; Roy, S.; Corson, L.; Gravenmier, C.; Saha, S. *J. Am. Chem. Soc.* **2011,** *133,* 15256.
167. Guha, S.; Goodson, F.; Clark, R.; Saha, S. *CrystEngComm.* **2012,** *14,* 1213.
168. Farina, V. *J. Org. Chem.* **1991,** *56,* 4985.
169. Chen, Z.; Liang, X.; Zhang, H.; Xie, H.; Liu, J.; Xu, Y.; Zhu, W.; Wang, Y.; Wang, X.; Tan, S.; Kuang, D.; Qian, X. *J. Med. Chem.* **2010,** *53,* 2589.
170. Cardona, C. M.; Li, W.; Kaifer, A. E.; Stockdale, D.; Bazan, G. C. *Adv. Mater.* **2011,** *23,* 2367.
171. Reczek, J. J. *Aromatic electron donor-acceptor interactions in novel supramolecular assemblies;* Austin, TX, 2006.
172. Kurosawa, H. *Inorg. Chem.* **1976,** *15,* 120.
173. Chandrasekhar, S.; Reddy, C. R.; Rao, R. J. *Tetrahedron* **2001,** *57,* 3435.
174. Cadot, C.; Dalko, P. I.; Cossy, J. *Tetrahedron Lett.* **2002,** *43,* 1839.
175. Bartmann, E. J. *Organometal. Chem.* **1985,** *284,* 149.
176. Kolhe, N.; Nandini Devi, R.; Senanayak, S. P.; Jancy, B.; Narayan, K. S.; Asha, S. K. *J. Mater. Chem.* **2012,** *22,* 15235.
177. Kirchmeyer, S.; Reuter, K. *J. Mater. Chem.* **2005,** *15,* 2077.
178. The Nobel Prize in Chemistry 2000 - Advanced Information. http://www.nobelprize.org/nobel_prizes/chemistry/laureates/2000/advanced.html (accessed April 3, 2013).
179. Hopkins, A.; Reynolds, J. *Macromolecules* **2000,** *33,* 5221.

Vita

Paul Michael Alvey II was born the oldest of two children of Michael and Linda Alvey. He was raised in Woodbridge, VA and graduated from Evangel Christian High School in 2003. He attended James Madison University where he obtained his B.S. in chemistry under the research direction of Professor Debra Mohler. Following his graduation from James Madison University in 2007, he entered the graduate program at the University of Texas at Austin and joined the research group of Professor Brent Iverson.

Permanent address: 3009 Arbor Court, Woodbridge, VA 22193

This dissertation was typed by the author